11-26-2011

International Conference on Advances in Engineering and Technology

Prof.Srikanta Patnaik Mentor
IRNet India, patnaik_srikanta@yahoo.co.in

Proceedings of International Conference on

Advances in Engineering and Technology

(ICAET-2011)
26th November, 2011
BHUBANESWAR, India

Interscience Research Network (IRNet)
Bhubaneswar, India

Editorial

The new economic millennium is surprisingly rushing with Innovation and Technology. There is a sharper focus on deriving value from the widespread global integration in almost all spheres of social, economic, political and technological subsystems. All the dignified fields of Engineering are becoming highly interdisciplinary and endowed with computational complexities. In the present era of science and technology, much attention has been given to the association of Soft Computing with other engineering disciplines. Soft Computing as a computational science dedicated to system solutions using certain logically enriched techniques. It is basically a high profile study deals with a fusion of research Evolutionary Algorithm and Genetic Programming, Neural Science and Neural Network Systems, Fuzzy Set theory and Fuzzy Systems, Chaos Theory and Chaotic Systems. In all perspectives the core objective is to reduce the complexity and uncertainty in the functioning of various engineering designs. The broad area provides a unifying platform that fosters comparisons, extensions and new applications.

In the advent of modern research there is a significant growth in Mechanical Engineering as Computer Aided Design has become instrumental in many industrialized nations like USA, European Countries, Scotland and GermOther CAE programs commonly used by mechanical engineers include product lifecycle management (PLM) tools and analysis tools used to perform complex simulations. Analysis tools may be used to predict product response to expected loads, including fatigue life and manufacturability. These tools include Finite Element Analysis (FEA), Computational Fluid Dynamics (CFD), and Computer-Aided Manufacturing (CAM). Using CAE programs, a mechanical design team can quickly and cheaply iterates the design process to develop a product that better meets cost, performance, and other constraints. No physical prototype need be created until the design nears completion, allowing hundreds or thousands of designs to be evaluated, instead of a relative few. In addition, CAE analysis programs can model complicated physical phenomena which cannot be solved by hand, such as viscoelasticity, complex contact between mating parts, or non-Newtonian flows.

Almost every researcher will not deny the fact that Computational Complexity is increasing with the advanced trend multidisciplinary approach to the field of Computation. In many instances the intricacies are not being solved through programming languages. MATLAB is an interactive environment designed to perform scientific and engineering calculations and to create computer simulations. MATLAB is a customized computing solution to the engineering researchers. MATLAB is a high-level language and interactive environment that enables you to perform computationally intensive tasks faster than with traditional programming languages such as C, C++, and FORTRAN. MATLAB is attributed to the pioneering work of Cleve Moler, head of Computer

Science Department, University of New Mexico during 1970s. The development of the field is credited to the works of MathWorks during 1984.

As the area is broad and requires cross functionally expert reviewers for technical scrutiny of the papers, we have tried to impart justice to all the paper in its publication in the proceeding. In all sense we have been transcendental in this field in developing the fauna of the conference. In meeting the professional commitments we maintained the sanctity by adhering to ethics, ontology and semiotics. I beg apology for any inconveniency caused to the participants and delegates in the journey of this conference. I have regards for the IRNet family members, reviewers, and support staffs for their generous gifts of time, energy and effort. Specifically I owe indebtedness to the authors for their intellectual contributions in this conference.

Prof. (Dr.) Srikanta Patnaik
President, IRNet India and Chairman IIMT
Intersceince Campus, Bhubaneswar
Email: patnaik_srikanta@yahoo.co.in

Utility of Resource Allocation and Frequency Off-set Estimation for MB-OFDM based UWB

Ravi Gugulothu & Vijaya

Vaagdevi College of Engineering, Jawaharlal Nehru Technological University, Hyderabad, Warangal-506002, India

Abstract - Most of the wireless services (like MB-OFDM, OFDM-MIMO) with variable rate transmission; both average rate and rate oscillation are important performance metrics. The traditional performance criterion, utility of average transmission rate, boosts the average rate. We introduce a utility function of instantaneous transmission rates. It is capable of facilitating the resource allocation with flexible combinations of average rate. Based on the new utility, we consider the time and power allocation in a time-shared wireless network. Two adaptation policies are developed, namely, time sharing (TS) and joint time sharing and power control (JTPC). We address low-complexity; highly-accurate frequency offset estimation for multi-band orthogonal frequency division multiplexing (MB-OFDM) based ultra-wide band systems in time-invariant as well as time-variant channels. We investigate the unique characteristics of MB-OFDM systems, namely, different frequency offsets, channel responses, received energies, and preamble structures in different frequency bands. Utilizing them, we develop frequency offset estimators based on the best linear unbiased estimation principle for the utility of resource allocation. If compared to the reference estimators, our proposed methods achieve significantly better estimation performance (4 to 6.4 dB (5 to 20 dB) estimation mean-square error advantage in the time-invariant (time-variant) channels) for all preamble patterns of the MB-OFDM system.

Keywords - *Utility function, Time sharing, UWB, BLUE, frequency offset, OFDM, JTPC.*

I. INTRODUCTION

One promising approach for addressing this issue is to dynamically allocate limited resources based on channel information and system preferences. Traditional investigations on wireless resource allocation pay much attention to hard real-time services. There in, the goal is to smooth out channel variation and build “bit pipes” that deliver data at a fixed rate. The rapid growth of the Internet has led to an increasing demand for supporting transmissions of best-effort service in wireless systems. These applications allow variable-rate transmission. Therefore, opportunistic communications [1] have been introduced to achieve higher system throughput. The concept of opportunistic communications is essentially to transmit more information in good channel states and less in poor ones. If constant-rate transmission algorithms are used, the transmission efficiency would be very low. On the other hand, opportunistic scheduling schemes, such as [2] and [3], whose objective is to maximize a utility of average rates, can improve efficiency in terms of average rate but result in high oscillation in instantaneous transmission rates. This thus motivated the need for a new criterion that can be used to facilitate the choice of the combinations of average rate and rate oscillation.

Ultra-Wide band (UWB) systems (e.g., impulse radios [4], [5] and transmitted reference schemes [6] to name a few) offer improved ranging precision, better penetration through obstacles, higher data rate, and increased multipath or frequency diversity. Due to ultra-wide bandwidth, UWB systems can operate at low power spectral density which allows overlay with other narrow-band systems. The coexistence issue and the spectral analysis of UWB systems have been investigated in [7] . Another approach to realize UWB systems is multi-band orthogonal frequency division multiplexing (MB-OFDM) which has been proposed for the IEEE 802.15.3a standard and adopted in European Computer Manufacturers Association (ECMA) standard . The very high data rate (480 Mbps and beyond) capability of the UWB technology would provide a compelling cable-replacement wireless technology. OFDM is a relatively mature technology and has been adopted in digital broadcasting, wireless LAN and MAN standards. OFDM has several advantages such as low complexity equalization in dispersive channels and the spectral density scalability/adaptability (e.g., adaptive bit loading). However, OFDM has some is advantages such as larger susceptibility to nonlinear distortion at the transmit power amplifier and larger sensitivity to frequency

offsets. The application of OFDM technology in UWB systems demands highly accurate frequency offset estimation, since frequency offset causes a loss of orthogonality among the subcarriers thereby introducing inter sub-carrier interference and significantly degrading the error performance. In the MB-OFDM system in [8] , a preamble is used to aid receiver algorithms related to timing and frequency synchronization, and channel estimation. There are several preamble-based frequency offset in the research literature. However, we have not observed frequency offset estimators derived for the MB-OFDM systems. In MB-OFDM systems, the oscillator frequency offset (OFO) causes different carrier frequency offsets (CFOs) for the different bands. The channel frequency responses and the channel energies for the different bands are different as well.

The frequency hopping of the MB-OFDM system results in different preamble structures for some of the frequency bands. These characteristics neither exist in typical OFDM systems nor have been fully reported in the MB-OFDM literature. To our best knowledge, no frequency offset estimator has been developed utilizing all of the above characteristics of MBOFDM systems for performance improvement. The statistics of UWB channels reported in the literature are mainly time-invariant. However, moving scatterers can cause time-varying UWB channels. The typical channel variations due to moving persons in UWB applications would be very slow and their effects on frequency offset estimation are negligible. Best knowledge, there is no frequency offset estimator designed to be robust against sudden channel changes. In this paper, we characterize the unique features of MBOFDM systems. Using a simple channel model capturing occasional abrupt channel change behavior, we develop an efficient detection algorithm to track a sudden channel change and propose frequency offset estimators suitable for (sudden) time-variant as well as time-invariant UWB systems. We apply the best linear unbiased estimation (BLUE) principle and fully utilize the unique characteristics of the MB-OFDM systems in developing our frequency offset estimators. Our proposed estimators offer significant MSE improvement over the reference estimators (about 4-6.4 dB (5-20 dB) estimation mean-square error (MSE) advantage in time-invariant (time-variant) UWB channels).

The rest of this paper is organized as follows. Section II describes the signal and channel models and the proposed frequency offset estimation methods are presented. Section III discusses the design parameters Simulation results and discussions are provided, in Section IV the paper is concluded.

II. SYSTEM MODEL

A. *Time-average Aggregate concave Utility of resource allocation and transmission Rate*

We consider a single cell consisting of *N* mobile users communicating with a common base station. The communication link between each user and the base station is modeled as a slowly time-varying fading channel with additive white Gaussian noise (AWGN). The channel coefficients remain approximately unchanged during each time frame, but can vary from one frame to another. Let the instantaneous channel gain of user *i* at any given time frame *t* be denoted by $g_i(t)$ The network channel gain is denoted by the N_{tuple} g(*t*) _ (*g*1(*t*), *g*2(*t*), . . . , $g_N(t)$), and has a joint probability density function (PDF) *f*(**g**). Let $p_i(t)$ denote the transmit power allocated to or from user *i*. The achievable transmission rate of user *is* in the absence of other users can be expressed

$$c_i(t) = \log_2[1 + \frac{p_i(t)g_i(t)}{\beta N_O}] \quad (1)$$

Where N_0 is the noise power, and β is the signal-to-noise ratio (SNR) gap [4]. We assume that each time frame can be accessed by all the *N* users in an adaptive time-sharing fashion. Let $\rho(g) = (\rho 1, \rho 2, \ldots, \rho N)$ denote the time-sharing adaptation policy with respect to the network channel gain **g**, where ρ_i represents the fraction of the frame duration allocated to user *i*. Without loss of generality, the interval of a time frame is normalized. The actual transmission rate of user *i* at the *t*-th time frame, $r_i(t)$ is given by $r_i(t) = \rho_i c_i(t)$ .The frame index *t* in $r_i(t)$ and $g_i(t)$ may be omitted hereafter if no confusion occurs. The utility considered here is a function of the instantaneous transmission rate. For user *i*, we denote its utility as $U_i(r_i(t))$. The analysis throughout this paper is valid for any utility function that is increasing, differentiable and concave.

B. *Time sharing*

In this section, we assume that the transmission powers between BS and mobiles are constant and identical for different users, i.e., $p_i(t) = p, \forall_i, t$, and that the wireless network is fully loaded. We choose the aggregate utility, which is the sum of individual user utilities, as the performance measure. The goal is to find the optimal time-sharing adaptation policy $\rho*$(g) relative to the instantaneous network channel condition g, so as to maximize the TAUR of the system. Since the channel

processes are ergodic, the optimization problem can be expressed mathematically as

$$\underset{\rho(g)}{Max}\, I_{Ts} \triangleq E_t[\sum_{i=1}^{N} U_i(r_i(t))] \quad (2)$$

$$= \int_g \sum_{i=1}^{N} U_i(\rho_i(g), g_i) f(g) dg$$

$$\sum_{i=1}^{N} p_i(g) = 1 \quad (3)$$

Where notation E*t*[·] represents the time average. Since the constraint (3) is defined for all channel states, the average aggregate utility maximization in (2) is equivalent to maximizing the instantaneous aggregate utility for every channel state. Furthermore, since the utility $U_i(.)$ is a concave function of r_i by assumption, $U_i(.)$ is also concave in p_i.

C. Signal and channel models

C.1. UWB Signal Model

We will adopt two types of UWB technologies which are presently emerging for technical and commercial purposes: the impulse radio UWB (IR-UWB) and the multiband OFDM UWB (MB-OFDM UWB) [8]. IR-UWB uses a short pulse (less than 1ns) that occupies a large bandwidth to modulate the information. Three typical modulation techniques are: time hopping pulse position modulation (TH-PPM), time hopping pulse amplitude modulation (TH-PAM), and direct sequence pulse amplitude modulation (DS-PAM) .The PPM-TH-UWB signal can be written as:

$$s_1^{(k)}(t) = \sum_{j=-\infty}^{\infty} g(t - jT_s - C_j^{(k)} T_c - \varepsilon d^{(k)}_{[j/Ns]}) \quad (4)$$

The PAM-TH-UWB signal may be expressed as follows:

$$S_2^{(k)}(t) = \sum_{j=-\infty}^{\infty} e^{(k)}_{[j=j/N_s]} g(t - jT_s - C_j^{(k)} T_c) \quad (5)$$

PAM-DS-UWB signal is donated as:

$$S_3^{(k)}(t) = \sum_{j=-\infty}^{\infty} d_j g(t - jT_s) \quad (6)$$

In Equation (1)-(3), *Ts* represents the pulse repetition period without modulation; $C_j(k)$ is the j_{th} symbol of the pseudorandom time hopping sequence of the k_{th} user; T_c is donated as the unit transmit pulse delay controlled by time hopping symbol; ε is a constant term; ei €*{-1,+1},* di *(k)* €*{0,1}*; "[]" represents rounding operation, and one binary symbol is transmitted within every *Ns* pulses; *g(t)* is the

Gaussian pulse waveform and may be given by:

$$g(t) = \pm \frac{t^2 - \sigma^2}{\sqrt{2\Pi\sigma^5}} e^{\frac{r^2}{2\sigma^2}} \quad (7)$$

Where σ is an index correlated to the width of pulse, indicating the shape of pulse.

In this paper, MB-OFDM PHY layer model is based on IEEE802.15.3a proposal, as shown in Fig. 1. And fig. 2.

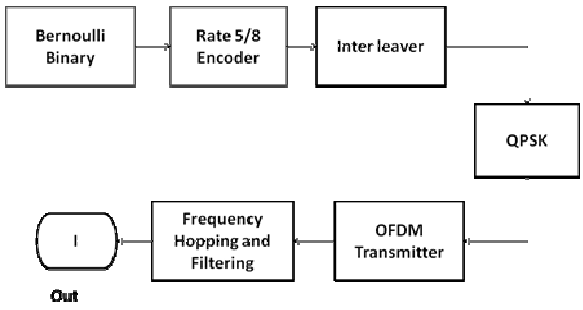

Fig.1 : PHY layer model of MB-OFDM

C.2. UWB Channel Model:

The Saleh and Valenzuela (S-V) multipath channel model proposed by IEEE802.15.3a, which is on the basis of modification of classical broadband indoor S-V model, is used as UWB channel model. The modified model retains the characteristics of the classical model, e.g. multiple paths appear in the form of clusters, and energy is subject to double-exponential distribution. Moreover, S-V model with a lognormal fading distribution on the amplitudes is superior to Rayleigh channels.

C.3. The MB-OFDM-based UWB system

The carrier frequency is hopped within a pre-defined set of carrier frequencies *{f1, f2, f3}* (corresponding to disjoint frequency bands) from symbol to symbol, according to a time-frequency code. The MB-OFDM system from has 4 different preamble patterns (for 4 pico-nets), each associated with a different time-frequency code. Each preamble pattern is constructed by successively repeating a time-domain preamble sequence(symbol) over 21 periods as *{*PS0, PS1, . . . , PS20*}* . The preamble patterns 1 and 2 (or, 3 and 4) have the same structure, except for the ordering

of the carrier frequencies. The preamble pattern 3 or 4, however, has a structure distinct from pattern 1 or 2. For details of the preamble structures of preamble 3 or4,In the MB-OFDM-based system from [8], zero-padded guard intervals N_{pre} prefix and N_{suf} suffix zero samples; $Ng = N_{pre} + N_{suf}$ are used instead of the conventional cyclic prefix guard interval.

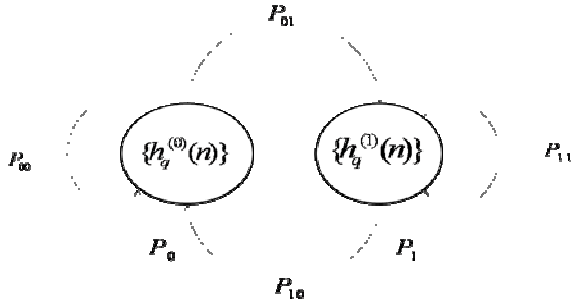

Fig. 2 : A simple time-variant UWB channel model capturing occasional sudden channel changes.

The total number of samples in one OFDM symbol (including the guard samples) is $M0 = N + Ng$. The low-pass-equivalent time-domain samples $\{sq(k = mM0 + N_{pre} + n) : n = -N_{pre}, \ldots, N + N_{suf} - 1\}$ (sampled at $N/T = 1/Ts$, N times the sub-carrier spacing) transmitted during the m-th symbol interval in the q-th frequency band are generated by taking the N-point inverse discrete Fourier transform of the corresponding sub-carrier symbols $C_{q,m}(l)$ (zeros for null sub-carriers; all zeros if no symbols are transmitted in the q-th band during the m-th interval) and inserting zero guard-samples as

$$S_q(k) = \begin{cases} 1/N \sum_{t=0}^{N-1} C_{q,m}(l) e^{j2\pi \ln/N}, 0 \le n \le N-1 \\ 0, -N_{pre} \le n < 0; N \le n < N + N_{suf} \end{cases} \quad (8)$$

The IEEE 802.15.3a UWB RF channel model described and is given by

$$h_{RF}(t) = X \sum_{l=0}^{L_k} \sum_{k=0}^{k} \alpha_{k_l}(t - T_i - T_{k,l}) \quad (9)$$

where $\alpha_{k,l}$, Tl, $\tau_{k,l}$, and X are random variables representing the multipath gain coefficients, the delay of the l-th cluster, the delay (relative to the l-th cluster arrival time) of the k-th multipath component of the l-th cluster, and the log-normal shadowing on the amplitude, respectively. L_{h+1} is the number of the clusters and $K + 1$ is the number of the multi-path components per cluster. In this paper, we consider a low-pass equivalent system that absorbs the carrier-frequency hopping into the channel impulse response (CIR). The sample-spaced low-pass-equivalent CIR for the q-th band is given by

$$h_q(n) = X \sum_{l=0}^{L_h} \sum_{k=0}^{k} \alpha_{k,l} e^{-2\pi f_q (T_l + T_{k,l})} p^{(nT - T_i - T_{k,l} - t_0)} \quad (10)$$

where the effect of the combined transmit and receive filter with the impulse response $p(t)$ has been included in the CIR and $t0$ is a delay for the causality.

The above UWB channel model does not include time varying behavior. However, the movements of the transmitter, the receiver, and/or the scatterers result in a time-varying channel. For the UWB system in [8], the channel variations due to the Doppler spread are too slow and can be neglected in the CFO estimation. However, occasionally when a fast scatterer moves through and thus blocks one or more of the UWB channel paths, an abrupt change in the CIR will occur. A scatterer can move into or out of a position that blocks some channel paths. We consider that the paths affected by the fast moving scatterer correspond to the L_c-th cluster, which is a random variable.

For convenience, we assume that arbitrary J adjacent rays of the L_c-th cluster are completely blocked. Note that $0 \le J \le K$ and $J = 0$ corresponds to a time invariant channel while $J = K$ with $k0 = 0$ defines that the whole L_c-th cluster is blocked. Due to non-negligible physical sizes of moving scatters in typical UWB environments, after an abrupt change occurs, the channel will most likely remain the same for the mandatory Mode-1 of the MB-OFDM system , the three carrier frequencies are generated from one oscillator. The normalized (by the sub-carrier spacing) OFO v causes different normalized CFOs $\{vq\}$ for the three bands, and their relationship4 is given by

$$V_q = b_q V \text{ , for q=1,2,3} \quad (11)$$

$$[b_1, b_2, b_3] = [\frac{13}{16}, \frac{15}{16}, \frac{17}{16}] \quad (12)$$

We assume that the timing synchronization eliminates inter symbol-interference. Define $\{t_q\} = \{t_{ql}(i) : i = 0, \ldots, N-1; l = 1, \ldots, L_q\}$ where $\{t_{ql}(i) : i = 0, 1, \ldots, N-1\}$ denotes the time-domain sample index set corresponding to the l-th non-zero preamble symbol period in the q-th band. Lq is the number of nonzero preamble symbols in the q-th band and depends on the preamble pattern and band index q. Let $\{x_q(k)\}$ denote the low-pass-equivalent time domain channel output

(noise-free) signal samples corresponding to the q-th band, where $x_q(k) \Delta = x_q(t0 + kT_s)$.

D. Frequency offset estimation

As discussed in the previous section, UWB systems may undergo abrupt channel changes. When an abrupt channel change occurs in the middle of the preamble transmission, the CFO estimation can be significantly affected due to the coherence loss in the periodicity of the received preamble symbols. In this section, we develop a BLUE-based OFO estimator for time-invariant/time-variant UWB channels. The novelty of the proposed approach compared to existing BLUE based approaches is the incorporation of the MB OFDM characteristics in the estimator development. For time-variant UWB channels, we first split the preamble in each band into two5 parts (left and right) by a simple abrupt channel change detection algorithm, which will be described in Section IV. We denote these parts by p-th preamble part with p = 1 and 2 for the left and right part, respectively.

The underlying idea is that correlation-based estimators require identical channel output preamble symbols, and due to the abrupt change, the channel outputs corresponding to these two parts will not be identical, and hence should not be cross correlated. Next we estimate CFO based on each part, and then appropriately average the CFO estimates. For time-invariant UWB channels, since they are the special cases of time-variant channels with the steady-state probability vector $[1, 0]T$, we can apply the method developed for the time-variant channel except with the following changes: we skip the abrupt channel change detection step, set the left part of the preamble in each band to be the preamble itself and hence null the right part. 4Our proposed estimator can be applied to other implementations of carrier frequencies generation by changing the values in (7) accordingly. 5Due to non-negligible physical sizes of moving scatters, the channel change occurs only once (if it does) during the preamble transmission, and hence we just need to consider two parts.

D.1. OFO Estimation:

The proposed OFO estimator is based on the BLUE principle and the correlation among the non-zero received preamble symbols within the same part of the band. For every preamble pattern, the channel output preamble of each part in a single band has identical symbols. The channel output preambles of different preamble parts are not the same due to distinct channel responses.

III. EXPERIMENTAL RESULTS

We use the simulation parameters as specified in :N = 128, $_{Ng}$ = 37, carrier frequencies f_1 = 3432 MHz,$_{f2}$ = 3960 MHz, $_{f3}$ = 4488 MHz, the sub-carrier spacing $1/T$ = 4.125 MHz, and four different preambles. The channel model CM-2 with L_h = 6 and K = 6 is adopted.

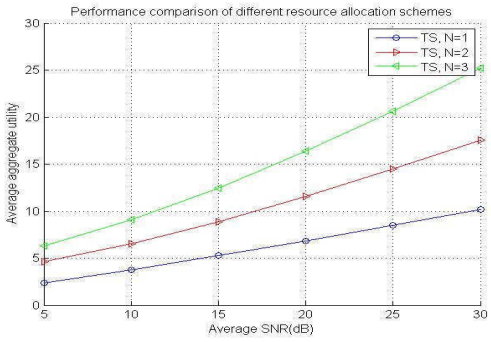

Fig. 3 : Performance comparison of different resource allocation schemes.

Fig.3 shows the no. of users for different resource allocation and the utility considered here is a function of the instantaneous transmission rate. For user i, we denote its utility as $U_i(r_i(t))$. The exact expression for the utility $U_i(.)$ is not crucial. The analysis throughout this paper is valid for any utility function that is increasing, differentiable and concave.

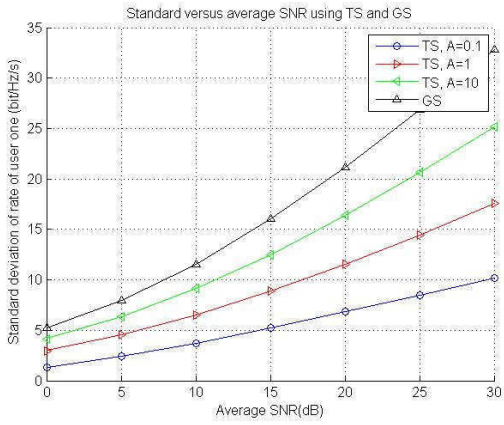

Fig. 4 : Average rate and standard deviation of rate versus average SNR using TS and GS

In Fig. 4 compares the mean and the standard deviation of the transmission rate achieved by TS and GS policies for A = 0.1, 1 and 10 with N = 32. The performances of the GS policy at different values of A are identical due to the channel symmetry among the users. In fact, it is an extreme case of our TS.

Fig. 2 shows the simulated TAUR in the network by using the proposed TS policy and the existing GS policy. Here the utility of both policies is specified to have the form

$$U(r) = \ln(1 + \frac{r}{A}) \tag{13}$$

where $A > 0$ is a concavity indicator. The channels are assumed to be Rayleigh fading and the SNR gap is set to 8.2 dB for all users which corresponds to a bit-error-rate requirement of $10-5$ when adaptive quadrature amplitude modulation (QAM) is used. The number of users in the network varies from 8 to 32 and their channel conditions are symmetric.

The concavity indicator A is set at 0.1.

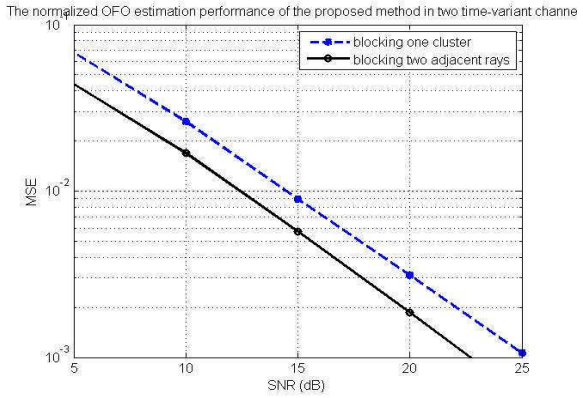

Fig. 5 : The normalized OFO estimation performance of the proposed method in two time-variant channels (defined by blocking one whole cluster and blocking two adjacent rays, respectively, when an abrupt

In Fig. 5, we evaluate the proposed method in two time Variant channels. In the first channel, we use J = K and k0 =0, i.e., the whole cluster is blocked when a moving scatterer affects the channel. In the second channel, we use J = 2, i.e., only two adjacent rays are blocked when a moving scatterer affects the channel. We only apply method B here since the estimation performance of the other method is similar. The simulation result shows that the proposed method works well in both channels.

IV. CONCLUSION

We develop a new framework for resource allocation in wireless networks for variable-rate transmission. The time-average aggregate utility of instantaneous transmission rate is proposed to jointly optimize the resulting average rate and rate oscillation. In particular, a time-sharing policy and a joint time-sharing and power control policy are designed to exploit the channel fluctuation.We have presented enhanced OFO estimators based on the BLUE principle for MB-OFDM based UWB systems by exploiting several characteristics of the MB-OFDM system –such as different CFOs, channel responses, received energies and preamble structures in different bands. We develop our estimators to be robust against sudden channel changes which can occur in some UWB systems with fast moving scatters. The proposed estimators are adaptive such that when a sudden channel change is detected during the preamble duration, the estimator designed for such a time-variant scenario is used, otherwise the estimator developed for the time-invariant channel is applied. For systems with no sudden channel changes, the latter estimator can be solely implemented for implementation simplicity. Our proposed approach can be applied to other multi-band systems or similar frequency hopped systems.

REFERENCES

[1] P. Viswanath, D. Tse, and R. Laroia, "Opportunistic beamforming using dumb antennas," IEEE Trans. Inform. Theory, vol. 48, no. 6, pp. 1277–1294, June 2002.

[2] A. Jalali, R. Padovani, and R. Pankaj, "Data throughput of CDMA-HDR a high efficiency-high data rate personal communication wireless system," in Proc. Veh. Technol. (VTC), 2000.

[3] A. L. Stolyar, "On the asymptotic optimality of the gradient scheduling algorithm for multiuser throughput allocation," Operation Research, vol. 53, no. 1, pp. 12–25, Jan. 2005.

[4] M. Z. Win and R. A. Scholtz, "Impulse radio: how it works," IEEECommun. Lett, vol. 2, no. 2, pp. 36-38, Feb. 1998.

[5] M. Z. Win and R. A. Scholtz, "Ultra-wide bandwidth time-hopping spread-spectrum impulse radio for wireless multiple-access communications,"IEEE Trans. Commun., vol. 48, no. 4, pp. 679-691, Apr. 2000.

[6] T. Q. S. Quek and M. Z. Win, "Analysis of UWB transmitted reference communication systems in dense multipath channels," IEEE J. Select Areas Commun., vol. 23, no. 9, pp. 1863-1874, Sept. 2005.

[7] A. Giorgetti, M. Chiani, and M. Z. Win, "The effect of narrowband interference on wideband wireless communication systems," IEEE Trans. Commun., vol. 53, no. 12, pp. 2139-2149, Dec. 2005.

[8] M. Z. Win, "A unified spectral analysis of generalized time-hopping spread-spectrum signals in the presence of timing jitter," IEEE J. Select. Areas Commun., vol. 20, no. 9, pp. 1664-1676, Dec. 2002.

Hybrid Neuro Fuzzy Temperature Controller using High Resolution Multifunction Card

R.T.Jadhav[1] & R.T.Patil[2]

[1]Dept. of Technology, Shivaji University, Kolhapur, Maharashtra, India
[2]Dept. of Electronics, TKIET College, Warananagar, Maharashtra, India

Abstract - The performance of Neuro-fuzzy techniques for a real time temperature controller system has been investigated in detail. A study of efficiency and superiority of control techniques of Neuro-fuzzy controller related to structure, system and design experience over conventional controller is carried out. The construction of circuit, design of the neuro-fuzzy system and experimental investigations has been reported. The designed controller was based on user friendly interface LabVIEW, one of the most important industrial platforms, which allows us to move from design to implementation in only few steps. The experimental result shows the system performance improvement with respect to oscillations around set point and settling time.

Key words *- Neuro-fuzzy controller; conventional controller; PCI add-on card; temperature measurement; LabVIEW.*

I. INTRODUCTION

The past decade has witnessed a significant breakthrough in the field of intelligent controllers. The field has been experiencing constant upgrades at a rate considered to be revolutionary. This tremendous breakthrough was a strong motivation for expanding our research in this field.

Real time control of non-linear systems is often a quite complex and computationally intensive task. It is for this reason that Neural Networks (NNs) and Fuzzy Systems (FSs) which are two branches of artificial intelligence are gaining widespread acceptance in the field of learning and intelligent control. This is due mainly to their intrinsic parallelism, their learning and adaptation capabilities and, to some extent, also to their increased fault tolerance. Fuzzy control and Neural Network control have many control advantages as above, but fuzzy control also has a drawback that you have to set new control laws and membership functions every time types of system change even after you set control laws and membership functions. And neural network has a drawback that while learning, it can easily fail onto local minimum instead of global minimum, and it take much time to make as many neurons learn as how complicated the system.

In order to make up for the defects, research on integration of neural network and fuzzy logic that is hybrid Neuro-fuzzy controller (HNFC) is under way. A proposed HNFC is an intelligent system that combines qualitative knowledge of symbolic fuzzy rules and learning capabilities of neural networks. Temperature control is an important factor in many process control system. If the temperature is too high or too low, the final product or the product under observation is seriously affected. Therefore it is necessary to reach some desired temperature points quickly and avoid large overshoot. Since the process control system are often non linear, complex in nature and tend to change in an unpredictable way, they are not easy to control accurately. Therefore, the proposed HNFC is expected to be a better alternative in accurately modeling and controlling the non linear thermal system.

In this paper the performance of neuro-fuzzy controller is tested on real time temperature controller system. To train the neuro-fuzzy controller generally input-output characterization or desired output of the plant is sufficient. The error and derivative error is given as an input to the system and the neural network's output is given to the fuzzy logic. Neural network will decided which fuzzy set is selected out of five fuzzy sets. The maximum membership set is selected [1].

II. FUZZY SYSTEMS

A. Fuzzy variables and basic operations

In contrary to Boolean logic where variables can have only binary states in fuzzy logic all variables may have any values between zero and one. The fuzzy logic consists of the some basic Λ - AND, V - OR and NOT operations.

$A \wedge B \wedge C \Rightarrow$ min (A, B, C) - Smallest value of A or B or C

$A \vee B \vee C \Rightarrow$ max (A, B, C) - Largest value of A or B or C.

$\bar{A} \Rightarrow 1 - A$- One minus value of A

For example: $0.1 \wedge 0.8 \wedge 0.4 = 0.1$, $0.1 \vee 0.8 \vee 0.4 = 0.8$, $0.3 = 0.7$

All above rules are known as zadeh AND, OR and NOT operators

B. Fuzzy Controller

The principle operation of fuzzy controller is different from neural networks. The fuzzy controller is divided in to three steps .In first step, analog inputs are converted into a set of fuzzy variables. In this step we use five fuzzy sets which is given in (1). Each fuzzy variable has analog value between zero and one. In the next step, a fuzzy logic is applied to the input fuzzy variables and resulting set of output variables is generated. The last step is known as defuzzification. From the set of output fuzzy variables one output variable is selected [2]

{very small, small, medium, large, very large} (1)

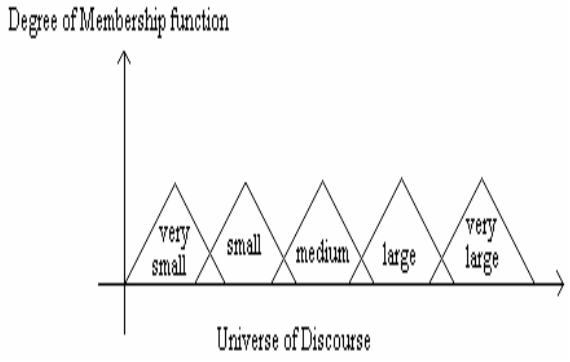

Fig. 1 : Fuzzy set.

III. HYBRID NEURO FUZZY SYSTEM

Neural networks and fuzzy systems are different in two aspects. First, neural networks are adaptable and trainable. Secondly, the neural networks are in nature large scale and parallel. The weights attached to data play an important role in the operation of a neural network .It is however difficult to understand the behavior of neural network. Fuzzy logic is mainly concerned with the imprecision and can express knowledge of field experts. Since fuzzy logic rules are constituted by human intuitions fuzzy logic has no adaptable and trainable properties. In a complex system, the more rules, the more complex the calculations is the longer it will take to identify and set up this rules. These properties limit the applicability of fuzzy logic [3]. When two technologic are combined, the advantages of both are useful for various applications. Advantages of hybrid system is given below

- Amalgamation of different pieces of knowledge is possible by application of fuzzy rules.
- A large scale knowledge base can be effectively handled and reduced by fuzzy front end or backend processor making learning easy and fast.
- Non precise and context depend knowledge is represented using fuzzy logic.
- Reorganization and learning from noisy data is possible.
- The neural network processes the data and knowledge by combining these two constructed inductively and dependently.
- The technique is robust in that only some rules in fuzzy knowledge base require to be updated with changing input condition avoiding the need to retrain the neural network. [4]

IV. CASCADE NEURO – FUZZY CONTROLLER

There are several fusion techniques to fuse the neural network and fuzzy logic out of that most suitable and simple is cascade. In this type the neural network gives output to fuzzy logic and selects the fuzzy set accordingly (Fig.2). There is another way is that the fuzzy logic gives input to the neural network. In this paper we use first approach.

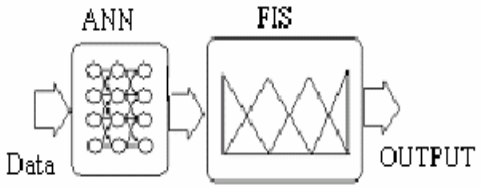

Fig. 2 : Cascade Control Syste

The function of the neural fuzzy compensator is to compensate for any unsatisfactory performance of the basic fuzzy controller. The model structure of neuro-fuzzy compensator is shown in Fig.3. The neural network has one hidden layer and one output layer. All the neurons have sigmoid function .The neural fuzzy compensator is trained in an on line back propagation algorithm. The updating of weight is given in (2).

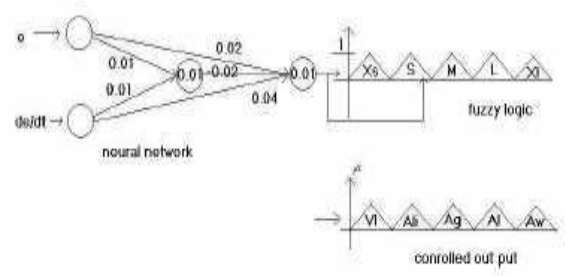

Fig. 3 : Neuro Fuzzy Controller.

$$W_{ij}(t+1) = W_{ij}(t) + \Delta W_{ji} \quad (2)$$

Where $W_{ij}(t)$ is the weight from unit i to unit j at time t (or t^{th} iteration) and ΔW_{ji} is the weight adjustment. The weight change is computed by

$$\Delta W_{ji} = \eta\, \delta_j\, o_i \quad (3)$$

Where η is a trial independent learning rate, δ_j is the error gradient at unit j and o_i is activation level [5].

The neural network select the one set out of five fuzzy set .When error is more the output category is very large. When the error is minimum or zero, the selected category is zero set. The defuzzified output is given to the DAC.

V. DESCRIPTION OF THE SYSTEM

The schematic diagram of the implemented control system is shown in Fig.4. The system consists of six main components, a heater assembly, a sensor (K-type thermocouple) and an instrument amplifier (IC AD 595), 16-bit, 250kS/s high-resolution multifunction, I/O interface card (PCI 1716, Advantech make), a PC in which the software for neuro- fuzzy controller is written in LabVIEW and final control element.

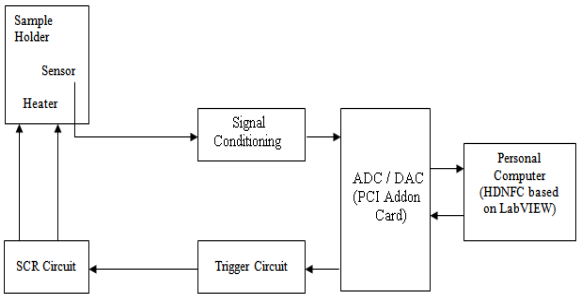

Fig. 4 : System Diagram

VI. HARDWARE SYSTEM

A. *Temperature Measurement*

The heater assembly consists of a sample holder (heating element) made of kanthol metal strip of size 3 × 1.5 cm is used. The chromel alumel (K- type) thermocouple is spot welded on the bottom of the sample holder (kanthol metal strip) to measure the temperature of the sample. A 4 V, 50 amps transformer is used to heat the kanthol strip.

The signal generated by the junction of the K-type thermocouple due to thermal changes was fed to an instrumentation amplifier (IC AD595) specially designed for cold junction compensation and very low signal amplification as shown in figure 5. It combines an ice point reference with a precalibrated amplifier to produce a high level (10 mV/°C) output directly from a thermocouple signal. The output of the instrumentation amplifier IC AD595 is fed to the single ended analog channel of PCI 1716 PC add-on card.

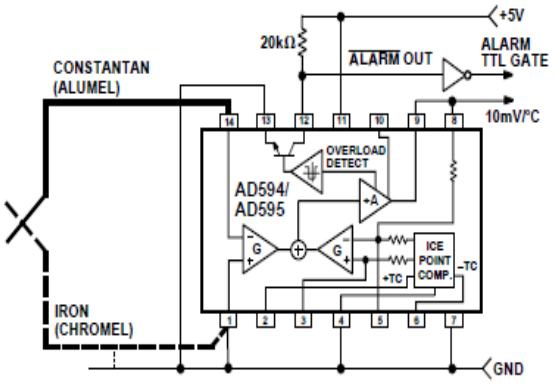

Fig. 5 : Temperature measurement circuit

B. *High Resolution Data Acquisition Card*

The PCI 1716 is a high performance, multifunction analog interface card for IBM/PC/XT/AT and compatible computers. It uses the hardware based analog to digital conversion process, providing a conversion time of 2.5 µs and 250K samples per second acquisition rate. The output channel provides fast settling time of 5µs with high accuracy. A high quality multiplexer in the input stage provides 16 single ended analog inputs or 8-channel Differential A/D Input. Standard input and output voltage ranges is user selectable, independent of each other. The A/D trigger and data transfer are controlled through programming. The block diagram is shown in figure 6.

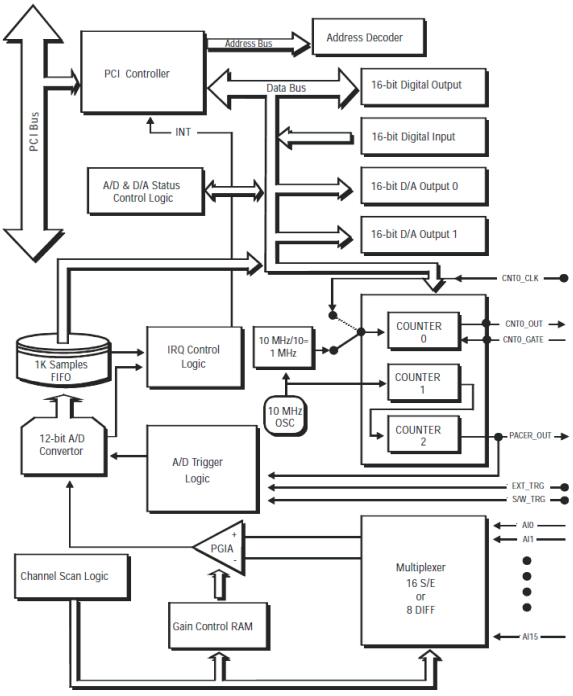

Fig. 6 : Block Diagram of PCI 1716 Card

C. *Final Control Element*

The temperature of the system through K-type thermocouple is measured with the help of PCI 1716 PC add-on card at constant intervals of a few milliseconds and is compared with the setpoint. The difference forms the digital error 'μ'. The heater power controlling signal is derived from this Neuro-fuzzy controller program residing in the PC. This digital value'μ' is converted to analogue in the range of 0V to 10V using an on board 16-bit digital to analogue converter. This analogue signal is fed to the triac based power controller for the heater. The power controller works on the principle of phase delay technique (7-8) (which is dependent on the analogue controlling signal) to fire the triac which delivers the final power to the heater. In this, unijunction transistor 2N2646 is used for triggering SCR 2N2326 which in turn triggers TRIAC 15A6. As the output of DAC was changing, the frequency of the relaxation oscillator using unijunction transistor 2N2646 was changing. In turn, the firing angle of the SCR 2N2326 and hence the TRIAC 15A6 was changing accordingly. Fig.7 shows solid-state power controller, which is used to control the power to the heater.

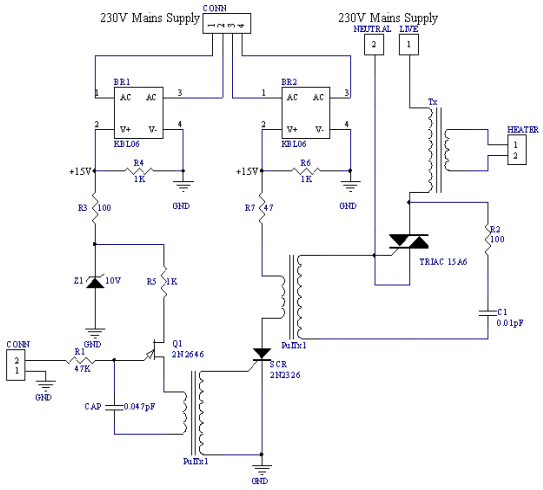

Fig. 7: Circuit diagram of solid-state power controller

VII. SOFTWARE

Software running on a standard PC controls the temperature of the system. This software mainly consists of controlled heating program modules which is described below .

A. *Controlled Heating Program*

This program essentially implements the Neuro-fuzzy algorithm (4) to generate the power controlling signal required by the control unit from the error signal developed between the actual temperature and the expected programmed temperature at frequent intervals. The Neuro-fuzzy algorithm includes process constants of the system required to generate controlled signal for the generated error. This way temperature controlling is achieved in a closed feedback loop. Controlling the temperature from software provides significant advantages in the flexibility of the measurement. Fig.8 shows the flow chart for temperature control system.

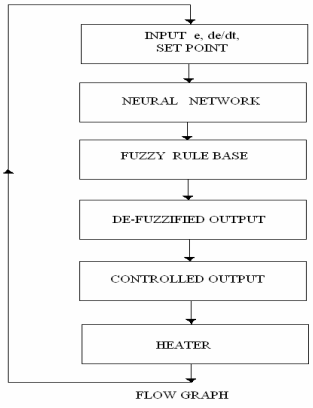

Fig. 8 : Flow chart for temperature control system

VIII. RESULT

A simple PC program was written in LabVIEW and experiments were conducted on the system. In this experiment we measured temperature at constant intervals of a few milliseconds. First open-loop heating characteristic of the controller was observed and recorded. As it can be shown in Fig.9, heating characteristic is a non-linear process. For non-linear system control, neuro-fuzzy logic is a powerful and useful tool.

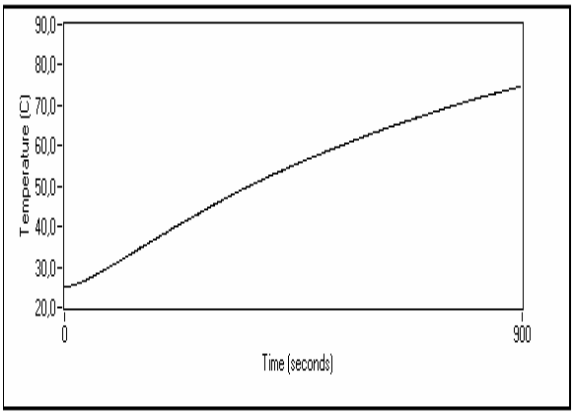

Fig. 9 : Heating Graph.

As presented in figure 10, the desired temperature is set to 45°C and initial temperature is about 24°C (room temperature). After one overshoot, the environmental temperature is arranged to desired set point by neuro-fuzzy logic.

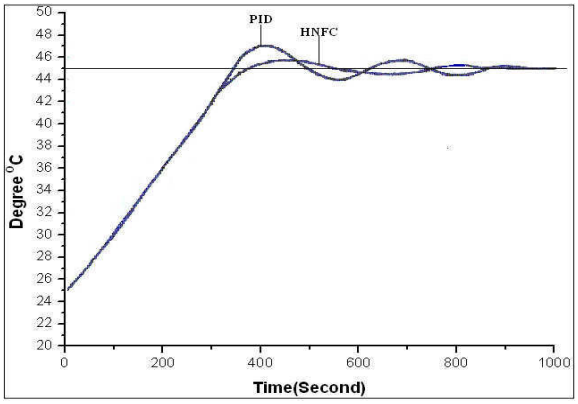

Fig. 10 : Measured temperature for 45°C set point.

As shown in Fig.11, the desired set point is 45°C. The measured temperature starts from 40°C and in a short time period it rises to the set point. Also the fluctuations about desired point could be seen.

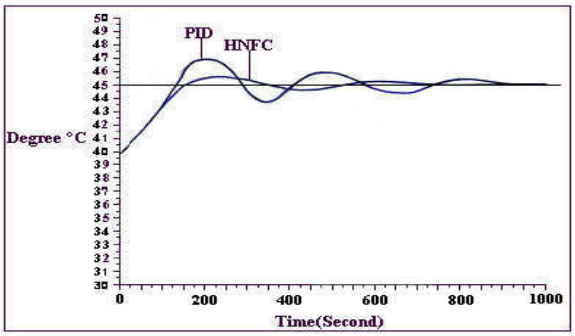

Fig. 11: Measured temperature rises from 40°C to the set point 45°C.

IX. CONCLUSION

This paper gives an idea that superiority of control techniques of neuro-fuzzy hybrid controller. In this paper the experimental results is also shown the better result when we theoretically compare with conventional controller. Neuro-fuzzy logic controller designed and implemented in this study has a range of from room temperature to 300°C. In this range, maximum fluctuations of ±0.1 °C around the set point are observed. Figure 10 and figure 11 are selected examples of desired set points in given range. The system performance improves in setting time, rise time, overshoots as compared to conventional controller. In this paper has gone over how fuzzy logic and neural networks can be combined to work with one another. If necessary the neural network can be altered for the needs of the user. This technique is robust in that only some rules in fuzzy knowledge required to be updated with change in input condition (set point), avoiding the need to retraining of the neural network. The neural network processes the data and knowledge representation in fuzzy logic is easy by combining these two technologies constructed inductively and independently found better result. This paper has gone over the simplest manner to investigate the connection between fuzzy logic and neural networks. These are two technologies that can work together to help people complete their jobs more efficiently and with a greater amount of accuracy especially in the field of uncertainty.

REFERENCES

[1] Hideyuki Takagi., "Fusion technology of neural network and fuzzy Systems: a chronicled progression from the laboratory to our daily live," Int. Journal of Applied Mathematics and Computer Science, vol. 10, no.4 pp. 647-673 (2000).

[2] Bogdan M. Wilamowki, "Neuro –Fuzzy System and Their Application,"IEEE 1998 pp.T35-T50.

[3] Weihong wang, xiaoming zhao, "A New Model of Fuzzy Neural Networks and its applications" 5th world congress on intelligent control and automation, pp2020-2022 June 15-19 2004.

[4] D.Srinivasan, A.C.Liew, C.S.Chang, "Forecasting daily load curves using a hybrid fuzzy-neural approach" IEEE pro-General Trans Distrib, Vol141, No6 Nov.1994.

[5] Dr. Valluru B. Rao and Hayagriva V. Rao. C++ neural networks and fuzzy logic, MIS: press, New York, NY, 1995.

[6] J.B.Mhatre, M.R.Ponkshe and J.K.Samuel. BARC/I-499 (1978)

[7] A.G.I.Dalvi, M.D.Sastry, and B.D. Joshi Journal of Physics E. Science 13, 1106 (1980).

◈◈◈

Development of VLIW Processor by using SIME and GALS Concept

A. Rama Krishna & B.V.V. Subramanya Kumar

Dept. of Department of ECE, A.S.R Engineering College

Abstract - Modern FPGA chips, with their larger memory capacity and re-configurability potential, are opening new frontiers in rapid prototyping of embedded systems. With the advent of high density FPGAs it is now possible to implement a high performance VLIW processor core in an FPGA Architecture based on Very Long Instruction Word (VLIW) processors is an optimal choice in the attempt to obtain high performance level in embedded system. In VLIW architecture, the effectiveness of these processors depends on the ability of compilers to provide sufficient instruction level parallelism (ILP) in program code. In this project we are developing VLIW architecture. In superscalar architecture there is SIME(single instruction multiple execution) concept but in VLIW technique there is both SIME and GALS(Globally asynchronous locally synchronous) in order to work VLIW processor more efficiently and to reduce the power consumption GALS is sometimes used in system-on-a-chip (SoC).GALS is a compromise between a completely synchronous system (a single clock domain, perhaps with clock gating on some registers) and a completely asynchronous circuit. Each synchronous subsystem can run on its own independent clock frequency. For the entire development VLIW processor VHDL code is used. VHDL code is simulated by using tool MODELSIM simulator.

Key words - *Rapid Prototyping, VLIW, Super Scalar, FIR, VHDL-Code, FPGA.*

I. INTRODUCTION

For the design of systems on chip (SoCs), the usage of FPGAs is increasing more and more. In many situations, where normally an ASIC would have been designed, an FPGA design has more advantages. Designing for FPGAs brings lower non-recurring engineering (NRE) costs than designing the same SoC for an ASIC. This is mainly caused by the fact that no external NRE costs have to be made, the IC itself is already manufactured. The manufacturing process of the IC is responsible for a large part of the costs. A mask set for an ASIC in the 90 nm process cost about $1M[4]. The FPGA (Field Programmable Gate Array), with its re-configurability and easy integration capacity becomes a key solution for rapid prototyping of embedded system. In the standard FPGA base prototyping methodology, algorithms are first developed on a personal computer or workstation in standard software programming languages such as C or Matlab. When the algorithm is later implemented in hardware, that code is translated into a hardware description language such as VHDL or Verilog. Finally, the design is synthesized for an FPGA-based environment where it can be tested [5].

A) Globally asynchronous locally synchronous

GALS is a circuit that consists of a set of locally synchronous modules communicating with each other via asynchronous wrappers. Advantages include lower power consumption and electromagnetic interference (EMI). GALS is sometimes used in system-on-a-chip (SoC). GALS is a compromise between a completely synchronous system (a single clock domain, perhaps with clock gating on some registers) and a completely asynchronous circuit (every register can be considered its own independent clock domain). Each synchronous subsystem ("clock domain") can run on its own independent clock frequency.

II. EXISTING TECHNIQUE

A) Super scalar architecture

A superscalar architecture Implements a form of parallelism called Instruction level parallelism" within a single processor. Super scalar structure executes on current operations. But it is not having the capability in which order they should have to do.

B) Instruction-level parallelism

ILP is a measure of how many of the operations in a computer program can be dealt with at once. Consider the following program:

```
e = a+b
f = c+d
g = e*f
```

Operation 3 depends on the results of operations 1 and 2, so it cannot be calculated until both of them are completed. However, operations 1 and 2 do not depend on any other operation, so they can be calculated simultaneously. If we assume that each operation can be completed in one unit of time then these three instructions can be completed in a total of two units of

time, giving an ILP of 3/2.to go for any excellent technique.

C) Existing block diagram

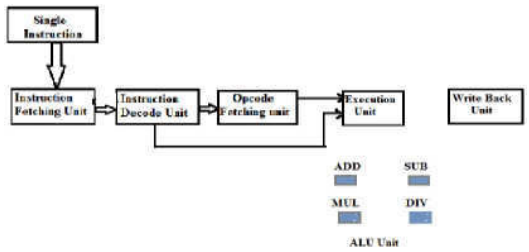

Fig. 1: Existing block diagram

III. PRESENT TECHNIQUE

The GALS basically consists of a large number of synchronous modules, which are synchronized by a clock locally and communicate asynchronously with other synchronous blocks. As the global clock net gets divided, the constraints of clock skew on the synchronous modules get eased. The self-timed approach is efficient, since it does away with the need to time align the operation of all modules within the frame work of a common base clock period we can reduce power by power by applying clock pulse to selected components through control logic.

A) Present block diagram

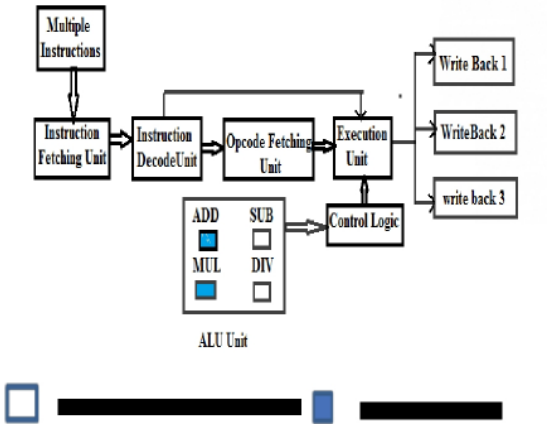

Fig. 2 : Present block diagram

B) Globally Asynchronous Locally Synchronous Systems (GALS)

Globally Asynchronous Locally Synchronous (GALS) Systems have provoked renewed interest over recent years as they have the potential to combine the benefits of asynchronous and synchronous de- sign paradigms. It has been applied to ASICs, but not yet applied to FPGAs. In this paper we propose applying GALS techniques to FPGAs in order to overcome the limitation on timing imposed by slow routing.

IV. VLIW PROCESSOR

VLIW processor use a long instruction word that is a combination Information about the machine needed by the compiler is broken down into six types of information, each of which has an associated hierarchy of sections.

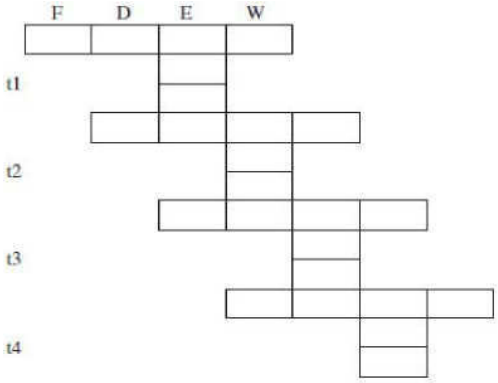

Fig. 3 : The instruction for a VLIW microprocessor (F =Fetch, E = Decode, E = Execute, and W = Write back)

Register information several operations combined into one single long instruction word. This allows a VLIW microprocessor to execute multiple operations in parallel [1] [3] [7]. Figure 2 shows the instruction execution for a VLIW microprocessor. Although both superscalar pipeline and VLIW microprocessors can execute multiple instructions in parallel, each microprocessor is very different and has its own set of advantages and disadvantages.

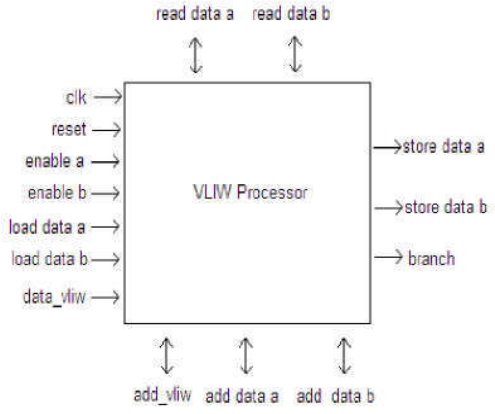

Fig. 4 : VLIW Processor signaling model.

V. EXPERIMENTAL RESULTS

The experimental results can be observed by using the simulator tool ModelSim simulator. The simulation results for synchronous and asynchronous operation for FIR filter in VLIW processor can observed in the simulation results.

The following figure5 represents the simulation result of SIME (Single instruction single execution) for asynchronous operations. Where the mathematical operations can perform asynchronously in SIME.

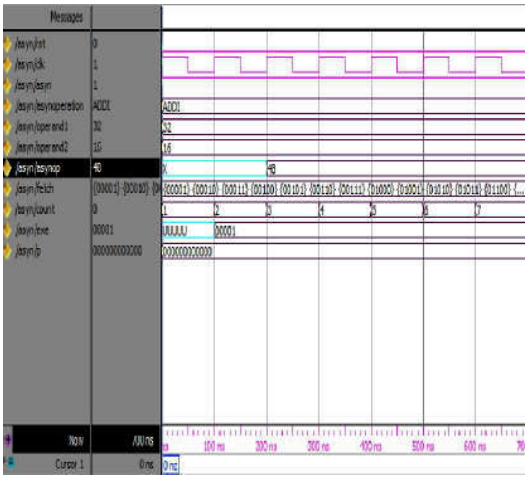

Fig. 5 : Simulation result of SIME (single instruction single execution) for asynchronous operation,

The following figure 6 represents the simulation result of SIME (Single instruction single execution) for synchronous operations. Where the mathematical operations can perform synchronously in SIME.

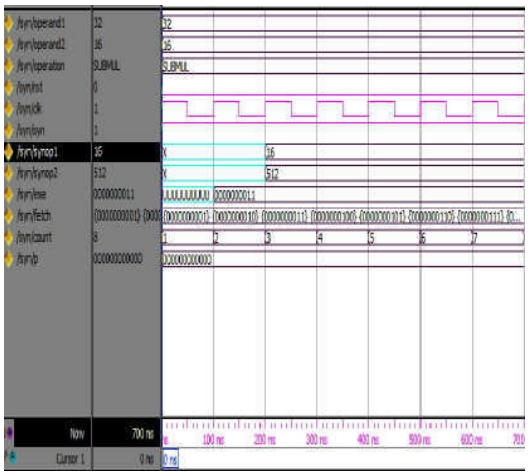

Fig. 6 : Simulation result of SIME (single instruction single execution) for synchronous operation

The following figure 7 represents the simulation result of asynchronous fir filter. Where the mathematical operations can perform asynchronously in FIR filter.

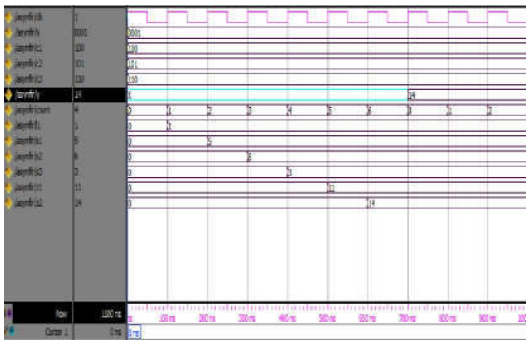

Fig. 7: Simulation result for asynchronous fir filter

The following figure 8 represents the simulation result of synchronous fir filter. Where the mathematical operations can perform synchronously in FIR filter.

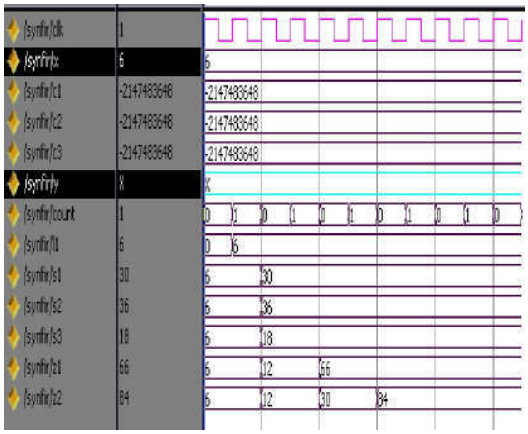

Fig. 8: Simulation result for synchronous fir filter

The following figure 9 represents the simulation result of GALS FIR Filter. Where the mathematical operations can perform in GALS FIR filter.

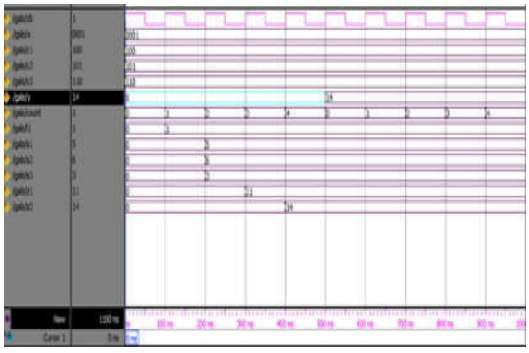

Fig. 9: Simulation Result For GALS FIR Filter

VI. CONCLUSION AND PERSPECTIVES

This project describes how to develop execution unit of VLIW processor by using Single instruction multiple execution and global asynchronous and local synchronous concepts. FIR filter is used in Global Asynchronous Local synchronous concepts. In Previous technique single instruction single execution is developed. In the present technique Single instruction Multiple execution is developed along with GALS (global asynchronous local synchronous) that is two instruction is executed instead of executing single instruction. So by using SIME (single instruction multiple execution) within the less time multiple instructions can be executed and by using GALS(global asynchronous local synchronous) delay of execution unit will be reduced. This technique is implemented in order to optimize the execution time and improve the performance with low power & energy efficient processor. The entire design of the project can be designed by using VHDL code. The MODELSIM simulator tool is used for the simulation results.

REFERENCES

[1] "Design Space Exploration for a custom VLIW Architecture : Direct photo printer hardware setting using VEX Compiler," In Proc of the 4th International Conference of SITIS 2008, November 2008.

[2] Gelato.org, "Impact Advanced Compiler Technology", http://gelato.uiuc.edu, 2009.

[3] " Embedded Computing : A VLIW Approach to Architecture, Compilers and Tools, Elsevier Morgan Kauffman, New York, 2005.

[4] "HMDES Version 2.0 Specification Technical Report IMPACT-96-3, 1996.

[5] " Rapid protoyping for wireless design," the five-ones approaches, Signal Processing, 2003.

[6] " Cost effective strategies for asic masks", In Cost and Performance in Integrated Circuit Creation, 2003.

[7] "VLIW Microprocessor Hardware Design For ASIC and FPGA", Mc Graw Hill Proffesional,2008.

[8] " Multiple modular VLIW processors based on FPGA", Journal of Electronic Imaging, *SPIE*, 16(2):110, April-June 2007.

◈◈◈

OFDM Based Bit Interleaved Coded Analysis

P. Hareesh & B. Jaya

Vaagdevi College of Engineering, Warangal – 506002,
Jawaharlal Nehru Technological University, Hyderabad, India.

Abstract - Bit interleaved coded space–time modulation (BICSTM) for Orthogonal frequency division multiplexing (OFDM) is an attractive strategy to achieve high power– and bandwidth–efficiency over multiple–input and multiple–output (MIMO) fading channels due to coding and diversity gains promised by the serial concatenation of an outer convolutional code, a bitwise interleaved and an inner high order space– time modulation (STM). In this paper, Bit interleaved coded space time modulation with iterative decoding (BICSTM-ID) for OFDM including non-iterative decoding as a special case is considered. For designing the inner STM, two parameters based on bitwise pairwise error probabilities (B-PEP) for the cases with and without a priori knowledge are proposed as new measures for designing labeling rules for the STM code words set suited to iterative decoding. On the other hand, the BICSTM-ID scheme is analyzed from an information theoretical aspect, and Information Processing Characteristic (IPC) analysis is developed for MIMO systems in order to fully characterize the BICSTM-ID scheme based on a new equivalent model of combined binary input channels. The analysis results show that the IPC analysis offers a unified perspective for BICSTM and BICSTM-ID from an information theoretical point of view and provides a comprehensive insight into the whole BICSTM-ID scheme as well. Additionally, IPC based upper and lower bounds on bit error ratio (BER) performance are extended to BICSTM-ID, and are confirmed by simulations. These bounds are of significant practical interest for estimating the BER performance of the bit-interleaved concatenated schemes with general nonlinear inner systems.

Key words - *Bit interleaved coded space–time modulation (BICSTM), Iterative Decoding, EXIT chart, MIMO fading channels. OFDM.*

I. INTRODUCTION

It was recognized first by Zehavi in [1] that a bit–interleaved coding scheme provides a diversity order for transmission over flat Rayleigh fading channels equal to the smallest number of distinct bits along any error event (rather than channel symbols). This scheme was later referred to as bit-interleaved coded modulation (BICM) in [2], where non–iterative decoding was considered and Gray labeling was thereby preferred. For frequency–selective fading channels, BICM schemes could also provide a high diversity order together with orthogonal frequency division multiplexing (OFDM) technique as discussed in [3], where again Gray labeling is chosen for a non–iterative decoding strategy. On the other hand, a question naturally arises whether Gray labeling is still preferred if an enhanced decoding method is applied to take the inter-dependence between the labeling bits into account.

By addressing the former problem of investigating an optimal decoder, a possible way is to consider the encoder, bit-interleaving and the mapper jointly with maximum likelihood (ML) decoding by means of a super-trellis diagram [4], but the trellis complexity may be extremely high in most cases with long interleaver. As an alternative, a suboptimal, iterative decoding method, which has been originally proposed for Turbo codes [5] could be adapted in principle to BICM with necessary modifications to take advantage of the inter-dependence between coded bits by updating *a-priori* information on labeling bits. This has been originally introduced by Li and Ritcey in [6] with a harddecision feedback method and the effects of different labeling strategies were discussed with the result that set partitioning (SP) [6] rather than Gray labeling performs best. Furthermore, iterative decoding (ID) employing soft decision feedback, cf. [7], [8], was applied to BICM (i.e., BICM-ID), too, yielding the result that when the inter–dependence introduced by high order modulation is somewhat exploited, a properly designed labeling rule different from Gray labeling will bring significant benefits. Later on, this iterative decoding with bit interleaver was further adapted to multiple input and multiple output (MIMO) systems in several different approaches, cf. [9], and we preferred to denote this by bit interleaved coded space–time modulation with iterative decoding (BICSTM-ID) in [10], since it closely resembles BICM in many aspects. As a natural consequence, designing a well suited labeling rule for space–time mod -ulation (STM) is certainly essential as well. For designing the labeling rules, some analytical methods for BICM-ID can serve as a good starting point

such as the harmonic mean of the minimum squared distance d^2 h in [2] and modified one in[11] by assuming ideal feedback information. The advantage of this modified parameter in [11] is that an analytical bit error ratio (BER) upper bound for the nonlinear scheme can be provided. However, in the low signalto- noise ratio (SNR) region, this upper bound is not reliable and even lower than the simulation results due to the fact that in this region only part of ideal *a-priori* information may be actually fed back by iterative decoding. Moreover, it suffers from its inability to predict the cliff region. In addressing the convergence issue, an alternative approach, namely extrinsic information transfer (EXIT) chart technique for visualizing the convergence behavior of Turbo codes becomes attractive, andis already applied to BICM-ID in [7]. Although the EXIT chart analysis provides a powerful tool for selecting a suitable labeling by investigating the transfer characteristic (TC) of the soft demapper, it may become problematic for large constellation sizes. Because this method is simulation-based, the generation of a high number of TC curves for all possible labeling rules would be very complex.

Due to limitations of the existing analysis for designing the labeling rule, in this paper, we propose two analytical parameters based on pairwise error probability, which effectively yield almost the same results as those obtained from TCs without having to resort to extremely long simulations. Beside EXIT chart analysis, Information Processing Characteristic (IPC) analysis is another attractive tool for analysis and design of the (concatenated) coding scheme with soft output decoding. It was originally proposed in [13] for binary coding over the additive white Gaussian noise (AWGN) channel (single transmit and receive antenna) and is closely related to EXIT chart analysis, because both of them are based on bitwise mutual information. However, the IPC is a function mapping the capacity of the underlying channel to the bitwise mutual information between input bits and soft output *a posteriori* knowledge.In the second part of this work, we extend the IPC analysis to the BICSTM-ID scheme over a MIMO system to provide a comprehensive insight into BICSTM-ID schemes. In order to obtain the IPC for BICSTM-ID, we propose a new equivalent model for BICSTM-ID with two combined binary input channels, by which available *a priori* information can also be taken into account. With this simple model, IPC is calculated directly from EXIT chart analysis by taking advantage of information combining [14], [15]. The results show that IPC provides the same insight as capacity of BICSTM when assuming no *a priori* information and gives an interpretation of the superiority of BICSTM-ID with some non-Gray mapping schemes compared to Gray mapping when assuming *a priori* information is available. On the other hand, tight upper and lower bounds on BER performance based on IPC analysis are extended to BICSTM-ID as well, which allow for an analytical performance estimation for the concatenated coding scheme with general inner STM. For the sake of clarity we apply the following rules on notation:

- Lower case symbols in boldface denote column vectors, e.g. **s**.
- Upper case symbols in boldface denote matrices, e.g. X and we do not distinguish between random matrices and their realizations.
- Upper case symbols in calligraphic typeface denote sets, e.g. $\mathcal{X}$.
- $(\cdot)^H$ denotes Hermitian transposition of a matrix.
- $H(\cdot)$ refers to the entropy of a random variable (please notice the difference to the channel matrix H of MIMO channels).
- $p(\cdot)$ denotes a probability density function (pdf), e.g. $p(Y)$, $p(\cdot|\cdot)$ a conditional pdf, e.g. $p(Y|X,H)$, $Pr(\cdot)$ the probability of a discrete event, e.g. $Pr(X)$ and $P(\cdot \rightarrow \cdot)$ pairwise error probability, e.g. $P(X \rightarrow \hat{X})$.
- $Ex\{\cdot\}$ denotes the expectation with respect to x.
- trace$(\cdot)$ denotes the trace of a matrix.
- diag$(\cdot)$ denotes a diagonal matrix.

Trellis coded modulation is a transmission technique to combine channel coding and modulation. However, the combination of channel coding and modulation may not be the best solution for fading channels, especially for fast Rayleigh fading channels. In fading channel environments, we can achieve better performance by separating the channel coding and modulation [16][17]. Bit-interleaved Coded OFDM is a technique which separates the coding and modulation with a bit-level interleaver. For the decoding of the received signal, it is necessary to obtain a soft-bit metric for the input of the Viterbi decoder.

The remainder of the paper is organized as follows: In section II, we propose system model of BICSTM-ID and MIMO In section III, Proposed OFDM concept and Bit interleaved coded OFDM. In section IV, Decoding of code Modulation. In section V Simulation results. Finally in section VI, we conclude illustrating the performance of proposed system with BER.

II. SYSTEM MODEL

A. System model of BICSTM-ID

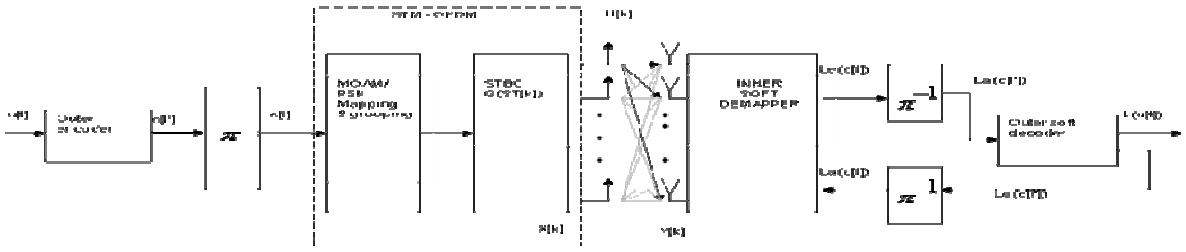

Fig.1 : Block diagram of bit interleaved coded space time modulation with iterative decoding

An outer encoder with code rate *R*c operates on the binary information sequence $u[\imath]$, $i \in Z$. The output data of the encoder are serialized to a binary sequence $c[l']$ and organized to frames of length N, $l' \in \{1, \ldots, N\}$. Within one frame the data stream is permuted bitwise by an interleaver. The interleaved data $c[l]$ are mapped onto signal points taken from an M-ary quadrature amplitude modulation/ phase–shift keying (QAM)/(PSK) constellation applying a suitable labeling rule. Here, we assume $N/n_c \in \mathrm{N}$ and let $K = N/n\mathrm{c}$. Finally, these groups of modulation symbols $\mathbf{s}\mathrm{T}[k]$ are the inputs of the encoder of an STBC, which can be fully specified by a code matrix $\mathrm{G}T\times n\mathrm{T}(\mathbf{s}\mathrm{T}[k])$. The actual codeword X[$k$] is given by $\mathrm{X}[k] = \mathrm{G}T\times n\mathrm{T}(\mathbf{s}\mathrm{T}[k])\mathrm{T}$, which will be transmitted at the k-th time interval consisting of T MIMO channel uses. Thus, the overall rate of the concatenated coded modulation scheme measured in bits per MIMO channel use is

$$\mathrm{R}_{\text{overall}} \triangleq \mathrm{Re}\times\frac{\mathrm{Q}}{\mathrm{T}}\times\log 2(\mathrm{M}) \qquad (1)$$

Transmission of a matrix code word X[k] through the MIMO channel can be modeled in normalized form by

$$Y[k] = \sqrt{\frac{\overline{Es}}{N_0 n_T}} H[k]X[k] + N[k], k = 1, \ldots, K, \qquad (2)$$

with $\overline{Es}$ denoting average received energy per MIMO channel use and receive antenna and N0 the one-sided noise power spectral density of complex additive white Gaussian noise (AWGN). Moreover, the code words X[k] are normalized to have unit variance elements. Y[k] $\in \mathrm{CnR}\times T$ denotes the received symbol at nR receive antennas in the k-th time interval and N[k] $\in \mathrm{C}n\mathrm{R}\times T$ is the corresponding complex $\in$ additive noise with independent $CN(0,1)$ elements.. H[k] $\in \mathrm{C}_n\mathrm{R}\times n\mathrm{T}$ denotes a complex matrix of spatially independent normalized Rayleigh fading variables with $CN(0, 1)$.

This model can be assumed when the transmit and receive antennas are spatially sufficiently separated Furthermore, the channel coefficients are assumed to be constant in each time interval representing one STM codeword duration. In addition, the long bitwise interleaved involved in this scheme ensures mutual independence between groups of coded bits associated with one matrix codeword, and thus can be considered as a symbol wise interleaver, too. Therefore, the products of H[k]X[k] are fully interleaved, spatially and temporally independent according to

$$\varepsilon H,X\left\{\left(H[k]X[k]\right)\left(X^H[k+\kappa]H^H[k+\kappa]\right)\right\} = \begin{cases} Diag(n_T T,\ldots,n_T T) & for \kappa = 0 \\ 0 & for \kappa \neq 0 \end{cases} \qquad (3)$$

In addition, the channel state information (CSI) is assumed to be perfectly known at the receiver. With the above normalization, $\overline{E_S} / No$ in Eq. (2) is linked to SNR as

$$SNR \triangleq \frac{\overline{Es}}{N_0 n_T} \frac{\varepsilon H,X\left\{trace\left((HX)^H HX\right)\right\}}{\varepsilon\left\{trace\left(N^H N\right)\right\}} = \frac{\overline{Es}}{N_0} \qquad (4)$$

For comparing the power efficiency of coding schemes, another important measure is the ratio of the average received energy per information bit $\overline{E_b}$ and the one-sided noise power spectral density $N0$. For the BICSTM scheme, it is related to E_s/N_0. At the receiver side, the iterative decoder uses a module with BCJR algorithm for the outer convolutional code (CC) and a soft-in soft-out demapper for the inner space-time modulation. The soft demapper can be simply derived

from Bayes' theorem. In order to present the iterative decoding with sufficient clarity, we briefly review the soft demapper for our scheme. We collect *n*c consecutive coded symbols $C_v[k] = C[(k-1)n_c + 1 + v]$, *v* € {0,..... , n_c − 1}, which are mapped onto one transmit matrix codeword X[*k*], in a row vector of binary symbols, i.e.,

$$C^T[k] \triangleq \left[C^0[k].....C^{n_c-1}[k]\right] \quad (5)$$

then, with the use of the long bitwise interleaver and the notation in , the log-likelihood ratio (LLR) *a posteriori* information of each coded bit *cv* conditioned on Y in one time interval can be derived as

$$J^{\nu}(X) \triangleq \left\{ j \,/\, j = 0,...,n_c - 1, j \neq \nu, \delta^j = 1 \right\}. \quad (6)$$

Moreover $$L_a\left(c^{\nu}\right) \triangleq \ln \frac{\Pr\left(c^{\nu}=1\right)}{\Pr\left(c^{\nu}=0\right)} \quad (7)$$

denotes the LLR *a priori* information on *cv* and *Le*(*cv*) denotes the LLR *extrinsic* information on coded bits as usual. The extrinsic knowledge of code bits is exchanged between inner demapper and outer decoder as shown in Fig.

III. OFDM CONCEPT

An OFDM signal consists of a number of closely spaced modulated carriers. When modulation of any form - voice, data, etc. is applied to a carrier, then sidebands spread out either side. It is necessary for a receiver to be able to receive the whole signal to be able to successfully demodulate the data. As a result when signals are transmitted close to one another they must be spaced so that the receiver can separate them using a filter and there must be a guard band between them. This is not the case with OFDM. Although the sidebands from each carrier overlap, they can still be received without the interference that might be expected because they are orthogonal to each another. This is achieved by having the carrier spacing equal to the reciprocal of the symbol period.

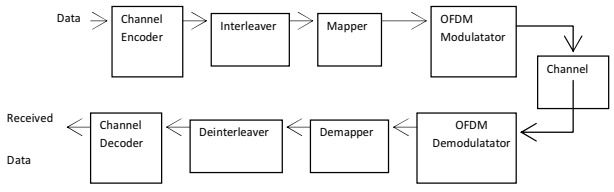

Fig. 2 : A block diagram of Bit-interleaved coded OFDM

A. Bit interleaved coded OFDM

Trellis coded modulation is a transmission technique to combine channel coding and modulation. However, thecombination of channel coding and modulation may not be the best solution for fading channels, especially for fast Rayleigh fading channels In fading channel environments, we can achieve better performance by separating the channel coding and modulation. Bit-interleaved Coded OFDM is a technique which separates the coding and modulation with a bit-level interleaver. For the decoding of the received signal, it is necessary to obtain a soft-bit metric for the input of the Viterbi decoder. Figure 2 shows a block diagram of a transmitter and receiver using bit-interleaved coded modulation. Input data are encoded with a channel encoder which is characterized by the coding rate and the minimum distance between two nearest data sequences. The coded bits are interleaved at the interleaver. The interleaved bits are mapped to a point in a modulation constellation. The modulation scheme can be *M*-ary PSK or QAM, where *M* is assumed to be a power of 2. A mapper is a memory less mapper between the interleaved bits *bk* and a constellation symbol *xn* that will be sent over the channel. Log2*M* interleaved bits are mapped to one modulation symbol. The relation between the position *k* of interleaved bit position *bk* and the position of the modulation symbol is

$$n = k/\log 2M$$

$$i = k \bmod \log 2M$$

where *i* is the location of the interleaved bit in a modulation symbol. The channel response for the *n*-th modulation symbol is assumed to be ρ_n. The received signal y_n at the receiver is given as

$$y_n = \rho_n I_n + n_n \quad (8)$$

At the receiver, a demapper computes the maximum-likelihood (ML) soft metric of each interleaved bit based on the received signal. The ML soft metric is deinterleaved and sent to a Viterbi decoder. The Viterbi decoder chooses a sequence ˆ*c* which satisfies

$$\hat{C} = \max_{C\mu \in C} \Pr\left\{ y_1, ..., y_N / \hat{C} \right\} \quad (9)$$

where *C* is the set of all possible data sequence and *N* is the number of modulation symbols.

A.1 Coded OFDM

Coded OFDM (COFDM) is one of the widely used transmission techniques for overcoming the frequency selectivity of the channel. The basic idea of coded OFDM is to encode input data and interleave the coded

symbols. The interleaved symbols are split into several sub channels to achieve frequency diversity. Even though the uncoded symbol error rate is high for the subcarriers with low channel gains, with the channel coding and interleaving it is possible to correct the errors in the low gain channels. With the channel coding and interleaving, coded OFDM provides a robust communication link for many wireless channel environments. This technique is very effective for channels with narrow coherence bandwidth. However, if the coherence bandwidth is large, then the channel gains of neighboring subchannels are highly correlated, and this may limit the diversity gain of coded OFDM systems.

IV. DECODING OF CODE MODULATION

The optimum decoding scheme for Trellis-coded modulation is to find the data sequence ĉ. The Maximum likelihood (ML) decoding can be implemented with a Viterbi decoder . The ML detection of multi-level bit-interleaved coded modulation requires a joint demodulation and decoding . However, this joint detection is very complex to implement in real systems because of the interleaver located between the mapper and the channel coder. Zehavi proposed a sub-optimal simple detection scheme which includes computation of a soft metric to be used in a Viterbi decoder. For each received symbol y_n, the receiver computes the soft metric $mi(yn, ck)$

$$m_i\left(y_n, c_k\right) = \log \Pr\left\{c_k = b / y_n\right\} \tag{10}$$

where $i = 1, 2, ..., \log_2 M$ and $b = 0, 1$. Based on the soft metrics, the ML decoding is performed to find the data sequence which satisfies With no a priori information assumption and the approximation of $\log_i zi \approx \max i \log zi$, we have a soft metric of

$$\hat{C} = \arg \max_{C^{\mu} \in C} \sum_{k} m_i\left(y_n, C_k\right) \tag{11}$$

$$m_i\left(y_n, c_k\right) = \log \sum_{\alpha \in S_i^{ck}} \Pr\left\{y_n / x_n = \alpha\right\}$$

$$m_i\left(y_n, c_k\right) \approx \log \max_{\alpha \in S_i^{ck}} \Pr\left\{y_n / x_n = \alpha\right\} \tag{12}$$

where S_{ck} i is the set of constellations for which the i-th bit is ck. The conditional probability $Pr\{yn|xn = \alpha\}$ is a complex Gaussian distribution with pdf where σ_2 is the variance of the AWGN. With the distribution of Equation (11), the metric is equivalent to

$$P_r\left\{y_n / x_n = \alpha\right\} = \frac{1}{\sqrt{2\pi\sigma}} \exp[-\frac{(y_n - \rho_n.\alpha)^2}{2\sigma^2}] \tag{13}$$

$$m_i(y_n, c_k) = \min \left| y_n - \rho.\alpha \right|^2 \tag{14}$$

Tosato proposed a decoding scheme which includes a simple soft-output demapper and a standard soft-input Viterbi decoder . The demapper computes the soft decision information of the coded bit b_k of which the sign is the hard decision bit and the absolute value is the reliability of the decision. The soft outputs of the demapper are deinterleaved and decoded by the standard soft-input Viterbi decoder.

V. SIMULATION RESULTS

The BER performance curves of OFDM BICSTM-ID schemes employing Gray and modified SP labeled 16-QAM symbols with corresponding upper and lower bounds are depicted in Fig.3 As described in the channel coefficients are assumed to be constant during the transmission of one STBC codeword but may vary from one codeword to another in a statistically independent manner. The interleaver length is $N = 120000$ coded bits and sufficiently many iterations that yield convergence are performed for both cases. Moreover, since the Gray labeling can not gain from iterative decoding, its BER curve goes slowly down to about $2.4X10^{-2}$ at $^{-}E_b/N_0 = 5$ dB. Significantly better and as predicted by IPC and EXIT charts, a cliff occurs in the BER diagram at about 4.2 dB, which results in a BER below 10^{-4} at that $^{-}E_b/N_0$, only 1.5 dB away from the theoretical limit of $(^{-}E_b/N_0)min \approx 2.7$ dB. Although the simulation curve for this case is slightly above the upper bound in the cliff region. The reason is that in the cliff region, much more iterations are required and hence, a very large interleaver (much larger than $N = 120000$) is needed to ensure the assumed independence of *a-priori* and *extrinsic* information. However, in spite of this little deficiency of the upper bound in the cliff region, these upper and lower bounds are still very useful for the performance estimation of the STBC MIMO OFDM scheme.

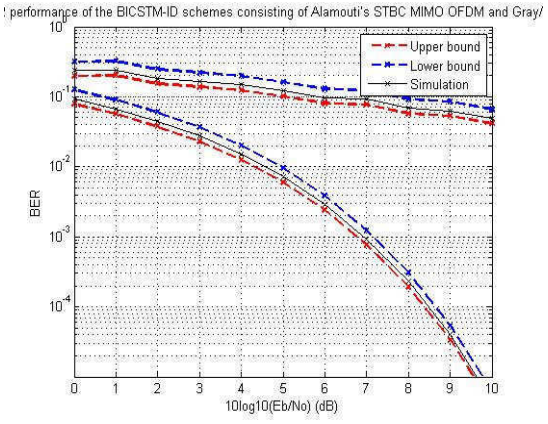

Figure3. Bounds and BER performance of the BICSTM-ID schemes consisting of Alamouti's STBC MIMO OFDM Gray/modified SP labeled 16QAM symbols with nT = 2 and nR = 1 as inner STM and a recursive systematic convolutional code with generator $G1$ =7, $G2$ = 5 in octal form as the outer code

VI. CONCLUSIONS

In this paper the BICSTM-ID scheme has been investigated. For the purpose of designing a both power and bandwidth efficient scheme with low complexity, two analytical parametersare proposed to evaluate different labeling rules. These parameters predict the properties of the TCs of the soft demapper and allow a quick comparison among possible labeling rules without having to simulate the real soft demapper. Based on the comparison of the proposed parameters, a very power efficient scheme employing an STBC and a 16QAM mapper with suitable labeling rule as inner space-time modulation and a simple rate 1/2 memory 2 convolutional code as outer code is proposed. The scheme can achieve a BER below 10^{-4} at only about 4.2 dB at the transmission rate of 2 bits per channel use with two transmit and one receive antenna, which is only about 1.5 dB off from the theoretical limit for reliable communications for this scenario. The BER and FER of a coded OFDM system are bounded by sums of exponential functions or Q-functions. In this dissertation, we have shown that the FER and BER bounds are convex functions. We have also shown that the FER and BER bounds are log-convex. With a feedback link from the receiver to the transmitter, the transmitter can optimize the power of each carrier to minimize the FER or BER with a constant total transmission power constraint. We have shown that the power optimization is a convex optimization problem, since the cost and constraint functions are shown to be convex. The proposed scheme can provide a near-optimum power allocation for a code OFDM system, since the BER and FER bound are tight to the actual performance for the E_b/N_0 range of interest. In this dissertation, we have provided a different view of the power optimization problem. In a coded system, the most important parameter is the minimum distance between two nearest data sequence. We have shown that maximizing the minimum distance is a convex optimization problem.

REFERENCES

[1] E. Zehavi, "8-PSK trellis codes for a Rayleigh channel," IEEE Trans. Commun., vol. 40, no.5, pp. 873–884, May 1992.

[2] G. Caire, G. Taricco, and E. Biglieri, "Bit-interleaved coded modulation," IEEE Trans. Inform. Theory, vol. 44, no. 3, pp. 927–946, May 1998.

[3] E. Akay and E. Ayanoglu, "Achieving full frequency and space diversity in wireless systems via BICM, OFDM, STBC and Viterbi decoding," IEEE Trans. Commun., vol. 54, no. 12, pp. 2164–2172, Dec. 2006.

[4] M. Breiling and L. Hanzo, "The super-trellis structure of turbo codes," IEEE Trans. Inform. Theory, vol. 46, no. 6, pp. 2212–2228, Sept. 2000.

[5] C. Berrou, A. Glavieux, and P. Thitimajshima, "Near Shannon limit error correcting coding and decoding: turbo-codes (1)," in Proc. International Conference on Communications (ICC), pp. 1064-1070, 1993.

[6] X. Li and J. A. Ritcey, "Bit-interleaved coded modulation with iterative decoding," IEEE Commun. Lett., vol. 1, no. 6, pp. 169–171, Nov. 1997.

[7] S. ten Brink, J. Speidel, and R. H. Yan, "Iterative demapping for QPSK modulation," Electron. Lett., vol. 34, no. 15, pp. 1459–1460, July 1998.

[8] X. Li and J. A. Ritcey, "Bit-interleaved coded modulation with iterative decoding," in Proc. International Conference on Communications (ICC),pp. 858–863, June 1999.

[9] A. M. Tonello, "Space-time bit-interleaved coded modulation with an iterative decoding strategy," in Proc. IEEE VTC 2000-Fall, Boston, pp. 24–28, Sept. 2000.

[10] L. Zhao, L. Lampe, and J. Huber, "Study of bit-interleaved coded spacetime modulation with different labeling," Proc. IEEE Information Theory Workshop 2003, pp. 199–202, Paris, France, Mar./Apr. 2003.

[11] A. Chindapol and J. A. Ritcey, "Design, analysis, and performance evaluation for BICM-ID with square QAM constellations in Rayleigh fading channels," IEEE J. Select. Areas Commun., vol. 19, no. 5, pp. 944–957, May 2001.

[12] Y. Huang and J. A. Ritcey, "Optimal constellation labeling for iteratively decoded bit-interleaved space-time coded modulation," IEEE Trans. Inform. Theory, vol. 51, no. 5, pp. 1865–1971, May 2005.

[13] S. Huettinger, J. Huber, R. Johannesson, and R. Fischer, "Information processing in soft-output decoding," in Proc. 39th Annual Allerton

Conference on Communications, Control and Computing, UIUC University, Oct. 2001.

[14] J.Huber and S. Huettinger, "Information processing and combining in channel coding," in Proc. 3rd International Symposium on Turbo Codes & Related Topics, Brest, France, Sept. 2003.

[15] I. Land, S. Huettinger, P. A. Hoeher, and J. Huber, "Bounds on information combining," in Proc. 3rd International Symposium on Turbo Codes & Related Topics, Brest, France, Sept. 2003.

[16] E. Zehavi, "8-PSK Trellis Codes for a Rayleigh Channel," IEEE Trans. on Commun.,vol. 40, no. 5, pp. 873-884., May 1992.

[17] G. Caire, G. Taricco and E. Biglieri, "Bit-Inreleaved Coded Modulation," IEEETrans. on Inf. Theory, vol. 44, pp. 927-946, May 1998.

◈◈◈

Design of Pipelined Architecture of 9/7

Lifting-Based DWT using FPGA

Maninee Patel & Jobbin Abraham Ben

Dept. of Electronics & Communication Engineering,
Hindustan Institute of Technology & Science, Chennai, India

Abstract - This paper presents a high speed 9/7 lifting 2-D algorithm which is implemented on FPGA with multi-stage pipelining structure. Compared with the architecture which without multi-stage pipeline, the proposed architecture has higher operating frequency. The hardware architecture is suitable for high speed implementation. An advanced two dimensional (2-D) discrete wavelet transform (DWT) implementation, with an efficient memory area, is designed to produce one output in every clock cycle. As a result, a very high speed is attained.

Key words *- Discrete wavelet transform (DWT); lifting scheme; multi-stage pipelining.*

I. INTRODUCTION

The discrete wavelet transform has been widely used as a powerful tool in many applications such as signal analysis, image processing and compression due to its characters of multi-resolution analysis[1], and it has also become an ingredient of many new image compression standards, such as JPEG2000.

Early implementations of the wavelet transform were based on filters' convolution algorithms[2-3]. This approach requires a huge amount of computational resources. In fact at each resolution, the algorithm requires the convolution of the filters used with the approximation image. A relatively recent approach uses the lifting scheme for the implementation of the discrete wavelet transform (DWT). This method still constitutes an active area of research in mathematics and signal processing.

Image compression techniques can compress with or without loss of data of original image. The lossy compression can achieve higher ratio than lossless compression. As a result, the 9/7 DWT which is recommended by JPEG2000 for lossy compression has been widely used in image compression area. The high-speed implementation of lifting-based 9/7 DWT on field-programmable gate array (FPGA) using multi-stage pipelining is presented in this paper.

A. Discrete Weblet Transform.

The transform of a signal is just another form of representing the signal. It does not change the information content present in the signal. The Wavelet Transform provides a time-frequency representation of the signal. It was developed to overcome the short coming of the Short Time Fourier Transform (STFT), which can also be used to analyze non-stationary signals. While STFT gives a constant resolution at all frequencies, the Wavelet Transform uses multi-resolution technique by which different frequencies are analyzed with different resolutions.

A wave is an oscillating function of time or space and is periodic. In contrast, wavelets are localized waves. They have their energy concentrated in time or space and are suited to analysis of transient signals. While Fourier Transform and STFT use waves to analyze signals, the Wavelet Transform uses wavelets of finite energy.

The wavelet analysis is done similar to the STFT analysis. The signal to be analyzed is multiplied with a wavelet function just as it is multiplied with a window function in STFT, and then the transform is computed for each segment generated. However, unlike STFT, in Wavelet Transform, the width of the wavelet function changes with each spectral component. The Wavelet Transform, at high frequencies, gives good time resolution and poor frequency resolution, while at low

frequencies; the Wavelet Transform gives good frequency resolution and poor time resolution.

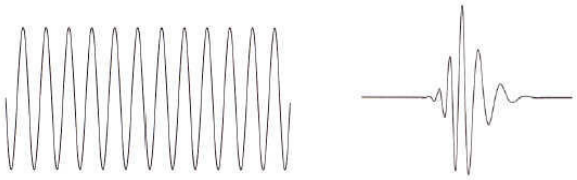

(a) (b)

Fig. 1 : Demonstrations of (a) a Wave and (b) a Wavelet

B. Multi-resolution Analysis using Filter Banks.

Filters are one of the most widely used signal processing functions. Wavelets can be realized by iteration of filters with rescaling. The resolution of the signal, which is a measure of the amount of detail information in the signal, is determined by the filtering operations, and the scale is determined by upsampling and downsampling (sub sampling) operations.

The DWT is computed by successive lowpass and highpass filtering of the discrete time-domain signal as shown in Fig.2. This is called the Mallat algorithm or Mallat-tree decomposition. Its significance is in the manner it connects the continuous-time multiresolution to discrete-time filters. In the figure, the signal is denoted by the sequence x[n], where n is an integer. The low pass filter is denoted by G_0 while the high pass filter is denoted by H_0. At each level, the high pass filter produces detail information; d[n], while the low pass filter associated with scaling function produces coarse approximations, a[n].

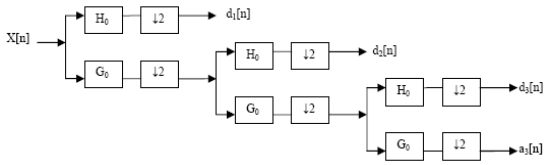

Fig. 2 : Three-level wavelet decomposition tree.

At each decomposition level, the half band filters produce signals spanning only half the frequency band. This doubles the frequency resolution as the uncertainty in frequency is reduced by half. In accordance with Nyquist's rule if the original signal has a highest frequency of ω, which requires a sampling frequency of 2ω radians, then it now has a highest frequency of ω/2 radians. It can now be sampled at a frequency of ω radians thus discarding half the samples with no loss of information. This decimation by 2 halves the time resolution as the entire signal is now represented by only half the number of samples. Thus, while the half band low pass filtering removes half of the frequencies and thus halves the resolution, the decimation by 2 doubles the scale. With this approach, the time resolution becomes arbitrarily good at high frequencies, while the frequency resolution becomes arbitrarily good at low frequencies. The filtering and decimation process is continued until the desired level is reached. The maximum number of levels depends on the length of the signal. The DWT of the original signal is then obtained by concatenating all the coefficients, a[n] and d[n], starting from the last level of decomposition.

Fig.3 shows the reconstruction of the original signal from the wavelet coefficients. Basically, the reconstruction is the reverse process of decomposition. The approximation and detail coefficients at every level are upsampled by two, passed through the low pass and high pass synthesis filters and then added. This process is continued through the same number of levels as in the decomposition process to obtain and the original signal. The Mallat algorithm works equally well if the analysis filters, G_0 and H_0, are exchanged with the synthesis filters, G_{11}.

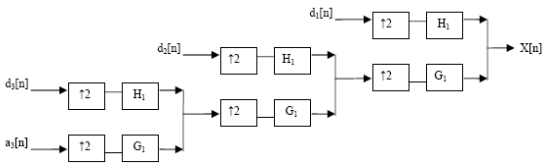

Fig. 3 : Three-level wavelet reconstruction tree.

II. LIFTING BASED WAVELET TRANSFORM

A. DWT & Lifting Implementation.

In traditional convolution (filtering) based approach for computation of the forward DWT, the input signal (x) is filtered separately by a low-pass filter (˜h) and a high-pass filter (˜ g). The two output streams are then sub-sampled by simply dropping the alternate output samples in each stream to produce the low-pass (yL) and high-pass (yH) sub band outputs as shown in Fig. 4. The two filters (˜h, ˜ g) form the analysis filter bank. The original signal can be reconstructed by a synthesis filter bank (h, g) starting from yL and yH as shown in Fig.4. Given a discrete signal x (n), the output signals yL(n) and yH(n) can be computed as follows:

$$y_L(n) = \sum_{i=0}^{T_L-1} \tilde{h}(i)x(2n-i),$$
$$y_H(n) = \sum_{i=0}^{T_H-1} \tilde{g}(i)x(2n-i) \quad (1)$$

Where τL and τH are the lengths of the low-pass (˜h) and high-pass (˜g) filters respectively. During the inverse transform computation, both yL and yH are first up-sampled by inserting zeros in between two samples and then filtered by low-pass (h) and high-pass (g) filters respectively. Then they are added together to obtain the reconstructed signal (x') as shown in Fig. below.

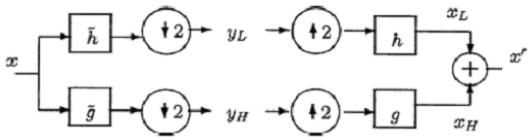

Fig. 4 : Signal analysis and reconstruction in 1D DWT

For multi resolution wavelet decomposition, the low pass sub band (yL) is further decomposed in a similar fashion in order to get the second-level of decomposition, and the process repeated. The inverse process follows similar multi-level synthesis filtering in order to reconstruct the signal.

Since two dimensional wavelet filters are separable functions, 2D DWT can be obtained by first applying the 1D DWT row-wise (to produce L and H sub bands in each row) and then column-wise as shown below:

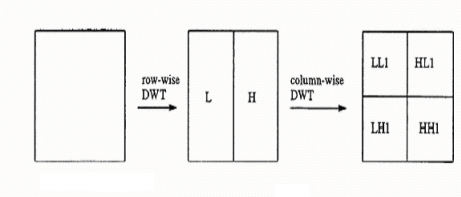

Fig. 5 : First level of decomposition

In the first level of decomposition, four sub bands LL1, LH1, HL1 and HH1 are obtained. Repeating the same in the LL1 sub band, it produces LL2, LH2, HL2 and HH2 and so on, as shown below:

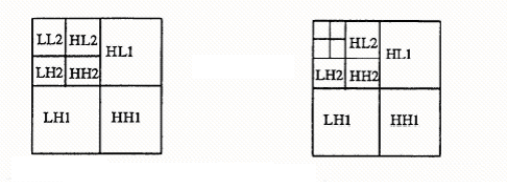

Fig. 6 : Second & Third of decomposition

The conditions for perfect reconstruction of a signal are given by

$$h(z)\tilde{h}(z^{-1}) + g(z)\tilde{g}(z^{-1}) = 2,$$
$$h(z)\tilde{h}(-z^{-1}) + g(z)\tilde{g}(-z^{-1}) = 0 \quad (2)$$

Where h(z) is the Z-transform of the FIR filter h. h can be expressed as a Laurent polynomial of degree p as:

$$h(z) = \sum_{i=0}^{p} h_i z^{-i} \quad (3)$$

Which can also be expressed using a poly phase representation as:

$$h(z) = h_e(z^2) + z^{-1}h_o(z^2) \quad (4)$$

Where ***he*** contains the even coefficients and ***ho*** contains the odd coefficients of the FIR filter h. Similarly,

$$g(z) = g_e(z^2) + z^{-1}g_o(z^2),$$
$$\tilde{h}(z) = \tilde{h}_e(z^2) + z^{-1}\tilde{h}_o(z^2),$$
$$\tilde{g}(z) = \tilde{g}_e(z^2) + z^{-1}\tilde{g}_o(z^2) \quad (5)$$

Based on the above formulation, we can define the poly phase matrices as:

$$\tilde{P}(z) = \begin{bmatrix} \tilde{h}_e(z) & \tilde{h}_o(z) \\ \tilde{g}_e(z) & \tilde{g}_o(z) \end{bmatrix},$$
$$P(z) = \begin{bmatrix} h_e(z) & g_e(z) \\ h_o(z) & g_o(z) \end{bmatrix} \quad (6)$$

Often P(z) is called the dual of ˜P (z) and for perfect reconstruction, they are related as P(z) ˜P (z−1)T = I , where I is the 2 × 2 identity matrix. Now the wavelet transform in terms of the poly phase matrix can be expressed as:

$$\begin{bmatrix} y_L(z) \\ y_H(z) \end{bmatrix} = \tilde{P}(z) \begin{bmatrix} x_e(z) \\ z^{-1}x_o(z) \end{bmatrix},$$
$$\begin{bmatrix} x_e(z) \\ z^{-1}x_o(z) \end{bmatrix} = P(z) \begin{bmatrix} y_L(z) \\ y_H(z) \end{bmatrix} \quad (7)$$

B. 2D DWT Architecture.

The basic idea of lifting based approach for DWT implementation is to replace the parallel low pass and high pass filtering by sequence of alternating smaller filters. The computations in each filter can be partitioned into prediction and update stages as shown in Fig. 7. Here the row module reads the data from MEM1, performs the DWT along the rows (H and L) and writes the data into MEM2. The prediction filter of the column module reads the data from MEM2, performs column wise DWT along alternate rows (HH and LH) and writes the data into MEM2. The update filter of the column

module reads the data from MEM2, performs column wise DWT along the remaining rows, and writes the LL data into MEM1 for higher octave computations and HL data to external memory.

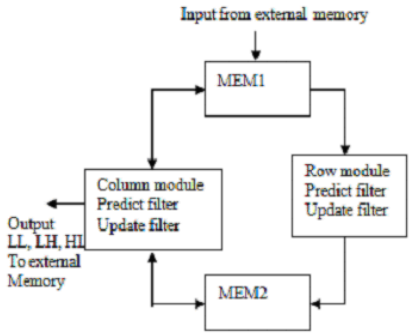

Fig. 7 : Overview of lifting based 2D DWT architecture.

The architecture can compute a large set of filters for both the 2D forward and inverse transforms. It supports two classes of architectures based on whether lifting is implemented by one or two lifting steps. The one step architecture corresponds to implementation using one lifting step.

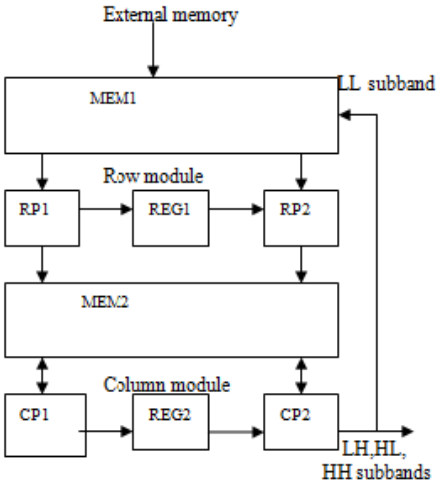

Fig. 8 : One step lifting based architecture.

RP1, RP2-row processors

CP1, CP2- column processor

MEM1, MEM2- memory

The block diagram shows one step lifting architecture is shown in Fig. 8. It consists of the row and column computation modules and two memory units, MEM1 and MEM2. The row module consists of two processors RP1 and RP2, along with a resister file REG1, and column module consists of two processors CP1 and CP2 along with register file REG2. All the four processor RP1, RP2, CP1, CP2 contain 2 adders, 1 multiplier and 1shifter. RP1 and CP1 are predicting filters and RP2 and CP2 are update filters.

C. Lifting Scheme.

The second generation of wavelets, which is under the name of lifting scheme, was introduced by Sweldens. The main feature of the lifting-based discrete wavelet transform scheme is to break up the high-pass and low-pass wavelet filters into a sequence of smaller filters that in turn can be converted into a sequence of upper and lower triangular matrices[4]. The basic idea behind the lifting scheme is to use data correlation to remove the redundancy.

The lifting algorithm can be computed in three main phases, namely: the split phase, the predict phase and the update phase, as illustrated in Fig. 9.

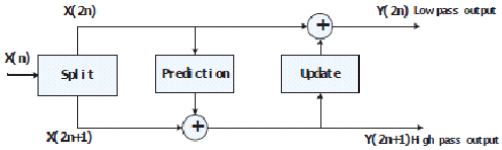

Fig. 9 : Split, predict, update phases of lifting based DWT

A. ***Split phase:*** In this split phase, the data set x(n) is split into two subsets to separate the even samples from the odd ones:

$$Xe = X(2n),\ Xo = X(2n+1) \qquad (8)$$

B. ***Prediction phase:*** In the prediction stage, the main step is to eliminate redundancy left and give a more compact data representation.

At this point, we will use the even subset x(2n) to predict the odd subset x(2n+1) using a prediction function P.

$$Y(2n+1) = Xo(2n+1) - P(Xe) \qquad (9)$$

C. ***Update phase:*** In this stage the coefficient x(2n) is lifted with the help of the neighboring wavelet coefficients.

$$Y(2n) = Y(2n+1) + U(Xe) \qquad (10)$$

Where, U is the new update operator.

After the two-dimensional wavelet transform of the first level, the image is divided into four parts. There are the horizontal low frequency-vertical low frequency component (LL), the horizontal low frequency-vertical high frequency component (LH), the horizontal high frequency-vertical low frequency (HL), and the

horizontal high frequency-vertical high frequency (HH), respectively.

D. Block Diagram of 9/7 Lifting DWT.

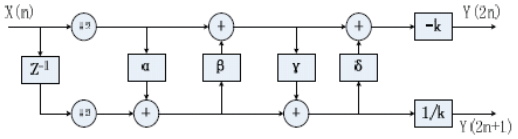

Fig. 10 : Block Diagram of 9/7 Lifting DWT

There are four lifting coefficient α, β, γ, δ and scaling factor k.

TABLE I. LIFTING COEFFICIENTS: ORIGINAL 9/7, RATIONAL 9/7 AND FIXED POINT BINARY OF RATIONAL 9/7

Coefficient	Rational 9/7	Fixed point binary of rational 9/7
α	-3/2	11.1
β	-1/16	10.0001
γ	4/5	00.1100110011001100
δ	15/32	00.0111100000000000
k	4/5	00.1100110011001100
1/k	5/4	01.01

III. PROPOSED SYSTEM

A. Pipeline Architecture of Lifting Based DWT.

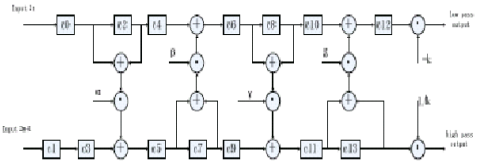

Fig. 11: Basic pipeline architecture of 1D-DWT

Generic multipliers usually have high area cost. Multiplication by constant can be performed by shifted additions when the number of bits in the multiplication is large.

According to the binary representation of multiplier constants presented in table1, the multiplication by γ needs 9 adders, the first one performs c6+c8, the next seven are to perform the sum of shifted partial products of c6+c8, and the last one performs the sum with c9. The multiplication by α needs 4 adders β needs 3 adders and the multiplication by δ needs 5 adders. The architecture of lifting DWT can be naturally pipelined, but the add/shift stages represent the worst delay path between registers. Pipelining these stages increases the data throughput (operating frequency).

The original arithmetic stage structure to perform the multiplication by γ is shown as:

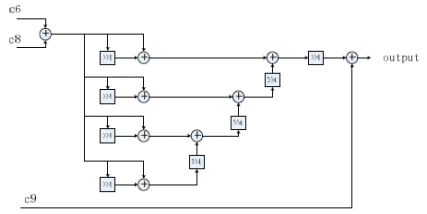

Fig. 12 : Original arithmetic stage structure

If x=c6+c8, the multiplication by γ can be expressed as

$$x(2^{-1}+2^{-2}+2^{-5}+2^{-6}+2^{-9}+2^{-10}+2^{-13}+2^{-14}) = 2^{-1}((((x+2^{-1}x)+2^{-4}(((x+2^{-1}x)+2^{-4}((x+2^{-1}x) +2^{-4}(x+2^{-1}x)))) \quad (11)$$

Hence, this design promotes only integer sums, reducing the area cost thus increasing the maximum operating frequency.

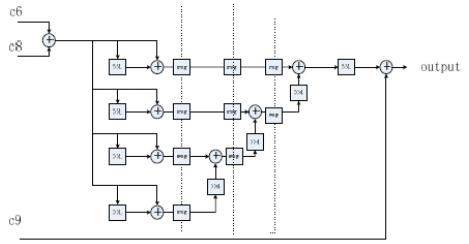

Fig. 13 : The pipelining arithmetic stage structure

B. Algorithm for Piprlined LDWT.

First, the input sequences Xi are split into even and odd parts s_i^0 and d_i^0. After the Splitting step, the two split sequences then perform the lifting steps respectively and the outputs are denoted as s_i^n and d_i^n,(n = 1,2). Finally, through the normalization factor K0 and K1, we can obtain the low-pass and high-pass wavelet coefficients si and di.

1. Splitting Step:

$$d_i^0 = x_{2i+1}; \quad (12)$$

$$s_i^0 = x_{2i}; \quad (13)$$

2. Lifting Step:

(First Lifting Step)

$$d_i^1 = d_i^0 - \alpha \times (s_i^0 + s_{i+1}^0); \quad \text{(Predictor)} \quad (14)$$

$$s_i^1 = s_i^0 + \beta \times (d_{i-1}^1 + d_i^1); \quad \text{(Updater)} \quad (15)$$

(Second Lifting Step)

$$d_i^2 = d_i^1 - \gamma \times (s_i^1 + s_{i+1}^1); \quad \text{(Predictor)} \quad (16)$$

$$s_i^2 = s_i^1 + \delta \times (d_{i-1}^2 + d_i^2); \quad \text{(Updater)} \quad (17)$$

3. Scaling Step:

$$d_i = K_1 \times d_i^2; \quad (18)$$

$$s_i = K_0 \times s_i^2. \quad (19)$$

In the pipeline design method, the critical path is dominated in the propagation delay between two registers (2 adders and 1 multiplier). To solve the delay time problem, we reschedule the pipe stage and propose a fast-pipeline architecture for 2D DWT.

Since the prediction or update step dominants the propagation delay in the direct mapping hardware implementation, we substitute Eq (15) into Eq (14) to merge the predictor and updater into one equation only. Thus, we can obtain a flattened equation and each computation is processed by one addition or multiplication at a time. The first lifting step equations are written as

$$\begin{aligned} s_i^1 &= s_i^0 + \beta\times(d_{i-1}^1 + d_i^1) \\ &= s_i^0 + \beta\times\{[d_{i-1}^0 - \alpha\times(s_{i-1}^0 + s_i^0)] + [d_i^0 - \alpha\times(s_i^0 + s_{i+1}^0)]\} \\ &= s_i^0 + (\beta\times d_{i-1}^0 - \beta\alpha\times s_{i-1}^0 - \beta\alpha\times s_i^0) + (\beta\times d_i^0 - \beta\alpha\times s_i^0 - \beta\alpha\times s_{i+1}^0) \\ &= s_i^0 + (\beta d_{i-1}^1) + (\beta d_i^1). \end{aligned} \quad (20)$$

In the second lifting step, we substitute Eq (17) into Eq (16) as the first lifting step.

Finally, since the effect of high pass coefficients, the scaling step can be rewritten as

$$d_i = \frac{K_1}{\delta}\times d_i^2, \qquad s_i = K_0 \times s_i^2. \quad (21)$$

From the above modified equations, six constant multipliers

$$\beta,\ \beta\alpha,\ \frac{\delta}{\beta},\ \delta\gamma,\ \frac{K_1}{\delta},\ K_0$$

are used in the process of lifting and scaling steps as the primitive algorithms. Then, we adopt the pipeline design method to implement the transformation.

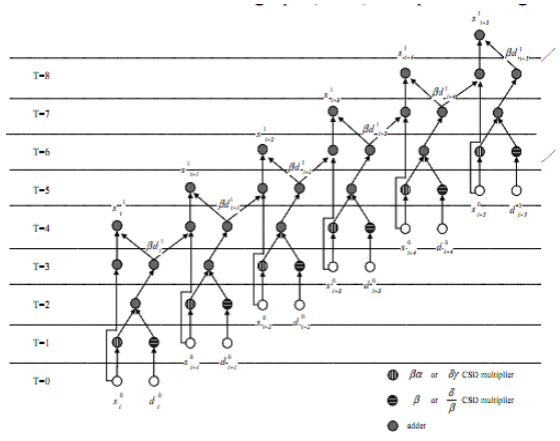

Fig. 14: DFG for pipeline scheduling

IV. IMPLEMENTATION RESULTS

A 2D input is first simulated by using MATLAB. Pipelining is implemeted by using XILINX, then again MATLAB code is used to obtain denoised 2D output or image. Now the local changes in brightness in the original image can be determined. The pipelined increases the area cost but reduces worst dalay path between registers, hence increases operating frequency.

Design 1 is shown in Fig. 12 and design 2 in Fig. 13. These 2 designs are compiled and simulated using XILINX.

TABLE II. IMPLEMENTATION RESULTS

Architecture	Maximum operating frequency(MHz)
Design1	68.36
Design2	96.64

From one observation the operating frequency of design 2 is higher than design 1 as shown in above table. The value of operating frequency can be different for different observation.

V. CONCLUSION

This paper presents an efficient FPGA implementation of the DWT algorithm with lifting scheme. It uses the multi-stage pipeline technique architecture for the purpose of speeding up the performance. The performance evaluation has proven that the proposed architecture has much higher operating frequency than the architecture which without multi-stage pipelining.

REFERENCES

[1] A. S. Lewis and G. Knowles, "Image compression using the 2-D wavelet transform," IEEE Trans. Image Process., 1992, 1(3), pp. 244–250

[2] T. Park and S. Jung, "High speed lattice based VLSI architecture of 2D discrete wavelet transform for real-time video signal processing," IEEE Trans. Consum. Electron., 2002, 48(4), pp. 1026–1032

[3] K. A. Kotteri, S. Barua,et.al,"A Comparison of Hardware Implementations of the Biorthogonal 9/7 DWT: Convolution Versus Lifting,"IEEE Trans. on circuit and systems,2005,52(5),256-260

[4] S.Khanfir, M. Jemni, "Reconfigurable Hardware Implementations for Lifting-Based DWT Image

Processing Algorithms," ICESS'08, 2008, pp. 283-290.

[5] S.V. Silva, S. Bampi, "Area and Throughput Trade-Offs in the Design of Pipelined Discrete Wavelet Transform Architectures," Proceedings of the Design Automation and Test in Europe Conference and Exhibition (DATE'05), 2005,1530-1591

[6] W.Sweldens, "The lifting scheme: a custom-design construction of biorthogonal wavelets," Applied and Computational Harmonic Analysis, 1996, 3(15), pp. 186-200

[7] K.K. Parhi, "VLSI digital signal processing systems: design and implementation", John Wiley & Sons, Inc, 1999, pp.508-510

◈◈◈

Design of Advanced On-Chip Bus Implementation with Open Core Protocol Interface using Finite State Machines

T. Subhasri & P. Krishna Chaitanya

Dept. of Electronics & Communication Engineering, NOVA College of Engineering & Technology, Vegavaram, India

Abstract - The on-chip bus design can be divided into two parts, the interface and the internal architecture of the bus. Here we adopt the well-defined interface standard, the Open Core Protocol (OCP), and focus on the design of the internal bus architecture. We develop an efficient bus architecture to support most advanced bus functionalities defined in OCP, including burst transactions, lock transactions, pipelined transactions, and out-of-order transactions. We first model and design the on-chip bus with transaction level modeling for the consideration of design flexibility and fast simulation speed. We then implement the RTL models of the bus for synthesis and gate-level simulation. Experimental results show that the proposed TLM model is quite efficient for the whole system simulation and the real implementation can significantly save the communication time.

I. INTRODUCTION

A group of lines shared for interconnection of the functional modules by a standard interface is called a Bus. The interconnections may be point-to-point, on-chip bus and on-chip network. The characteristic of a traditional bus is that I/O pins are fixed and form a shared I/O with dedicated address decoding. But for an OCB, the routing resource is in a target device like FPGA, ASIC. OCP (Open Core Protocol) is an interface standard that interconnects IP cores to on-chip bus. A designer selects only those signals and features from the palette of OCP configurations needed to fulfill all of an IP coreXs unique data, control and test signaling requirements. The bus interface involves a set of interface signals and their corresponding timing relationship, while the bus architecture refers to the internal components of buses and the interconnections among the IP cores. When the number of integrated IP cores increases, the communication between IP cores also increase and it becomes quite frequent that two or more master IPs would request data from different slaves at the same time. The shared bus architecture often cannot provide efficient communication since only one bus transaction can be supported at a time. To solve this problem, two bus protocols have been proposed recently. One is the Advanced eXtensible Interface protocol (AXI) and the other is bus interface protocol is proposed by a non-profitable organization, the Open Core Protocol.

The main features of OCP interface are: 1) Master - slave interface with unidirectional signals: 2) Driven and sampled by the rising edge of the OCP clock; 3) Fully synchronous, no multi-cycle timing paths; 4) All signals are strictly point-to point (except clock & reset); 5) Simple request / acknowledge protocol; 6) Supports data transfer on every clock cycle; 7) Allows master or slave to control transfer rate; 8) Configurable data word width; 9) Configurable address width; 10) Pipelined or blocking reads; 11) Specific description formats for core characteristics, interfaces (signals, timing & configuration), performance OCP interface is a user-settable, so the designer can define interface attribute, such as address and data bus width.

OCP is an interface (or socket) aiming to standardize and thus simplify the system integration problems. It facilitates system integration by defining a set of concrete interface (I/O signals and the handshaking protocol) which is independent of the bus architecture. In this paper we propose a high performance on-chip bus design with OCP as the bus interface. We choose OCP because it is open to the public and OCP-IP has provided some free tools to verify this protocol.

Our proposed bus architecture features crossbar/partial-crossbar based interconnect and realizes most transactions defined in OCP, including 1) single transactions, 2) burst transactions, 3) lock transactions, 4) pipelined transactions, and 5) out-of-order transactions.

Basic OCP includes only data flow signals and is based on simple request and acknowledge protocol. However, the optional extensions support more functionality in control, verification and testing. Simple Extension and Complex Extension support burst transaction and pipelined write operations. In addition, Sideband Extension supports user-defined signals and

asynchronous reset. Also, Debug and Test Interface Extension supports JTAG (Join Test Action Group) and clock control. This is the reason why, when integrated in SoC, the OCP protocol allows debugging and IP block test generating.

In addition, the proposed bus is flexible such that one can adjust the bus architecture according to the system requirement. One key issue of advanced buses is how to manipulate the order of transactions such that requests from masters and responses from slaves can be carried out in best efficiency without violating any ordering constraint. In this work we have developed a key bus component called the scheduler to handle the ordering issues of out-of-order transactions. We will show that the proposed crossbar/partial-crossbar bus architecture together with the scheduler can significantly enhance the communication efficiency of a complex SOC. We employ both transaction level modeling (TLM) and register transfer level (RTL) modeling to design the bus.

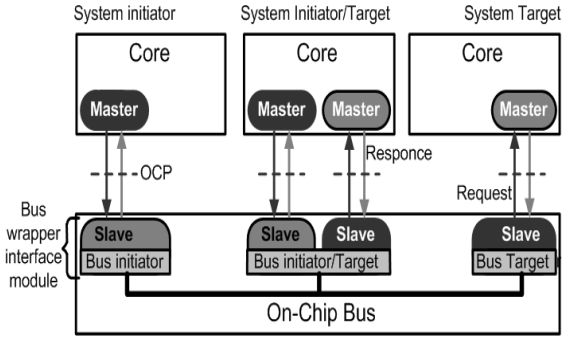

Fig. 1 : On-chip bus overview

We start from the TLM for the consideration of design flexibility and fast simulation speed. We then refine the TLM design into synthesizable and cycle-accurate RTL codes which can be synthesized into gate level hardware to facilitate accurate timing and functional simulation. The remainder of this paper is organized as follows. The various advanced functionalities of on-chip buses are described in Section 2. Section 3 details the hardware architecture of the proposed bus. Section 4 gives the experimental results which show the efficiency on both simulation speed and data communication. Conclusions are then drawn in Section 5.

II. ON-CHIP BUS FUNCTIONALITIES

The various bus functionalities include 1) burst, 2) lock, 3) pipelined, and 4) out-of-order transactions.

- The burst transactions allow the grouping of multiple transactions that have a certain address relationship, and can be classified into multi-request burst and single-request burst according to how many times the addresses are issued. FIGURE 1 shows the two types of burst read transactions. where the address information must be issued for each command of a burst transaction (e.g., A11, A12, A13 and A14). This may cause some unnecessary overhead

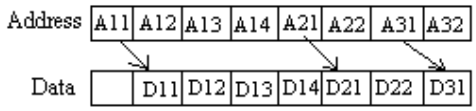

Fig. 2 : Burst transactions

- Lock is a protection mechanism for masters that have low bus priorities. Without this mechanism the read/write transactions of masters with lower priority would be interrupted whenever a higher-priority master issues a request. Lock transactions prevent an arbiter from performing arbitration and assure that the low priority masters can complete its granted transaction without being interrupted.
- For a pipelined transaction as shown in FIGURE 3 this hard link is not required. Thus A21 can be issued right after A11 is issued without waiting for the return of data requested by A11 (i.e.,D11-D14)

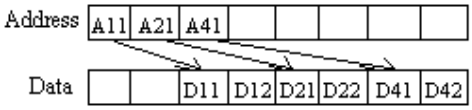

Fig. 3: Pipelined transactions

- The out-of-order transactions allow the return order of responses to be different from the order of their requests. These transactions can significantly improve the communication efficiency of an SOC system containing IP cores with various access latencies as illustrated in FIGURE 4.

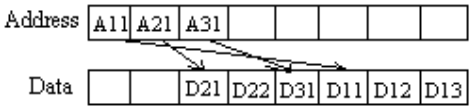

Fig. 4 : With-out-order transactions

III. HARDWARE DESIGN OF THE ON-CHIP BUS

The architecture of the proposed on-chip bus is illustrated in FIGURE 5, where we show an example with two masters and two slaves. A crossbar architecture is employed such that more than one master can

communicate with more than one slave simultaneously. If not all masters require the accessing paths to all slaves, partial crossbar architecture is also allowed.

For a crossbar or partial crossbar architecture, resource contention occurs when more than one master is to access the same slave simultaneously. In the proposed design each slave IP is associated with an arbiter that determines which master can access the slave.

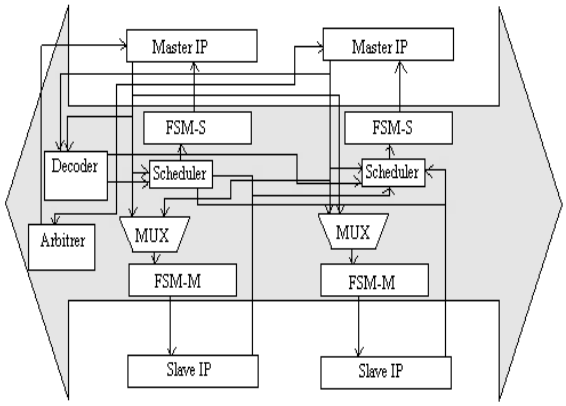

Fig. 5 : Top view of proposed architecture

3.1 Decoder

Since more than one slave exists in the system, the decoder decodes the address and decides which slave return response to the target master. In addition, the proposed decoder also checks whether the transaction address is illegal or nonexistent and responses with an error message if necessary.

3.2 FSM-M & FSM-S

Depending on whether a transaction is a read or a write operation, the request and response processes are different. For a read operation, the address of the target slave is first sent out and the target slave will issue an accept signal when it receives the message. The slave then generates the required data and sends it to the bus where the data will be properly directed to the master requesting the data. The read transaction finally completes when the master accepts the response and issues an acknowledge signal. For a write transaction, the data to be written is sent out together with the address of the target slave, and the transaction is complete when the target slave accepts the data and acknowledges the reception of the data. FSM-M acts as a master and generates the OCP signals of a master, while FSM-S acts as a slave and generates those of a slave. These finite state machines are designed in a way that burst, pipelined, and out-or-order read/write transactions can all be properly controlled.

3.3 Scheduler

The OCP protocol, each out-of order transaction is tagged with a TagID by a master. For those transactions with the same TagID, they must be returned in the same order as requested, but for those with different TagID, they can be returned in any order. Conventional bus scheduling algorithms tend to favor the in-order transactions, while the ordering mechanism favors out-of order transactions.

3.4 Multiplexer

In FIGURE 6 MUX1 is used to solve the problem of resource contention when more than one slave returns the responses to the same master. It selects the response from the slave that has the highest priority. The recorder shown in the figure is used to keep track of the ID of the target slave and the TagID of every out-of-order transaction. Whenever a response arrives, the comparator determines whether the ordering restriction is violated or not by comparing the ID of the target slave and TagID. If no ordering restriction is violated, the response is sent forward to the priority setter. If the restriction is violated, the response is sent backward to one of the inputs of MUX2, which is always a preferred input over the input from MUX1. For the transactions without TagID, which are regarded as in-order transactions, the priority setter sets the priority to 0 or the largest value to reflect whether in-order first or out-of-order first policy is used. To further improve the efficiency of the scheduler, the response can be forwarded to the master directly without going through the priority queue when the priority queue is empty.

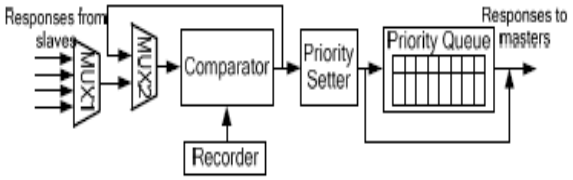

Fig. 6 : Block diagram of scheduler

IV. EXPERIMENTAL RESULTS

We design the proposed bus with both TLM and RTL models. The RTL model can be further synthesized into gate-level description. The specification and the synthesis results when 4 masters and 6 slaves are used are shown in TABLE 1, where all masters can issue burst, lock, pipelined and out-of-order transactions.

TABLE 1.Bus specifications and synthesis results

Architecture of bus	Factor
Address width Data width	64-bits 128-bits
Number of Slave Ports Number of Master Ports	12 8
Total area (μm^2) Operating frequency	About 60K gates 333.33MHz

The total area of the proposed on-chip bus at 333MHz using TSMC 0.13_m CMOS process is 153,823 um2 (about 60K gates). We find that for each additional master, about 3,682 x2 and 4,531x2 more gates are needed for a port without and with the out-of-order capability, respectively. On the other hand, about 1,456x2 gates are required for one slave port. Originally the on-chip bus is a multi-layer bus consisting of two AHB-lite busses modeled with a commercial bus library (CoWare [4]). The ARM9 processor is connected to one AHB-lite bus, and the PAC DSP processor is connected to the other. In the experiment, we replace the AHB-lite bus connecting the PAC DSP processor with the proposed on-chip bus and verify the whole SOC design with an H.264 decoding procedure. Experimental results show that the proposed on-chip bus deals with all the communications in the SOC well.

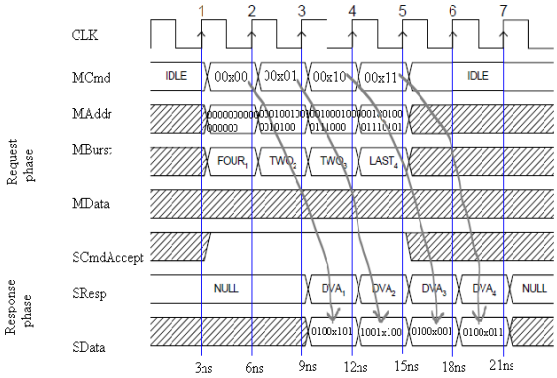

Fig. 7 : Burst Transactions

The simulation times of decoding one frame are about 48.6 and 44.3 seconds before and after the replacement, respectively. It should be pointed out that even though both the proposed bus and the one using CoWare bus library are cycle-accurate; our proposed bus is further a pin-accurate one but the one from CoWare is not. Thus the proposed TLM bus model provides better simulation speed since it contains more implementation details. To focus on the efficiency evaluation of the crossbar bus architecture, we design an SOC system as shown in FIGURE 8 which contains two masters (IP1 and IP2) and three slaves (IP3, IP4 and IP5).

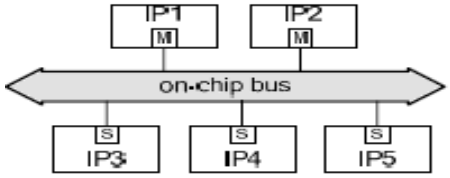

Fig. 8 : SOC System for bus evaluation

In this experiment we compare the communication efficiency of the SOC systems with the shared bus architecture and the crossbar bus architecture. The transactions used in the experiment are described as follows:

1. Master IP2 first requests a series of burst WR transactions to slave IP4 and a WR transaction to slave IP3.
2. Master IP1 then requests a series of burst RD transactions to slave IP4.
3. Master IP1 then requests a series of burst WR transactions to slave IP5, and master IP2 requests a series of burst WR transactions to slave IP4.
4. Master IP2 requests a series of burst RD transactions to slave IP5.

The procedure from step2 to step4 is iterated for 100 iterations. The execution of these transactions on the factor architecture can be illustrated in FIGURE 9, where parallel communication between different masters and slaves happens in time intervals B, D, F, H and J. The behavior on the shared bus architecture is all in series without any parallel communication.

Experimental results show that the proposed bus with crossbar interconnection reduces about 23.35% communication cycles as comparing to the tradition shared bus architecture such as AHB. In the last experiment, we evaluate the efficiency of out-of-order transactions using the proposed scheduler. We assume that the access latency of the slave IP3 and IP4 in FIGURE 8 are 1 cycle and 3 cycles, respectively. The slave IP5 has the access latency of 5 cycles when it is accessed by master IP1 and two cycles when it is accessed by master IP2.

In the simulation, IP1 first requests a series of out-of-order WR transactions, IP2 then requests a series of out-of-order RD transactions. After that, IP2 requests a series of out-of-order WR transactions, and IP1 finally requests a series of out-of-order RD transactions. The simulation results show that when each series of these requests contain 6000 transactions, the proposed

scheduler reduces 67.16% communication cycles as comparing to a bus that supports only in-order transactions.

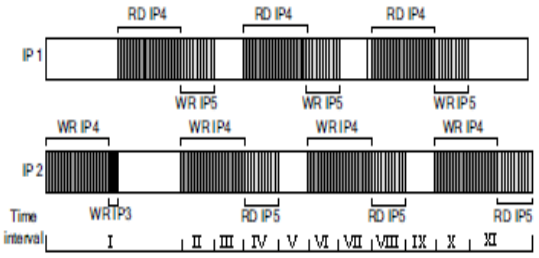

Fig. 9 : Performance analysis of parallel transactions

V. CONCLUSION

The bus standard must be able to define an explicit bus interface and leave the internal bus architecture to the bus designer. The design which complies with the bus interface protocol to carry out the various advanced bus functionality consequently dominates the communication efficiency of an SOC system. In this work, we develop an on-chip bus employing OCP as the bus interface. Various bus transactions defined in AXI and OCP to reduce the communication latency and increase the bus throughput are supported by the proposed bus architecture. Experimental results demonstrate the efficiency of the proposed bus in both simulation speed and execution performance.

REFERENCES

[1] Open Core Protocol (OCP) Specification, http://www.ocpip.org/home.

[2] C.-K. Lo and R.-S. Tsay, "Automatic Generation of Cycle Accurate and Cycle Count Accurate Transaction Level Bus Models from a Formal Model," Asia and South Pacific Design Automation Conference, pages 558-563, 2009.

[3] N.Y.-C. Chang, Y.-Z. Liao and T.-S. Chang, "Analysis of Shared-link IET Computers & Digital Techniques, Volume 3, Issue 4, pages 373-383, 2009.

[4] CoWare website, http://www.coware.com

[5] Sudeep Pasricha & Nikil Dutt "On-chip communication architectures (system on-chip interconnect)"

◈◈◈

Power Quality Improvement by Utilizing Super Capacitor in Electrical Power Transmission System

W. A. Augusteen, V. Nandhakumar & R. K. Balaji

Indira Institute of Engineering and Technology, India

Abstract **-** Power quality problem manifested in voltage, current or frequency deviations that result in failure or mis-operation of customer equipment. In distribution network, the sensitive industrial loads and critical commercial operations suffer from outages and service interruptions which cause financial losses to both utility and consumers. This paper is to improve the power quality in transmission system by adopting and replacing the super capacitor instead of existing capacitor bank. This super capacitor resembles a regular capacitor with the exception that it offers very high capacitance in a small package and considerably improves the power factor and efficiency of the transmission system. This approach has been tested in T type & PI type model of medium and long transmission distribution systems by replacing super capacitor with existing capacitor bank. This approach simulated through the software package of Matlab 6.5 and the results shows considerable Power Quality improvements.

I. INTRODUCTION

Power quality is an issue that is becoming increasingly important to electricity consumers at all levels of usage. Sensitive equipment and non-linear loads are commonplace in both the industrial and the domestic environment; because of this a heightened awareness of power quality is developing. The source of problems that can disturb the power quality are: power electronic device ,arcing device, load switching, large motor starting ,embedded generation, sensitive equipment storm and environment related damage, network equipment and design.

The solution to improve the energy quality (PQ-Power Quality) at the load side is of great importance when the production processes get more complicated and require a bigger liability level, which includes aims like to provide energy without interruption, without harmonic distortion and with tension regulation between very narrow margins. The devices that can fulfill these requirements are the custom power; a concept that we could include among the super capacitor, but that is different to them because of their final use. In fact the topologies that they employ are identical to the ones in the super capacitor device with little modification and adaptations to tension levels, therefore they are most oriented to be used in distribution networks of low and medium tension, sometimes replacing the active filters.

Recent developments in electrical powers system such as deregulation, open access, and cogeneration are creating scenarios of transmission congestion and forced outage. Addition of new transmission lines is an almost impossible solution due to environmental and other consideration, and developing new approaches to power system operation and control is the need of the hour for overload relief, efficient and reliable operation [1].

Benefits of utilizing Super capacitor:

The benefits of utilizing super capacitor in electrical transmission system can be summarized as follows: Electrochemical Double Layer Capacitors (EDLCs) – also called super capacitors (SC) - are electrochemical capacitors that have high capacitance and high energy density when compared to common capacitors, and higher power density when compared to batteries.

Most EDLC's are constructed from two carbon based electrodes (mostly activated carbon with a very high surface area), an electrolyte (aqueous or organic) and a separator (that allows the transfer of ions, but provides electronic insulation between the electrodes). As voltage is applied, ions in the electrolyte solution diffuse across the separator into the pores of the electrode of opposite charge. Charge accumulates at the interface between the electrodes and the electrolyte (the double layer phenomenon that occurs between a conductive solid and a liquid solution interface), and forms two charged layers with a separation of several angstroms – the distance from the electrode surface to the center of the ion layer (in Fig. 1). The double layer capacitance is the result of charge separation in the interface. Since capacitance is proportional to the

surface area and the reciprocal of the distance between the two layers, high capacitance values are achieved.

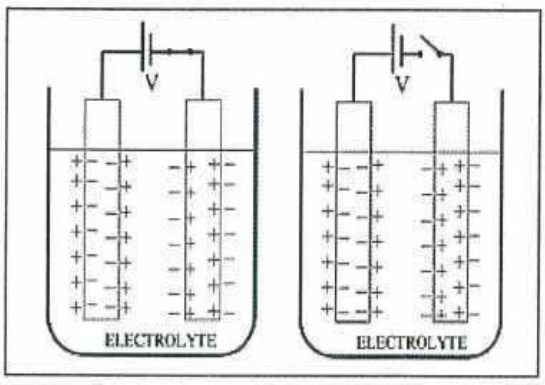

Fig.1

Electrical double layer capacitor constructed by inserting two electrodes in a beaker and applying a voltage. The voltage persists after the switch is opened (right), creating two series-connected capacitors. Charges in the electric double layer are separated by only about 1 nm [4].

EDLC's store electrical charge electro statically, and almost no reaction occurs between the electrodes and the electrolyte. Consequently, electrochemical capacitors can undergo hundreds of thousands of charge and discharge cycles.

The first electrical device using double layer charge storage was reported in 1957 by General Electric. This was followed by the development from the Standard Oil Company of Ohio (SOHIO), who patented a device that shaped the format commonly used today. In 1978, NEC was the first to introduce super capacitors commercially as low voltage devices with high ESR, primarily designed for backup applications. Since then, EDLC's have evolved: high voltage and very high capacitance (thousands of Farads) on the one hand, and low ESR pulse super capacitors with a capacitance range of few milli -Farads, up to 1- 2 Farads, on the other hand.

Significant improvements in materials, design and the process of production of pulse super capacitors has lead to low profile prismatic devices that can supply high peak currents of up to 2 – 3 A. These devices are suited to meet the peak power demands of many battery-powered electronics and other consumer and industrial devices with current-limited energy sources.

Why we use super capacitors for energy storage?

Supercapacitors represent one of the latest innovations in the field of electrical energy storage, and find their place in many applications where energy storage is needed, or can help in smoothing strong and short-time power solicitations of a distribution network. In comparison with classical capacitors, these new components allow a much higher energy density, together with a high power density. Even if the energy density is not comparable to that of electrochemical accumulators, the possible amount of stored energy, along with storage time are compatible with many industrial requirements [5], [6].

Batteries are widely used for energy storage in industrial and consumer electronic devices because of their high energy density, but are limited in their power density. With its limited power the battery often cannot supply the required power while still retaining its open circuit voltage. The larger the voltage drop of the battery the larger the load on the battery. Often, when a battery needs to supply high power at short pulse widths, the voltage drop may be too large, causing lower voltage than required by the end product. The large load decreases the energy stored in the battery, harming it and shortening its life-span.

When high power is required in battery operated devices (i.e. in pulse applications), the combination of the super capacitor connected in parallel to the battery gives the advantages of both, enhancing the performance of the battery and extending its life, exploiting the batteries to its maximum potential. The super capacitor connected to the battery in parallel produces a voltage damping effect - low impedance super capacitors can be charged in seconds with a low current during standby times between high current pulses. Adding the super capacitor to the battery in parallel decreases the voltage drop, leading to: Better energy and power management, Battery life and operational range extension, Superior energy density in the battery, Power to be produced by both the EDLC and the battery, each supplying power inversely to its own ESR, Fewer battery replacements in some of the applications .

Batteries are very inefficient at low temperatures. Their internal resistance increases due to the slower kinetics of the chemical reaction within the battery. The internal resistance is reduced by incorporating a super capacitor into the system with the battery. The internal resistance of pulse type super capacitors is much lower than that of batteries, even at low temperatures down to -40°C. Super capacitors have several advantages and disadvantages relative to batteries.

II. PROBLEM FORMATION

This paper is to obtain the design and operation of a transmission line by determination of voltage drop, line losses and efficiency of transmission system. These values are greatly influenced by the line constants R, L,

and C of the transmission line. For instance, the voltage drop in the line depends upon on the value of above three line constants .Similarly, the resistance of the transmission line conductor is the most important cause of power loss in the line and determines the transmission of efficiency.

In this paper, we shall develop problem formation by calculating voltage regulation, line losses and efficiency of transmission lines. In this paper we have taken the formation of Nominal π Method and Nominal T Method of radial distribution systems

Nominal π Method:

In this method in which capacitance is divided into two halves with one half lumped near sending end and other half near the receiving end. This is shown in the following figure 2.1. The capacitor near the sending end does not contribute any line voltage drop but it should be added with line current to get total sending end current. The phasor diagram is shown in the following figure2.2. V_R is taken as the reference phasor. The current $\bar{I}_R$lags behind V_R by angle $\emptyset_R$.

The current through capacitor C_1 is leading the voltage V_R by an angle of 90°. The phasor sum of I_R

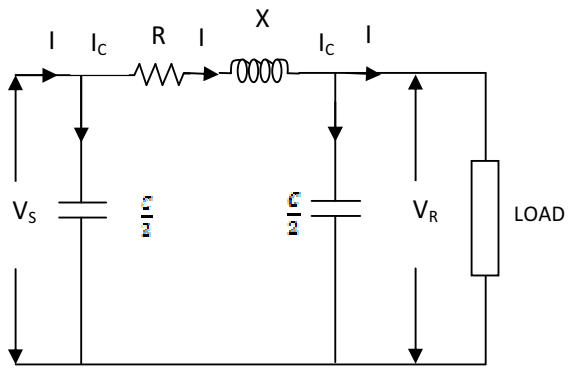

Schematic Fig. 2.1

and I_{C1} gives the line current I_L. The drop I_LR is in phase with I_L whereas drop I_LX_L is leading by 90°. The phasor sum of these drops with V_R gives the sending end voltage V_S. The capacitor current I_{C2} is leading voltage V_S by 90°. The phasor sum of I_S and I_{C2} gives the sending end line current I_S.

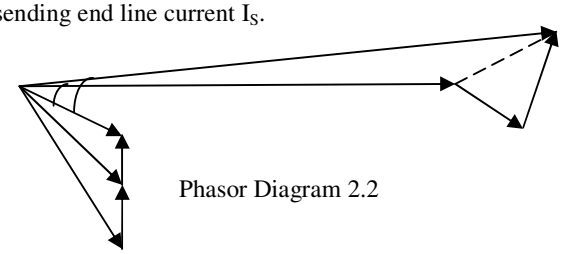

Phasor Diagram 2.2

Thus sending end voltage is given as

$$\bar{V}_S = \bar{V}_R + \bar{I}_L\bar{Z} = \bar{V}_R + \bar{I}_L[R + jX_L] \quad (2.1)$$

%Voltage Regulation= $\frac{VS - VR}{VR} \times 100$ (2.2)

Efficiency=$\frac{\text{Power delivered}}{\text{Power delivered + Losses}} \times 100$ (2.3)

Where

V_S = Sending end voltage

V_R = Receiving end voltage

I_R = Load current or receiving end current

R = Resistance per phase

X_L = Inductive reactance per phase

C = Capacitance per phase

$\cos\emptyset_R$ = P.f at receiving end

$$\bar{V}_R = V_R + j0 \quad (2.4)$$

Load current,

$$\bar{I}_R = I_R(\cos\emptyset_R - j\sin\emptyset_R) \quad (2.5)$$

Charging current at receiving end,

$$\bar{I}_{C_2} = j\omega\left(\frac{C}{2}\right)\bar{V}_S = j\pi fC\bar{V}_S$$

$$\bar{I}_{C_1} = j\omega\left(\frac{C}{2}\right)\bar{V}_R = j\pi fC\bar{V}_R$$

We get the line current as,

$$\bar{I}_L = \bar{I}_R + \bar{I}_{C_1} \quad (2.6)$$

Sending end current, $\bar{I}_S = \bar{I}_L + \bar{I}_{C_2}$ (2.7)

The efficiency and the regulation of the transmission line can be obtained in the similar manner as explained in the earlier sections.

Nominal T Method:

In this paper we have taken Nominal T Method additionally and especially this method of calculation is utilized for medium transmission line.

In this method the total line capacitance is lumped or concentrated at the midpoint of the line. The resistance and reactance of the line are divided with half the resistance and reactance on one side and remaining half on other side of capacitor. Half of the line carries full charging current with this arrangement. The following diagram shows the arrangement used in nominal T method for one phase. It is desirable to work in phase instead of line values.

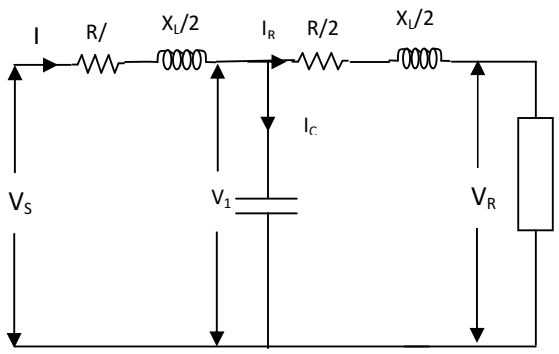

Schematic Diagram 2.3

The corresponding phasor diagram is represented as follows

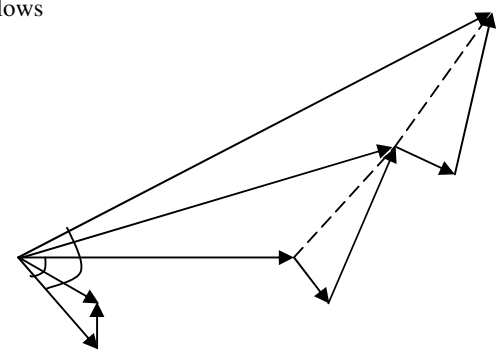

Phasor Diagram 2.4

Here the receiving end voltage V_R is taken as reference. The drop PQ $\left(I_R.\frac{R}{2}\right)$ is in phase with I_R. The drop QR $\left(I_R.\frac{X_L}{2}\right)$ is leading I_R by $90°$. The phasor sum of these drops with V_R gives the voltage V_1 which is the voltage across the capacitor. The capacitor current I_C leads V_1 by $90°$. The phasor sum of I_R and I_C gives I_S. The drop $R_S\left(I_S.\frac{R}{2}\right)$ is in phase with I_S whereas drop ST $\left(I_S.\frac{X_L}{2}\right)$ is loading I_S by $90°$. The phasor sum of these drops along with V_1 gives the sending end voltage V_S.

Let

I_R = Receiving end load current per phase

R = Resistance per phase

X_L = Inductive resistance

C = Capacitance per phase

$\cos \emptyset_R$ = p.f. at receiving end

V_S = Sending end voltage

V_1 = Voltage across capacitor

%Voltage Regulation= $\frac{VS-VR}{VR} \times 100$

Transmission Efficiency= $\frac{\text{Power delivered}}{\text{Power delivered}+\text{Losses}} \times 100$

Receiving end voltage, $\overline{V}_R = V_R + j0$ (2.8)

Load current, $\overline{I}_R = I_R(\cos \emptyset_R - j \sin \emptyset_R)$ (2.9)

Voltage across capacitor, $\overline{V}_1 = \overline{V}_R + \overline{I}_R\left(\frac{\overline{Z}}{2}\right)$

$=[V_R + j0] + [I_R(\cos \emptyset_R - j \sin \emptyset_R)]\left(\frac{R}{2} + j\frac{X_L}{2}\right)$

Current through capacitor, $\overline{I}_C = j\omega C \overline{V}_1 - j2\pi fC\,\overline{V}_1$

Sending end current, $\overline{I}_S = \overline{I}_R + \overline{I}_C$

Sending end voltage,

$\overline{V}_S = \overline{V}_1 + \overline{I}_S\left(\frac{\overline{Z}}{2}\right) = \overline{V}_1 + \overline{I}_S\left(\frac{R}{2} + j\frac{X_L}{2}\right)$ (2.10)

The efficiency and regulation can be calculated in the similar manner explained in earlier sections.

III. TEST SYSTEM

A supercapacitive-storage-based substation for the compensation of resistive voltage drops in transportation networks has been proposed. It allows to feed as a current source in any voltage conditions of the line. The system has been designed as a compensation substation to be placed at week points like end-of-line stations, instead of additional feeding substations. A dedicated control system for the stabilization of the voltage level in case of strong perturbations is also proposed. Practical results have been recorded from a reduced-size prototype and are also presented[2].

Super capacitor Specification	Ratings
Charging Current	200A
Voltage	60v
Super Capacitor Rating	75F
Tank/Bank Size	24*1800F

A scaled prototype of the "Val-Vert" substation has been realized in order to show the operation and behavior of such a system. The scaled system is represented in the pic of figure.8.the model has the following characteristics: 60-v dc rectifier and line voltage, 100-a maximum load current, 60-v/200-a/75F super capacitor tank ($24 \times 1800F$) series - connected. The power converter is realized with standard IGBT modules[2].

By taking a sample of A 3 phase,50 Hz overhead transmission line 100 km long has the resistance/km/phase=.1Ω,inductive reactance/km/phase=.02Ω , capacitance susceptance /km/phase = 0.04×10^{-4} mho[3].

The result shows the high build up in voltage and also much improved efficiency for a sample of 1800F much improved in sending end voltage.

IV. CONCLUSION

In this paper we would like to replace the existing capacitor bank with the new proposed super capacitor. By applying this supper capacitor results shows the improved efficiencies and much improved sending and receiving end voltages depends about the requirement. By using this super capacitor in much less size we can get the same performances of existing capacitor. In this paper work opens up the research ideas towards radial distribution systems, optimization etc., and also opens up the designing of capacitor etc.

REFERENCES:

[1] M.P.Donsion , J. A. Guemes, J. M. Rodgriguez "Power quality. Benefits of utilizing Facts Devices in electrical power systems" university of Vigo Spain, university of Basque country.

[2] Alfred Rufer,senior Member,IEEE ,David Hotellier and Philippe , Member ,IEEE "A Supercapacitor-Based Energy Storage Substation for Voltage Compensation in Weak Transportation Networks" .

[3] U.A.Bakshi , M.V.Bakshi Text Book Reference "Transmission and Distribution" Technical Publication.

[4] "Fundamentals Of Electrochemical Capacitor Design And Operation" by John R. Miller and Patrice Simon.

[5] A. Rufer and P. Barrade, "Key developments for supercapacitive energy storage: Power electronic converters, systems and control," in Proc. Int. Conf. Power Electron. Intell. Motion Power Quality, Nuernberg, Germany, June 19–21, 2001, ISBN 3-928 643-27-4, pp. 17–25.

[6] "A supercapacitor-based energy-storage system for elevators with soft commutated interface," IEEE Trans. Ind. Applicat., vol. 38, pp. 1151–1159, Sept./Oct. 2002.

◈◈◈

Blind Adaptive Equalization using CMA Algorithm with Variable Step Size

T. Rambabu[1] & P. Rajesh Kumar[2]

[1]Dept. of ECE, Sarojini Institute of Technology, Telaprolu, Krishna(Dt.)
[2]Dept. of ECE, A. U. college of Engineering, Andhra University,Visakhapatnam

Abstract - The approach in this paper integrates a technique for variable-step- size (VSS) with the constant-modulus algorithm(CMA) for blind adaptive equalization for QAM signals.. This leads to the saving of some amount of computations for the VSS technique. Simulation results show that algorithms with the VSS technique exhibit lower steady-state mean-squared error (MSE) for the same speed of convergence.

Key words - *component; Blind Adaptive Equalization, CMA, MMA,VSS, QAM, MSE.*

I. INTRODUCTION

Blind adaptive equalization achieve channel equalization without the need of a training sequence [1][2]. The constant-modulus algorithm (CMA) has gained widespread practical use for equalizing channels in digital communication systems [3]. The multi modulus algorithm (MMA) [4] separates the equalizer output into in-phase and quadrature components and penalizes the dispersion of each around separate straight contours. Hybrid approaches for blind equalization are reported in [5]-[8].

It is known that the choice of the step size determines the performance characteristics of the adaptive algorithm in terms of the convergence rate and the amount of steady-state mean-square-error (MSE). In general, a smaller step size results in a smaller state-state MSE but also a slower rate of convergence. On the other hand, a larger step size results in a faster rate in convergence but a large steady-state MSE. To eliminate the trade off between the convergence rate and the **state**-state MSE, one would use a variable-step-size (VSS) technique [9]-[11].

In this paper, we propose a VSS technique suitable for QAM signals and integrate it with a stop-and-go (SAG) procedure to reduce the amount of computations. The technique is applied to CMA and MMA. Simulation results show that the VSS technique integrated with either CMA or MMA exhibits faster time to convergence than the original algorithm.

The rest of the paper is organized as follows. Section II presents fractionally-spaced equalizers. Section III reviews CMA and MMA for blind adaptive equalization while the proposed VSS technique is introduced in section IV. Simulation results applied to CMA presented in section V, while conclusions are given in section VI.

II. FRACTIONALLY-SPACE CMA

Figure 1 represents a noisy communication system with an FIR channel model and a fractionally-spaced equalizer (FSE) [12] with sampling interval $T/2$ where T is the sampling period. In the figure, $s(n)$ represents the baud-spaced source symbol, $\mathbf{c}$ is the N_c-length vector representing the fractionally-spaced channel impulse response, $\mathbf{h}$ is the N_h-length vector comprising the fractionally-spaced equalizer coefficients, and $y(n)$ is the baud-spaced equalizer output. In addition to the inter symbol interference, the $T/2$-spaced received signal $x(k)$ is also corrupted by an additive noise process $v(k)$. The received signal can be put in the form:

$$\mathbf{x}(n) = \mathbf{C}\mathbf{s}(n) + \mathbf{v}(n)$$

where $\mathbf{x}(n)$ and $\mathbf{v}(n)$ are N_h-length vectors containing the previous values for received signal and the channel noise process, respectively, and $\mathbf{C}$ is the $N_h \times \lfloor (N_h + N_c - 1)/2 \rfloor$ fractionally-spaced convolution matrix of the form [12]:

$$\mathbf{C}=\begin{bmatrix} c_1 & c_0 & & & & & \\ \vdots & \vdots & c_1 & c_0 & & & \\ c_{N_c-1} & c_{N_c-2} & \vdots & \vdots & \ddots & c_1 & c_0 \\ & & c_{N_c-1} & c_{N_c-2} & \ddots & \vdots & \vdots \\ & & & & & c_{N_c-1} & c_{N_c-2} \end{bmatrix}^T$$

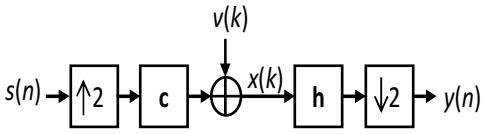

Fig. 1 : Fractionally spaced equalizer(T/2)

III. BLIND ADAPTIVE ALGORITHMS

In the following, CMA briefly presented.

3.1 CMA

CMA is a stochastic gradient algorithm minimizes the dispersion of the equalizer output around a circular contour. The CMA coefficient update algorithm is equivalent to the Godard coefficient update algorithm when $p = 2$, and is defined as [3];

$$\mathbf{h}(n+1) = \mathbf{h}(n) + \mu\, e_{CMA}(n)\, \mathbf{x}^*(n) \text{ with}$$
$$e_{CMA}(n) = y(n)\left(\gamma_C - |y(n)|^2\right)$$

where $\mathbf{h}(n+1)$ and $\mathbf{h}(n)$ are the vectors comprising the next and current equalizer coefficients, respectively, μ is the step size, $y(n)$ is the complex equalizer output, $\mathbf{x}(n)$ is the vector of equalizer input samples in the tapped-delay line, while * denotes the complex conjugate operation. The constant γ_C is referred to as the dispersion constant and is chosen in accordance chosen in accordance with the source statistics according to the relation:

$$\gamma_C = \frac{E\left\{|s(n)|^4\right\}}{E\left\{|s(n)|^2\right\}}$$ Where $E\{\cdot\}$ is the expectation operation with $s(n)$ being the transmitted signal.

$$\gamma_M = \frac{E\left\{a^4(n)\right\}}{E\left\{a^2(n)\right\}}$$ Where $a(n) = \mathrm{Re}\{s(n)\}$.

IV. PROPOSED VSS TECHNIQUE

When using an adaptive step size, The equalizer coefficient update takes the form:

$$\mathbf{h}(n+1) = \mathbf{h}(n) + \mu\, e(n)\, \mathbf{x}^*(n)$$

Where $\mu(n)$ is adjusted according to a certain rule and $e(n)$ is the error signal. The proposed VSS technique is a modified version of that which has been proposed in [11] for least-mean-square (LMS) algorithm integrated with a SAG algorithm and is summarized in the following steps:

1. Input $\mu(0)$
2. Initialize $\mathbf{h}(0)$
3. Loop $n = 0, 1, 2, \ldots$

   Calculate $e(n) = e_{CMA}(n)$ or $e(n) = e_{MMA}(n)$

$$\mathbf{h}(n+1) = \mathbf{h}(n) + \mu(n)\, e(n)\, \mathbf{x}^*(n)$$

$$\mu(n+1) = \frac{\mu(n)}{1 + \lambda\mu(n)\,|e(n)|^2}$$

where

$$\lambda = \begin{cases} 1 & \text{if } n = 0 \\ 0 & \text{if } \mathrm{sgn}(\mathrm{Re}\{e(n)\}) = \mathrm{sgn}(\mathrm{Re}\{e(n-1)\}) \,\&\, \\ & \quad \mathrm{sgn}(\mathrm{Im}\{e(n)\}) = \mathrm{sgn}(\mathrm{Im}\{e(n-1)\}) \\ 1 & \text{otherwise} \end{cases}$$

with $\mathrm{sgn}\{\cdot\}$ denotes signum function.

V. SIMULATION RESULTS

Simulations were carried out in a 35-dB SNR environment using 4-QAM. The channels were T/2-spaced microwave channels from SPIB where T is the symbol period. The equalizers were 16-tap T/2-spaced finite-duration impulse response (FIR) filters, initiated by a unitary double center spike as in [5]. The MSE was calculated as the average instantaneous-squared error over 100 trials using microwave channel #2 [13].

Figure 2 shows the convergence curves for CMA and CMA with VSS for $\mu(n) = \mu = 2^{-7}$ for the CMA, and for $\mu(0) = 2^{-7}$ for the CMA with VSS. It is clear that VSS technique has resulted in less steady-state MSE for the same convergence speed as shown by the MSE curves in the transient region. Figure 3 demonstrates the constellation diagrams for the outputs which also shows the advantage of using the VSS technique. Figure 4 illustrates the variations of the step

size with the iterations. It was calculated that the step size does not change in 25% of the number of samples due to the SAG approach within the VSS technique. This leads to reduction in the amount of computations in calculating the step size update.

VI. CONCLUSION

In this paper, a VSS has been proposed to suit blind equalization for QAM signals. The technique has also used a SAG approach to either vary the stepsize or to hold the previous step depending on the relative sign of the current-sample error from that of the previous sample error. This leads to the reduction of the amount of computations involved. Simulation results show that integrating the proposed VSS to the CMA the exhibits in lower steady-state MSE for the same speed of convergence which means better overall performance of the receiver system.

REFERENCES

[1] S. Haykin, Adaptive Filter Theory, 3rd Ed., Prentice-Hall, 2003.

[2] S. Bellini, "Blind equalization and deconvolution", SPIE vol. 1565 Adaptive Signal Processing, pp. 88-101, 1991.

[3] J.R. Treichler and B. G. Agee, "A new approach to multipath correction of constant modulus signals", IEEE Trans. Acoustics, Speech, Signal Processing, vol. 31, pp. 459-472, Apr 1983.

[4] J. Yang, J.-J. Werner, and G. A. Dumont, "The multimodulus blind equalization and its generalized algorithms," IEEE Journal on selected areas in communication, 20(5):997–1015, June 2002.

[5] K. Banovic, E. Abdel-Raheem, and M.A.S. Khalid, "A novel radius-adjusted approach for blind adaptive equalization," IEEE Signal Processing Lett., vol. 13, No.1, pp. 37-40, Jan. 2006.

[6] K. Banovic, Blind Adaptive Algorithms for QAM Signals: New Algorithms and Hardware Implementation, M.Sc. Thesis, University of Windsor, Canada, 2006.

[7] Godard, D. N., "Self-recovering equalization and carrier tracking in two-dimensional data communication systems," IEEE Trans. on Communications.1980

[8] Fijalkow, I., C. E. Manlove, and C. R. Johnson, Jr., "Adaptive fractionally spaced blind CMA equalization: Excess MSE," IEEE Trans. on Signal Processing, Vol. 46, No. 1, 227–231, 1998.

[9] Ding, Z., R. A. Kennedy, B. D. O. Anderson and C. R. John- son, Jr., "Ill-convergence of godard blind equalizers in data communication systems," IEEE Trans. on Communications, Vol. 39.

[10] Johnson, Jr., C. R., S. Dasgupta, and W. A. Sethares, "Averaging analysis of local stability of a real constant modulus algorithm adaptive filter," IEEE

[11] Brown, D.R., P. B. Schniter, and C. R. Johnson, Jr., "Computationally efficient blind equalization," 35th Annual Allerton Conference on Communication, Control, and Computing, September 1997.

[12] Casas, R. A., C. R. Johnson, Jr., R. A. Kennedy, Z. Ding, and R. Malamut, "Blind adaptive decision feedback equalization: A class of channels resulting in ill-convergence from a zero initialization," International Journal on Adaptive Control and Signal Processing Special Issue on Adaptive Channel Equalization

[13] Johnson, Jr., C. R. and B. D. O. Anderson, "Godard blind equalizer error surface characteristics: White, zero-mean, binary source case," International Journal of Adaptive Control and Signal Processing, Vol. 9, 301–324.

[14] Al-Kamali, F. S., M. I. Dessouky, B. M. Sallam, and F. E. Abd El-Samie, "Frequency domain interference cancellation ," Progress In Electromagnetics Research.

[15] Hanks and H.Zeng and Lang Tong "The Mse Perfromance Of Constant Modulus Algorithm".

[16] Sridha vambu, Sergio Verdu, Rodney A. Kennedy and William Sethares "Convex Cost functions in Blind Equalization". IEEE trans on signal processing vol 42., no. 8. 1994.

[17] J. J. Shynk et al., "A comparative performance study of several blind equalization algorithms", SPIE vol. 1565 Adaptive Signal Processing, pp. 102-117, 1991.

[18] L. He, M. G. Amin, Jr. C. Reed, and R. C. Malkemes. A hybrid adaptive blind equalization algorithm for QAM signals in wireless communications. IEEE Transactions on Signal Processing, 52(7):2058–2069, July 2004.

[19] T. Aboulnasr and K. Mayyas, "A robust variable step-size LMS algorithm: analysis and simulation," IEEE Trans. Signal Processing, vol. 45, no. 3, pp. 631-639, March 1997.

[20] P. Sristi, W.-S. Lu, and A. Antoniou, "A new variable-step-size LMS algorithm and its

application in subband adaptive filtering for echo cancellation," Proc. IEEE Int. Symp. On Cir. & Syst., pp. II-721-724, May 2001.

[21] Z. Ramadan and A. Poularikas, "Performance analysis of a new variable step-size LMS algorithm with error nonlinearities," Proc. IEEE ISSEC, pp. 384-388, 2004.

[22] C.R. Johnson, Jr. et al. "Blind equalization using the constant modulus criterion: A review," Proc. of the IEEE, vol. 86, pp. 1927-50, Oct. 1998.

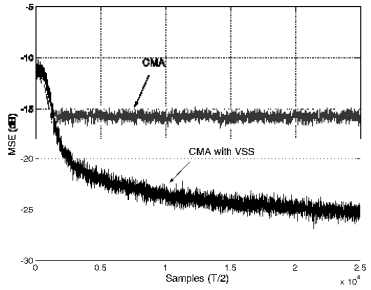

Fig. 2: Convergence Analysis with CMA and VSS CMA

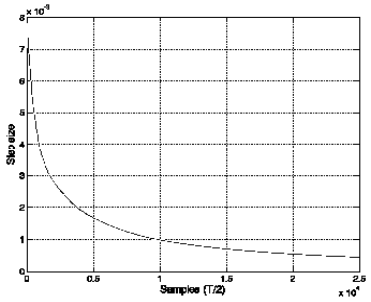

Fig. 3 : The variation of μ versus samples.

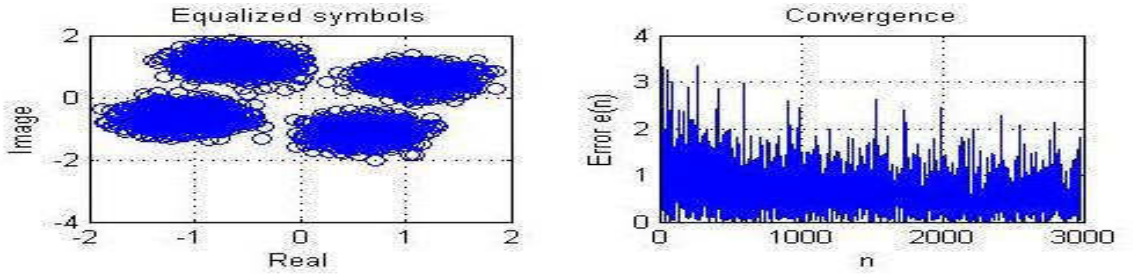

Fig. 4 **:** Adaptive blind equalization using CMA without variable step size(μ)

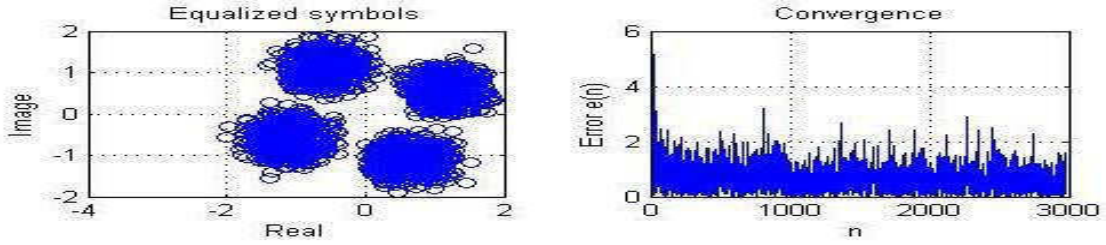

Fig. 5 **:** Adaptive blind equalization using CMA with variable step size (μ)

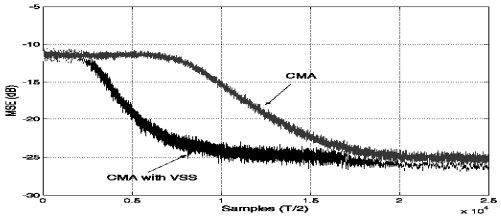

Fig. 6 : Convergence curves for CMA using $\mu(n) = \mu = 2^{-11}$, and for CMA with VSS using $\mu(0) = 2^{-9}$

A fast and Accurate Method for Computing Semi Analytic BER for PSK with ISI and AWGN

Naveen Kumar. M & Baskar Reddy

Dept. of ECE, QISCET, Ongole, A.P.,

Abstract - Digital modulation is undoubtedly significant portion in wireless communication technology. It allows the transmission of digital data via the air on high frequency carrier waves. In, Digital transmission the number of bit errors is the number of received bits of a data stream over a communication channel that have been altered due to noise, interference, distortion or bit synchronization errors. There are several techniques for accelerating the estimation of BER. The method considered here is called the semi analytic or quasi analytic method.

Semi analytic bit error rate (New approach) estimation is a well-known method for evaluating the BER of a digital communication system. The main utility of the method is the significant time savings in computation relative to Monte Carlo simulation. Despite this advantage, no known reference defines the procedure for computing exact BER for M-array phase shift keying(PSK) with ISI and AWGN using the semi analytic method. This paper defines an efficient procedure for computing exact semi analytic BER for modulation formats with circular constellations when the noise component of the decision variable has a circularly symmetric Gaussian distribution. Technique is demonstrated for 8-PSK over Digital Video Broadcasting Satellite Second Generation (DVB-S2) channel.

Key words - *Computer aided analysis, digital communication, error analysis, phase shift keying, simulation.*

I. INTRODUCTION

COMPUTER methods for determining the probability of bit error P***b*** or BER of a digital communication system are widely used when an accurate Analytic expression for BER is not available. The most general technique for BER estimation is the Monte Carlo method. A simulation is performed by passing a known data sequence through a system model and counting the bit errors at the receiver decision device. A simple and unbiased estimator of the BER is the sample mean of the simulated BER. If N is the number of bits evaluated, then as $N \rightarrow \infty$ the estimate will converge to the true BER. In practice, the rule of thumb that N should be on the order of $10/Pb$ produces a 90% confidence interval of about two on the BER estimate. Simulations of systems operating at very low error probabilities therefore require prohibitively large run times to accurately estimate BER using the Monte Carlo method.

There are several techniques for accelerating the estimation of BER [1]-[4]. The method considered here is called the semi analytic or quasi analytic method.With this method the problem is broken into two parts, the first dealing with the signal component, and the second dealing with the noise component of the decision variable at the receiver. For a known data sequence and a static channel, the demodulated and sampled signal component at the decision device is deterministic and can be evaluated by simulation.

The Data sequence used in the simulation should have specific properties in order to emulate random data with equi probable symbols. Using this noise free sequence of demodulated and detected decision variables, then if the probability density of the noise component is known, the BER can be computed. This is done by integrating the noise probability density function (pdf) centered about each of the simulated noise free decision variable points over each error event region. Each integral is then weighted by the corresponding number of bit errors and the sample mean over all the weighted integrals produces the BER. Because of the complexity of this procedure for M-array PSK, previous references have presented only approximations [4]. For ideal M-array PSK with known symbol probabilities and arbitrary symbol bit-mapping it is possible to compute the exact BER for the additive white Gaussian noise (AWGN) channel in an efficient way [5]. By extending these methods to include the effects of inter symbol interference(ISI), an efficient procedure for computing semi analytic BER was developed.

II. PSK CONSTELLATION WITH ISI AND AWGN

The M signal waveforms for ideal M-ary PSK are represented as

$$s_m(t) = g(t)\cos(\omega_c t + \theta_m) \qquad m = 0, 1, ..., M-1 \quad (1)$$

Where g(t) is a pulse waveform used to shape the spectrum of the transmitted signal and θm is the information-bearing phase angle which takes M possible values

$$\theta_m = \frac{(2m+1)\,\pi}{M} \qquad m = 0, 1, ..., M-1. \quad (2)$$

If an ideal PSK signal is optimally demodulated, then using complex phasor notation, each of the complex decision variables takes one of the following M values

$$S_m = \varepsilon e^{j\theta_m} \qquad m = 0, 1, ..., M-1 \quad (3)$$

Where ε is the energy of the spectrum shaping pulse and is given in terms of bit energy Eb by

$$\varepsilon = \log_2(M)\, E_b.$$

Fig. 1 shows the ideal symbol locations Sm and decision regions Rm for 8PSK.

When distortions due to channel effects or modem imperfections are present, the received decision variables will differ from the M ideal points, and their locations will data dependent due to ISI. In this context, ISI will refer to the effects of both linear and non-linear time invariant distortions with memory. Assuming equi probable symbols, then in order to completely characterize the ISI of a channel with L symbol periods of memory, it is sufficient to consider all possible sequences of L symbols.

A maximal length pseudorandom M^L symbol sequence will satisfy this property. For M=2, linear feedback shift registers can be used to generate maximal length pseudorandom bit sequences.For M>2, efficient methods for generating maximal length pseudorandom symbol sequences have also been proposed [6][7].With the addition of cyclic prefixes and postfixes of L symbols each, a simulation using one cycle of a M^L length pseudorandom symbol sequence is sufficient to emulate equi probable data symbols. Therefore, performing a simulation using $M^L + 2L$ Symbols from a maximal length M^L symbol sequence, and discarding the first and last L demodulated and detected decision variable points, the resulting M^L decision variable points will completely characterize the effect of the system ISI on the signal. This set of decision variables can be defined in terms of their respective magnitudes and phases or in-phase and quadrature components

$$s_k = r_k e^{j\theta_k} = i_k + jq_k \qquad k = 0, 1, ..., M^L - 1. \quad (4)$$

When AWGN is present at the receiver input, the decision variables are

$$y_k = s_k + n_k \qquad k = 0, 1, ..., M^L - 1. \quad (5)$$

For a receiver having an arbitrary discrete time detection filter with impulse response h(n), the noise component nk at the filter output is a sequence of complex Gaussian distributed random variables each with mean zero and variance given by

$$\sigma^2 = \sigma_r^2 + \sigma_i^2 = N_0 \sum_{n=-\infty}^{\infty} |h(n)|^2 = \frac{N_0}{2\pi} \int_{-\pi}^{\pi} |H(e^{j\omega})|^2 \, d\omega. \quad (6)$$

where σ2 r and σ2 i are the variances of the real and imaginary components respectively, and N0 is the one-sided power spectral density (psd) of the AWGN.

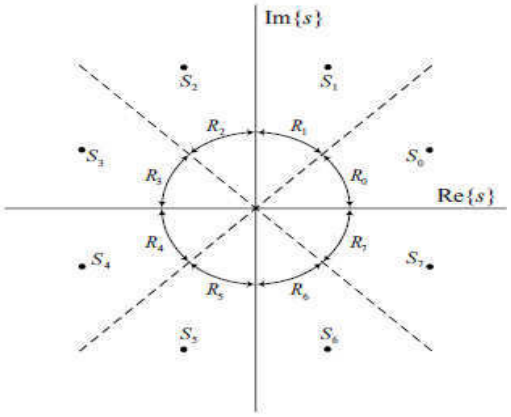

Fig. 1. Ideal 8PSK symbols S_m and decision regions R_m.

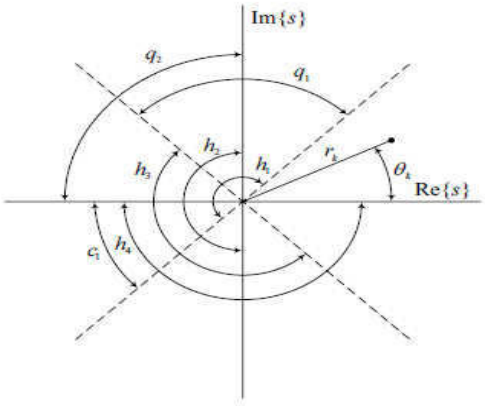

Fig. 2. 8PSK decision regions showing half-planes, quadrant planes, and correction planes. A single noise free decision variable s'_k with ISI is also shown.

III. BIT ERROR RATE CALCULATION

Since a pseudorandom symbol sequence emulates equiprobable symbols, averaging the BER over all of the resulting decision variable points will determine the BER of the system. The bit error probability is therefore given by

$$P_b = \frac{1}{M^L} \sum_{k=0}^{M^L-1} P_b(s_k, m) \qquad (7)$$

Where Pb(sk,m) is the bit error probability for decision variable sk with correct decision region Rm. An expression for Pb(sk,m) is

$$P_b(s_k, m) = \frac{1}{\log_2(M)} \sum_{n=0}^{M-1} w_{mn} P_{n/m}(s_k). \qquad (8)$$

The term $P_{n/m}(s_k)$ is the probability that the received decision variable s_k from region R_m would fall in decision region R_n under the influence of noise, and w_{mn} is the number of bit errors that occurs in this event. For an arbitrary bit mapping, the bit error weight matrix **W** with elements w_{mn} can be generated from the weight matrix for the binary bit mapping by swapping rows and then columns according to the desired symbol assignment.

Equation (8) can be simplified by noting that each received decision variable can be rotated to decision region R_0 provided that the bit error weight matrix **W** is appropriately tansformed as well. The rotated decision variable from decision region R_m is

$$s'_k = e^{-\mathrm{j}\frac{2\pi m}{M}} s_k. \qquad (9)$$

The required transformation for the **W** matrix consists of a cyclic left shift of row m by m positions. This operation can be expressed as

$$w'_{mn} = w_{m(n+m) \bmod M}. \qquad (10)$$

In terms of the transformed variables, (8) becomes

$$P_b(s_k, m) = \frac{1}{\log_2(M)} \sum_{n=1}^{M-1} w'_{mn} P_{n/0}(s'_k). \qquad (11)$$

In this way, only the error event probabilities for decision variables from decision region R0 need to be computed. This situation is depicted in Fig. 2. Expressing (11) in vector notation produces

$$P_b(s_k, m) = \frac{1}{\log_2(M)} \boldsymbol{w}^T(k)\boldsymbol{p}(k) \qquad (12)$$

Where **p**(k) is a column vector with elements $P_{n/0}(s'_k)$ for n=1,2,. . . ,M-1 and $\boldsymbol{w}^T(k)$ is a row vector with elements taken from row m and columns 1 through M-1 of the weight matrix **W**'. Note that column 0 need not be included because this corresponds to a correct decision, and the weight is therefore always 0. Substituting (12) into (7) produces

$$P_b = \frac{1}{M^L \log_2(M)} \sum_{k=0}^{M^L-1} \boldsymbol{w}^T(k)\boldsymbol{p}(k). \qquad (13)$$

The main difficulty in evaluating (13) is the computation of the individual error event probabilities $P_{n/0}(s'_k)$ for n=1,2,. . . ,M-1. The probabilities could be evaluated for each decision variable point by numerically computing M-1 double integrals over the error event regions. By generalizing the method presented in [5] to include ISI, a significant improvement in computational speed and accuracy can be achieved relative to direct numerical integration. This is done by expressing a set of half-plane, quarter-plane, and correction plane probabilities in terms of the desired $P_{n/0}(s'_k)$ and solving this system of equations for $P_{n/0}(s'_k)$ For an M-ary PSK decision variable specified by s'_k as shown in Fig. 2 and circularly symmetric additive Gaussian distributed noise, M/2 independent half-plane probabilities and M/4 independent quarter-plane probabilities can be written as

$$h_i(k) = \frac{1}{2}\mathrm{erfc}\left(\frac{r_k \sin\left(\frac{2\pi i}{M} - \theta_k\right)}{\sigma}\right) \quad i = 1, 2, \ldots, \frac{M}{2} \qquad (14)$$

$$q_i(k) = h_i(k)\left(1 - h_{i+M/4}(k)\right) \quad i = 1, 2, \ldots, \frac{M}{4}. \qquad (15)$$

In addition to the 3M/4 probabilities specified by (14) and (15), the remaining required M/4-1 independent probabilities can be found using the following correction plane probabilities

$$c_i(k) = \frac{1}{\pi\sigma^2} \int_0^{\infty} \int_{\tan\left(\frac{2i\pi}{M}\right)x}^{\tan\left(\frac{2(i-1)\pi}{M}\right)x} e^{\frac{-\left((x+i_k)^2+(y+q_k)^2\right)}{\sigma^2}} dy dx$$
$$i = 1, 2, \ldots, \frac{M}{4} - 1 \qquad (16)$$

Where ik = rk cos(θk) and qk = rk sin(θk). The expressions for the probabilities (14)-(16) are given by integrating the circularly symmetric Gaussian pdf over the specified regions.

Evaluating the inner integral of (16) produces

$$c_i(k) = \frac{1}{2\sqrt{\pi\sigma^2}} \int_0^\infty e^{\frac{-(x+q_k)^2}{\sigma^2}} f(x;i,M,q_k,\sigma)\ dx \qquad (17)$$
$$i = 1,2,...,\frac{M}{4}-1$$

Where the integrand term is

$$f(x;i,M,q_k,\sigma) = \operatorname{erfc}\left(\frac{\tan\left(\frac{2(1-i)\pi}{M}\right)x+q_k}{\sigma}\right) - \operatorname{erfc}\left(\frac{\tan\left(\frac{2i\pi}{M}\right)x+q_k}{\sigma}\right). \qquad (18)$$

The values for the correction plane probabilities ci(k) specified by (17) and (18) can be evaluated by numerical integration. Expressions for the half-plane, quarter plane, and correction plane probabilities can also be written in terms of the desired probabilities Pn/0(s'k)

$$h_i(k) = \sum_{n=i}^{\frac{M}{2}+(i-1)} P_{n/0}(s'_k) \qquad i = 1,2,...,\frac{M}{2} \qquad (19)$$

$$q_i(k) = \sum_{n=i}^{\frac{M}{4}+(i-1)} P_{n/0}(s'_k) \qquad i = 1,2,...,\frac{M}{4} \qquad (20)$$

$$c_i(k) = \sum_{n=\frac{M}{2}-(i-1)}^{\frac{M}{2}+(i-1)} P_{n/0}(s'_k) \qquad i = 1,2,...,\frac{M}{4}-1\,. \qquad (21)$$

The system of linear equations specified by (19)-(21) can be expressed compactly in matrix-vector notation as

$$\boldsymbol{z}(k) = \boldsymbol{A}\boldsymbol{p}(k) \qquad (22)$$

Where **z**(k) is a known column vector of h(k), q(k), and c(k) values, **A** is a matrix of known coefficients, and **p**(k) is an unknown column vector of Pn/0(s'k) values. The matrix **A** and the form of the vector **z**(k) are determined by the PSK modulation order M. For 8PSK they are given by

$$\boldsymbol{A} = \begin{bmatrix} 1 & 1 & 1 & 1 & 0 & 0 & 0 \\ 0 & 1 & 1 & 1 & 1 & 0 & 0 \\ 0 & 0 & 1 & 1 & 1 & 1 & 0 \\ 0 & 0 & 0 & 1 & 1 & 1 & 1 \\ 1 & 1 & 0 & 0 & 0 & 0 & 0 \\ 0 & 1 & 1 & 0 & 0 & 0 & 0 \\ 0 & 0 & 0 & 1 & 0 & 0 & 0 \end{bmatrix} \quad z(k) = \begin{bmatrix} h_1(k) \\ h_2(k) \\ h_3(k) \\ h_4(k) \\ q_1(k) \\ q_2(k) \\ c_1(k) \end{bmatrix}. \qquad (23)$$

The system of equations specified by (22) can be solved for the unknown probabilities

$$\boldsymbol{p}(k) = \boldsymbol{A}^{-1}\boldsymbol{z}(k). \qquad (24)$$

Substituting (24) into (13) produces the desired expression for the bit error probability

$$P_b = \frac{1}{M^L \log_2(M)} \sum_{k=0}^{M^L-1} \boldsymbol{w}^T(k)\boldsymbol{A}^{-1}\boldsymbol{z}(k). \qquad (25)$$

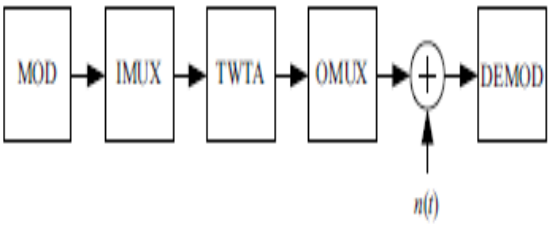

Fig. 3 : Simulation Model

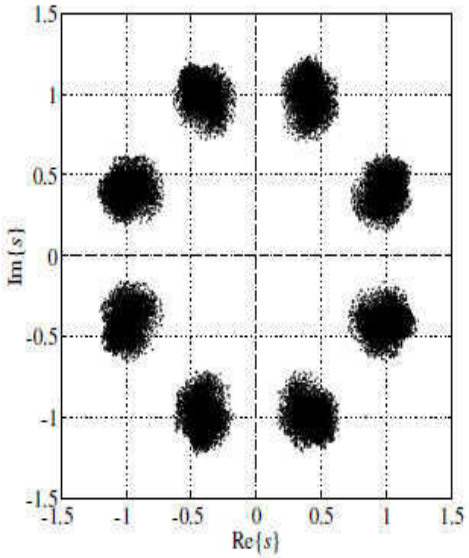

Fig. 4. Noise free decision variable points s_k used for the semianalytic BER computation of uncoded 8PSK and the DVB-S2 channel.

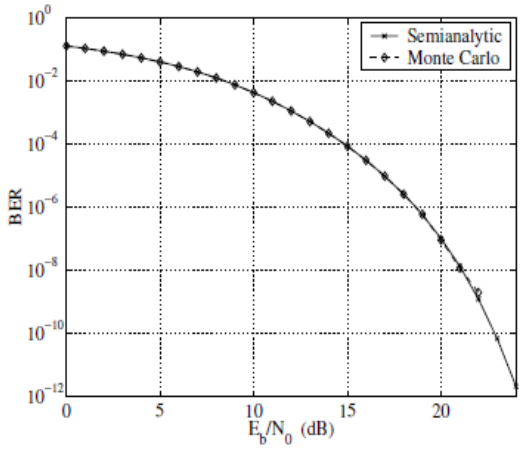

Fig. 5. Semianalytic and Monte Carlo BER as a function of SNR for uncoded 8PSK and the DVB-S2 channel.

IV. APPLICATION EXAMPLE

To serve as an example of the proposed method, the BER for un coded 8PSK with the DVB-S2 satellite channel was evaluated and compared to the results of Monte Carlo simulation. A block diagram of the model used for the simulations is shown in Fig. 3. The characteristics of the channel model are specified in the DVB-S2 standard [8].The complex baseband simulations were performed using an 8PSK pseudorandom symbol sequence sampled at 16 samples/symbol. A Gray coded symbol bit mapping was used and the symbol pulse shaping filter had a square-root raised cosine magnitude response with a roll-off factor of 0.35. A 10th order rational transfer function was used to approximate the specified frequency response of the input multiplexer (IMUX) filter and a 6th order rational transfer function was used for the output multiplexer (OMUX) filter. The signal at the traveling wave tube amplifier (TWTA) model input was scaled to a level corresponding to 1dB of input back off (IBO). The TWTA produces a pass band nonlinearity that was modeled using the non-linearised amplitude modulation-to amplitude modulation (AM/AM) and amplitude modulation to-phase modulation (AM/PM) conversions specified in the standard. The output from the OMUX filter was applied to a square-root raised-cosine detection filter with roll-off factor 0.35 and then interpolated by 4. The optimal sample phase, carrier phase, and gain were then jointly determined to produce decision variables with the minimum mean squared error relative to the ideal symbol locations.

From [8] it can be seen that the pass band channel memory spans approximately 5 symbol periods due to the IMUX and OMUX filters, so a value of L=5 was chosen. For the Semi analytic BER computation, only one cycle of a length 32768 pseudorandom symbol sequence with a small cyclic prefix and postfix was simulated. After discarding the decision variable points corresponding to the prefix and postfix, the resulting set of points shown in Fig. 4 was used to compute the BER according to (25).

For the Monte Carlo BER estimate, 10173 cycles of the 32768 length pseudorandom symbol sequence were simulated for a total of approximately 109 bits. AWGN was applied to the receiver detection filter and the resulting decision variable noise components were scaled and added to the deterministic components to emulate the desired effective SNR at the receiver input. Bit errors were then counted to produce BER estimates. The results of the semi analytic and Monte Carlo simulations are plotted in Fig. 5. The differences between the results are consistent with the expected estimation error for a Monte Carlo simulation of 109 bits in length. While the Monte Carlo simulation produced no errors when the SNR was greater than 22dB, the semi analytic method produced accurate results at all signal-to-noise ratios.

V. CONCLUSION

A fast and accurate method for computing semi analytic BER for PSK with ISI and AWGN has been presented. Two simplifications were applied relative to directly evaluating the Semi analytic BER using numerical integration. First, the decision variable points were each rotated to decision region $R0$, and the bit error weight matrix was appropriately transformed. Second, the process of numerically computing M-1 double integrals for each decision variable point was simplified to require only the evaluation of complementary error functions and M/4-1 single integrals. The technique is applicable to ideally demodulated and matched filter detected PSK with a static channel distortion, and produces an exact BER result when the received noise has a circularly symmetric Gaussian distribution. The basic approach can also be applied for any circularly symmetric noise distribution by simply re-deriving the half-plane and correction-plane probabilities of (14) and (16) for the desired pdf.

An extension of the technique to include synchronization errors in the demodulator is described in [3] and is referred to as the statistical averaging method. In a similar way, the technique can also be extended to frequency non-selective slowly fading channels [9]. The BER specified by (25) that accounts for time invariant distortions such as high power amplifier nonlinearity and non-ideal filtering is first expressed as a function of αrk, αik , and αqk, where α accounts for the effect of fading. The resulting expression is then averaged over the pdf of α. Depending on the pdf considered, some of the integrals may be evaluated analytically to produce a computationally efficient procedure for determining exact BER in a flat fading environment.

REFERENCES

[1] M. Jeruchim, “Techniques for estimating the bit error rate in the simulation of digital communication systems," IEEE J. Select. Areas Commun., vol. SAC-2, pp. 153-170, Jan. 1984.

[2] W. Tranter and K. Kosbar, “Simulation of communication systems," IEEE Commun. Mag., vol. 32, no. 7, pp. 26-35, July 1994.

[3] M. Jeruchim, P. Balaban, and K. Shanmugan, Simulation of Communications Systems. New York: Plenum,

[4] F. Gardner and J. Baker, Simulation Techniques: Models of Communications Signals and Processes. New York: Wiley, 1997.

[5] M. Irshid and I. Salous, “Bit error probability for coherent M-ary PSK systems," IEEE Trans. Commun., vol. COM-39, pp. 349-352, Mar. 1991.

[6] E. Pinto and J. Brandao, “On the efficient use of computer simulated digital signals to evaluate performance parameters," IEEE J. Select. Areas Commun., vol. SAC-6, pp. 52–57, Jan. 1988.

[7] M. Kavehrad and P. Balaban, “Digital radio transmission modeling and simulation," in Proc. IEEE GLOBECOM ‘89, Dallas, TX, pp. 1289-1294,Nov. 1989.

[8] ETSI EN 302 307 V1.1.1 (2005-03); “Digital video broadcasting (DVB);second generation framing structure, channel coding and modulation systems for broadcasting interactive services, news gathering and other broadband satellite applications."

[9] J. Proakis, Digital Communications, 3rd ed. New York: McGraw Hill, 1995.

◈◈◈

Performance Analysis of Mimo Wireless System in Frequency Selective Channel

Shuvabrata Bandopadhaya, Soumya Mishra & Jibendu Sekhar Roy

Dept. of E&TC, Silicon Institute of Technology, Bhubaneswar, Odisha, India

Abstract - The frequency-selectivity property of channel is the major bottleneck for the next generation wireless communication systems, which demands both high data rate transmission and a better quality of service guarantee. This paper analyses the impact of frequency selectivity on signal and the system performance through fading channel with feasible combinations of antennas at transmitter and receiver.

Key words - *Frequency selectivity, MIMO, R.M.S.delay-spread, Rayleigh Fading channel, Rician- K factor.*

I. INTRODUCTION

The frequency-selectivity property of channel is the major bottleneck for the next generation wireless communication systems, which demands both high data rate transmission and a better quality of service guarantee. Frequency selectivity occurs only if the signal's bandwidth is too large as compared to the channel's coherence bandwidth. The capacity of the fading channel is severely effected by frequency selectivity and described by

$$C = \underset{P(\gamma)}{Max} \int P(\gamma)\, P_a(\gamma) d\gamma \qquad (1)$$

Where $P_a(\gamma)$ is the power adaptation and $P(\gamma)$ is the distribution of fading SNR(γ)[1]. Implementation of multiple transmissions and receiving antenna popularly known as MIMO system exploits spatial diversity to combat feeding and considerably increase capacity.

This paper analyses the impact of frequency selectivity on signal and the system performance through fading channel with feasible combinations of antennas at transmitter and receiver. The performance of the system is judged considering the Rayleigh and Rician fading channels with different Doppler frequency

II. FREQUENCY SELECTIVE PROPERTY OF CHANNEL

In wireless communication systems, the transmitted signal propagates via several paths from transmitter to receiver leading to multi-path propagation. The multi-path components experiences different attenuations and phase changes, sum up at the receiver. This phenomenon leads to frequency selectivity. Generally the received multi-path band pass waveform can be written as [2]:

$$R(t) = R_e\left[\sum_{n=1}^{M} an \exp(j2\pi(f_c + f_d)(t-\tau_n)\right]\tilde{S}(t-\tau_n)] \qquad (2)$$

Where $\tilde{S}(t)$ = complex envelope of transmitter signal, f_c = carrier frequency.

f_d =Doppler's Frequency and n is number of multi-path.

More over due to non-static behavior of the channel impulse response, the channel parameters like path attenuation (a_n) and path delay (τ_n) undergoes random variation. Hence the channel may be described with it's statistical parameters like average delay $D_\tau(1)$ and rms delay spread $D_\tau(2)$ which are derived from power delay profile described by

$$G_\tau(\tau) = \int_{-\infty}^{\infty} G(\tau, f) df \qquad (3)$$

Where $G_\tau(\tau)$ is a 2D-scattering function. The average delay $D_\tau(1)$ is the first moment of the power delay profile described by

$$D_{\tau_k}(1) = \frac{\sum_k G_{\tau_k}(\tau_k)\tau_k}{\sum_k G_{\tau_k}(\tau_k)} \qquad (4)$$

The rms delay spread $D_\tau(2)$ is the second central moment of the power delay profile given by [3]

$$D_\tau(2) = \sqrt{D_\tau^2(1) - [D_\tau(1)]^2} \quad (5)$$

A channel is called as frequency selective when the rms delay spread $D_\tau(2)$ is greater than the bit duration.

A Rayleigh frequency selective fading signal having Doppler power spectrum s(v) is modeled as[4]

$$s(v) = \frac{1}{\pi f_d \sqrt{1 - \left(\frac{v}{f_d}\right)^2}} \quad (6)$$

Where v is the frequency shift relative to the carrier frequency and

$-fd \le v \le f_d$,

Where fd is the Doppler frequency.

The Rician distribution of a circularly symmetric complex Gaussian random variable (Z) applying central limit theorem is given by

$$P(Z,\theta) = \frac{Z}{2\pi\sigma^2} \exp[-(z^2 - 2C_u z\cos\theta + C_u^2)/2\sigma^2], \; Z \ge 0 \quad (7)$$

The Rician k-factor is defined as the ratio of signal power in dominant component over the local mean scattered power. Thus

$$K = \frac{C_u^2}{2\sigma^2} \quad (8)$$

Where C_u is the amplitude of the dominant component of line of sight(LOS) signal and σ^2 is the local mean scattered power .Assuming the scatterers being uniformly distributed around a circle at angle α_n with "k" rays emerging from each scatterer and with 'M' such scatterers, the Rayleigh frequency selective fading of the kth waveform over time t, can be modeled as[5]:

$$R(t,K) = \sqrt{\frac{2}{M}} \sum_{n-1}^{M} A_k(n)(\cos\beta_n + j\sin\beta_n) Cos(2\pi f_n t + \theta_n) \quad (9)$$

Where $A_k(n)$ is the weighting function used in eq-(9)

Here α_n, β_n, $\theta_{n,k}$ are model parameters with α set to zero.

$$\beta_n = \frac{\pi n}{M+1} \quad (10)$$

And $\theta_{n,k}$ used to generate multiple waveforms.

$$\theta_{n,k} = \beta_n + \frac{2\pi(K-1)}{M+1} \quad (11)$$

III. IMPLEMENTATION OF DIVERSITY THROUGH MIMO

Spatial diversity exploits the random nature of radio propagation by finding independent but highly uncorrelated signal path for communication. If $P(\gamma<\gamma_s)$ is the probability that a SNR of path will flow below the given threshold γ_s, then we can describe the Cumulative Density Function of a Rayleigh channel as[6]:

$$P(\gamma < \gamma_s)_N = (1 - e^{\frac{\gamma_s}{\Gamma}})^N \quad (12)$$

Where Γ= mean SNR

γ= instantaneous SNR

N=No of antennas/branches

In a MIMO system, the equivalent low pass channel, impulse response between j^{th} transmitting antenna and i^{th} receiving antenna.

$H_{ji}(\tau;t)$ where 'τ' is the delay & 't' is the time variable.

$$H(\tau,t) = \begin{bmatrix} h_{11}(\tau,t) & h_{12}(\tau,t) & \cdots & h_{1N}(\tau,t) \\ h_{21}(\tau,t) & h_{22}(\tau,t) & \cdots & h_{1N}(\tau,t) \\ \cdot & \cdot & \cdots & \cdot \\ \cdot & \cdot & \cdots & \cdot \\ \cdot & \cdot & \cdots & \cdot \\ h_{NR1}(\tau,t) & h_{NR2}(\tau,t) & \cdots & h_{NRNT}(\tau,t) \end{bmatrix} \quad (13)$$

If a signal $X_{j(t)}$ is transmitting antenna then the receiving signal at i^{th} receiving antenna is

$$r_i(t) = \sum_{j=1}^{N_t} \int_{-\infty}^{\infty} h_{ij}(\tau,t) * X_j(t-\tau) d\tau + \eta_i(t) \quad (14)$$

Where $\eta_i(t)$ is the additive noise.[7,8]

IV. SIMULATION RESULTS

A. *Fading envelope.*

Fig.-1 shows the fading envelope of various fading channel having different r.m.s. delay spreads. The channel having higher delay spread undergoes deeper fades.

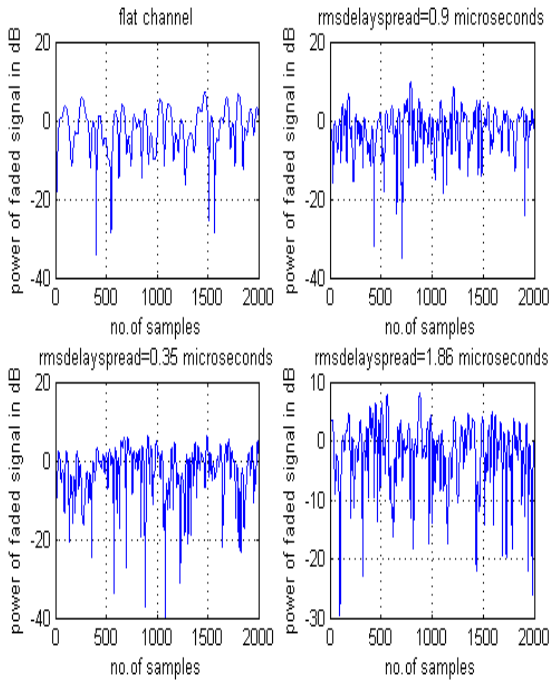

Fig. 1: Envelope of various fading channel having different r.m.s. delay spreads

B. Space diversity effect

Fig.-2 shows the impact of space diversity in a communication system. The performance curve is plotted for various feasible combinations of transmitting and receiving antennas.

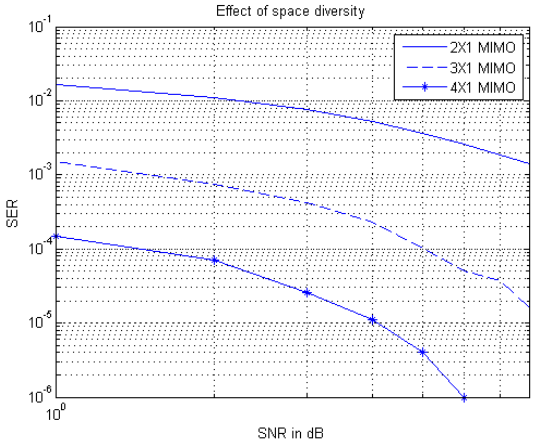

Fig. 2 : Impact of space diversity in a communication system

C. Effect of line of sight component on MIMO channel.

The strength of line of sight component of a communication channel is measured through K-factor. Fig-3 shows that with the increase of K-factor the system performance increase.

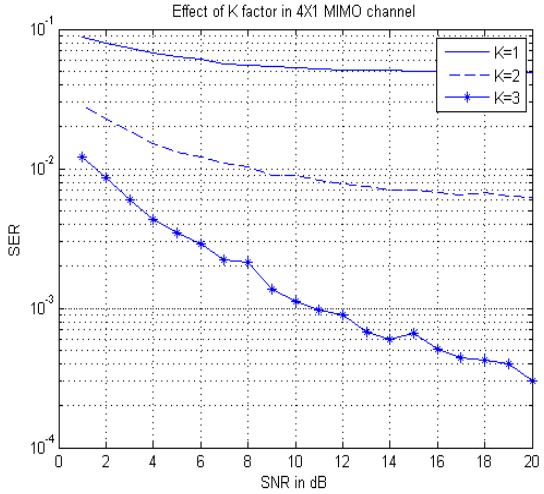

Fig.3 : Effect of K-factor in 4X1 MIMO channel

D. Doppler's effect on MIMO channel

Doppler's effect is a measure of the relative velocity between the transmitter and receiver causing spread in signal frequency. Fig-4 shows that increase of Doppler shift degrades the Quality of Service of a communication system

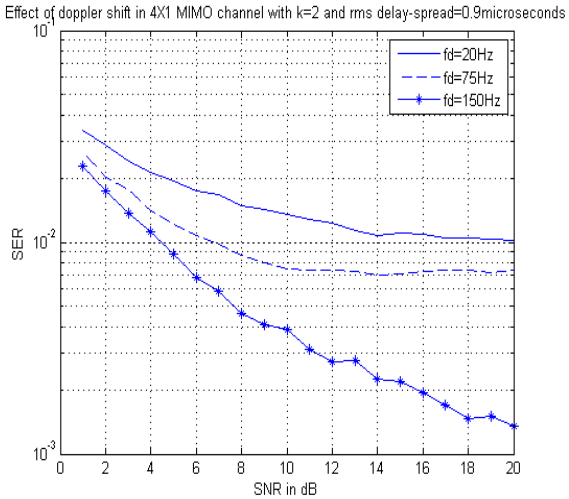

Fig. 4 : Effect of Doppler shift in MIMO channel

V. CONCLUSION

This paper analyses various aspects of frequency selective nature of the channel on communication system. The paper discusses varying combinations of multiple transmitting antenna with single receiving antenna to optimize design circuitry and power drain of small hand-held receiving devices. Additionally. the paper highlights the effect of frequency dispersion leading to signal fading. The paper also shows the effect of LOS component, improving the system performance with increase in K-factor. OFDM technique can be implemented on a frequency selective channel through proper equalization in order to mitigate the signal degradation due to fading.

REFERENCES

(1) A Blurr, "Evaluation of Capacity of indoor wireless MIMO channelizing ray racing" Proc. International Zurich Seminar on Communication, pp 28.1-6, 2002

(2) M. Patzold, "Methods of Modeling of Specified and Measured Multipath Power-Delay Profiles". IEEE Transactions on Vehicular Technology, Vol.51, NO.5, Sep 2002

(3) R.H Clarke "A statistical theory of Mobile Radio reception", Bell systems Technical Journal 47(6):pp-957-1000, 1968.

(4) W..C.Jakes, Microwave Mobile Communications.New York:John Wiley & Sons Inc., 1975.

(5) S. Bandopadhaya et al,"Design of DFE Based MIMO Communication System for Mobile Moving with High Velocity".S. Bandopadhaya et al. / (IJCSIT) International Journal of Computer Science and Information Technologies, Vol. 1 (5) , 2010,pp-319-323.

(6) J.G. Proakis, and Salehi, M, Communication system Engineering, Prentice Hall, 1994.

(7) S.M. Bahari, F.T. Bendi Merad , "Transmitter Design for LMS-MIMO-MCCDMA system with pilot channel estimates and Zero forcing equalizer". International Journal of Computer pp-258-263, Feb 2008

◈◈◈

A Low Complexity Fast Converging Selective Partial Update Adaptive Algorithm Employing Variable Step-Size for Acoustic Echo Cancellation

Andy W. H. Khong[1] , Woon-Seng Gan[2], Patrick A. Naylor[3] & Mike Brookes[4]

[1,3&4]Dept. of Electrical and Electronic Engineering, Imperial College London, UK
[2]School of Electrical and Electronic Engineering, Nanyang Technological University, Singapore

Abstract - Partial update adaptive algorithms have been proposed as a means of reducing complexity for adaptive filtering. The MMax tap-selection is one of the most popular tap-selection algorithms. It is well known that the performance of such partial update algorithm reduces with reducing number of filter coefficients selected for adaptation. We propose a low complexity and fast converging adaptive algorithm that exploits the MMax tap-selection. We achieve fast convergence with low complexity by deriving a variable step-size for the MMax normalized least-mean-square (MMax-NLMS) algorithm using its mean square deviation. Simulation results verify that the proposed algorithm achieves higher rate of convergence with lower computational complexity compared to the NLMS algorithm.

Key words - *acoustic echo cancellation, partial update adap- tive filtering, variable step-size, adaptive algorithms.*

I. INTRODUCTION

The profound interest in adaptive filtering with finite impulse response (FIR) arises due to its extensive application in signal processing. One of the most popular adaptive algorithms is the normalized least-mean-square (NLMS) algorithm [1][2] which has been applied to many applications including acoustic echo cancellation (AEC). To achieve effective echo cancellation, a replica of the echo is generated by means of modelling the Loudspeaker-Room-Microphone (LRM) system using an adaptive filter as shown in Fig. 1. Implementation of an acoustic echo canceller poses great challenges due to (i) the highly time-varying nature of the impulse response [3] and (ii) the long duration of the LRM system, which can require several thou- sands of filter coefficients for accurate modeling. Much recent re- search has aimed to develop fast converging algorithms that are necessary to track time variations in the LRM system. In addition, a typical room impulse response in the region of 50 to 300 ms re- quires an FIR adaptive filter with 400 to 2400 taps at 8 kHz sampling frequency. Since the NLMS algorithm requires $O(2L)$ multiply-accumulate (MAC) operations per sampling period, it is very desirable to reduce the computational workload of the processor, especially for the real-time implementation of AEC algorithms in portable devices where power budget is a constraint. As a result, a class of partial update adaptive filtering algorithms has been pro- posed that share the characteristic of executing tap update operations on only a subset of the filter coefficients at each iteration.

Partial update adaptive algorithms differ in the criteria used for selecting filter coefficients to update at each iteration. The Periodic-LMS and Sequential-LMS algorithms [4] employ tap-selection schemes that are independent of the input data. In the Periodic-LMS algorithm, reduction in computation is achieved at x(n)

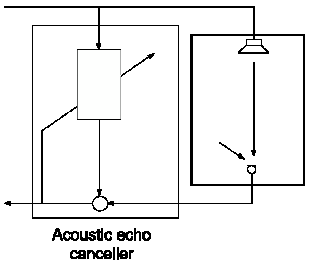

Fig. 1: Acoustic echo cancellation.

each time iteration by updating a subset of filter coefficients periodically whereas the Sequential-LMS algorithm employs the instantaneous gradient estimate at each time iteration by decimation in the tap space. In contrast, data dependent tap-selection criteria are employed in later algorithms including

Max-LMS [5] and MMax- NLMS [6][7]. Block-based and transform domain algorithms which generalized MMax-NLMS [8] have also been proposed. More recently, the MMax tap-selection criterion has been extended to a class of selective-tap algorithms including the MMax affine projection (MMax-AP) and MMax recursive least squares (MMax-RLS) algorithms [9]. The performance of these MMax-based adaptive algorithms for time-varying LRM systems has also been analyzed [9] and extended for the multichannel case [10]. It has been shown that the performance of MMax tap-selection is better than Periodic- and Sequential-LMS algorithms [11].

It is found that as the number of filter coefficients updated per iteration in a partial update adaptive filter is reduced, the computational complexity is also reduced but at the expense of some loss in performance. Hence the goal of the designers of such algorithms is to find ways to reduce the number of coefficients updated per iteration in a manner which degrades algorithm performance as little as possible. The aim of this paper is to propose a low complexity, fast converging adaptive algorithm for AEC. It has been shown in [9] that the convergence performance of MMax-NLMS is dependent on the step-size when identifying a LRM system. This motivates us to jointly utilize the low complexity of MMax tap-selection and the improvement in convergence performance brought about by a vari- able step-size. We begin by first analyzing the mean-square deviation of MMax-NLMS and deriving a variable step-size in order to increase its rate of convergence. We show through simulation examples that the proposed variable step-size MMax-NLMS (MMax- NLMS$_{VSS}$) algorithm achieves *higher rate of convergence* with *lower computational complexity* compared to NLMS for both white Gaus-sian noise (WGN) and speech inputs.

II. THE MMAX-NLMS ALGORITHM

Figure 1 shows an echo canceller in which, at the n^{th} iteration, $y(n) = \mathbf{x}^T(n)\mathbf{h}(n)$ where $(n) = [x(n), \ldots, x(n-L+1)]^T$ is the tap-input vector while the unknown LRM system $\mathbf{h}(n) = [h0\ (n), \ldots, hL-1\ (n)]^{\mathrm{T}}$ is of length L. An adaptive filter $\mathbf{h}(n) = [h0\ (n), \ldots, hL-1\ (n)]^{\mathrm{T}}$, which we assume [3] to be of equal length to the unknown system $\mathbf{h}(n)$, is used to estimate $\mathrm{h}(n)$ by adaptively minimizing the *a priori* error signal $e(n)$ using $n)$ defined by

$$e(n) = \mathbf{x}^T(n)\mathbf{h}(n) - y(n) + w(n), \qquad (1)$$

$$y(n) = \mathbf{x}^T(n)\mathbf{h}(n-1) \qquad (2)$$

with $w(n)$ being the measurement noise.

In the MMax-NLMS algorithm [6], only those taps correspond- ing to the M largest magnitude tap-inputs are selected for updating at each iteration with $1 \le M \le L$. Defining the subselected tap-input vector

$$\mathbf{x}(n) = \mathbf{Q}(n)\mathbf{x}(n), \qquad (3)$$

Where $\mathrm{Q}(n) = \mathrm{diag}\{\mathrm{q}(n)\}$ is a $L \times L$ tap selection matrix and $\mathbf{q}(n) = [q0\ (n), \ldots, qL-1\ (n)]$, element $qi\ (n)$ for $i = 0, 1, \ldots, L-1$ is given by,

$$qi(n) = \begin{cases} 1 & |x(n-i)| \{M \text{ maxima of } |\mathbf{x}(n)|\} \\ 0 & \text{otherwise} \end{cases} \qquad (4)$$

Where $|\mathbf{x}(n)| = |x(n)|, \ldots, |x(n-L+1)|^T$. Defining. ^{2} as the squared $l2$ -norm, the MMax-NLMS tap-update equation is then

$$\mathbf{h}(n) = \mathbf{h}(n-1) + \frac{\mu\mathbf{Q}(n)\mathbf{x}(n)e(n)}{\mathbf{x}(n)^2 + \delta}, \qquad (5)$$

Where δ is the regularization parameter. Defining $\mathbf{I}_{L\times L}$ as the $L \times L$ identity matrix, we note that if $\mathbf{Q}(n) = \mathbf{I}_{L\times L}$, i.e., with $M = L$, the update equation in (5) is equivalent to the NLMS algorithm. Similar to the NLMS algorithm, the step-size μ in (5) controls the ability of MMax-NLMS to track the unknown system which is re- flected by its rate of convergence. To select the M maxima of $|\mathbf{x}(n)|$ in (4), MMax-NLMS employs the SORTLINE algorithm [12] which requires $2\log_2 L$ sorting operations per iteration. The computational complexity in terms of multiplications for MMax-NLMS is $O(L + M)$ compared to $O(2L)$ for NLMS.

As explained in Section 1, the performance of MMax-NLMS normally reduces with the number of filter coefficients updated per iteration. This tradeoff between complexity and convergence can be illustrated by first defining

$$\eta(n) = \mathrm{h}(n) - \mathrm{h}(n)^2 \quad \mathrm{h}(n)^2 \qquad (6)$$

as the normalized misalignment. Figure 2 shows the variation in convergence performance of MMax-NLMS with M for the case of $L = 2048$ and $\mu = 0.3$ using a white Gaussian noise (WGN) input. For this illustrative example, WGN $w(n)$ is added to achieve a signal-to-noise ratio (SNR) of 20 dB. It can be seen that the rate

of convergence reduces with reducing M as expected. The dependency of the asymptotic performance and rate of convergence on M for MMax-NLMS has been analyzed in [9].

III. MEAN SQUARE DEVIATION OF MMAX-NLMS

It has been shown in [9] that the convergence performance of MMax- NLMS is dependent on the step-size μ when identifying a LRM system. Since our aim is to reduce the degradation of convergence performance due to partial updating of the filter coefficients, we propose to derive an adaptive step-size for MMax-NLMS. A similar approach was adopted in [13] for NLMS by analyzing the mean square deviation (MSD) of NLMS. Similar to the analysis of MMax-NLMS under time-varying unknown system conditions as shown in [9], we assume that the MMax-NLMS algorithm is able to track the unknown system.

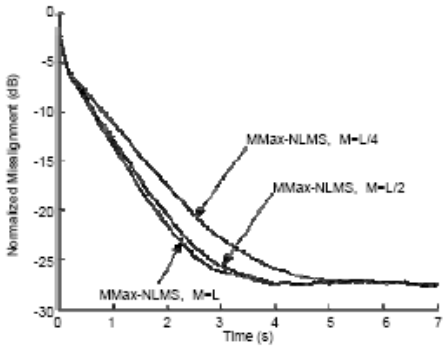

Fig. 2 : MMax-NLMS: Variation of convergence rate with number of filter coefficients selected for adaptation M for L = 2048, μ = 0.3, SNR=20 dB.

The MSD of MMax-NLMS can be obtained by first defining the system deviation as

$$(n) = \mathbf{h}(n) - \mathbf{h}(n), \quad (7)$$
$$(n-1) = \mathbf{h}(n) - \mathbf{h}(n-1). \quad (8)$$

Subtracting (8) from (7) and using (5), we obtain

$$(n) = (n-1) - \frac{\mu \mathbf{Q}(n)\mathbf{x}(n)e(n)}{\mathbf{x}^T(n)\mathbf{x}(n) + \delta}. \quad (9)$$

Defining $E\{\cdot\}$ as the expectation operator and taking the mean square of (9), the MSD of MMax-NLMS can be expressed iteratively as

$$E\ \|(n)\|^2 = E\ {}^T(n)\ (n)$$
$$= E\ \|(n-1)\|^2 - E\ \psi(\mu), \quad (10)$$

Where

$$E\ \psi(\mu) = E\ \frac{2\mu \mathbf{x}^T(n)\ (n-1)e(n)}{\|\mathbf{x}(n)\|^2} - \frac{\mu^2\ \|\mathbf{x}(n)\|^2 e^2(n)}{\|\mathbf{x}(n)\|^2\ {}^2} \quad (11)$$

and similar to [13], we assume that the effect of the regularization term δ on the MSD is small. The subselected tap-input vector (n) is defined by (3). As can be seen from (10), in order to increase the rate of convergence for the MMax-NLMS algorithm, we choose step-size μ such that $E\{\psi(\mu)\}$ is maximized.

IV. THE PROPOSED MMAX-NLMSVSS ALGORITHM

Following the approach of [13], we differentiate (11) with respect to μ. Setting the result to zero, we obtain,

$$E\ \frac{\mu(n)e(n)\|\mathbf{x}(n)\|^2 e(n)}{\|\mathbf{x}(n)\|^2\ {}^2} = E\ {}^T(n-1)\mathbf{x}(n)\ \|\mathbf{x}(n)\|^2\ {}^{-1} e(n)$$

giving the variable step-size

$$\mu(n) = \mu_{\max} \times \frac{\mathbf{x}\ {}^{-1}\ \mathbf{x}\ (n)\ (n\ \ 1)\ \mathbf{x}(n)\ {}^2}{{}^T(n-1)\ (n)\ \|\mathbf{x}(n)\|^2\ \ {}^T\ \ - \ \times\ \times}$$
$$\|\mathbf{x}(n)\|^2\ {}^T(n-1)\mathbf{x}(n)\ \|\mathbf{x}(n)\|^2\ \ {}^{-1}\mathbf{x}^T(n)\ (n-1) + \sigma_w^2 M(n)$$

where $0 < \mu\max \leq 1$ limits the maximum of $\mu(n)$ and we have defined [9]

$$M(n) = \frac{\|\mathbf{x}(n)\|^2}{\|\mathbf{x}(n)\|^2} \quad (12)$$

as the ratio between energies of the sub selected tap-input vector (n) and the complete tap-input vector x(n), while $\sigma^2 w = E\{w2\ (n)\}$. To simplify the numerator of $\mu(n)$ further, we utilize the relationship $x(n)x^T(n) = x(n)\ x^T(n)$ giving

$$\mu(n) = \mu_{\max} \times \frac{{}^T(n-1)\mathbf{x}(n)\ \|\mathbf{x}(n)\|^2\ {}^{-1}\mathbf{x}^T(n)\ (n-1)\times\|\mathbf{x}(n)\|^2}{\|\mathbf{x}(n)\|^2\ {}^T(n-1)\mathbf{x}(n)\ \|\mathbf{x}(n)\|^2\ {}^{-1}\mathbf{x}^T(n)\ (n-1) + \sigma_w^2 M(n)}.$$

We can now simplify $\mu(n)$ further by letting

$$\mathbf{x}(n)[\mathbf{x}^T(n)\mathbf{x}(n)]^{-1}\mathbf{x}^T(n)\ (n-1), \quad (13)$$
$$\|(n)\|^2 = M(n)\ {}^T(n-1)\mathbf{x}(n)\ \ \|\mathbf{x}(n)\|^2\ {}^{-1}\mathbf{x}^T(n)\ (n-1), \quad (14)$$

$$\|\mathbf{p}(n)\|^2 = M(n)\ {}^T(n-1)\mathbf{x}(n)\ \ \|\mathbf{x}(n)\|^2\ {}^{-1}\mathbf{x}^T(n)\ (n-1),$$
$$\|\mathbf{p}(n)\|^2 = {}^T(n-1)\mathbf{x}(n)\ \ \|\mathbf{x}(n)\|^2\ {}^{-1}\mathbf{x}^T(n)\ (n-1).$$

$$\|\mathbf{p}(n)\|^2 = M(n)\ {}^T(n-1)\mathbf{x}(n)\ \ \|\mathbf{x}(n)\|^2\ {}^{-1}\mathbf{x}^T(n)\ (n-1),$$
$$\|\mathbf{p}(n)\|^2 = {}^T(n-1)\mathbf{x}(n)\ \ \|\mathbf{x}(n)\|^2\ {}^{-1}\mathbf{x}^T(n)\ (n-1).$$

Following the approach in [13], and defining $0 << \alpha < 1$ as the smoothing parameter, we can estimate (n) and $\mathrm{p}(n)$ iteratively by

$$\mathrm{x}(n)[\mathrm{x}^T(n)\mathrm{x}(n)]^{-1}e_a \\ \mathrm{p}(n-1)+(1-\alpha) \qquad (n), \quad (15)$$

$$\mathrm{p}(n)=\alpha\mathrm{p}(n-1)+(1-\alpha)\mathrm{x}(n)[\mathrm{x}^T(n)\mathrm{x}(n)]^{-1}e(n), \quad (16)$$

where we have used $e(n) = \mathrm{x}^T(n)\ (n-1)$ in (16) while the error $e_a(n)$ due to active filter coefficients $\mathrm{x}(n)$ in (15) is given as

$$e_a(n) = \mathrm{x}^T(n)\ (n-1) = \mathrm{x}^T(n)[\mathrm{h}(n)-\mathrm{h}(n-1)]. \quad (17)$$

It is important to note that since $\mathrm{T}(n)\mathrm{h}(n)$ is unknown, we need to approximate $ea\ (n)$. Defining $\mathrm{Q}(n) = \mathrm{I}L\times L - \mathrm{Q}(n)$ as the tap-selection matrix which selects the inactive taps, we can express

$$e_i(n) = \overline{\mathrm{Q}}(n)\mathrm{x}(n)^T\ (n-1)$$

as the error contribution due to the inactive filter coefficients such that the total error $e(n) = ea\ (n) + ei\ (n)$. As explained in [9], for $0.5L \le M < L$, the degradation in $M(n)$ due to tap-selection is negligible. This is because, for M large enough, elements in $\mathrm{Q}(n)\mathrm{x}(n)$ are small and hence the errors $ei\ (n)$ are small, as is the general motivation for MMax tap-selection [7]. We can then approximate $ea\ (n) \approx e(n)$ in (15) giving

$$\mathrm{x}(n)\ \mathrm{x}^T(n)\mathrm{x}(n)\ ^{-1}e(n). \quad (18) \\ \mathrm{p}(n-1)+(1-\alpha)$$

Using (16) and (18), the variable step-size is then given as

$$\mu(n) = \mu_{\max}\frac{\mathrm{p}(n)^2}{M^2(n)\ \mathrm{p}(n)^2 + C} \quad (19)$$

Where $C = M2\ (n)\sigma 2$. Since $\sigma 2$ is unknown, it is shown that we can approximate C by a small constant, typically 0.01 [13].

We note that the computation of (16) and (18) each requires M additions. In order to reduce computation even further, and since for M large enough the elements in $\mathrm{Q}(n)\mathrm{x}(n)$ are small, we can approximate $\mathrm{p}(n)^2 \approx \mathrm{p}(n)^2$ giving

$$\mu(n) \approx \mu\max\ \frac{\mathrm{p}(n)^2}{\mathrm{M2(n)\ p(n)}} + \mathrm{C} \quad (20)$$

Table 1. The MMax-NLMSvss algorithm

$0 << \alpha < 1,$	$0 < \mu_{\max} \le 1, \quad C = 0.01,$
$e(n)$	$= y(n) - \mathrm{x}^T(n)\mathrm{h}(n-1) + w(n)$
$\mathrm{Q}(n)$	$= \mathrm{diag}\{\mathrm{q}(n)\}$
$q_i(n)$	$= \begin{cases} 1 & \lvert x(n-i)\rvert \in \{M \text{ maxima of } \lvert x(n)\rvert\} \\ 0 & \text{otherwise} \end{cases}$
$\mathrm{x}(n)$	$= \mathrm{Q}(n)\mathrm{x}(n)$
$\mathrm{p}(n)$	$= \alpha\mathrm{p}(n-1) + (1-\alpha)\mathrm{x}(n)[\mathrm{x}^T(n)\mathrm{x}(n)]^{-1}e(n)$
$M(n)$	$= \mathrm{x}(n)^2 / \mathrm{x}(n)^2$
$\mu(n)$	$= \mu_{\max}\ \mathrm{p}(n)^2 / M^2(n)\ \mathrm{p}(n)^2 + C$
$\mathrm{h}(n)$	$= \mathrm{h}(n-1) + \mu(n)\dfrac{\mathrm{Q}(n)\mathrm{x}(n)e(n)}{\mathrm{x}(n)^2 + \delta}$

When $\mathrm{Q}(n) = \mathrm{I}L\times L$, i.e., $M = L$, MMax-NLMS is equivalent to the NLMS algorithm and from (12), $M(n) = 1$ and $(n) = \mathrm{p}(n)\ 2$. As a consequence, the variable step-size $\mu(n)$ in (20) is consistent with that presented in [13] for $M = L$. The proposed MMax-NLMSvss is summarized in Table 1.

V. COMPUTATIONAL COMPLEXITY

We now discuss the computational complexity in terms of the number of multiplications required for the proposed MMax-NLMSvss algorithm at each sample iteration. Computation of (18) and $p(n)^2$ for (20) require M multiplications each. The computation of $\mathrm{x}(n)^2$ and $\mathrm{x}(n)^2$ for $M(n)$ in (12) requires 2 multiplications and a division using recursive means [11]. More importantly, since the term $\mathrm{x}(n)[\mathrm{x}^T(n)\mathrm{x}(n)]^{-1}\ e(n)$ is already computed in (18), no multiplications are now required for the update equation in (5).

Hence, including the computation of $\mathrm{x} = (n)\mathrm{h}\ (n-1)$ for $e(n)$MMax-NLMSvss requires $O(L + 2M)$ multiplications per sample period compared to $O(2L)$ for NLMS. The number of multiplication required for MMax-NLMS is thus less than NLMS when $M < L/2$. We note that although MMax-NLMSvss requires an additional 2 log2 L sorting operations per iteration using the SORTLINE algorithm [12], its complexity is still lower than NLMS. As with MMax-NLMS, we would expect the convergence performance for MMax-NLMSvss to degrade with reducing M. However, we shall show through simulation results that any such degradation is offset by the improvement in convergence rate due to $\mu(n)$.

VI. SIMULATION RESULTS

We demonstrate the performance of MMax-NLMSvss in terms of the normalized misalignment $\eta(n)$ defined in (6) using both WGN and speech inputs. Impulse response h(n) is generated using the method of images [14] in a room of dimension 4 × 5 × 3 m. The microphone and source positions are placed at coordinates $\{2.01, 2.5, 1.6\}$ and $\{2.1, 1.5, 1.6\}$ respectively. With a sampling rate of 8 kHz and a reverberation time of 256 ms, the length of the impulse response is L = 2048. Similar to [13], we have used C = 0.01, α = 0.95 and we added WGN $w(n)$ to $y(n)$ in order to achieve an SNR of 20 dB. We have used μmax = 1 for MMax-NLMSvss while step-size μ for the NLMS algorithm is adjusted so as to achieve the same steady-state performance for all simulations.

We illustrate first the improvement in convergence rate due to the variable step-size $\mu(n)$ for the MMax-NLMSvss algorithm. Figure 3 shows the improvement in convergence performance of MMax-5N1L2M. Svss over MMax-NLMS for the cases of M = 1024 and 512.

For each case, the proposed MMax-NLMSvss algorithm achieves an improvement of approximately 7 and 5.5 dB over MMax-NLMS in terms of normalized misalignment during initial convergence.

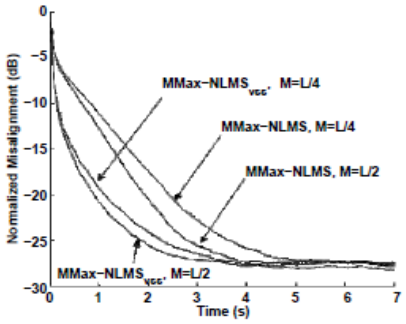

Fig. 3 : Comparison between MMax-NLMSvss and MMax-NLMS for L =2048 and SNR= 20 dB using WGN input.

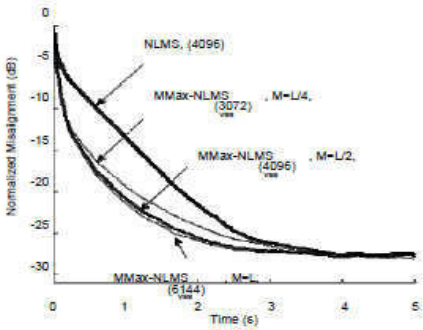

Fig. 4 : WGN input: Comparison between convergence performance of MMax-NLMSvss with NLMS for L = 2048 and SNR= 20 dB.

We next illustrate the tradeoff between computational complexity and convergence performance for the MMax-NLMSvss algorithm. We also compare the performance of MMax-NLMSvss and NLMS for a WGN input as shown in Fig. 4. The step-size of NLMS has been adjusted in order to achieve the same steady-state normalized misalignment. This corresponds to μ = 0.3. The number of multiplications per sample iteration required for each case is depicted between braces in the figure. As can be seen from Fig.4, for the same number of multiplications of 4096, the improvement of MMax-NLMSvss in terms of normalized misalignment compared with NLMS is approximately 8 dB during initial convergence. More importantly, the proposed MMax-NLMSvss algorithm outperforms NLMS even with lower complexitywhen M = 512. This improve- ment in normalized misalignment of 7 dB (together with a reduction of 25% in terms of multiplications) over NLMS is due to variable step-size for MMax-NLMSvss . The MMax-NLMSvss achieves the same convergence performance as the NLMSvss [13] when $M = L$.

The performance of MMax-NLMSvss for a male speech input is depicted in Fig. 5. For this simulation, we have used L =2048 and an SNR=20 dB as before. In order to illustrate the benefits of our proposed algorithm, we used M = 512 for both MMax-NLMS and MMax-NLMSvss . This gives a 25% savings in multiplications per iteration for MMax-NLMSvss over NLMS. As can be seen, even with this computational savings, the proposed MMax-NLMSvss al- gorithm achieves an improvement of 3.5 dB in terms of normalized misalignment over NLMS.

VII. CONCLUSIONS

We have proposed a low complexity fast converging partial update SPU-NLMSvss algorithm by introducing a variable step-size during adaptation.

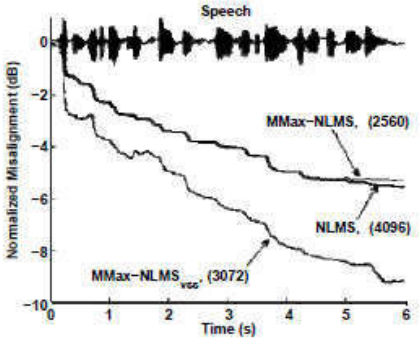

Fig. 5 : Speech input: Comparison between convergence performance of MMax-NLMSvss with NLMS for L = 2048, M = 512 and SNR= 20 dB.

This is derived by analyzing the mean-square deviation of SPU-NLMSvss. In terms of convergence performance, the proposed MMax-NLMSvss algorithm achieves approximately 5 dB improvement in normalized misalignment over NLMS for WGN and speech input respectively. More importantly, the proposed algorithm can achieve higher rate of convergence with lower computational complexity compared to NLMS.

REFERENCES

[1] B. Widrow, "Thinking about thinking: the discovery of the LMS algorithm," IEEE Signal Processing Mag., vol. 22, no. 1, pp. 100–106, Jan.2005.

[2] S. Haykin, Adaptive Filter Theory, 4th ed., ser. Information and System Science. Prentice Hall, 2002.

[3] E. Ha¨nsler, "Hands-free telephones- joint control of echo cancellation and postfiltering," Signal Processing, vol. 80, no. 11, pp. 2295–2305, Nov. 2000.

[4] S. C. Douglas, "Adaptive filters employing partial updates," IEEE Trans. Circuits Syst. II, vol. 44, no. 3, pp. 209–216, Mar. 1997.

[5] "Analysis and implementation of the MAX-NLMS adaptive filter," in Proc. Twenty-Ninth Asilomar Conference on Signals, Systems and Computers, vol. 1, 1995, pp. 659–663.

[6] T. Aboulnasr and K. Mayyas, "Selective coefficient update of gradient based adaptive algorithms," in Proc. IEEE Int. Conf. Acoustics Speech Signal Processing, vol. 3, 1997, pp. 1929–1932.

[7] "MSE analysis of the M-Max NLMS adaptive algorithm," in Proc. IEEE Int. Conf. Acoustics Speech Signal Processing, vol. 3, 1998, pp. 1669–1672.

[8] K. Dogancay and O. Tanrikulu, "Adaptive filtering algorithms with selective partial updates," IEEE Trans. Circuits Syst. II, vol. 48, no. 8, pp. 762–769, Aug. 2001.

[9] A. W. H. Khong and P. A. Naylor, "Selective-tap adaptive filtering with performance analysis for identification of time-varying systems," IEEE Trans. Audio Speech Language Processing, vol. 15, no. 5, pp. 1681 –1695, Jul. 2007.

[10] "Stereophonic acoustic echo cancellation employing selective tap adaptive algorithms," IEEE Trans. Speech Audio Processing, vol. 14, no. 3, pp. 785–796, Jul. 2006.

[11] A. W. H. Khong, "Adaptive algorithms employing tap selection for single channel and stereophonic acoustic echo cancellation," Ph.D. dissertation, Imperial College London, Feb. 2006.

[12] I. Pitas, "Fast algorithms for running ordering and max/min calculation," IEEE Trans. Circuits Syst., vol. 36, no. 6, pp. 795–804, Jun. 1989.

[13] H. C. Shin, A. Sayed, and W.-J. Song, "Variable step-size NLMS and affine projection algorithms," IEEE Signal Processing Lett., vol. 11, no. 2, pp. 132–135, Feb. 2004.

[14] J. B. Allen and D. A. Berkley, "Image method for efficiently simulating small-room acoustics," J. Acoust. Soc. Amer., vol. 65, no. 4, pp. 943–950, Apr. 1979.

◈◈◈

Study of Software Maintenance is Optional

M. D. Acharya[1] & R. R. Deshmukh[2]

[1]Yogeshwari College, Ambajogai
[2]Dr. B.A.M.University, Aurangabad

Abstract - Software maintenance and evolution is a considerably understudied area while taking into account its cost effects. thirty years ago software maintenance was characterized as an iceberg. We hope that what is immediately visible is all there is to it but we know that an enormous mass of potential problems and cost lies under the surface. The maintenance of existing software can account for over 60 percent of all effort expended by a development organsation and the percentage continues to rise as more software is produced. There is very low maintenance when we concentrate on the first two stages of software that is Analysis and design.

I. SOFTWARE MAINTENANCE

Maintenance takes up a considerable amount of software engineer's time. The goal of the study was to gain insight into the origin of maintenance and reduced the intensity of maintenance. The study is an example of analysis and design of the software engineering process. Analysis and design of a software process should lead to improvement of that process. data on the development process are required to be able to analyze it. The need for measurement and data collection of software development and maintenance is often stressed.

Software engineering research is on the development of new software products means that software engineer is finished by the time the product fulfills the requirements and the software is installed Boehm suggest that the three kinds of maintenance.

1) Corrective maintenance is maintenance performed in response to processing, performance, or implementation failures.

2) Adaptive maintenance is maintenance in response to chances in data and processing environments.

3) Perfective maintenance is maintenance performed to eliminate processing inefficiences, enhance performance or improve maintainability.

Software maintenance is often associated with software faults and failures. An error is defined as a defect in the human thought process. Faults are concentrate manifestations of errors within the software. Failures are departures of the software system form software requirements

II. ANALYSIS

The requirements gathering process is intensified and focused on software, to understand the nature of the programs to be built, the software analyst must understand the information domain behavior, performance and interface. requirements for both the system and the software are documented and reviewed with the customer. The distinction of construction of a software product and analysis of the software process is useful to direct improvement efforts. Analytic and constructive activities are distinguished

Analytic and constructive activities are distinguished, as well as analytic and constructive methods and tools are concerned with building products, analytic methods and tools are concerned with analyzing the constructive process and the resulting products. 'We need to clearly distinguish between the role of constructive and analytical activities. Only improved construction process will result in higher quality software. Quality cannot be tested or inspected into software. Analytic process (e.g. quality assurance) cannot serve as a substitute for constructive process but will provide control of the constructive process".

This distinction as made by Basili and Rombach provides insight into the control of software development. Data on the development process are required to be above to analyze software development. This is the appropriate place to quote Lord Kelvin from a century ago: 'When you measure what you are speaking about, and express it in numbers, you know something about it: but when you cannot measure it, when you cannot express it in numbers, you knowledge is of a meager and unsatisfactory kind; it may be the beginning of knowledge, but you have scarcely in your thoughts advanced to the stage of science.

Analysis and measurements should focus on one or a few aspects of the software process because they are time consuming activities. For example, it is possible to focus on reasons for delay in software development, on the impact of new tools, or on the impact of change requests on the development process. Anyway, the goal of the analysis should be clear. The goal should be quantified to allow for analysis and measurement. The Goad/Question/Metric paradigm can be an aid in goal setting and operationalization of analysis of software development. The paradigm represents an approach by which analysis goals are tailored to the needs of an organization. The goals are relined into a set of quantifiable questions that, in tits turn, specifies a set of metrics and data for collection. As such, analysis of software development is incorporated into the development process. The study described in this paper can be perceived as an example of the application of the Goal/Question/Metric paradigm.

III. DESIGN

It is actually a multistep process that focuses on four distinct attributes of a program. Data structure, software architecture, interface representations and algorithmic detail. The design process translates requirements into representation of the software that can be assessed for quality before coding begins, the design is documented and becomes part of the software configuration. The maintenance study took place in a department that was concerned with development and integration of system software in the operating system and data communications field. The department employed 175 software engineers and covered a range of 300 products. The quality assurance department consisted of 10 people and the methods and tools department employed five people. The maintenance study was a consequence of an earlier study on reasons for delay in software development[9]. Reasons for delay were studied because insight revealed from these can lead to improvement measures that should enable future projects to follow the plan more closely.

Analysis of 160 activities, comprising over 15 000 hours of work, resulted in a number of improvement measures, of which two will be named. The first measure was the introduction of maintenance weeks. Analysis of the collected data showed that maintenance activities in particular were a constant interruption to development and caused a considerable part of the delay. A number of possible ways of separating development and maintenance was discussed. It was decided to concentrate the maintenance work as far as possible in maintenance weeks and to include two maintenance weeks in each quarter. By carrying out most of the maintenance during these two weeks, development could proceed more quickly and with fewer interruptions during the other weeks.

A second measure was the start of the study that is discussed in this paper. The goal of the study was to increase the insight into the origin of maintenance. The reasons for the delay study focused on the control aspects of time and cost, while the maintenance study focused on the aspect of quality. This study focused on maintenance reports. Pettijohn[10] pointed out that maintenance reports are one of the two primary sources of quality data; the other source is inspection data. Maintenance reports were named 'problem reports' by the department concerned. A problem report can be written by engineers within the development department, employees outside the development department, or customers who perceive a problem. A problem can be a software failure. Problem reports can, however, also be abused, An additional requirement may be formulated, incorrectly, by a user as a problem in a problem report. The term problem will in this paper refer to a shortcoming of a software product, as perceived by the writer of a problem report. Whether a problem is related to a software fault is still to be determined.

The study addressed four questions that will be discussed subsequently. They will be referred to as 'analysis questions' and represent the questions in the Goal/ Question/Metric paradigm.

(1) How much efforts does it take to solve a problem?

The study of reasons for delay made it clear that maintenance troubled development. It was not yet clear how much effort it took to correct faults. Knowledge of the distribution of the correction time can, for example, be used to plan maintenance activities.

(2) How is error occurrence distributed over the development phases?

Knowledge of the distribution of error occurrence over the phases of development pinpoints software construction problems and, as such, identifies areas for improvement. The long-term solution is improvement of the construction process. A short-term improvement measure may be to focus inspection and test emphasis on the phases that are most error prone.

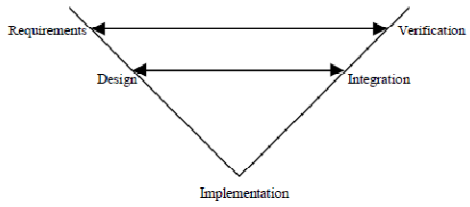

V- Model of development and testing

3) Do late corrections require more effort?

It would be expected that the cost of fix faults increases towards the end of the project because when an error is detected in a test not only must the fault be corrected, but also the upstream documents must be updated as well. Figure I gives the relative cost to fix failures in subsequent phases of development, as they were found by Boehm[11].

The authors wanted to check whether the figure reflected the experience in the department concerned. Additional efforts can be spent to avoid errors in the earlier phases of development if the figure reflected experience. If not, the department should ask itself why it does not behave as expected.

(4) Does the V model of development and resting work?

The department had adopted the V model of development and testing introduced by Myers[12] (see Figure 2).

Table 1 . Three multiple-choice questions added to problem report

(1) How many hours did it take to solve the problem?

Less than one hour

1 to 2 hours

2 to 4 hours

4 to 8 hours

Over 8 hours

(2) In what phase did the error occur?

Requirements

Design

Implementation

Other ..

(3) In what test was the fault detected?

Integration test

Verification test

Validation test

The V model shows the phases as distinguished by the department concerned. The phase are requirements, architectural design, implementation, integration, and verification and validation.

The V model shows that a development team test a concept exploration document in the validation test, a requirements specification in the verification test, and a design document in the integration test. It would be expected that the fault-detection phase is related to the error-occurrence phase.

The metric is derived from the four analysis questions above. The metric consisted of the answers to three multiple-choice questions are derived from questions proposed by Basili and Rombach[14]. The three questions were stated for every problem that was solved during four months. Eleven project leaders and some of their team members were involved in data collection. The data collection did not take much time for the project leaders involved. The authors' experience is that this is a prerequisite for successful data collection in software development. Another prerequisite is feedback of the results to the participating project leaders. This will be returned to when the results of the study are discussed in the next section.

IV. RESULTS

Over 400 problem reports were analyzed. The most important results of the study are presented in Table . Table comprises the answer to the first two analysis questions sated in the previous section. It shows the correction time versus the phase of error occurrence. For example, 22 errors that were incurred in the requirements phase took less than an hour to solve.

A large number of errors is classified in Table as 'other'.

Phase of occurrence	Time to correct fault hours						
Requirements design	<1	1-2	2-4	4-8	>8	Total (%)	
Implementation other	22	10	7	0	1	40	10
	12	8	6	1	4	31	7
	93	37	15	6	12	163	40
	103	25	16	7	26	177	43
	230	80	44	14	43	411	100
Total	56	20	11	3	10	100	

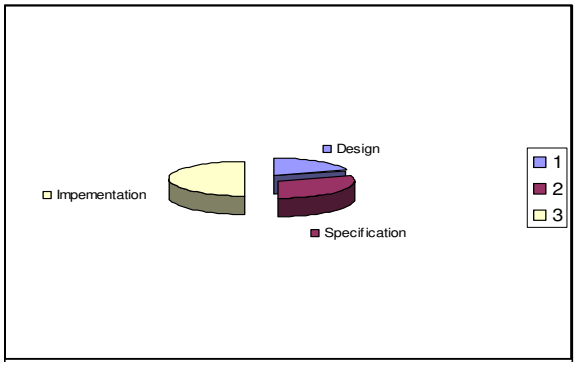

Distribution of error occurrence

It became clear during the study that some problems that were reported were not related to software errors or could not be attributed to a particular phase.

Number of problem reports, distributed over correction time and error occurrence Table Number of problem reports, distributed over correction time and error occurrence.

An example of the first case is change requests that are reported as problems.

Now focus is switched to the analysis questions that were stated in the third section. The first analysis question was 'How much effort does it take to solve a problem?' Table shows that over 50 per cent of the problems are solved within must one hour. Apparently, most of the problems are not too difficult to solve. A conclusion is that the maintenance problem is more a lead-time than an effort problem: it takes more time to get the problem to the right developer than to solve the problem.

The second analysis question was 'How is the occurrence of efforts distributed over the project?' The distribution of errors over the requirements, design, and implementation phases is given in Table 2 and is presented in the pie chart in Figure 3. The errors that were classified as other are left out of the diagram.

Figure 3 shows that the majority of errors was reported as implementation errors. A comparison with other studies shows that errors distributions depend on the development process and environments. Two studies by Basili et al. show different result. The first study concerned a general-purpose program for satellite planning studies. The error distributions shows that 48 per cent of the errors was attributed to incorrect or misinterpreted functional specifications or requirements. The second study concerned a ground support system. A large amount of software was reused. The errors distribution showed that 78 percent of the errors was related to design or implementation errors of a single component . The two studies by Basili et al. and the study described in this paper show that the error distributions are determined by the software engineers, the kind of application, and the development process. It is recommended that every software development organization gains insight into the distribution of errors to be able to take improvement measures that allow the number of errors to be able to take improvement measures that allow the number of errors to be reduced in the future.

The third analysis question stated was 'Do late corrections require more effort?' Figure 4 shows the distribution percentage of requirements, design, and implementation errors, distributed over the classes of correction time. For example 55 per cent of requirements errors, 39 percent of design errors, and 57 per cent of implementation errors are solved within the hour.

It was expected to find that, for example, requirements efforts take more time to solve than design and implementation errors. At first sight there is no relation between error occurrence and correction time.

The analysis question was stated in terms of the hypothesis 'There is no relationship between the error occurrence phase and the solution time'. Non-linear analysis16 was used to test this hypothesis. Non-linear analysis can be used to analyze cross-table. The cross-table concerned gives the distribution of problems over the error-detection phase on the one hand and correction time of the fault on the other. The structure of the table can be described by the independence and the association model as well. The hypothesis is therefore not rejected. This indicates that there is no relation between error occurrence and solution time, contrary to what the authors expected and what Boehm has found. The reasons behind this will be discussed after the last analysis question, related to the one just discussed, has been dealt with.

The last analysis question was 'Does the V model of development and testing work?' Figure 5 the number of requirements, design, and implementation faults found in the various tests, with the integration, verification and validation test on the horizontal axis. The number of faults that are detected is distributed over the phases in which the errors occurred. For example, three requirements errors, and 19 implementation errors are found in the integration test.

At first glance, there is no clear relation between the kind of error and the phase in which a fault was detected. This was confirmed when the hypothesis. 'There is no relationship between the kind of error and the phase in which a fault is detected' was tested. Longlinear analysis showed that the hypothesis did not need to be rejected. It is concluded that the empirical data did not reflect the use of the V model.

The answer to the last two analysis questions did not confirm expectations. The result were discussed with the relevant project leaders and their manager. The authors consider it to be important to discuss the results with the participants. This is a general starting point that Bemelmans has called closed-loop information supply . The idea is that the people who have to provide input to an information system should benefit from the output of that information system. The fact that they

benefit from correct output and are harmed by incorrect output is the incentive to provide accurate input. The principle could be summarized by 'nothing for nothing'. The closed-loop principle can be applied to information supply in software development: the data that are collected by software engineers should support the engineers in doing their job.

From discussion of the results, the authors concluded that there was serious misfit between the methods as they were supposed to be applied and reality. There will always be some kind of gap between the theoretical concepts and the application in reality; its is important, however, to access the size of the gap. For example, one explanation for the fact that there was no relation between the kind of error and the solution time could be the fact that any fault is resolved in the code. It is to be expected that a requirements error that is detected in a test will take more time to solve because upstream documents, such as design and requirements documents, will have to be updated. If the upstream documents are not updated there is a serious gap between theory and practice, returning to code and fix practices. The fact illuminated the misfit between theoretical concepts and reality. This has led to a renewed discussion of the role of theoretical concepts and their application in the department concerned. A major difference is that the discussions can now be based on facts provided by this empirical study.

Another result of the study is the questions that it raised. For example, the fact that this study showed that handling maintenance is mainly a lead-time problem raised the question 'How can maintenance be organized so that lead time is shortened?' A second questions that was raised was: 'Are change requests handled properly?' This question was raised because this study has shown that many users formulated their change requests as problem reports. The answering of these and similar questions will require additional data collection and analysis that should result in future improvement of the software development process.

V. CONCLUSION AND RECOMMENDATIONS

This paper has discussed an empirical study of software maintenance. When we concentrate on two phases of SDLC modifications are reduced with the help of iterations.

Maintenance takes a considerable part of the total expenditure on software. The study is an example of analysis of the software process. The distinction of construction of a software product and analysis of the software process is useful to direct improvement efforts. Basili and Rombach state that there needs to be a clear distinction between the role of constructive and analytical activities. Analysis requires measurement and data collection in software development. The lack of data collection in current software process indicates a lack of interest in analysis of the software process.

This study is an example of the fact that measurement and analysis can be done in a way that is simple and provides useful insight. It is not possible to measure everything at the same time, and therefore attention should be limited to one or a few aspects of the software construction process. The Goal /Question/Metric paradigm may be helpful in this focus. Examples of analysis studies that are similar to this study have been reported .

This study focused on maintenance, particularly error occurrence and fault detection. It was not possible to show a relation between phase or error occurrence and phase of fault detection. It was also not possible to show a relation between the phase of error occurrence and solution time. This indicated a gap between the methods as they were supposed to be applied and reality. The study also showed, once more, that data should be collected and used by every software department. It makes little sense to try to gain insight from somebody else's data because software development differs considerably from place to place. An important requirement for data collection and analysis in software development is the cooperation of the engineers involved.

Another typical result of this study was that it raised more questions than in answered. The authors intend to continue to raise and answer questions that increase insight into the software engineering process.

ACKNOWLEDGEMENTS

The authors than the participating project leaders for their cooperation in the study. They also thank Ben Smit and Rob Stobberingh for their support and for entertaining discussion during the study. Finally, thanks to Stephen Speirs for his comments.

REFERENCES

1 Conte, S D, Sunsmore, H E And Shen, V Y Software engineering metrics and models Benjamin/Cummings (1986)

2 Lehman, M Mm Heemstra, F. J and van der Stelt, H 'Cost control in automation projects, an empirical study'

3 Genuchten, M.J.I.M.van towards a software kluwer academic. Dordreecht

4 IEEE 'IEEE standard glossary of software engineering terminology.

5 Bohem,B W software engineering economics Prentice Hall (1981)

6 Basili, V R and Rombach, H D 'Tailoring the software process to project goals and enironemtns/ in Proc. 9th Int. Conf. Software Engineering (1987).

7 Basili, V R and Perricone, B T 'Software errors and complexity : an empirical investigation' Common. ACM Vol 27 No. 1 (January 1984)

8 Bemelmans, T M A 'Management information systems; questions, no answers' Informatie Vol. 31 (June 1989) (in Dutch)

Connected Boundary RegionTracing for Object Hole Filling

Mokhtar M. Hasan & Pramod K. Mishra

Computer Science Department, Banaras Hindu University, Uttar Pradesh, India

Abstract - The object detection algorithms may result with some noises that affect the final object shape, a novel approach is introduced in this paper for filling the holes in that object for better object detection and for correct feature extraction, this method is based on the hole definition which is the black pixel surrounded by a connected boundary region, and hence trying to find a connected contour region that surrounds the background pixel using roadmap racing algorithm, our method shows a great results in 2D space for objects.

Keywords- *object filling; object detection; object holes; noise removal; scanning 2D objects.*

I. INTRODUCTION

We can define the object hole as *"a black pixel surrounded by a connected boundary region"*, this definition is mentioned for each pixel; another definition of the object holes taken from [1] literally is *"background region surrounded by a connected border of foreground pixels"*, the other definition from [2] literally is *"an object has a hole whenever it contains a closed path which cannot be transformed into a single point by a sequence of elementary deformations inside the object"*, one more final hole definition taken from [3] literally is *"break in a surface mesh"*.

The term "hole" has not good interpretation in case of 3D objects since in these objects the view is changed and we need to define a new term(s), 3D objects contain cavities and concavities [2], the cavity is the existence of a hollow [2] in the object, or a bounded connected component of the background [2], while the concavity is considered to be a contour with concave shape [2].

The image transformation and segmentation techniques cause some noise to be added inside the object that they working on [2], this detected object in his current state can cause some problems since some parts of that objects are missing due to the noise, for the correct feature extraction phase or any future manipulation with that object; the noise should be removed, and we are talking about the noise within the object which is more difficult to handle than outside.

Furthermore, for object fitting and building the best model [4] that describes the object distribution, we need to scan or formulate the model from a completed object, any missing in these data will can a false or incorrect fitting that will affect the simulation process, however, for a correct parameter estimations [4] and fitting process, a correct filling algorithm should be applied.

This step can be postponed to be a post-processing step after applying all the pre-processing steps on object and hence, the new emerged holes from pre-processing step will be processed as well [4], and also this will reduce the computational time since the operation will be applied close to hole area [4] rather than spending time with un-processed object .

We have present in this paper a 2D object filling model that based on locating the black pixels (background) surrounded by a connected white (foreground) region (pixels), we have applied a binary image representation for object filling operation.

II. GENERAL SYSTEM DESCRIPTION

Our suggested filling algorithm composed of two main stages, thee stages are show in Fig. 1, the second stage with more detailed is shown in Fig. 2.

III. DETERMINING MASK SIZE

The mask is very important to locate the pixel hole, we have applied a diamond mask shape with certain diameter which is the distance between two opposite vertex of the diamond, Fig. 3 shows some masks with difference diameters.

As seen by Fig. 3; the centre pixel of the mask is zero which means a black pixel which means a hole pixel, whereas the surrounded pixels are foreground pixels.

However, the mask size is important in this process since it is the tool for finding the pixel hole, we can estimate the mask size so that it covers the maximum hole region, the mask selection is controlled by the following assumption:

Let the H_{ij} represents the hole j of object i, which means the input image may has a collection of objects each with many holes, let d represent the diameter of the mask and chosen according to (1).

d > length (H_{ij}). (1)

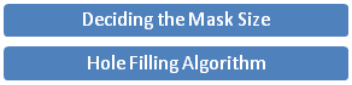

Figure 1.Two Stages of our Suggested System.

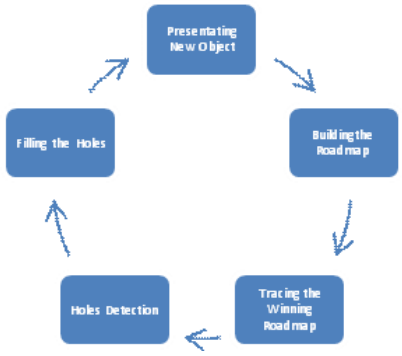

Figure 2. Hole Filling Algorithm

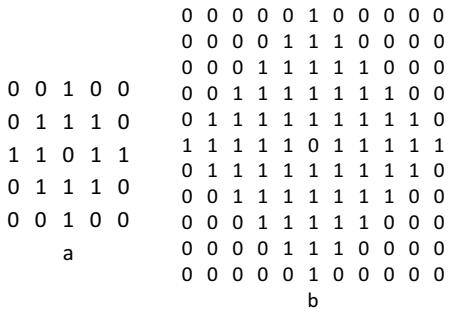

a) 5x 5 mask sizes. b) 11x11 mask size.

Figure 3. Different Mask Sizes Employed by our System.

Where *length (w)* is the maximum distance between each opposite hole region, in other words, the mask should cover the hole completely.

After deciding the mask size, the processing speed will be enhanced as the mask size goes down, we can make the mask size bigger enough to cover whole the input object but this will slow the algorithm down, so, a careful estimation of the mask size will enhance and speed up the processing time.

IV. SYSTEM IMPLEMENTATION

The following sections describe the detailed implementation of the proposed system, according to the cycle of Fig. 2.

A. Presenting New Input

In this stage a new input is presented to the system, the input take the form of an object or an image with multiple objects, however, the system performs pixel wide operations and the number of objects in the input image has no impact, this input is converted to binary image for discriminating between the foreground pixels and background pixels.

B. Building the Roadmap

The system iterates for each pixels in the input object and seeking for a hole pixel which is the background pixel, and foreground pixels are ignored.

In order to understand the roadmap, we will consider the following objects in Fig. 4.

Both of the latter objects are convolved with the mask of size 11x11 that mentioned in Fig. 3b, the resulting will be in Fig. 5 which is called the masked window.

We can notice that the resulting convolved window is 11x11 since the mask size is. After that convolution operation, we have to look to see if there is any way out starting from the middle of the masked window to the border, there are many possibilities and combinations of such path, in either meaning, we try to find a border that surrounding the centre background pixel, the pixel to be considered as a hole pixel if such border exists. Fig. 6 shows differed samples of sub-masked window which is very difficult to trace.

As seen in latter figure, we have presented a two sub-masked window, Fig. 6a shows that this background pixel x is a hole pixel whereas Fig. 6b shows not.

Now, to find such connected border around the centre window background pixel, we expanded the above masked window into an equal length of tracing paths, each path represents a full diamond, so, we will have r tracing paths where r represents the vertical radius of the diamond (vertical and horizontal are the same).

0	0	0	0	0	0	0	0
0	0	1	1	1	1	1	0
0	0	1	0	0	0	1	0
0	0	1	0	0	0	1	0
0	0	1	0	0	0	1	0
0	0	1	1	1	1	1	0
0	0	0	0	0	0	0	0
0	0	0	0	0	0	0	0

a

0	0	0	0	0	0	0	0
0	0	1	1	1	1	1	0
0	0	1	0	0	0	1	0
0	0	0	0	0	0	1	0
0	0	1	0	0	0	1	0
0	0	1	1	1	1	1	0
0	0	0	0	0	0	0	0
0	0	0	0	0	0	0	0

b

a) closed object, b) opened object

Figure 4. Two Objects Will be Considered as an Example.

0	0	0	0	0	0	0	0	0	0	0
0	0	0	0	0	0	0	0	0	0	0
0	0	0	**1**	**1**	**1**	**1**	**1**	0	0	0
0	0	0	**1**	0	0	0	**1**	0	0	0
0	0	0	**1**	0	0	0	**1**	0	0	0
0	0	0	**1**	0	0	0	**1**	0	0	0
0	0	0	**1**	**1**	**1**	**1**	**1**	0	0	0
0	0	0	0	0	0	0	0	0	0	0
0	0	0	0	0	0	0	0	0	0	0
0	0	0	0	0	0	0	0	0	0	0
0	0	0	0	0	0	0	0	0	0	0

0	0	0	0	0	0	0	0	0	0	0
0	0	0	0	0	0	0	0	0	0	0
0	0	0	**1**	**1**	**1**	**1**	**1**	0	0	0
0	0	0	**1**	0	0	0	**1**	0	0	0
0	0	0	0	0	0	0	**1**	0	0	0
0	0	0	**1**	0	0	0	**1**	0	0	0
0	0	0	**1**	**1**	**1**	**1**	**1**	0	0	0
0	0	0	0	0	0	0	0	0	0	0
0	0	0	0	0	0	0	0	0	0	0
0	0	0	0	0	0	0	0	0	0	0
0	0	0	0	0	0	0	0	0	0	0

a) convolution of figure(4a) and figure (3b)
b) convolution of figure(4b) and figure (3b)

Figure 5. Convolution Operation Applied Between Object Window And 11x11 Mask

1	1	0	0	0	0	0	0	0
1	1	1	1	1	1	1	1	1
0	1	1	0	0	0	1	0	0
0	1	0	**1**	**1**	**1**	**1**	**1**	0
0	0	0	**1**	x	0	0	**1**	0
0	**1**	**1**	**1**	1	1	0	**1**	0
0	**1**	0	1	0	0	0	**1**	1
0	**1**	0	0	0	1	0	0	**1**
0	0	**1**	**1**	**1**	**1**	**1**	**1**	**1**

a

0	1	1	1	1	1	1	1	1
0	1	**0**	**0**	**0**	**0**	**0**	**0**	1
0	1	**0**	1	1	1	1	**0**	1
0	1	**0**	1	1	0	1	**0**	1
0	1	**0**	1	**x**	0	1	**0**	**0**
0	1	**0**	**0**	**0**	0	1	1	1
0	1	1	1	1	1	1	0	0
0	1	0	0	0	0	0	0	0
0	1	1	1	1	1	1	1	1

b

a) hole pixel, b) non hole pixel

Figure 6: two different sub-masked window.

There is a problem facing this expansion which is; the number of pixels in each tracing path is different since produced from different size diamond, the formula in (2) shows the size for each diamond in the mask, considering the diamond diameter is d and radius is r.

$$NOP=DN * 4 \qquad (2)$$

Where NOP =number of pixels, and DN=diamond number, the diamonds are start numbering from the centre of the mask, the following example shows the 5x5 mask with their diamonds and the tracing paths. Consider we have 9x9 mask coded as in Fig. 7 for a better understanding.

We have labeled the diamond pixels with symbols so the expansion will be more digested. In order to make the length of the tracing path for each one equal, we have to repeat some points, these repeated points is the vertices of the diamond. This repetition is controlled by (3).

$$RP=r_{global} - r_{local} \qquad (3)$$

Where RP is the number of repeated points, rglobal is the radius of the bigger diamond (mask), and rlocal is the radius of that diamond, in this equation we have controlled the number of repeated pixels in order to formulate a unique length tracing paths, Table 1 shows the tracing paths of the latter figure.

0	0	0	0	5	0	0	0	0
0	0	0	5	L	5	0	0	0
0	0	5	K	g	M	5	0	0
0	5	H	f	4	h	N	5	0
5	G	e	3	x	1	a	A	5
0	5	F	d	2	b	B	5	0
0	0	5	E	c	C	5	0	0
0	0	0	5	D	5	0	0	0
0	0	0	0	5	0	0	0	0

Figure 7. 9x9 Labeled Mask.

What we have done is, starting with vertex 1 of the inner diamond and places it in the path, then we are repeating the next point as equation (3), the shaded cells represent the repeated codes. As seen in latter figure, all the tracing paths are equally length which enable us to proceed to the next level for hole pixel discovering.

C. *Tracing the Winning Roadmap*

In this level we are trying to trace the road paths (maps) that are produced for each pixel, the key point is to find a full paths starting from the beginning and reaching to the end of path.

Consider a path P={w0, w1, ..., wt}, where t is the roadmap length, and consider RMbk is the roadmap for a given background pixel bkx, y , then this pixel is said to be a hole pixel hx, y the following formula (4) and(5) holds:

$$P=Tracing\ (r, t, RM_{bk}) \qquad (4)$$

and then,

(5)

Where Tracing(r, t, P, RM) is our tracing algorithm. For better understanding, we can put this in two cases, each road path in Table 1 represents a full diamond, furthermore, if this path are connected without any black pixel; this means the diamond is closing the centre pixel which, in turns, leads to hole pixel declaration, since it is surrounded by a connected region, this is the first case, the other and the most encountered case, like Fig. 6a, there is no connected diamond but these is an connected region formed by multiple diamonds, our aim is to verify the first case which is faster, it not, we continue with second case which finds the hole pixels if such exist.

Table 2 shows the paths expansion corresponding to Fig. 4a which has a connected region around pixel (3, 3).

As we have seen above, this point is considered to be a hole pixel since we traced a connected path from start point to end point, on the contrary, Fig. 4b should declare no hole point since there is a crack in the structure, Table 3 shows the trace.

The trace stops since there is no more connection, and furthermore, you can notice that there are a gap in the middle of tracing paths, this gap of zeroes is caused since the structure is opened.

.

TABLE 1 . TRACING PATHS THAT CORRESPONDS TO FIG. (7).

diamond r=1	1	2	2	2	2	3	3	3	3	4	4	4	4	1	1	1
diamond r=2	a	b	c	c	c	d	e	e	e	f	g	g	g	h	a	a
diamond r=3	a	b	c	d	d	e	f	g	g	h	k	l	l	m	n	a
diamond r=4	5	5	5	5	5	5	5	5	5	5	5	5	5	5	5	5

TABLE 2 . TRACING THE PATHS FOR FIGURE (4A).

start point	0	0	0	0	0	0	**1**	**1**	**1**	**1**	**1**	0	0	0	0	0	0	0	0	0	end point
	0	0	**1**	**1**	**1**	**1**	**1**	0	0	0	0	**1**	**1**	**1**	**1**	**1**	0	0	0	0	
	1	0	**1**	0	0	0	1	0	0	0	0	0	1	0	0	0	**1**	**0**	**1**	**1**	
	0	**1**	**1**	0	0	0	0	0	0	0	0	0	0	0	0	0	0	1	1	0	
	0	0	1	0	0	0	0	0	0	0	0	0	0	0	0	0	0	0	1	0	

TABLE 3. TRACING THE PATHS FOR FIGURE (4B).

start point	0	0	0	0	0	0	0	0	0	0	0	0	0	0	0	0	0	0	0	0	end point
	0	0	**1**	**1**	**1**	**1**	**1**	0	0	0	0	1	1	1	1	1	0	0	0	0	
	1	0	**1**	0	0	0	**1**	0	0	0	0	0	1	0	0	0	1	0	1	1	
	0	**1**	**1**	0	0	0	0	0	0	0	0	0	0	0	0	0	0	1	1	0	
	0	0	1	0	0	0	0	0	0	0	0	0	0	0	0	0	0	0	1	0	

Tracing Algorithm

Input: r represents mask radius, t represents total number of points in bigger diamond (roadmap length)

StatusMap is a matrix with size r x t contains the on, off pixels of the road paths

Output: background pixel or hole pixel.

Method:

Step 1: [initialization]

initialize k[i] for all i=0, .., r-1 with true values, k represents the tracing status vector at each step.

StepCounter=0;

Step 2: [repeat]

Repeat to step ( ) while StepCounter<t

Step 3: [repeat for the current step]

For each i where i=0, 1,…, r-1 do up to step (7) the following:

CurrentStatus=StatusMap(i, StepCounter)

Step 4: [update the upper pixels in the current step]

If CurrentStatus is on and k[i] is on then update all k[j] for all j<i with the following:

k[j]=k[j] ANDing StatusMap (j, StepCounter)

Step 5: [update the lower pixel in the current step]

Update k[j] where j=i+1 with the following:

k[j]=k[j] ANDing StatusMap (j, StepCounter)

Step 6: [update the current status of tracing status vector]

k[i]=CurrentStatus ANDing k[i]

Step 7: [gap checking checking]

If all k[j] for j=0, 1,.., r-1 are off, then declare that this is an background pixel, stop.

Else go back to step (3).

Step 8: [stop]

Declare that this is a hole pixel, stop.

V. EXPERIMENTAL RESULTS

We have tested our suggested algorithm with different of images, some of them with objects and other with text images and the result was as expected, the following Fig. 8 shows some of these tested images.

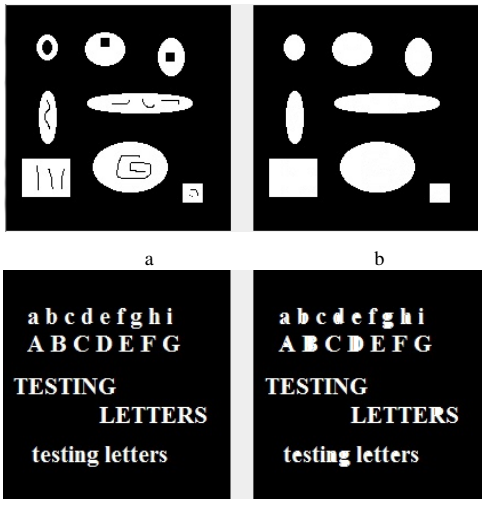

(a and c) are input images, (b and d) are output images

Figure 8. Some Testing Images.

VI. SUMMARY

Hole filling algorithms are considered to be important to close the fill the noise inside the object, especially before the feature extraction phase for an object since these noises may give a wrong feature translation, and also help to fill the un wanted holes during the scanning operation for images that has some artifacts.

In this study we have introduced an algorithm for hole filling that looks and seeks for the a background pixel lie inside a connected region, and hence, this background pixel is announced as hole pixel.

REFERENCES

[1] Rafael C. Gonzalez, Richard E. Woods, "Digital Image Processing",Pearson Prentice Hall, First Impression, 2009.

[2] Zouina Aktouf, Gilles Bertrand, and Laurent Perroton, "A threedimensional holes closing algorithm", ELSEVIER Pattern Recognition Letters, vol. 23 :523–531, 2002.

[3] Eric Firestone, "An Exploration Of Hole Filling Algorithms", M.Sc. Thesis, Faculty Of California Polytechnic State University, San Luis Obispo, 2008.

[4] Elaine Cohen , Lavanya Sita Tekumalla , and Elaine Cohen,"A Hole-Filling Algorithm for Triangular Meshes", School of Computing, University of Utah, USA, 2004.

[5] Matteo Dellepiane, Andrea Venturi, and Roberto Scopigno," Image guided reconstruction of un-sampled data: a coherent filling for uncomplete Cultural Heritage models", International Journal of Computer Vision, vol. 94(1), USA, 2011.

[6] Kwan-Jung Oh, Sehoon Yea,and Yo-Sung Ho," Hole-Filling Method Using Depth Based In-Painting For View Synthesis in Free Viewpoint Television (FTV) and 3D Video", IEEE 27th conference on Picture Coding Symposium, Chicago, IL, 2009, pp. 1-4.

[7] Alan Brunton, Stefanie Wuhrer, Chang Shu, Prosenjit Bose, and Erik Demaine, "Filling Holes in Triangular Meshes Using Digital Images by Curve Unfolding", International Journal of Shape Modeling, vol. 16(1-2), NRC Institute for Information Technology, 2011.

[8] Mingqiang Wei, Jianhuang Wu, and Mingyong Pang, "An Integrated Approach To Filling Holes In Meshes", IEEE International Conference on

Artificial Intelligence and Computational Intelligence, 2010, pp. 306 – 310.

[9] Xiao J. Wu, Michael Y. Wang, and B. Han, "An Automatic Hole-Filling Algorithm for Polygon Meshes", Computer-Aided Design and Applications, vol. 5(6):889-899, 2008.

[10] Chun-Yen Chen, Kuo-Young Cheng, and H. Y. Mark Liao," ASharpness Dependent Approach to 3D Polygon Mesh Hole Filling", Proceedings of EuroGraphics, 2005, pp. 13-16.

[11] Amitesh Kumar, Alan Shih, Yasushi Ito, Douglas Ross, and Bharat Soni,"A Hole-filling Algorithm Using Non-uniform Rational B-splines", Department of Mechanical Engineering, University of Alabama at Birmingham, Birmingham, AL, U.S.A., >2008.

◈◈◈

AUTOMATIC MELAKARTA RAAGA IDENTIFICATION SYSTEM FOR CARNATIC MUSIC USING K-NEAREST NEIGHBOUR AND EARTH MOVER DISTANCE

B. Tarakeswara Rao[1], Sivakoteswararao Ch[2], & Prasad Reddy P.V.G.D[3]

[1 & 2] School of Computing, Vignan University, Guntur, India

Department of CS&SE, Andhra University, Visakhapatnam, India

Abstract **-** Perhaps the most straightforward classifier in the arsenal or machine learning techniques is the Nearest Neighbour Classifier – classification is achieved by identifying the nearest neighbours to a query example and using those neighbours to determine the class of the query. This approach to classification is of particular importance today because issues of poor run-time performance are not such a problem these days with the computational power that is available. This paper presents an overview of techniques for Nearest Neighbour classification focusing on; mechanisms for finding distance between neighbours using Cosine Distance, Earth Movers Distance and formulas are used to identify nearest neighbours, algorithm for classification in training and testing for identifying Melakarta raagas. From the results it is concluded that Earth Movers Distance is producing better results than Cosine Distance measure.

Keywords **-** Music, Melakarta Raaga, Cosine Distance, Earth Movers Distance, K-NN.

I. INTRODUCTION

Underlying the two systems of classical music in the Indian subcontinent is a melodic system known as *raaga*. Performance in Indian classical music is always within a Melakarta raaga, except for solo percussion. Melakarta raaga is a system within which performers improvise and compose. Melakarta raagas are often summarized by the notes they use, though many Melakarta raagas in fact share the same notes. Melakarta raaga recognition is a difficult task even for humans. A Melakarta raaga is popularly defined as a specified combination, decorated with embellishments and graceful consonances of notes within a mode which has the power of evoking a unique feeling distinct from all other joys and sorrows. It possesses something of a transcendental element. A Melakarta raaga is characterized by several attributes, like its Vaadi-Samvaadi, Aarohana-Avrohana and Pakad [17], besides the sequence of notes. It is of utmost importance to note here that no two performances of the same Melakarta raaga, even two performances by the same artist, will be identical. A certain music piece is considered a certain Melakarta raaga, as long as the attributes associated with it are satisfied. This concept of Indian classical music, in that way, is very open.

Given an audio sample, find the underlying Melakarta raaga for the input, complexity of a Melakarta raaga is highly variable in performance. Though tried to be very general in the approach, some constraints have to be placed on the input.

Through this work the following major contributions to the study of musical raagas and KNN with CD and EMD are made. In first place, our solutions based primarily on techniques from speech processing and pattern matching, which shows that techniques from other domains can be purposefully extended to solve problems in computational musical raagas, Secondly, the two note transcription methods presented are novel ways to extract notes from sample raagas of Indian classical music. This approach has given very encouraging results.

The rest of the paper is organized as follows. Section 2 highlights some of the useful and related previous research work in the area. The solution strategy is discussed in detail in Section 3. The test procedures and experimental results are presented in Section 4, Finally, Section 5 lists out the conclusions.

II. PEVIOUS WORK

Previous work in Carnatic music retrieval is on a slow pace compared to western music. Some work is being done in Swara identification [1] and Singer identification [2] of Carnatic music. In Hindustani music work has been done in identifying the Melakarta raaga of Hindustani music [3]. In [3][19] the authors have created a HMM based on which they have identified two

raagas of Hindustani music. The fundamental difference between Hindustani Raaga pattern and Carnatic Raaga pattern is that in Hindustani R1, R2 are present as against R1, R2, R3 in Carnatic. Similarly G, D, N all has three distinct frequencies in Carnatic music as compared to two frequencies in Hindustani [8]. This reduces the confusion in identifying the distinct frequencies in Hindustani music as compared to Carnatic music. The authors have not used polyphonic music signal and have assumed that the input music signal is a voice only signal. The fundamental frequency of the signal was also assumed and based on these features the Melakarta raaga identification process was done for two Hindustani raagas. On the western music aspect, melody retrieval is being performed by researchers. The one proposed by [9] is based on identifying the change in frequency in the given query. The query is received in the form a humming tune and based on the rise and fall in the pitch of the received query, the melody pattern that matches with the query's rise and fall of pitch is retrieved. The melody retrieval based on features like distance measures and gestalt principles. The approach is based on low level signal features and the Melakarta raaga is identified by considering different instrument signal as input to our system. In the present work Melakarta raaga identification is done using KNN with two different distance metrics one CD and the other EMD.

III. PRESENT WORK

K Nearest Neighbour has rapidly become one of the booming technologies in today's world for developing convoluted control systems. Melakarta raaga Recognition is one the fascinating applications of KNN – which is basically used in Melakarta raaga identification for many cases, Melakarta raaga detection is considered as a rudimentary nearest neighbour problem. The problem becomes more fascinating because the content is an audio – given an audio find the audio closest to the query from the trained database.

The intuition underlying Nearest Neighbour Classification is quite straight forward, classified based on the class of their nearest neighbours. It is often useful to take more than one neighbour into account so the technique is more commonly referred to as k-Nearest Neighbour (k-NN) Classification where k nearest neighbours are used in determining the class. Since the training examples are needed at run-time, i.e. they need to be in memory at run-time, it is sometimes also called Memory-Based Classification. Because induction is delayed to run time, it is considered a Lazy Learning technique. Because classification is based directly on the training examples it is also called Example-Based Classification or Case-Based Classification. The basic idea is as shown in Figure 6.1 which depicts a 3-Nearest Neighbour Classifier on a two-class problem in a two-dimensional feature space. In this example the decision for q1 is straightforward – all three of its nearest neighbours are of class O so it is classified as an O. The situation for q2 is a bit more complicated at it has two neighbours of class X and one of class O. This can be resolved by simple majority voting or by distance weighted voting (see below). So k–NN classification has two stages; the first is the determination of the nearest neighbours and the second is the determination of the class using those neighbours. The following section describes the techniques CD and EMD which is used to raaga classification.

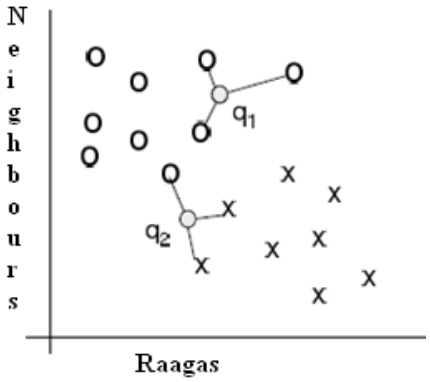

Fig. 1 A simple example of 3-Nearest Neighbour Classification

3.1 COSINE DISTANCE

Cosine similarity (CD) between two vectors x and y is defined as:

$CD(x; y) = (x^T * y)/(\|x\|*\|y\|)$ ------- (1)

Cosine similarity has a special property that makes it suitable for metric learning: the resulting similarity measure is always within the range of -1 and +1. this property allows the objective function to be simple and effective.

3.2 EARTH MOVER DISTANCE (EMD)

The EMD is based on the solution to a discrete optimal mass transportation problem. EMD represents the minimum cost of moving earth from some source locations to fill up holes at some sink locations. In other words, given any two mass (or probability) distributions, one of them can be viewed as a distribution of earth and the other a distribution of holes, then the EMD between the two distributions is the minimum cost of rearranging the mass in one distribution to obtain the other. In the continuous setting, this problem is known as the Monge-Kantorovich optimal mass transfer problem and has been well studied over the past 100 years the importance

here is that EMD can be used to measure the discrepancy between two multidimensional distributions.

3.3. METHODOLOGY/ALGORITHM FOR MELAKARTA RAAGA RECOGNITION SYSTEM

The following is the methodology is used for the Melakarta raaga Recognition for training and testing. Initially first k-Nearest Neighbour Classifier is determined on a two-class problem in a two-dimensional feature space which is shown in the following diagram raagas in horizontal axis and neighbours of raaga on the vertical axis. In this proposed approach the decision for raaga is straightforward – one of its nearest neighbours is of class O and one of class X.

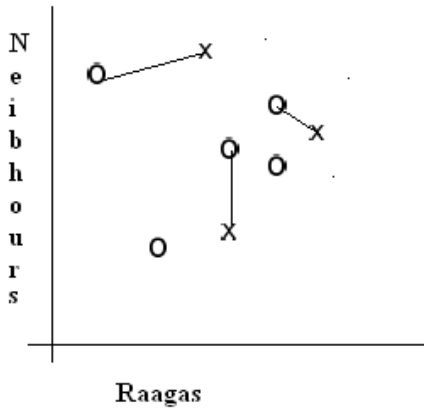

Fig. 2 1-Nearest Neighbour classification of Raagas

A training dataset D is made up of (xi), I Є[1,|D|] training samples where xi is the raaga. The raaga is divided in to 15 samples by eliminating unwanted frequencies (disturbances, accompanied instruments) by using low level filter-Fourier Transform of a Signal (Spft). The same process is repeated for each raaga in database D. Then these samples are trained by using Self- Organizing and Learning Vector Quantization Nets. The grouping process is carried by us. Each training example is labeled with a class label yj Є Y. Our objective is to classify an unknown example raaga q. Now training process is completed. Next the testing phase is performed by using KNN classification.

The KNN approach carried in two phases

1. Determination of Nearest Neighbours
2. Determination of the class using those neighbours

Determination of Nearest Neighbours :

For each xi Є D the distance between q and xi is calculated as follows:

$$d(q, x_i) = \sum_{f \in F} \varpi_f \delta(q_f, x_{if}) \quad \text{------(2)}$$

Where xi = trained raaga ,

q = testing raaga,

f = feature(flow pattern)

wf = weighted feature of raaga

There are huge ranges of possibilities for this distance metric; a basic version for continuous and discrete attributes would be:

$$\delta(q_f, x_{if}) = \begin{cases} 0 & f \text{ discrete and } q_f = x_{if} \\ 1 & f \text{ discrete and } q_f \neq x_{if} \\ |q_f - x_{if}| & f \text{ continuous} \end{cases} \quad (3)$$

The k nearest neighbours is selected based on this distance metric. In order to determine the class of q the majority class among the nearest neighbours is assigned to the query. It will often make sense to assign more weight to the nearer neighbours in deciding the class of the query.

Determination of the class using those neighbours:

If more than one of the neighbours is identified then it can be resolved by simple majority voting or by distance weighted voting. A fairly general technique to achieve this is distance weighted voting where the neighbours get to vote on the class of the query case with votes weighted by the inverse of their distance to the query.

$$Vote(y_i) = \sum_{c=1}^{k} \frac{1}{d(q, x_c)^n} 1(y_j, y_c) \quad \text{------ (4)}$$

Thus the vote assigned to class yj by neighbour xc is 1 divided by the distance to that neighbour, i.e. 1(yj , yc) returns 1 if the class labels match and 0 otherwise. From the above equation would normally be 1 but values greater than 1 can be used to further reduce the influence of more distant neighbours. Now the distance measures Cosine and EMD measures applied to our KNN process is discussed.

3.3.1 COSINE DISTANCE MEASURE

The cosine similarity measure is the cosine of the angle between these two vectors, suppose di and dj are the paths between ai and aj in instance xi and instance xj, respectively. di and dj are represented as vectors of term frequencies in the vector-space model. The cosine is calculated by using the following formula

_____ ----- (5)

3.3.2 EARTH MOVER DISTANCE

The Earth Mover Distance (EMD) is a distance measure that overcomes many of problems that arise from the arbitrariness of binning. As the name implies, the distance is based on the notion of the amount of effort required to convert one instrumental music to another based on the analogy of transporting mass from one distribution to another. If two instrumental music are viewed as distributions and view one distribution as a mass of earth in space and the other distribution as a hole (or set of holes) in the same space then the EMD is the minimum amount of work involved in filling the holes with the earth. Some researchers analysis of the EMD argue that a measure based on the notion of a signature is better than one based on a histogram. A signature {sj = mj ,wmj } is a set of j clusters where mj is a vector describing the mode of cluster j and wmj is the fraction of features falling into that cluster. Thus a signature is a generalization of the notion of a histogram where boundaries and the number of partitions are not set in advance; instead j should be 'appropriate' to the complexity of the instrumental music. The example in Figure 6.3 illustrates this idea. The clustering can be thought as a quantization of the instrumental music in some frequency space so that the instrumental music is represented by a set of cluster modes and their weights. In the figure the source instrumental music is represented in a 2D space as two points of weights 0.6 and 0.4; the target instrumental music is represented by three points with weights 0.5, 0.3 and 0.2. In this example the EMD is calculated to be the sum of the amounts moved (0.2, 0.2, 0.1 and 0.5) multiplied by the distances they are moved. Calculating the EMD involves discovering an assignment that minimizes this amount.

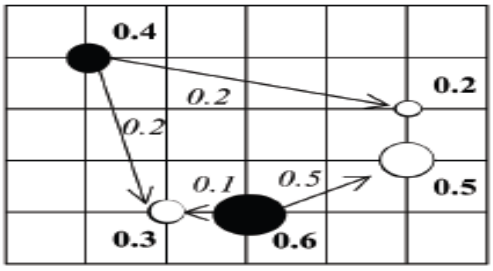

Fig. 3. An example of the EMD between two 2D signatures with two points (clusters) in one signature and three in the other.

For two instrumental music described by signatures S = {mj ,wmj }nj =1 and Q = {pk,wpk}r k=1 . The work required to transfer from one to the other for a given flow pattern F:

$$WORK(S,Q,F) = \sum_{j=1}^{n}\sum_{k=1}^{r} d_{jk} f_{ik} \quad \text{---- (6)}$$

where djk is the distance between clusters mj and pk and fjk is the flow between mj and pk that minimizes overall cost. Once the transportation problem of identifying the flow that minimizes effort is solved by using dynamic programming. The EMD is defined as:

$$EMD(S,Q) = \frac{\sum_{j=1}^{n}\sum_{k=1}^{r} d_{jk} f_{jk}}{\sum_{j=1}^{n}\sum_{k}^{r} f_{jk}} \quad \text{-----(7)}$$

EMD is expensive to compute with cost increasing more than linearly with the number of clusters. Nevertheless it is an effective measure for capturing similarity between instrumental music. It is identified that the EMD approach is giving better results than Cosine measure.

IV. RESULTS AND DISCUSSION

The input signal is sampled at 44.1 KHz. The identification of different Raagams for the purpose of evaluating this algorithm is considered. For the purpose of Melakarta raaga identification seven different instruments are considered. The signal is made to pass through the signal separation algorithm, and segmentation algorithm.

The result showing the segmentation points for one input is shown in below Figures. This is the first level of segmentation where the protruding lines indicate the points of segmentation. After identifying the segmentation points the frequency components are determined using the HPS algorithm and tabulated the frequency values which have the dominant energy. Using the raaga identification system, the confusion matrix is determined.

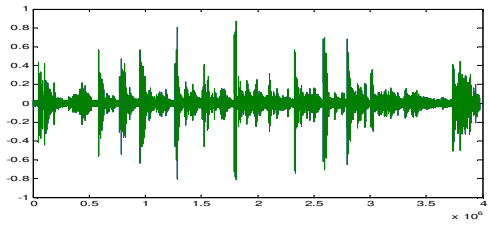

Fig.4 Plot Graph for Begada Raaga

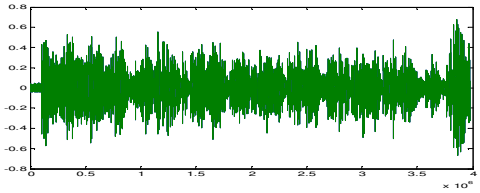

Fig. 5 Plot Graph for Kharaharapriya Raaga

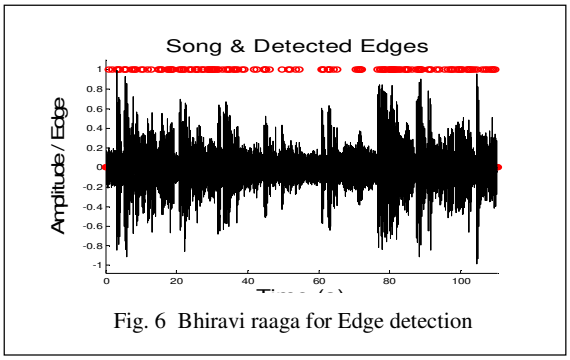

Fig. 6 Bhiravi raaga for Edge detection

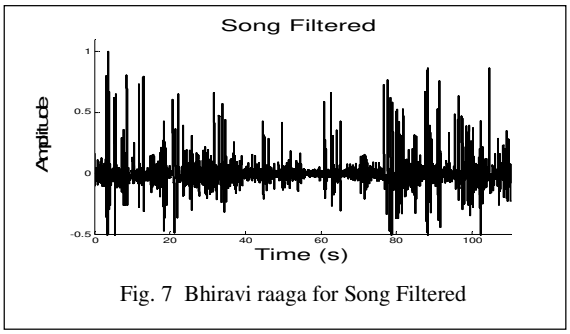

Fig. 7 Bhiravi raaga for Song Filtered

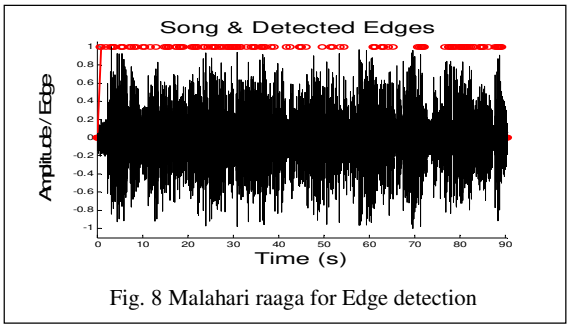

Fig. 8 Malahari raaga for Edge detection

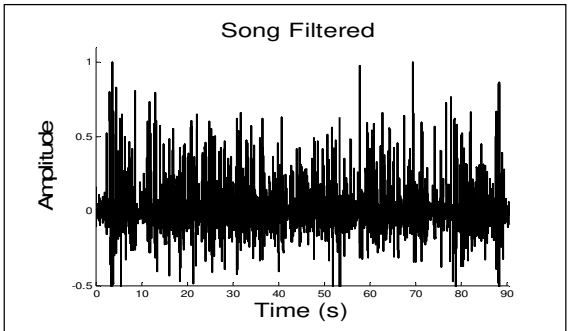

Fig. 9 Malahari raaga for Song Filtered

The following are the results obtained by applying Cosine Distance measure .

Cosine Distance: The Data is same for Train and Sample

Table 1 Confusion Matrix: Same data for Train and Sample

Name of the Raaga	Recognized Raagas (%)				
	Begada	Vanasapathi	sundavinodini	Desh	Hindilom
Begada	**92**	56	56	60	65
Vanasapathi	58	**92**	63	70	72
sundavinodini	58	68	**92**	68	70
Desh	62	70	76	**92**	75
Hindilom	65	72	70	85	**92**

Cosine Distance: The Data is different for Train and Sample

Table 2 Confusion Matrix: Different data for Train and Sample

Name of the Raaga	Recognized Raagas (%)				
	Begada	Vanasa pathi	sundavin odini	Desh	Hindilom
Sri	90	58	58	62	65
Bhiravi	58	88	63	70	72
Abheri	58	68	78	68	70
Malahari	62	70	76	84	75
Sahana	65	72	70	85	86

The following are the results obtained by applying EMD Distance measure

EMD: The Data is same for both Train and Sample

Name of the Raaga	Recognized Raagas (%)				
	Begada	Vanasa pathi	sundav inodini	Desh	Hindilom
Begada	**96**	66	57	74	68
Vanasapathi	78	**96**	65	82	80
sundavin odini	72	78	**96**	88	70
Desh	72	70	76	**96**	85
Hindilom	66	74	72	86	**96**

Table 3 Confusion Matrix: Same data for Train and Sample

Name of the Raaga	Recognized Raagas (%)				
	Begada	Vanasa pathi	sundav inodini	Desh	Hindilom
Begada	**96**	66	57	74	68
Vanasapathi	78	**96**	65	82	80
sundavin odini	72	78	**96**	88	70
Desh	72	70	76	**96**	85
Hindilom	66	74	72	86	**96**

Table 4 Confusion Matrix: Different data for Train and Sample

Name of the Raaga	Recognized Raagas (%)				
	Begada	Vanasap athi	sundav inodini	Desh	Hindilo m
Sahana	89	68	78	62	65
Todi	68	88	63	70	72
Sri	58	68	78	68	70
Bhiravi	72	70	76	84	75
Abheri	75	72	70	85	86
Malahari	70	75	68	78	80

VI. CONCLUSION

K-NN is very simple to understand and easy to implement. So it should be considered in seeking a solution to any classification problem. In some circumstances where an explanation of the output of the classifier is useful, K-NN can be very effective if an analysis of the neighbours is useful as explanation. In order to improve classification process an EMD approach is used for fast convergence. K-NN is very sensitive to irrelevant or redundant features because all features contribute to the similarity and thus to the classification. This can be ameliorated by EMD approach and feature selection or feature weighted voting. The EMD results are compared with Cosine distance measure and observed that EMD gives better results.

REFERENCES

[1] Rajeswari Sridhar, Geetha T. V, "Swara Indentification for South Indian Classical Music", ICIT '06 Proceedings of the 9th International Conference on Information Technology, IEEE Computer Society, ISBN:0-7695-2635-7.

[2] Youngmoo E. Kim, Brian Whitman" Singer Identification in Popular Music Recordings Using Voice Coding Features", citeseerx.ist.psu.edu/viewdoc/download?doi=10.1.1.115.

[3] Paul G., Corine G.M., Christophe C., Vincent F. "automatic classification of environmental noise events by hidden Markov models", citeseerx.ist.psu.edu/viewdoc/download?doi=10.1.1.52

[4] Berger. "Some factors in the recognition of timbre". J. Audio. Eng. Soc. 30, pp. 396-406.

[5] Clark, Milner. "Dependence of timbre on the tonal loudness produced by musical instruments". J. Audio. Eng. Soc. 12, pp. 28-31.

[6] Eagleson, H. W., Eagleson, O. W. "Identification of musical instruments when heard directly and over a public-address system". J. Acoust. Soc. Am. 19, pp. 338-342.

[7] Strong, Clark. "Perturbations of synthetic orchestral wind instrument tones". J. Acoust. Soc. Am., Vol. 41, pp. 277-285.

[8] Bhatkande.V (1934), Hindusthani Sangeet Paddhati.Sangeet Karyalaya, 1934.

[9] Schroeder.M.R (1968), " Period histogram and product spectrum: New methods for fundamental-frequency measurement", Journal of the Acoustical Society of America, , vol. 43, no. 4, 1968.

[10]. A. Ghias, J. Logan, D. Chamberlin and B. C. Smith: "Query by Humming – Musical Information Retrieval in an Audio Database": Proc. ACM Multimedia, pp. 231-236: 1995.

[11]. H. Deshpande, U. Nam and R. Singh: "MUGEC: Automatic Music Genre Classi-fication": Technical Report, Stanford University: June 2001.

[12]. S. Dixon: "Multiphonic Note Identification": Proc. 19th Australasian Computer Science Conference: Jan-Feb 2003.

[13]. W. Chai and B. Vercoe: "Folk Music Classification Using Hidden Markov Models": Proc. Internation Conference on Artificial Intelligence: June 2001.

[14]. A. J. Viterbi: "Error bounds for convolutional codes and an asymptotically optimal decoding algorithm": IEEE Transactions on Information Theory, Volume IT-13, pp.260-269: April 1967.

[15]. L. E. Baum: "An inequality and associated maximization technique in statistical estimation for probabilistic functions of Markov processes": Inequalities, Volume 3, pp. 1-8: 1972.

[16]. L. E. Baum and T. Petrie: "Statistical inference for probabilistic functions of finite state Markov chains": Ann.Math.Stat., Volume 37, pp. 1554-1563: 1966.

[17]. Gaurav Pandey, Chaitanya Mishra, and Paul Ipe "TANSEN: a system for automatic raga identification"

[18]. A. Prasad et al. "Gender Based Emotion Recognition System for Telugu Rural Dialects using Hidden Markov Models" Journal of Computing: An International Journal, Volume2 ,Number 6 June 2010 NY, USA, ISSN: 2151-9617

[19]. Tarakeswara Rao B et. All "A Novel Process for Melakartha Raaga Recognitionusing Hidden Markov Models (HMM)", International Journal of Research and Reviews in Computer Science (IJRRCS), Volume 2, Number 2,April 2011, ISSN: 2079-2557.

◈◈◈

Standardization of Requirement Elicitation For International Projects

[1]Pankaj Yadav, [2]Umesh Kumar Yadav & [3]Saru Bajwa
[1&3] Singhania University & [2]Bhagwant University

Abstract - The elicitation of end-user requirements is primarily focusing on the industry, where companies endeavor to discover and satisfy their customer's requirements. Increasingly however, companies which are working in the same or in different fields are getting together, in order to do joint research and development, despite the fact that they may be potential competitors. These kinds of projects have varying motivations, are often supported by governmental incentives, and participated by academic partners and other for-profit, as well as non-profit organizations. These projects also have to deal with the elicitation of end-user requirements. Current processes however, are not able to take the special characteristics, presented by such project consortia, into account. In this paper we are evaluating the suitability of the wide-audience requirements engineering method, with its new and unique characteristics, for the requirements elicitation process in such international research projects.

Keywords : Requirements Elicitation, Requirements Gathering, Wide-Audience Requirements Engineering (WARE) , WARE Method, International Cooperation, Research Projects.

I. INTRODUCTION

In requirements engineering, **requirements elicitation** is the practice of obtaining the requirements of a system from users, customers and other stakeholders. [1] The practice is also sometimes referred to as **requirements gathering**. The term elicitation is used in books and research to raise the fact that good requirements can not just be collected from the customer, as would be indicated by the name requirements gathering. Requirements elicitation is non-trivial because you can never be sure you get all requirements from the user and customer by just asking them what the system should do. Requirements elicitation practices include interviews, questionnaires, user observation, workshops, brain storming, use cases, role playing and prototyping.

Before requirements can be analyzed, modeled, or specified they must be gathered through an elicitation process. Requirements elicitation is a part of the requirements engineering process, usually followed by analysis and specification of the requirements.

Commonly used elicitation processes are the stakeholder meetings or interviews. For example, an important first meeting could be between software engineers and customers where they discuss their perspective of the requirements.

Especially in information and communication technology (ICT) research, but also in other fields, it has in recent years become increasingly common for researchers to work in international research projects. These kinds of projects often involve many different types of partners, even competitors, in a global and culturally very diverse environment. The projects are often funded in part by governmental and non-profit organizations, and in part by private companies and other institutions. The participating organizations form international project consortia, bringing together researchers from different countries, with varying backgrounds and with different interests and expertise.

II. INTERNATIONAL RESEARCH PROJECTS

While national research and development projects are often an attempt to promote local research, while bringing academia and industry closer together, international research projects are often motivated by the development of a common (technical) standard, or by promoting special, frequently new technologies or techniques. Often their wide-spread, even global introduction is most beneficial or even required for their success. Examples are typical standardization efforts, such as the GSM standard, or the research and development efforts of the World Wide Web Consortium (W3C[1]). In other cases the project goals are more politically oriented and include for instance the involvement of partners from specific countries, which are to be brought closer to ongoing global research and development.

Whereas challenges in the globalization of information systems have been covered in previous research (e.g., Ives, B. and Jarvenpaa, S. L. (1991), or Tractinsky, N. and Jarvenpaa, S. L. (1995)), this paper

focuses on the requirements engineering stage of international research projects. Although such projects have a specific set of goals, already the initial requirements are often not well understood. Current methods of requirement elicitation (RE) are geared towards the industry, which is trying to discover and satisfy the customer's needs. The methods are thus typically not very well suited for these kinds of research projects.

While the potential end-users can often be found within the project consortium itself, for example developers and researchers, their very special characteristics and constraints need to be taken into account as well. This concerns not only the varying cultural background and the physical distribution. Since the end-user is intimately involved with the project, it also involves the differing approaches towards research methodology and development work itself.

Many factors have to be considered, such as the background of the individual researcher or research groups, as well as the type and the goals of the organizations that take part in the project. Researchers that take part in such a project have often different backgrounds, different fields of expertise and different goals. For them the project often presents a mean to validate their particular research ideas. These different objectives can make the coordination of such project a major challenge, as conflicts have to be avoided. At the same time, the differing goals result in very different, potentially conflicting requirements for the whole project.

III. REQUIREMENTS ENGINEERING TECHNIQUES

The unique structure of these international research projects makes the process of finding requirements very difficult. Normal requirement elicitation techniques, such as group elicitation, prototyping, contextual or cognitive techniques, as classified by Nuseibeh, B. and Easterbrook, S. (2000) are difficult to apply, due to the varying goals of the participating parties, as well as their physical distribution over different countries.

Traditional techniques, such as questionnaires, surveys, etc. are not suitable due to their direct and immediate involvement of the end-user, which is limited by the international character of the projects discussed here. The prototyping technique as described by Davis, G. B. (1982) with its iterated approach is certainly more suitable in international projects, does however not fit with their research character, as the outcome cannot be prototyped easily. Group elicitation techniques, like brain storming or group support systems (GSS), such as TeamSpirit (Liou, YiChing, Chen, Minder, Fan, Y.W. and Jeffery Chi, Y.P. (2003)) would also be very suitable for the elicitation of end-user requirements, but lack the integration with existing software engineering processes (Herlea, D. E. (1998)). These techniques are furthermore not able to compensate for the lack of knowledge the end user may have, with regard to specific technologies or other contextual information. These are however addressed by contextual techniques (Goguen, J. and Linde, C. (1993)), such as ethno-methodology or conversation analysis. Even though, also those techniques are less suitable for the widely distributed end-users in an international research project. For very special fields, the use of cognitive techniques (Browne, G. J. and Ramesh, V. (2002)), such as protocol analysis can be useful, but it needs to be adapted for more general application.

IV. REQUIREMENTS ELICITATION TECHNIQUES IN INTERNATIONAL RESEARCH PROJECTS

Requirements elicitation techniques, such as wide-audience requirements engineering (WARE) (Tuunanen, T., Peffers, K. and Gengler, C. E. (2004)), which explicitly take the reach of the user into account, can help the RE process in international research projects significantly. Based on a laddering approach, it can be considered a model-driven technique, even though it does not necessarily rely on a very specific model of the type of information that is gathered. The WARE method also addresses other characteristics of international research projects, such as the differing context of the project participants and the flexible modeling of their goals, or the involvement of decision makers and their need for information.

Identification of end-users

In order to gather requirements it is necessary to identify the potential end-user, the targeted beneficiary of the effort. As mentioned earlier, international research projects can have a wide variety of goals which often already determine what kind of end-users are targeted. Occasionally it is the case that end-users are explicitly defined and at times not directly related to the project itself. While also in these cases the WARE method can be applied, they are not in the focus of this paper. Instead we are here concentrating on cases where the end-user, the beneficiary, is directly participating the project. Especially in the field of information and communication technology (ICT) one common goal is often the development and implementation of a common standard, in order to ensure later interoperability. In these kinds of cases the beneficiary – the end-user – is a group of companies, not primarily a group of individual persons, even though eventually those will benefit from the interoperability of, for instance, consumer products.

It needs to be taken into account that these companies are typically more in the role of competitors, but are in such a project driven by the common goal of profitability. Usually also involved are other types of groups, with varying goals and priorities. The different organizations that take part in these kinds of international projects can be divided at least into the following categories:

- Governmental funding organizations, such as the European Commission[2], which often provide partial funding for projects, while they are participating only on an advisory and management level, and ensure the proper use of funding. Their goal is typically more politically oriented, such as the general promotion of a particular industrial field, the promotion of international cooperation, or the integration of new member-countries.
- Other non-profit organizations, especially research organizations, which have a specific field of own research and expertise. These are usually heavily involved in the actual research and mostly interested in the successful dissemination of research results in the academic or industrial field. They are ideally not bound by concerns related to funding or profit, even though they may also benefit from it. This results in the possibility of doing long-term and more theoretical research.
- Industrial research centers, which are usually affiliated with a company, have typically a very high level of expertise and a lot of practical experience. While the final goal is for the company to make profit, the researchers and managers often have different levels of freedom of decision making and are able to direct efforts toward long term research. At the same time the practical experience and the close affiliation with the company itself enables the use of latest technologies and products, while bringing research results into early use.
- Companies and for-profit organizations are usually motivated to mature the research results as soon as possible and bring them to market, in order to ensure a competitive advantage of the company. These organizations share the goal of profitability, which forces them to focus on short-term and more practical research. Besides this goal of profitability, the organizations are often competitors in the same field and are driven by their own, internal goals, which often are not communicated to other members of the consortium.

These factors result in unique problems in such projects, already in the requirements elicitation process. While for instance a company may be interested in very concrete requirements that can be used in a product in the near future, a research organization may be interested in a more general approach and thus an entirely different set of requirements, whose benefits may be become apparent only over a longer period of time.

Other factors, such as cultural differences, also need to be taken into account, especially in the project management. Excluding possible localization requirements, they do however play a lesser role in the requirements elicitation process itself.

In this document we will focus on the different project participants themselves as the beneficiaries and thus as the considered end-users. Especially the researchers in these projects need to be motivated to actively and most of all creatively contribute to the project, which requires taking into account their perhaps individual fields of interest and expertise. The end-users discussed here cannot be considered to belong either to the group of external users or organizational users, as described by Kotonya, G. and Sommerville, I. (1998).

Applicability of the WARE method

In the past, ICT research projects have dealt with the problem of gathering requirements in different ways. In some cases it was possible to use conventional methods, such as described by Davis, A. M. (1993), to internally gather and present the elicited requirements. In most cases however the RE process has been less structured, as normal processes could not be applied, or required major adaptation efforts.

The WARE method of Tuunanen, T., Peffers, K. and Gengler, C. E. (2004) takes several of the key problems, such as the distribution of the end-users, into account and considers specific RE problems in wide-audience information systems (WAIS):

- Context, dealing with the relationship between the end-user and the firm, and the lack of context information available to the end-user. The significance of this problem depends on the research project itself. While sometimes the participants share a common field of expertise, there are often cases in which explicitly partners from different fields are involved.
- Reach: the problem of having the end-user available for further clarification of gathered requirements and the collection of further requirements for another product version. In international projects this problem can perhaps be considered less severe, as the participants are usually well known, and reachable by means of modern telecommunication. Project meetings also ensure the communication between partners, the exchange of further information and the clarification of difficult issues.

However, in practice there are limits to the ability of finding solutions by remote communication and, especially in the RE phase, a more efficient mechanism would be very beneficial.

- The Modeling and Model Aggregation issues deal with the lack of common knowledge between the actual product developer and the eventual end-user, as well as between different end-users. Similar to the problem of common context, mentioned above, this is often dependent on the project itself and the composition of the project consortium. Having the project participants themselves as potential end-users can reduce this problem. However, in case the project partners are from sufficiently different backgrounds, this problem can become very serious, as different experts have different backgrounds, knowledge and experience, which can easily lead to unnecessary misunderstandings and controversy. Sometimes this problem can be resolved by partners providing a basic level of education within the consortium.
- Presentation and Consensus making refer to the problem of differing perspectives and understanding between management and end-users or management and developers respectively. Also in the case of international research projects this problem is very frequent. The end-users, being members of the project, have typically different interests from those of the decision makers, who are constrained by the goals of the affiliated organization, as described earlier. Researchers are typically motivated by being able to do research in their own field of expertise, whereas management is typically driven by other goals. In same cases this problem can be decreased, or altered by having a researcher responsible for management tasks. If this is not the case, often also the understanding between decision makers and developers differs significantly, causing further problems.
- Eventually, WARE also deals with the problem of the Requirements-design interface, the methodology to model the results of the RE process in such a way as to be understandable by the end-user. This problem is perhaps less applicable in the case of research projects, where the end-user and the developer are essentially in the same group.

The WARE method addresses these problems directly. However, in international research projects another problem can be identified:

- Organizational restrictions and goals often play an integral part of the RE process of the individual organization. Even though this could be attributed to the Model Aggregation problem above, it is in fact a separate obstacle, as it refers not to the lack of common knowledge, but instead to un-communicated constraints of the individual organization. These can be related for instance to the long-term goals of the organization, or to established internal conventions.

This problem can however only be generally taken into account during the RE process, as it is more related to project management, whose problems with globalization have already been studied previously (e.g., Ives, B. and Jarvenpaa, S. L. (1991)).

V. EVALUATION

The WARE method applies altogether very well to the problems, faced in the requirements elicitation process of international research projects, especially in the field of ICT. At the same time, the size of these kinds of projects is sufficient to gather all requirements and also provides "lead users", which are quickly adopting new technologies (Rogers, E. M. (1995)). Within a limited amount of time it is possible to conduct the necessary interviews and gather the requirements, using the laddering method (Peffers, K., Gengler, C. E. and Tuunanen, T. (2003)), which WARE is based upon.

A follow-up analysis can then be carried out separately, and without the needed presence of all end-users, resulting in a well-defined set of functional, as well as non-functional requirements. If necessary it is still possible to consult with experts inside the consortium, in order to refine the results further.

In the case of an iterative development approach in the project, a very early evaluation of the use of the WARE method for the requirements elicitation process may be possible. The process provides the priorities for the different requirements, which can be implemented iteratively. As part of each iterative cycle, the fulfillment of requirements can be already be evaluated. It is possible to correct or refine requirements and select those requirements that should be implemented as part of the next development iteration. In case another development approach is taken, an evaluation can be done similar to the method described by Peffers, K. and Tuunanen, T. (2005).

VI. CONCLUSION AND FURTHER RESEARCH

In this paper we presented the requirements elicitation process of international research projects, specifically in the field of information and communication technology. We studied the suitability of the wide-audience requirements engineering (WARE) method for eliciting end-user requirements in these kinds of projects. We analyzed how the problems, identified for the WARE method relate to the special

restrictions in these types of projects and how the method itself can be applied in such an environment.

We intend to apply the WARE method in proposed and in currently starting projects, in order to evaluate its practical usability in such international research of projects. We believe that its application will significantly benefit the project and result in a set of well defined and clearly understood requirements, as well as their motivation.

REFERENCES

1. Browne, G. J. and Ramesh, V. (2002), Improving Information Requirements Determination: A Cognitive Perspective, Information & Management, 39, 625-645.
2. Davis, A. M. (1993), Software Requirements: Objects, Functions and States, Prentice-Hall.
3. Davis, G. B. (1982), Strategies for information requirements determination, IBM Systems Journal 21(1): 4-30.
4. Goguen, J. and Linde, C. (1993), Techniques for requirements elicitation, Requirements Engineering, IEEE, 152-164.
5. Herlea, D. E. (1998), Users involvement in requirements engineering, Proceedings of the Workshop on Internet-based groupware for users involvement in software development, Seattle, USA.
6. Kotonya, G. and Sommerville, I. (1998), Requirements Engineering: Processes and Techniques, John Wiley, 1998.
7. Liou, YiChing, Chen, Minder, Fan, Y.W. and Jeffery Chi, Y.P. (2003), TeamSpirits: The Design, Implementation, and Evaluation of a Web-based Group Problem Solving Support System for Distributed Teams, First Annual Pre-ICIS Workshop on Decision Support Systems: Research Directions on Decision Support, Seattle, WA, Dec. 14, 2003.
8. Nuseibeh, B. and Easterbrook, S. (2000), Requirements engineering: A roadmap, Proceedings of The Future of Software Engineering, ICSE 2000, Limerick, Ireland, pp. 35 – 46.
9. Peffers, K., Gengler, C. E. and Tuunanen, T. (2003), Extending Critical Success Factors Methodology to Facilitate Broadly Participative Information Systems Planning, Journal of Management Information Systems 20 (1), 51 – 85.
10. Rogers, E. M. (1995), Diffusion of Innovations, the Free Press, 2003.
11. Tuunanen, T., Peffers, K. and Gengler, C. E. (2004), Wide audience requirements engineering (WARE): a practical method and case study, working paper series W-378 Helsinki School of Economics; submitted to Journal of Management Information Systems, 52 – 100.
12. Ives, B. and Jarvenpaa, S. L. (1991), Applications of global information technology: Key issues for management, MIS Quarterly, 15 (1), 33-49.
13. Tractinsky, N. and Jarvenpaa, S. L. (1995), Information systems design decisions in a global versus domestic context, MIS Quarterly, 19 (4), 507-534.
14. Peffers, K. and Tuunanen, T. (2005), Using rich information to plan mobile financial services applications with maximum positive impact: A case study, Information and Management, 42 (3), 483-501.

❑❑❑

A Review of Correctness of Requirement Specifications

Pankaj Yadav[1], Saru Bajwa[2] & Shipra Srivastava[3]
[1&2] Singhania University, [3]Amity

Abstract - In order to identify the determinants for getting information requirements right, cognitive research has been conducted to study the process of information requirement analysis. As a result, three important determinants for the correctness of requirement specifications have been identified: the knowledge of information analysts, requirement analysis techniques, and problem domains. In order to identify and explain the important variables for the correctness of requirement specifications, various cognitive models have been built on the basis of different cognitive theories such as normative models, problem solving models, mental models, and comprehension models. However, they are inadequate because they are focused on some rather than all of the three determinants. As a result, two issues related to requirement analysis techniques cannot be accounted for: First, no requirement analysis technique can consistently outperform the others.

Second, experienced information analysts use multiple requirement analysis techniques in analyzing complex information systems. This research suggests that an adequate cognitive model need to meet two requirements: first, it can explicate the interactive relationships among the three determinants of information requirement analysis, and second, it can explain the two unsolved issues for requirement analysis techniques

The importance of an adequate cognitive model can be shown in four aspects: (1) it provides an adequate model for information requirement analysis; (2) it provides a basis for empirical validation; (3) it provides a framework for viewing and comparing important aspects of information requirement analysis; and (4) it provides a theoretical basis for the design of computer-aided software engineering tools.

I. INTRODUCTION

In order to identify the determinants for getting information requirements right, cognitive research has been conducted to study the process of information requirement analysis. One stream of research has investigated the differences in analytical behaviors between novice and expert information analysts. Richer domain knowledge and modeling knowledge have been recognized as the qualities of expert information analysts for better performance in information requirement analysis. Another stream of research has focused on comparing the effectiveness of various requirement analysis techniques in specifying information requirements. However, the research results are contradictory No requirement analysis technique has shown consistently better performance than the others (Kim and Larch, 1992; Yadav, Bravoco, Raikumar, 1988). In addition, experienced information analysts use multiple requirement analysis techniques in analyzing complex information systems (Littman, 1989). In order to explain the contradictory results, some researchers have suggested that requirement analysis techniques should be matched to types of problem domains (Fitzgerald, 1996; Jackson, 1994; Vessey and Glass, 1994). In addition, several frameworks have been proposed to classify requirement analysis techniques on the basis of problem domains (Davis, 1988; Iivari, 1989; Marca, and McGowan, 1993; Vessey and Glass; Fall 1994).In order to identify and explain the important variables for the correctness of requirement specifications, various cognitive models have been built on the basis of different cognitive theories such as normative models, problem solving models, mental models, and comprehension models.

However, they are inadequate because they are focused on some rather than all of the three determinants: the knowledge of information analysts, requirement analysis techniques, and problem domains. As a result, two issues related to requirement analysis techniques cannot be accounted for: First, no requirement analysis technique can consistently outperform the others. Second, experienced information analysts use multiple requirement analysis techniques in analyzing complex information systems.

Without an adequate model of information requirement analysis, research studies may miss important influential variables in viewing and comparing the cognitive processes of information requirement analysis, resulting in erroneous findings. Therefore, this research argues that an adequate cognitive model can not only explicate the interactive relationships among the three determinants of

information requirement analysis, but also explain the two unsolved issues for requirement analysis techniques.

The importance of an adequate cognitive model can be shown in four aspects: (1) it provides an adequate model for information requirement analysis; (2) it provides a basis for empirical validation; (3) it provides a framework for viewing and comparing important aspects of information requirement analysis; and (4) it provides a theoretical basis for the design of computer-aided software engineering tools.

The rest of this article will be organized into two sections. First, I review the cognitive Models used in current cognitive research of information requirement analysis. Then, the conclusion is made in the final section.

II. A REVIEW ON COGNITIVE MODELS OF INFORMATION REQUIREMENT ANALYSIS

In order to identify and explain important variables for the correctness of requirement specifications, various cognitive models have been proposed on the basis of different cognitive theories. Basically, four approaches have been used to derive cognitive models of information requirement analysis: normative models, problem solving models, mental models, and comprehension models.

First, normative models are referred to as the models of information requirement analysis

That is built on the basis of the researchers' experiences or opinions. Normative models are often built for comparing or evaluating requirement analysis techniques. Examples can be found in the research papers of Yadav, Bravoco and Raikumar (1988). This class of models provides a set of criteria about what should be achieved by good requirement analysis techniques. However, without an understanding of the cognitive behaviors of information analysts, those models provide no guideline for how to support information analysts in understanding problem domains and in specifying correct information requirements.

Second, some researchers believe that information requirement analysis is similar to the Cognitive process of problem solving (Amphora, etal., 1980; Schenk, Vitalari, and Davis, 1998; Sutcliffe and Mainden, 1992). They focus on the reasoning processes that information analysts use to analyze information requirements. Specifically, they focus on "the frequency, ordering, and association with analysts' performance of the clues, goals, strategies, heuristics, hypotheses, information, and knowledge manifested in the thought process of the information analysts" (Vitalari and Dickson, 1983, p. 949). Some examples can be found in the research papers of Malhotra, et al. (1980); Vitalari and Dickson (1983); and Sutcliffe and Mainden (1992). On the basis of the problem solving paradigm, this class of cognitive models provides a framework for understanding the influence of knowledge and reasoning processes on the correctness of requirement specifications. However, these models cannot identify the interaction among cognitive variables in determining the correctness of requirement specifications. In addition, problem domains have not been identified as a variable in these models. Third, mental models have also been used to identify important determinants for the correctness of requirement specifications. A mental model is a collection of interconnected autonomous objects (Williams, Hollan, and Stevens; 1983, p.133). According to Williams, Hollan, and Stevens, autonomous objects are mental objects that have their own internal rules to guide their behaviors. The interactions among autonomous objects achieve the task of human reasoning. Some mental models for information requirement analysis can be found in the research papers of Adelson and Soloway (1985); Guindon and Curtis (1988); Guindon, Krasner, and Curtis (1990); and Vessey and Conger (1993). On the basis of the mental models, problem statements, domain knowledge of information analysts, and methodology knowledge of information analysts are identified as three sources of knowledge for specifying information requirements. However, those models provide no theoretical basis for explaining the interactive relationships between problem domains and requirement analysis techniques.

Finally, some researchers view information requirement analysis as a comprehension process. They believe that information requirement analysis is a process of translating the knowledge of problem statements into that of requirement analysis techniques. Therefore, good requirement analysis techniques should be able to make the translation process easy for information analysts. For example, Kim and Lerch (1992) focus the required skills for the translation of information requirements. They believe that object-oriented techniques are better than functional oriented techniques because the required skill for object oriented techniques (symbolic simulation) is easier than that for functional-oriented techniques (test case). Batra and Sein (1994), on the other hand, suggest that the constructs used by requirement analysis techniques should be close to those of problem domains. By modeling information requirement analysis as a comprehension process, the above two models provide some insights about the required features for good requirement analysis techniques. However, they do not explain the interactive relationships between requirement analysis techniques and problem domains.

In addition, the knowledge of information analysts is not included in those models.

In this section I have discussed various cognitive models used by researchers to explain the cognitive process of information requirement analysis. The cognitive models have focused on different aspects of information requirement analysis like knowledge of information analysts, requirement analysis techniques, or modeling behaviors of information analysts. However, due to the lack of an integrated view of information requirement analysis, it is unknown what the Interactive relationships between the different cognitive variables are. Even worse, some research Studies may reach conflicting or contradictory conclusions because of the negligence of confounding Variables.

III. CONCLUSION

This research argues that an adequate cognitive model of information requirement analysis needs to meets two requirements: first, it can explicate the interactive relationships among the three determinants for the correctness of requirement specifications; and second, it can provide an explanation for the two unsolved issues related to requirement analysis techniques.

An adequate cognitive model is important and deserves further research because it contributes to the research in information requirement analysis in four aspects as follows.

First, the cognitive model provides a more adequate theory of information requirement analysis. In addition to explicating the relationships among the knowledge of information analysts, requirement analysis techniques, and problem domains, the cognitive model can explain two important phenomena in information requirement analysis: (1) no requirement analysis technique can consistently outperform the others; and (2) experienced information analysts use multiple requirement analysis techniques in analyzing complex information systems.

Second, the cognitive model provides a basis for empirical validation. On the basis of this cognitive model, empirical research can be conducted to test the influence of the knowledge of information analysts, requirement analysis techniques, problem domains, and the interactive relationships among the three determinants on the correctness of requirement specifications.

Third, the cognitive model provides a framework to view and to compare important aspects of information requirements. According to the cognitive model, the knowledge of information analysts, requirement analysis techniques, and problem domains are interactive in determining the correctness of requirement specifications. Therefore, effective research studies in the cognitive processes of information requirement analysis should consider interactive relationships among these three determinants.

Finally, the cognitive model provides a theoretical basis for the development of compute raided software engineering (CASE) tools.

REFERENCE :

[1] Adelson, B., and Soloway, E. (1985). The role of domain experience in software design. IEEE Transactions On Software Engineering, se-11 (11), 1351-1360. Allied Academies International Conference page 243, Proceedings of the Allied Academies, Volume 15, Number 2 Reno, 2008

[2] Batra, D., and Sein, M. K. (1994). Improving conceptual database design through feedback. International Journal of Human-Computer Studies, 40, 653-676.

[3] Davis, A. M. (1988). A comparison of techniques for the specification of external system behavior. Communications of the ACM, 31(9), 1098-1115.

[4] Guindon, R., and Curtis, B. (1988). Control of cognitive process during software design: what tools are needed? Proceedings of CHI'88. 263-268.

[5] Guindon, R., Krasner, H., and Curtis, B. (1987). Cognitive process in software design: Activities in early, upstream

[6] Design. in Bullinger, H. J., and Shackel, B. (eds). Human-computer Interaction-INTERACT'97. North-Holland, 383-388.

[7] Kim J., and Lerch, F. J. (1992). Towards a model of cognitive process in logical design: Comparing object-oriented and traditional functional decomposition software methodologies. Proceedings of CHI'92, 489-498

[8] Malhotra, A., Thomas, J. C., Carroll, J. M., and Miller, L. A. (1980). Cognitive processes in design. International Journal of Man-Machine Studies, 12, 119-140.

[9] Schenk, K.D., Vitalari, N.P., and Davis, K.S. (1998). Differences between novice and expert system analysts: What do we know and what do we do? Journal of Management Information Systems, 15(1), 9-50.

[10] Sutcliffe, A., and Maiden, N. (1992). Analysing the novice analyst: cognitive model in software

engineering. International Journal of Man-Machine Studies, 36, 719-740.

[11] Vessey, I., and Conger, S. (1993). Learning to specify information requirements: the relationship between application and methodology. Journal of Management Information Systems, 10 (2), 177-201.

[12] Vitalari, N. P., and Dickson, G. W. (1983). Problem solving for effective system analysis: An experimental exploration. Communications of the ACM, 26(11), 948-956.

[13] Williams, M. D., Hollan, J. D., and Stevens, A. L. (1983). Human reasoning about a simple physical system. in Gentner.

[14] D., and Stevens, A. L. (eds). Mental Models. Lawrence Erlbaum Associates, Publishers, Hillsdale, New Jersey. 131-153.

[15] Yadav, S. B., Bravoco, R. R., Chatfield, A. T., and Rajkumar, T. M. (1988) Comparison of analysis techniques for information requirement determination. Communication of the ACM, 31(9), 1090-1097.

◈◈◈

Speech Analysis and Synthesis in MATLAB

Srishtee Chaudhary[1] & Jagdev Singh Kaleka[2]

[1]NITTTR, Chandigarh India

[2] Dept. of ECE, Government Polytechnic College for Girls, Patiala, Punjab, India

Abstract **–** The demand for telecommunications applications of automatic speech recognition has exploded in recent years. Simplifying the interface between user and machine is one major goal of speech recognition research and development. Speech coding refers to the process of reducing the bit rate of digital speech representations for transmission or storage, while maintaining a speech quality that is acceptable for the application. LPC (Linear Predictive Coding) is a technique for speech analysis-synthesis at low bit rates. The analysis consists finding a time-based series of n-pole IIR filters whose coefficients better adapt to the formants of a speech signal. Dynamic Time Warping is a technique for aligning some new recording with some known one. DTW is a cost minimization matching technique, in which a test signal is stretched or compressed according to a reference template. DTW is widely used in the small-scale embedded-speech recognition systems such as those embedded in cell phones. The reason for this is owing to the simplicity of the hardware implementation of the DTW engine, which makes it suitable for many mobile devices. Technological innovators around the world rely on MATLAB to accelerate their research, reduce analysis and development time, and produce advanced products. It integrates mathematical computing, visualization, and a powerful technical language. Unlike most traditional languages, MATLAB gives you the freedom to focus on high-level technical concepts and ignore programming details such as memory management and variable declarations. MATLAB and its companion products are used in a broad range of applications, including signal and image processing, DSP and control design, medical research, finance, and earth and space exploration.

Key words *- Speech recognition, analysis and synthesis, Linear Predictive Coding, Dynamic Time Warping, MATLAB.*

I. INTRODUCTION

Real time speech recognition is an active area of speech research. Human perception of speech is, in part, reliant on detection of formant frequencies and their transitions times. Subjects utilize formant transition length to categorize sounds. Speech recognition systems can be classified according to the type of speech, the size of the vocabulary, the basic units and the speaker dependence. The position of a speech-recognition system in these dimensions determines which algorithm can or has to be used. Speaker independence is the typical aspect of a speech-recognition application where the rate of success is independent of the user.

Speech coding refers to the process of reducing the bit rate of digital speech representations for transmission or storage, while maintaining a speech quality that is acceptable for the application. LPC (Linear Predictive Coding) is a well-known technique for speech analysis-synthesis at low bit rates. The model of the human vocal tract mechanism assumed by LPC presupposes that speech can be reduced to a succession of voiced or unvoiced sounds.

Technological innovators around the world rely on MATLAB to accelerate their research, reduce analysis and development time, and produce advanced products. MATLAB and its companion products are used in a broad range of applications, including signal and image processing, DSP and control design, medical research, finance, and earth and space exploration.

II. LINEAR PREDICTIVE CODING

The principle behind the use of LPC is to minimize the sum of the squared differences between the original speech signal and the estimated speech signal over a finite duration. This could be used to give a unique set of predictor coefficients. LPC takes into account the redundancy in the speech signal and thus enables speech coding at low bit rate possible.

Speech can generally be classified as voiced (vowels), unvoiced (consonants). Voiced speech is quasi-periodic in the time-domain and harmonically structured in the frequency-domain while unvoiced speech is random-like and broadband. In addition, the energy of voiced segments is generally higher than the energy of unvoiced segments. Unvoiced sounds are also of higher frequency.

The LPC analysis of each frame involves the decision-making process of concluding if a sound is voiced or unvoiced. If a sound is decided to be voiced, an impulse train is used to repesent it, with nonzero taps

occurring every pitch period. A pitch-detecting algorithm is employed to determine to correct pitch period / frequency. The autocorrelation function can be used to estimate the pitch period. However, if the frame is unvoiced, then white noise is used to represent it and a pitch period of T=0 is transmitted. Therefore, either white noise or impulse train becomes the excitation of the LPC synthesis filter. It is important to re-emphasize that the pitch, gain and coefficient parameters will be varying with time from one frame to another.

The linear prediction problem can be stated as finding the coefficients ak which result in the best prediction of the speech sample in terms of the past samples. The predicted sample is given by:

$$\hat{s}(n) = \sum_{k=1}^{P} (a_k s(n-k))$$

In order to find the filter coefficients that best match the current segment being analyzed the encoder attempts to minimize the mean squared error. The first step in minimizing the average mean squared error is to take the derivative.

$$\frac{\delta}{\delta a_j} E\left[(y_n - \sum_{i=1}^{M} a_i y_{n-i} + G\epsilon_n)^2\right] = 0$$

$$\rightarrow -2E\left[(y_n - \sum_{i=1}^{M} a_i y_{n-i} + G\epsilon_n)\, y_{n-j}\right] = 0$$

$$\rightarrow \sum_{i=1}^{M} a_i E[y_{n-i} y_{n-j}] = E[y_n y_{n-j}]$$

(Use fact that $E[y_n y_{n-j}] = 0$ if $j \neq 0$)

Autocorrelation requires that {yn} be stationary and that the {yn} sequence is zero outside of the current segment. In autocorrelation, each E[yn-iyn-j] is converted into an autocorrelation function of the form Ryy(| i-j |). The estimation of an autocorrelation function Ryy(k) can be expressed as:

$$R_{yy}(k) = \sum_{n=n_0+1+k}^{n_0+N} y_n\, y_{n-k}$$

Using Ryy(k), the M equations that were acquired from taking the derivative of the mean squared error can be written in matrix form RA = P where A contains the filter coefficients.

In order to determine the contents of A, the filter coefficients, the equation A = R-1P must be solved. This equation cannot be solved with out first computing R-1. This is an easy computation if one notices that R is symmetric and more importantly all diagonals consist of the same element. This type of matrix is called a Toeplitz matrix and can be easily inverted.

$$R = \begin{bmatrix} R_{yy}(0) & R_{yy}(1) & R_{yy}(2) & \cdots & R_{yy}(M-2) & R_{yy}(M-1) \\ R_{yy}(1) & R_{yy}(0) & R_{yy}(1) & \cdots & R_{yy}(M-3) & R_{yy}(M-2) \\ R_{yy}(2) & R_{yy}(1) & R_{yy}(0) & \cdots & R_{yy}(M-4) & R_{yy}(M-3) \\ \vdots & \vdots & \vdots & & \vdots & \vdots \\ R_{yy}(M-1) & R_{yy}(M-2) & R_{yy}(M-3) & \cdots & R_{yy}(1) & R_{yy}(0) \end{bmatrix}$$

$$A = \begin{bmatrix} a_1 \\ a_2 \\ a_3 \\ \vdots \\ a_M \end{bmatrix} \qquad P = \begin{bmatrix} R_{yy}(1) \\ R_{yy}(2) \\ R_{yy}(3) \\ \vdots \\ R_{yy}(M) \end{bmatrix}$$

The Levinson-Durbin (L-D) Algorithm is a recursive algorithm that is considered very computationally efficient since it takes advantage of the properties of R when determining the filter coefficients.

L-D Algorithm

1. Set $E_0 = R_{yy}(0)$, i=0

While (i < M) {

2. i++

3. Calculate $k_i = [\sum_{j=1}^{i-1} a_j^{(i-1)} R_{yy}(i-j+1) - R_{yy}(i)] / E_{i-1}$

4. Set $a_j^{(i)} = k_i$

5. Calculate $a_j^{(i)} = a_j^{(i-1)} + k_i a_{i-j}^{(i-1)}$, $\forall j = 1, \ldots, i-1$

6. Calculate $E_i = (1 - k_i^2) E_{i-1}$

}

For voiced segments a pulse is used as the excitement signal. For unvoiced segments white noise produced by a pseudorandom number generator is used as the input for the filter. This combination of voice/unvoiced determination and pitch period is the only things that are needed to produce the excitement signal.

At the encoder we use an analysis system that has as input the speech signal and uses linear prediction to determine the filter coefficients and the appropriate excitation signal. The synthesis system consists of an all pole filter that uses the coefficients obtained from the analysis system and by using appropriate excitation it generates a synthetic speech signal.

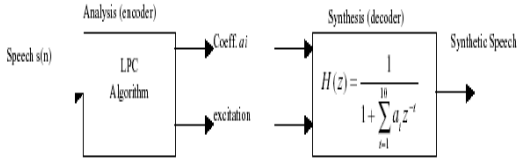

III. SPEECH ANALYSIS AND SYNTHESIS

The basic steps involved in analysis include:

Pre-emphasis : The speech signal is passed through low-order digital system to spectrally flatten the signal and prevent the precision effects to affect the analysis.

Frame Blocking : In this step, the already pre-emphasized signal is divided into frames of N samples (256), with adjacent frames being separated by M (128) samples. Since speech signals are not stationary, interest is in the similarities between signals only over a short time duration.

Windowing : Each frame is processed through a window to minimize the discontinuities at the beginning and end of each frame. A rectangular window has an abrupt discontinuity at the edge in the time domain. As a result there are large side lobes and undesirable ringing effects in the frequency domain representation of the rectangular window. To discard the large oscillations, we should use a window without abrupt discontinuities in the time domain.

Autocorrelation Analysis : Each windowed frame is auto-correlated to give:

$$r_\ell(m) = \sum_{n=0}^{N-1-m} \tilde{x}_\ell(n)\tilde{x}_\ell(n+m), \qquad m = 0,1,\ldots,p$$

LPC Analysis : Linear prediction is a method of modeling speech signals. In linear prediction, the human vocal tract is modeled as an infinite impulse response (IIR) system that produces the speech signal. Here, Durbin's method is used for converting auto-correlation coefficients to an LPC parameter set.

LPC Synthesis : The filter that is used by the decoder to recreate the original input signal is created based on a set of coefficients. These coefficients are extracted from the original signal during encoding and are transmitted to the receiver for use in decoding. Each speech segment has different filter coefficients or parameters that it uses to recreate the original sound.

IV. THE MATLAB CODE:

```
[x, fs] = wavread('f:\speech\eight.wav'); p=10;
p=number of predictor coefficients
 w=256;                    h=w/2;
                      %%  Analysis  %%
 npts = length(x);      nhops = 1+ floor((npts-w)/h);
 a = zeros(nhops, p+1);    e = zeros(1, npts);
 pre = [1 -0.9];              x = filter(pre,1,x);
 for hop = 1:nhops
              xx = x((hop - 1)*h + [1:w]);
              wxx = xx .* hamming(w);
              rxx = xcorr(wxx);
              rxx = rxx(w+[0:p]);
              R = toeplitz(rxx(1:p));
              an = inv(R)*rxx(2:(p+1));
              rs = filter([1 -an'],1,wxx);
              G = sqrt(mean(rs.^2)); a(hop,:) = [G -an'];
              e((hop - 1)*h + [(1+h/2):(w-h/2)]) =
          rs([(1+h/2):(w-h/2)])/G;
end
                      %% Synthesis %%
 e = [ ];                    [nhops,p] = size(a);
 npts = w + (nhops - 1)*h;
 if length(e) == 0          e = randn(1,npts);
 end
 if length(e) == 1
    pd = e;   e = sqrt(pd) * (rem(1:npts,pd) == 0);
end
d = 0*e;
for hop = 1:nhops
              hbase = (hop-1)*h;
              oldbit = d(hbase + [1:h]);
              aa = a(hop,:);
              G = aa(1);
              an = -aa(2:p);
              newbit = G*filter(1, [1 -an], e(hbase +
[1:w]));
d(hbase + [1:w]) = [oldbit, zeros(1,(w-h))] +
(hanning(w)'.*newbit);
%  d(hbase + [1:w]) = newbit;
end
pre = [1 -0.9];      % De-emphasis
d = filter(1,pre,d);
```

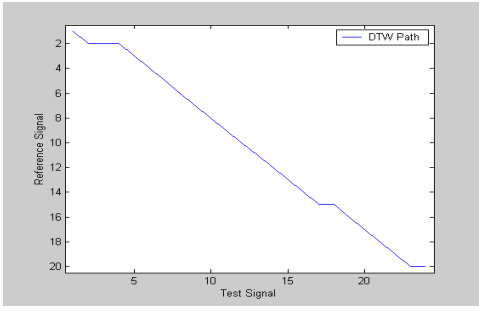

Fig. 4: DTW Simulation in MATLAB of same word

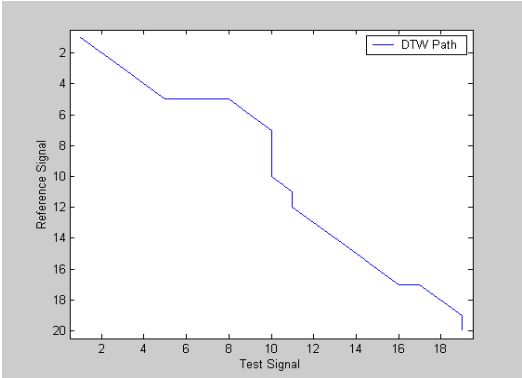

Fig. 5: DTW Simulation in MATLAB of different word

V. CONCLUSION

The demand for telecommunications applications of automatic speech recognition has exploded in recent years. This area seems a natural candidate for speech recognition systems, since it embraces a tremendous variety of applications that rely entirely on audio signals and serial interfaces. However, the telecommunication environment strains the capabilities of current technology, given its broad range of uncontrollable variables, from speaker characteristics to telephone handsets and line quality.

REFERENCES

[1] Claudio Becchetti, "Speech Recognition Systems", Wiley, April 1999.

[2] LR Rabiner, MR Sambur, "Speaker Independent Recognition of Connected Digits", IEEE International Conference on Acoustics, Speech, and Signal Processing, April 1976.

[3] L. R. Rabiner, R. W. Schafer, "Digital processing of speech signals", Prentice-Hall, Sept. 1978.

[4] Wai C. Chu, "Speech Coding Algorithms", Wiley, April 2003.

[5] "Speech Coding with Linear Predictive Coding", www.dspexperts.com/projects.

[6] Richard V. Cox, Peter Kroon, "Low Bit-Rate Speech Coders for Multimedia Communication", IEEE Communication Magazine, Dec 1996.

[7] O. M. Ibarra, F. Curatelli, "A Brief Introduction to Speech Analysis and Recognition", May 2000, www.mor.itesm.mx.

[8] Christian Plessl, Simon Maurer, Hardware/Software Codesign in speech compression applications", Feb 2000, www.tik.ee.ethz.ch

[9] Speech processing in MATLAB www.mathworks.com

◈◈◈

Modeling and Simulation of A Hysteresis Band Pulse Width Modulated Current Controller Applied to A Three Phase Voltage Source Inverter by using Mat lab

Madichetty Sreedhar & Sambeet Mishra

Dept. of Electrical Engineering, KIIT University, Bhubaneswar-751024, Odisha

Abstract - In This Paper It has been designed a hysteresis band PWM (HBPWM) current controller for a three level voltage source inverter (VSI) .The HBPWM approach has been selected for the research, since it has the potential to provide an improved method of deriving non-linear models which is complementary to conventional techniques. To illustrate the validity of this approach, an indirect vector controlled induction motor (IVCIM) drive has been considered as its application. The induction motor (IM) is modeled using *d-q* transform called Park's transformation as it adequately simulates the transient performance. network acquires the features of an HBPWM controller. The simulation model of an IVCIM drive employing HBPWM current controller is developed in SIMULINK/MATLAB environment. The performance of the proposed method is compared with conventional PWM current control scheme. HBPWM current controller is more efficient in terms of fault tolerance, switching loss and total harmonic distortion thus improving the performance of the drive.

Key words - *Hysteresis band pulse width modulated controller(HPWM),Indirect vector control of Induction Motor(IVCIM),Voltage source Inverter(VSI).*

I. INTRODUCTION

The effective way of varying speed of an Induction Motor(IM) drive is to supply with three phase Inverter of variable frequency and variable voltage. It can be obtained through a dc voltage link via a current controlled inverter. In order to maintain the proper magnetic conditions in the core the applied voltage /frequency ratio must be constant.

The various methods for the control of output voltage [6] of inverters are (i) External control of ac output voltage. (ii)External control of dc input voltage. If the available voltage is dc, then the dc voltage input to the inverter is controlled by means of chopper. This method is not much used as it involves more losses, reduced efficiency, high cost and complexity. (iii)Internal control of inverter control with in the inverter itself. The most efficient method of doing this is by Pulse Width Modulation (PWM) control used within the inverter. PWM inverters are quiet popular and most widely used in all industrial applications. In the present paper the output voltage of inverter is controlled by using HBPWM control.

The PWM principle, different methods of PWM techniques and HBPWM controller is discussed in detail and description of modeling of HBPWM controller in SIMULINK/MATLAB. Simulation block diagram of IVCIM using HBPWM current controller for the inverter is presented and the simulation results are Shown.

II. PWM CONTROL

In this method, a fixed dc input voltage is given to the inverter and a controlled ac output voltage is obtained by adjusting the on and off periods of the inverter components. Inverters employing PWM principle are called PWM inverters. PWM techniques are characterized by constant amplitude pulses. The width of these pulses is modulated to obtain inverter output voltage control and to reduce its harmonic content. The advantages possessed by PWM technique are [8]

(i) The output voltage control with this method can be obtained without any additional components.

(ii) With this method, lower order harmonics can be eliminated or minimized along with its output voltage control. As higher order harmonics can be filtered easily, the filtering requirements are minimized.[1]

The main disadvantage of this method is that the SCRs are expensive as they must possess low turn on and turn off times. This is the most popular method of

controlling the output voltage of an inverter in industrial applications.[2]

III. TYPES OF PWM TECHNIQUES

There are several types of PWM techniques [4] Sinusoidal PWM (SPWM),Selected harmonic elimination (SHE) PWM, Minimum ripple current PWM, Space vector PWM, Hysteresis band current control PWM (HBPWM),Sinusoidal PWM with instantaneous current control, Sigma-delta modulation

The hysteresis band current control PWM has been used because of its simple implementation, fast transient response, direct limiting of device peak current and practical insensitivity of dc link voltage ripple that permits a lower filter capacitor.

IV. HBPWM CURRENT CONTROL

The HBPWM is basically an instantaneous feedback current control method of PWM where the actual current continually tracks the command current within a specified hysteresis band.[3]

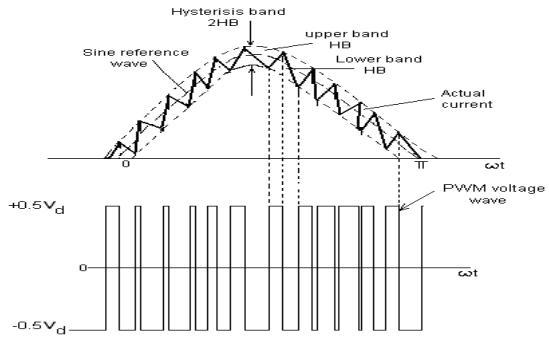

Fig. 1: Principle of Hysteresis Band current control

The Fig 1 explains the operation principle of HBPWM for a half bridge inverter. The control circuit generates the sine reference current wave of desired magnitude and frequency, and it is compared with the actual phase current wave. As the current exceeds a prescribed hysteresis band, the upper switch in the half-bridge is turned off and the lower switch is turned on. As a result the output voltage transitions from $+0.5V_d$ to $-0.5V_d$, and the current starts to decay. As the current crosses the lower band limit, the lower switch is turned off and the upper switch is turned on. The actual current wave is thus forced to track the sine reference wave within the hysteresis band by back- and-forth switching of the upper and lower switches. The inverter then essentially becomes a current source with peak to peak current ripple, which is controlled within the hysteresis band irrespective of V_d fluctuation. The peak-to peak current ripple and the switching frequency are related to the width of the hysteresis band. The HBPWM inverter control method is shown in the Fig 2. The inputs to the HBPWM controller are three phase current errors and the outputs are the switching patterns to the PWM inverter. k in the figure represents the normalization factor and is used for the purpose of scaling the current error input to the HBPWM controller. PS is the pulse separation circuit for the separation of pulses to the IGBTs in the upper and lower leg of the inverter.[4]

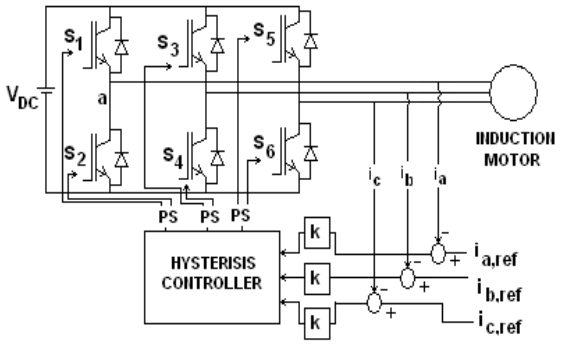

Fig. 2 : Conventional HBPWM Inverter Control method

The hysteresis current controller gives output pulses to the inverter according to this rule [7]

$|i_{m,ref} - i_m| < \varepsilon$ keeps the output pulse at the same state $i_{m,ref} - i_m > \varepsilon$ let output pulse =1(high)

$i_{m,ref} - i_m < -\varepsilon$ let output pulse =0(low)

Where m=a, b, c phases and ε is the hysteresis band

The algorithm for this scheme is:

$$i_{m,ref}(t) = I_{m,ref}\sin(wt)$$

Upper band $$i_u = i_{m,ref}(t) + \Delta i \quad (1)$$

Lower band $$i_l = i_{m,ref}(t) - \Delta i \quad (2)$$

Where Δi =hysteresis band limit

If $i_m > i_u$, $$V_{mo} = -V_{dc}/2 \quad (3)$$

If $i_m < i_l$, $$V_{mo} = V_{dc}/2 \quad (4)$$

Else, maintain the same state. Where m=a, b, c phases i is load current and V_{dc} is the dc link voltage of the inverter.[3]

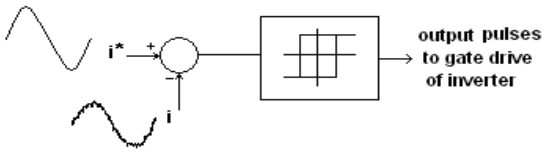

Fig. 3 : Control block diagram for HBPWM

The main drawback of this method is that the PWM frequency is not constant and, as a result non optimum harmonics will result.

V. SIMULINK MODELOF HBPWM CURRENT CONTROLLER

The HBPWM current controller block diagram using SIMULINK/MATLAB is shown below in Fig 4. Current errors for the three phases are determined and a hysteresis block is employed for each phase. The outputs of HBPWM controller, which are pulses, are given to inverter feeding the 3-ø IM. The hysteresis block is available in SIMULINK library in discontinuities and fixed point block set.

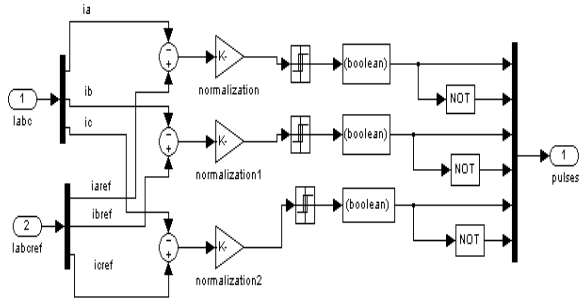

Fig. 4 : Block diagram of HBPWM current controller

VI. SIMULINK MODEL OF IVCIM DRIVE USING HBPWM CONTROLLER

To illustrate the operation of HBPWM current controller the simulation model of an IVCIM drive using HBPWM current controller is developed and simulated. The model is shown in Fig 5. The IM block is available in the SIMULINK library in Sim Power Systems block set. The motor specifications can be specified by double clicking the block. The IM is squirrel cage type and the synchronous reference frame is selected. The motor block is internally d-q modeled.[5]

The reference inputs to the system are the reference speed (ω_{ref}) in radians per second, the flux linkages (flux*) and the load torque (Load torque) The required outputs are the developed electromagnetic torque (T_e) and the rotor speed (ω_m).

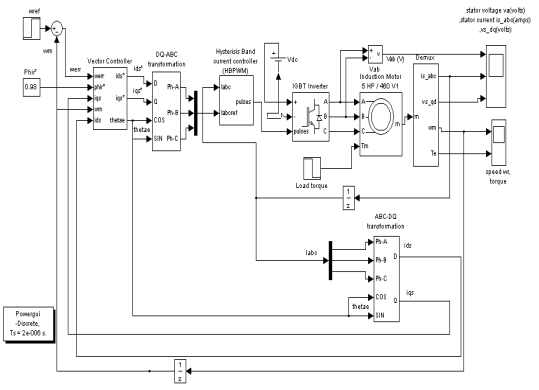

Fig. 5 : Block diagram of IVCIM drive using HBPWM current controller.

VI . VECTOR CONTROLLER

The Fig 6 shows the vector controller for the IM drive.

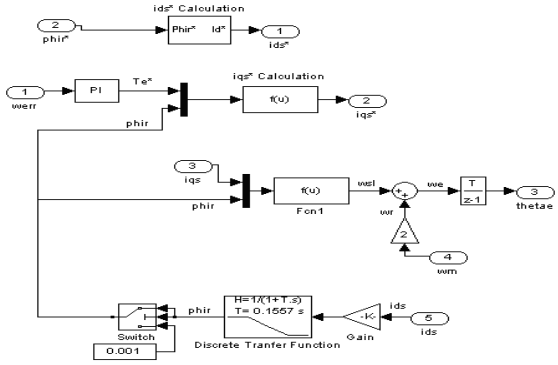

Fig . 6 : Vector Controller block diagram

The inputs to the vector controller are rotor reference flux (flux*) and difference in reference speed and actual motor speed (ω_{err}). Flux* is used to generate i_{ds}^* . $i_{ds}^*$is the control current to control i_{ds}, where i_{ds} is the d-axes component of stator current.

$$\Psi_r = L_m i_{ds}^* \qquad (5)$$

$$i_{ds}^* = \frac{\Psi_r}{L_m} \qquad (6)$$

i_{qs}^* is the control current to control i_{qs}, where i_{qs} is the q-axes component of stator current. ω_{err} is used to calculate i_{qs}^* using algorithm. A PI controller is used to generate the reference torque T_e^* from $\omega_{err.}$ The gain constants K_P

and K_I of the PI controller chosen are 16 and 32 and are selected by performance. The Rotor flux flux is calculated from the equation (5)

$$\Psi_r = L_m i_{ds} \Big/ \left[\frac{L_r}{r_r} s + 1 \right] \qquad (7)$$

The dynamic part of the flux is omitted while calculating the reference rotor flux. This is because the rotor flux is constant in steady state. The i_{qs}^* is calculated using T_e^* and flux*.

$$T_e^* = \frac{3}{2}\frac{P}{2}\frac{L_m}{L_r}\Psi_r I_{qs}^* \qquad (8)$$

$$i_{qs}^* = \frac{2}{3}\frac{2}{P}\frac{L_r}{L_m}\frac{1}{\Psi_r}T_e^* \qquad (9)$$

Slip speed denoted by ω_{sl} in rad/sec is calculated using Phir (rotor flux) and i_{qs} (q-axes component of stator current) from the following equation 4.

$$\omega_{sl} = (\omega_e - \omega_r) = L_m \frac{r_r^{'}}{L_r}\frac{i_{qs}}{\hat{\Psi} r} \qquad (10)$$

The synchronous speed ω_e and therefore theta are calculated using the equations 5 and 6 respectively.

$$\omega_e = \omega_r + \omega_{sl} \qquad (11)$$

$$\theta_e = \int \omega_e dt = \int (\omega_r + \omega_{sl}) dt = \theta_r + \theta_{sl} \qquad (12)$$

VII. a-b-c TO d-q TRASNFORMATION

The a-b-c to d-q transformation can be implemented by the SIMULINK model shown in the Fig 7.

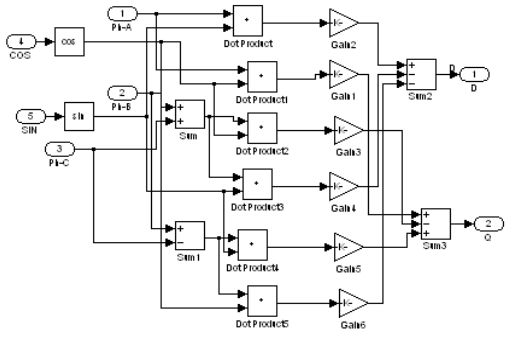

Fig. 7 : Block diagram for a-b-c to d-q Transformation

Transformation matrix used for a-b-c to d-q transformation is given by the following equation 13.

$$\left[T_{qd0}(\theta)\right] = \frac{2}{3}\begin{bmatrix} \cos(\theta) & \cos(\theta-\frac{2\pi}{3}) & \cos(\theta+\frac{2\pi}{3}) \\ \sin(\theta) & \sin(\theta-\frac{2\pi}{3}) & \sin(\theta+\frac{2\pi}{3}) \\ \frac{1}{2} & \frac{1}{2} & \frac{1}{2} \end{bmatrix} \qquad (13)$$

VIII. d-q to a-b-c (DQ-ABC) TRANSFORMATION

The d-q to a-b-c transformation can be implemented by the SIMULINK model shown in the Fig 8.

$$\left[T_{qd0}(\theta)\right]^{-1} = \begin{bmatrix} \cos(\theta) & \sin(\theta) & 1 \\ \cos(\theta-\frac{2\pi}{3}) & \sin(\theta-\frac{2\pi}{3}) & 1 \\ \cos(\theta+\frac{2\pi}{3}) & \sin(\theta+\frac{2\pi}{3}) & 1 \end{bmatrix} \qquad (14)$$

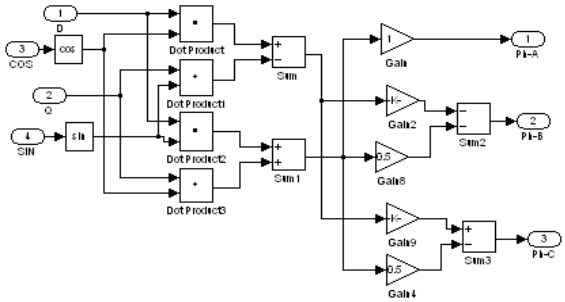

Fig. 8 : Block diagram for d-q to a-b-c Transformation

Transformation matrix used for d-q to a-b-c transformation is given by the equation (14).

IX. SIMULATION RESULTS AND DISCUSSIONS

The simulation results of the IVCIM drive employing HBPWM controller with an inverter and an IM with the following specifications are considered.

Inverter: DC link voltage (V_{dc}) = 428.76V

The dc link voltage V_{dc} should be around $1.453V_L$ where V_L is R.M.S value of line voltage.

Sampling time (T_s): 1.8μs,Hysterisis Band width of HBPWM current controller is 0.03.Induction motor: 3 phase, 6 hp, 440 V, 4-pole Frequency: 50 Hz Stator resistance (r_s): 0.007 ohm.Rotor resistance (r_r'): 0.028 ohm.Stator Leakage inductance (L_{ls}): 0.8 mH. Rotor Leakage inductance (L_{lr}'): 0.8 mH. Magnetizing inductance (L_m):34.7 mH

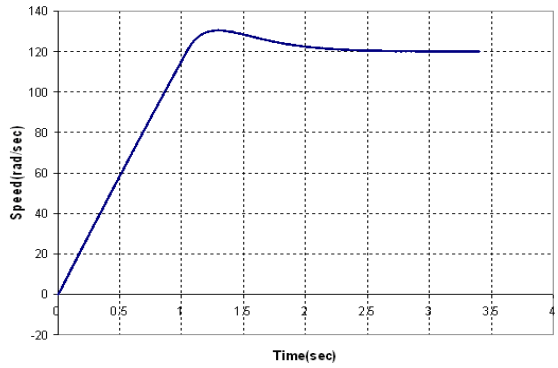

Fig. 9 : Speed response of IVCIM using HBPWM controller without any disturbance.

The motor has high starting torque of about 10 to 12 times the load torque. But in the graph the starting torque is seen to be constant at three times the load torque. In the vector controller circuit for i_{qs}^* generation where a PI controller is used to generate the reference torque, a saturation limit of three times the load torque is set.

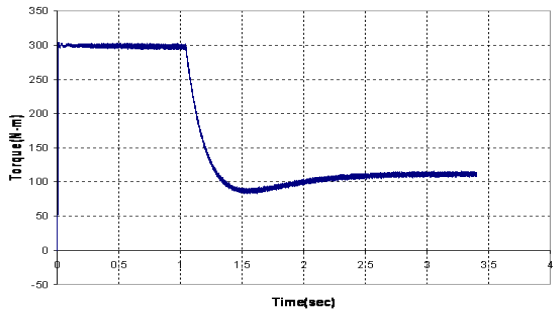

Fig. 10 : Torque response of IVCIM using HBPWM controller without any disturbance

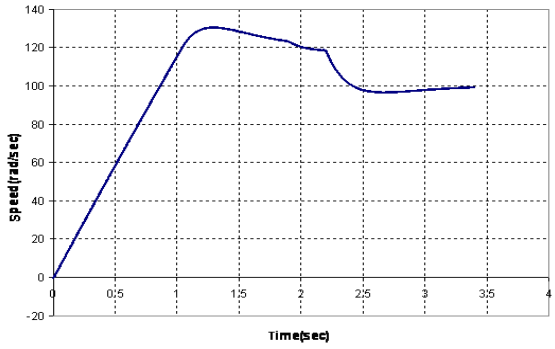

Fig. 11 : Speed response of IVCIM using HBPWM controller with step disturbance

It can be seen from the graph that the disturbance in load is given even before the drive reached the post disturbance speed 160 rad/sec. Now if the drive is left as such without any further disturbance, it stabilizes at around 3.277 sec. But the step disturbance of 50 rad/sec in speed given at 2.2 sec causes the drive to stabilize at around 3.5 sec.

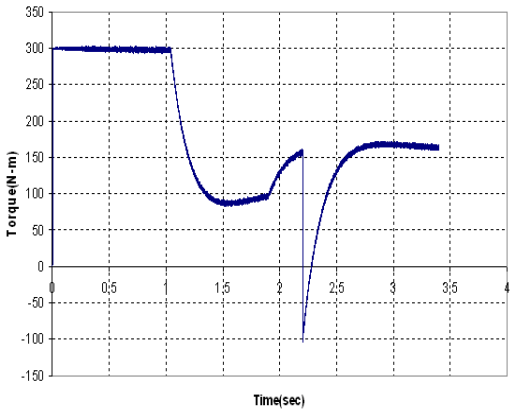

Fig. 12 : Torque response of IVCIM using HBPWM controller with step disturbance

HBPWM controller, when there is a step disturbance in load torque and speed at 1.9 sec and 2.2 sec respectively. Pre and post disturbance values of load torque are 100 N-m and 150 N-m respectively.. This dip can be reduced by proper selection of gain constants of the PI controller generating the reference torque T_e^*. As the speed of motor reaches the reference value of 100 rad/sec, the developed torque reaches a final value of 170 N-m.

Fig. 13: Stator current of IVCIM using HBPWM controller with normalization factor k=1

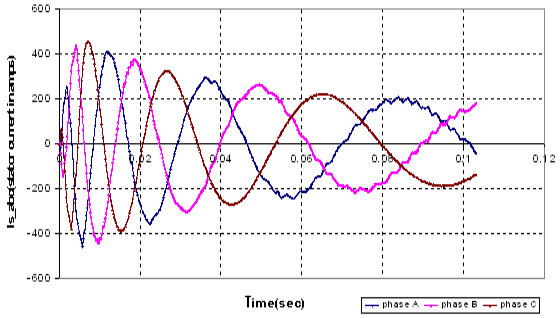

Fig. 14(a) : Stator current of IVCIM using HBPWM controller with k=0.003

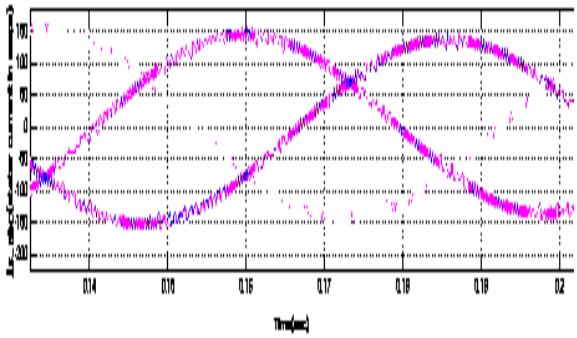

Fig. 14(b) : Zoomed portion of stator current of IVCIM using HBPWM controller with k=0.003

It can be observed from the graphs shown in Figs 13 and 14(a) that when the current error input to the HBPWM controller is not normalized i.e. k=1, the input current to the stator of IM is smooth but with the normalization factor k=0.003 the input current to the stator of IM is distorted and there is an increase in torque pulsations in the developed torque. The Fig 3.14(b) shows the zoomed portion of the stator current in the in the Fig 3.14 (a). Further normalization causes further distortion of input current and increase in the pulsations in the torque waveform.

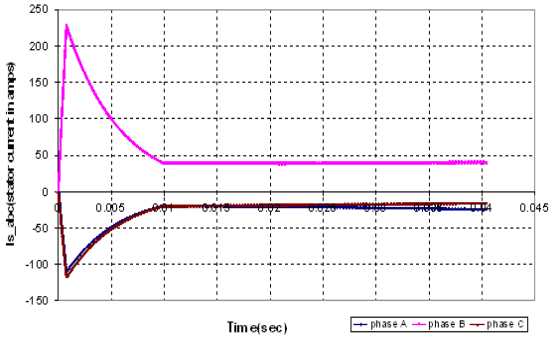

Fig. 15 : Stator current of IVCIM with HBPWM when A-phase current error is zero

The switching loss of the inverter using HBPWM controller in the IVCIM drive is calculated by defining a ratio α as follows:

$$\alpha = \frac{\text{number of actual device switchings}}{\text{number of possible switchings}}$$

Reduction of α decreases the inverter switching loss. The values of α calculated for different values k is given below:

α for k=1 is	0.26
α for k=0.1 is	0.64
α for k=0.003 is	0.96

Total Harmonic Distortion

The total harmonic distortion (THD) is a measure of closeness in shape between a waveform and its fundamental component and is defined as

$$\text{THD} = \frac{\left[\sum_{n=2,3,\ldots}^{\infty}\left(\frac{I_n^2}{n}\right)^2\right]^{1/2}}{I_1} = \frac{1}{I_1}\left(I^2 - I_1^2\right)^{1/2}$$

where, I_n = RMS value of the nth harmonic component of the current I_1 = RMS value of the fundamental component of the current . I = RMS value of the total current. The % total harmonic distortion (%THD) of the input current to the stator of the IVCIM using HBPWM controller for hysteresis band widths of 0.02 and 0.5 are shown in the Table 1:

Table 1: %THD

Hysteresis Band Width	%THD of stator current (phase-A) of IVCIM using HBPWM controller
0.02	3.679
0.5	4.210

X. CONCLUSIONS

In this Paper the working principle of HBPWM current controller and its modeling in SIMULINK for an inverter control is discussed. As its application, an IVCIM drive is modeled and the results are shown. The hysteresis band width of the HBPWM current controller is 0.02. The speed, torque responses, stator current waveforms, inverter switching losses and %THD of the stator current of the IVCIM .

REFERENCES

[1] Masao Yano, Shigeru Abe, Eiichi Ohno: "History of Power Electronics for Motor Drives in Japan", IEEE Publishers.

[2] Jacek M. Zurada: "Introduction to Artificial Neural Systems"-West Publishing Company, 2002.

[3] MATLAB 6.5: Help Documentation-Release Notes 13.

[4] I.Boldea & S.A.Nasar:"Vector control of AC Drives".

[5] Bimal K. Bose: "Modern Power Electronics and Ac Drives"-Pearson Education,

[6] Dr. P. S. Bimbhra: "Power Electronics"-Khanna Publications, 2nd Edition, 1998.

[7] Bor-Ren Lin and Richard G.Hoft: "Power Electronics Inverter Control with Neural Network", in IEEE-APEC, (San Diego), pp. 128-134, 1993.

[8] Fumio Harashima, Yuzo Demizu, Seiji Kondo, Hideki Hashinmoto: "Application of Neural Networks to Power Converter Control", IEEE-IAS, Ann. Mtg. conf. Record, pp.1086-1091, 1989.

[9] Marian P Kazmierkowski, Dariusz Sobczuk: "Improved Neural Network Current Regulator for VS-PWM Inverters" IEEE, pp. 1237-1241, 1994.

◈◈◈

Ant Colony Optimization and Gradient for Capacitor Placement in Electrical Systems

Bharat Solanki[1] & Manish Srivastava[2]

[1]R.G.P.V , Bhopal, India, [2]E.C Dept. T.I.T Bhopal, India

Abstract - The optimal capacitor placement problem involves determination of the location, number, type and sizes of capacitor to be placed in a distribution system in the most efficient manner. The main objective of optimal capacitor allocation is to reduce the peak power losses of the system while striving to minimize the cost of the capacitors in the system. This paper describes an approach to minimize the active losses in electrical distribution systems with the help of the optimal capacitor bank placement. Ant Colony Optimization (ACO) technique along with the gradient method is employed in order to have the perfect placement of the Capacitor Banks. We have used the gradient method along with the metaheuristic so as to accelerate the convergence of the ACO algorithm. The optimization algorithm described here has been applied successfully in two real systems. Results obtained by simulation of real systems, are presented to validate the proposed solution method.

Key words - *load flow, ACO metaheuristic, Gradient, Capacitor Placement*

I. INTRODUCTION

The complex social behaviors of insects have been intensively studied in science and in research of computer technology. The attempt is to develop algorithms inspired by insect behavior to solve optimization problems. These behavior patterns can offer models for solving difficult combinatorial (distributed) optimization problems. Real ants which can indirectly communicate by pheromone information without using visual cues are able of finding the shortest path between food sources and their nest. Artificial ants imitate the behavior of real ants how they forage the food [1], but can solve much more complicated problem than real ants can. One of search algorithms with such concept is Ant Colony Optimization (ACO) [3]. ACO has been widely applied to solving various combinatorial optimizations problems such as Travelling Salesman Problem (TSP) [2, 4, 5], Quadratic Assignment Problem (QAP) [3], Weapon-Target Assignment problems (WTA) [16, 17], etc

Since 1970s, researchers are working towards the goal of producing computational methods in order to optimize power systems. In the late 80s and early 90s, work oriented to distribution systems became more common, after the emergence of efficient computational methods, such as, the power summation load flow method [1] used for simulating electricity distribution radial systems. At that time, also began to emerge general purpose heuristics, called metaheuristics, applied successfully in many optimization problems. For capacitor placement optimization, it is emphasized the Tabu Search [2], [3], Genetic Algorithms [4], [5] and Ant Colony [6], [7], [8], due to the frequency with which they are addressed in technical literature and survey.

The capacitor placement problem consist of finding places to install capacitor bank in an electrical distribution network aiming to reduce losses due to the compensation of the reactive component of power flow. The capacitor placement is hard to solve in sense of global optimization due to the high non linear and mixed integer problem.

The current work presented here helps in the minimization of the active losses in distribution systems, with the help of placement of capacitor banks. In [9], the solution of this problem was formulated by the gradient method combined with a clustering algorithm that, may be fast, but does not guarantee to find the global optimized solution. The algorithm proposed here combines the gradient method with the ACO metaheuristic. The gradient vector provides a measure of the impact caused by the injection of reactive power losses in the system. The metaheuristic uses this measure to guide and accelerate the search. The final result is a method which is able to find the global optimum solution very easily.

This paper is organized as follows. Section II describes the problem of optimal capacitor placement. In Section III, it presents a brief introduction to the ACO metaheuristic. In Sections IV and V, it describes the proposed ACO algorithm for capacitor bank placement. In Section VI, it shows the various experimental results

of the proposed algorithm. Finally, it presents the conclusions in Section VII.

II. PROBLEM FORMULATION

Capacitor placement problem basically determines the location and sizes of capacitors in order to minimizing the active losses. An Alternate, application can be correction of the power factor, increase the capacity of transmission lines. In this work, the function to be optimized is defined as the total active losses of the system. In the form of the mathematical equation the problem can be written as:

Reduce $L_t = \sum L_i$ where i ranges from 1 to n (1)

Where n is the number of lines and Li is the active losses in line i.

III. ANT COLONY OPTIMIZATION

A. *Basic ACO*

Initially ants wander randomly, and upon finding food source return to their colony while laying down a pheromone trails. During the return trip, the quantity of pheromone that an ant leaves on the ground may depend on the quantity and quality of the food. When other ants find such a path, they are likely to follow the trail, rather than keep traveling at random.

On the passage of some time, the pheromone trail starts to evaporate, which reduces its attractive strength. If an ant takes more time to travel down and come back to colony, it gives more time to pheromones to evaporate. A shortest path, by comparison, gets marched over more frequently, and thus the pheromone density grows heavily on shortest path as compared to the other longer paths. With the help of the pheromone evaporation convergence to a locally optimized solution can be converged which is the main advantage of pheromone evaporation. This makes the ACO algorithm more accurate in finding the shortest and the most reliable path for the journey. If there were no evaporation at all, the paths chosen by the first ants would tend to be excessively attractive to the following ones. In that case, the exploration of the solution space would be constrained.

So when one ant finds a good or shortest path from the colony to a food source, other ants are more likely to follow that path, and this positive feedback eventually leads all the ants following a single path. The idea of the ant colony algorithm is to mimic this behavior with "simulated ants" walking around the graph which represents a method to solve a given problem.

B. *Basic ACO Methodology*

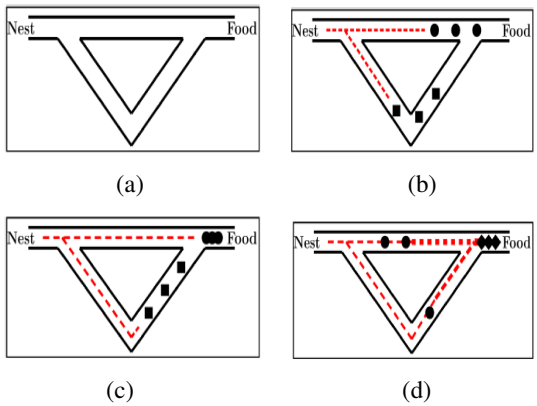

Fig. 1: Natural ACO

1. In Figure 1 (a), initially all ants are in the Nest. There is no pheromone in the environment.
2. In Figure 1 (b) the foraging starts. 50% of the ants take the short path (symbolized by circles), and 50% of the ants take the long path to the food source(symbolized rhombus).
3. As shown in figure 1 (c), the ants that have taken short path have arrived earlier than the ants which followed the longer path.. So while returning the probability to take short path is higher.
4. As shown in figure 1 (d), the pheromone trail on the short path receives in probability a stronger reinforcement and thus the probability to follow this path grows.
5. Finally due to the evaporation of the pheromone on the longer path, the whole colony will, in probability, use the short path.

C. *ACO metaheuristic Algorithm*

ACO metaheuristic is briefly described in this section. Further details can be found in [10].

In nature, after finding the food source an ant returns to its nest or colony. Ant leaves a trail of pheromone (a chemical) between the food source and its colony. If other ants manage to find this trail, they will be attracted by the pheromone as it is attractive in nature. So the other ants will mostly follow the same path with some probability. As a result these new ants reinforce the pheromone trail. Future ants choose to follow the same trail with higher probability, due to the increase in the percentage of pheromone on the trail. The final result is a strong pheromone scent on the trail connecting the colony to the food source, which attract even more ants. The ACO metaheuristic algorithm mimics this behavior of ants to build the solution of search and optimization problems.

1: initialize
2: while termination condition not met do
3: for all ant k do
4: repeat
5: add a bank to a node for ant k by rule of Eq. (3)
6: until there is no more improvement in $L_t^{(k)}$, Eq.(1)
7: compute $L_t^{(k)}$ by Eq.(1)
8: if $L_t^{(k)} < L^*$ then
9: $x^* = x^{(k)}$
10: $L^* = L_t^{(k)}$
11: end if
12: end for
13: update the pheromone by Eq. (5) and (6)
14: end while
15: return x^* (the best solution found)

Fig. 2 : ACO Algorithm

Artificial ants basically implement constructive algorithms. Generally, these algorithms start with a partial solution. With the help of step by step addition of a component (e.g., capacitors banks) to this partial solution, the algorithm builds a complete solution. At each step, the ant takes a decision which is probabilistic in nature, for the choice of the next component (capacitor bank) to be added to partial solution. This decision depends on two types of information:

1. The pheromone percentage which represents the desirability of a solution component.
2. The heuristic information which represents prior information about the problem statement.

As soon as artificial ant builds a solution (finds a path), it deposits pheromones on the path that lead the ant to the final solution. The amount of the pheromone deposited depends on the nature and quality of the food source. This procedure is repeated until it satisfies some predetermined criteria.

IV. THE PROPOSED APPROACH

This section describes the proposed algorithm for the efficient capacitor placement.

A. Representation of Solution

A solution for the capacitor placement problem statement is represented by a vector x of size n. The component x_i of the vector x represents the number of capacitor banks in node i of the system (e.g., if there are Seven capacitor banks in node i, then $x_i = 7$).

B. *Constructing the Solution*

Artificial ant builds a solution in a step by step manner. In each step, artificial ant selects a node where the capacitor bank is to be deposited and add a capacitor bank to this selected node. The ant stops addition of capacitor banks to the nodes, when there is no more improvement in the objective function value.

In the current work, ACO metaheuristic uses a probabilistic rule involving pheromone and heuristic information for the selection of the node in order to add capacitor bank. More specifically, an ant k with $x_j^{(k)}$ capacitor banks in node j, has probability p_j of selecting the node j. The value p_j is calculated by the following equation:

$$P_j^{(k)} = \frac{(\Gamma_{j,zj})^{\alpha} (\eta_j)^{\beta}}{\sum_{w=1}^{n} (\Gamma_{i,zw})^{\alpha} (\eta_w)^{\beta}} \qquad (2)$$

where

Γ is the performance matrix.

η_j is the heuristic information associated with node j.

α and β are the scaling factors defined by user.

z_j refers to the next bank to be added.

C. The Pheromone

The pheromone τ is a $n \times 7$ matrix. The row i of the matrix refer to node i and the column j refer to the number of capacitor banks in each node. The maximum number of capacitor banks in a node is limited to the seven banks. The matrix element τ_{ij} is a pheromone level representing the desirability of adding the jth capacitor bank to the node i.

D. Heuristic Information

The Heuristic Information is denoted as η_j and it represents the desirability of adding a capacitor bank of the node j. In the current work, η_j is defined as jth component of gradient vector η_j helps to provide a measure of the impact caused by the injection of reactive power losses in the system.

With the help of a mathematical equation η_j can be written as:

$$\eta_j = \frac{\delta L_t}{\delta Qc_{,i}} \qquad (3)$$

here $\delta Qc_{,j}$ is the capacitive reactive power at node j.

E. Updating status of Pheromone Trails

After the completion of tasks of all the artificial ants, the pheromone trail needs to be updated. There are

two important events which affects this process, the evaporation of pheromone and the deposition of pheromone.

Evaporation reduces the level of pheromone in the pheromone matrix Γ as follows:

$$\Gamma_{ij} = (1 - \rho)\,\Gamma_{ij} \quad (4)$$

for i = 1 to 7 and j = 1 to n. Γ is the pheromone evaporation rate, whose value ranges in between 0 to 1. The evaporation process avoids the pheromone level to grow rapidly. Thus it avoids convergence to suboptimal solutions.

After the evaporation process, pheromone deposition process continues. During the deposition process the pheromone matrix is updated as per the following equation:

$$\Gamma_{ij} = \Gamma_{ij} + \sum \Delta\, \Gamma_{ij}^{(k)} \quad (5)$$

Here k is the constant which takes values from 0 to m. (m is the ant population) for i = 1 to 7 and j = 1to n, the term $\Delta\, \Gamma_{ij}^{(k)}$ is the amount of pheromone that the ant k deposits on the element Γ_{ij}.

V. IMPLEMENTATION OF THE PROPOSED APPROACH

In the case of analytical method the computation of the, Eq. (1), demands the expensive analysis of a power flow. But the ACO algorithm requires a computation of the objective function in each simple step of the solution formation. As a result, much processing time would be needed to run the ACO algorithm. In the current work in order to reduce the processing time, it was implemented a memory to save the N last power flow computations. This approach significantly reduced the processing time.

VI. EXPERIMENTAL ANALYSIS

To analyze the performance of the algorithm proposed here we have used two distributed real time systems.

1. System I - 55 nodes with total load of 2.5 MVA;

2. System II - 27 nodes with total load of 1.4 MVA;

The proposed ACO algorithm uses populations of 55 and 27 ants, respectively, and a maximum of 25 iterations. For computation of power flow, we have used the algorithm given in [1].

Table 1 : Active Losses for different systems

	Initial State	100 kVAr	200 kVAr	300 kVAr
System 1	0.6793	0.5743	0.6791	0.6795
System 2	4.3017	3.5361	3.6223	4.3027

Second column of Table 1, shows the value of total losses for the initial configuration without the addition of the capacitor banks. The last three columns indicates the resultant losses obtained by proposed ACO algorithm using units of capacitor banks of 100, 200, and 300 kVAr, respectively.

Table 2 : Capacitor Banks Added

	100kVAr	200kVAr	300kVAr
System 1	1	0	0
System 2	3	1	0

Table 2 specifies the number of capacitor banks added in each system. From the results it can be said that the ACO algorithm worked perfectly in its task of placement as it has not added capacitors of 200 MVA and 300 MVA to the system 1, since these capacitors have high powers for the system 1 and its addition would lead to the increase in the losses.

Table 3 : Iterations for the optimal solution

	100kVAr	200kVAr	300kVAr
System 1	7	0	0
System 2	5	1	0

In Table 3, shows the number of iterations performed by the proposed ACO algorithm for obtaining the optimal solution. While the simulation, in all the cases, the best solution was found with few iterations only.

Table 4 : Gradient influence to the result

	With Heuristic	Without Heuristic
System 1	22	31
System 2	11	17

In Table 4 specifies a different experimental study results to know the influence of the gradient. In this study we have used heuristic information of the ACO algorithm, as per the according to Equation 3. The algorithm was applied to the systems using two different methods: with information heuristic and without

information heuristic. Table 4 shows the number of iterations to find the optimal solution. While using the heuristic information the number of iterations is less in both the cases.

VII. CONCLUSION

The ACO metaheuristic algorithm is proved to be efficient to find the optimal solution in the capacitor placement problems studied in this work. The proposed algorithm described here, which uses the gradient vector as heuristic information to the colony of artificial ants, was effective, efficient and promising in the experiments studied here. Also in this current work the ACO approach is implemented with innovations like method of finding solution and the use of the pheromone matrix.

REFERENCES

[1] E. Bonabeau, M. Dorigo, and G. Theraulaz, "Swarm intelligence from natural to artificial systems," Oxford University Press, 1999.

[2] M. Dorigo and L. M. Gambardella, "The colony system: A cooperative learning approach to the traveling salesman problem," IEEE Transactions on Evolutionary Computation, Vol.1, No.1, April, 1997.

[3] A. Colorni, M. Dorigo, and V. Maniezzo, "Distributed optimization by ant colonies," Proc. of ECAL91-European Conference on Artificial Life, pp. 134-142, 1991.

[4] M. Dorigo, V. Maniezzo, and A. Colorni, "The ant system: Optimization by a colony of cooperating agents," IEEE Transactions on System, Man, and Cybernetics, Part B, Vol.26, pp. 29-41, 1996.

[5] T. St¨utzle and H. H. Hoos, "Max-min ant system," Future Generation Computer System, Vol.16, pp. 889-914, 2000.

[6] Z.-J. Lee, S.-F. Su, and C.-Y. Lee, "An immunity based ant colony optimization algorithm for solving weapon-target assignment problems," Applied Soft Computing, Vol.2, pp. 39-47, 2002.

[7] Z.-J. Lee, S.-F. Su, and C.-Y. Lee, "A heuristic based ant colony system applied to weapon-target assignment problems," Journal of Applied Systems Studies, Vol.4, No.2, 2003.

[8] G. R. Cespedes, "New method for analysis of distribution networks," IEEE Transactions on Power Delivery, vol. 5, no. 1, 1990.

[9] R. A. Gallego, A. J. Monticelli, and R. Romero, "Optimal capacitor placement in radial distribution networks," IEEE Transactions on Power Systems, vol. 16, no. 4, pp. 630–637, 2001.

[10] Y.-C. Huang, H.-T. Yang, and C.-L. Huang, "Solving the capacitor placement problem in a radial distribution system using tabu search approach," IEEE Transactions on Power Systems, vol. 11, no. 4, pp. 868–873, 1996.

[11] T. Ghose, S. Goswami, and S. Basu, "Energy loss reduction in distribution system by capacitor placement through combined ga-sa technique," in TENCON '98 - IEEE Region 10 International Conference on Global Connectivity in Energy, Computer, Communication and Control, vol. 2, 1998, pp. 502–505.

[12] K.-H. Kim and S.-K. You, "Voltage profile improvement by capacitor placement and control in unbalanced distribution systems using ga," in IEEE Power Engineering Society Summer Meeting 1999, vol. 2, 1999, pp. 800–805.

[13] R. Annaluru, S. Das, and A. Pahwa, "Multilevel ant colony algorithm for optimal placement of capacitors in distribution systems," in Congress on Evolutionary Computation CEC2004, 2004.

[14] P. Gardel, B. Baran, H. Estigarribia, U. Fernandez, and S. Duarte, "Multiobjective reactive power compensation with an ant colony optimization algorithm," in The 8th IEE International Conference on AC and DC Power Transmission, 2006. ACDC 2006, 2006.

[15] C.-F. Chang, "Reconfiguration and capacitor placement for loss reduction of distribution systems by ant colony search algorithm," IEEE Transactions on Power Systems, vol. 23, no. 4, pp. 1747–1755, 2008.

[16] M. F. M. Junior and M. C. P. Filho, "Optimal power flow in distribution networks by newton' s optimization methods," in Proceedings of the 1998 IEEE International Symposium on Circuits and Systems, Montrey, CA, 1998.

[17] M. Dorigo and T. Stützle, Ant Colony Optimization. MIT Press, 2004.

◈◈◈

Real Time Implementation of Differential Time Lapse Video

Sardhara Ravin[1], Abhishek Choubey[2] & Bharat Solanki[3]

[1&3]R.G.P.V , Bhopal, India
[2] Dept. of E.C., R. K. D. F Bhopal, India

Abstract - Time lapse method is one of the cinematography technique in which each frame is captured with a rate which is very much lesser as compared to the speed in which it is played back. Recorded frames when played back at a normal rate, time seems to be running at a faster rate which is known as lapsing. The procedures such as plant growing, motion of the sun and stars in the sky generally appears to be stable for human eye. Times lapse approach is an efficient technique to record extremely slowly processing/developing/moving procedures. Basically in this approach, a series of snaps of the subject under study are taken at regular or irregular intervals and finally arranged sequentially to create a small movie of all those snaps. Generally video recording requires very less information as compared to the normal video. One of the main features of differential time-lapse technique is that it allows to remove unnecessary frames from the normal video, so that the time to visualize gets reduced and also decreases the storage requirements. A vital application of Time-lapse techniques can be for documentation of the processes for getting the finer details of the slowly changing processes, One of the drawback of the differential time lapse video is that it does not provide the information about the time at which an event is recorded. This limitation can be overcome by using real time loss less visual watermarking. The proposed algorithm has been implemented in MATLAB for generating the differential time lapse video along with the date and time stamping with the help of loss less visual watermarking. The results have been tested for five different processes.

Keywords - *Time Lapse Video, Lossless Watermarking, Pixel threshold value, Pixel difference value.*

I. INTRODUCTION

Time-Lapse is proved to be an effective tool for visualizing processes that changes too slowly and which needs to be perceived in real-time. Time-Lapse videos are mostly used to capture natural phenomenon like motion of sun, a plant growing or any other natural process which takes very large amount of time in terms of days or years for its completion. In the case of Time-lapse approach the frames are captured at a much slower rate as compared to its playback speed. Camera connected to the system captures the live streams of frames which can be directly accessed by the Matlab algorithm. Periodic form of Time Lapse Video can be created by sampling the live frames at regular interval. These Periodic Time Lapse Videos can be very much useful to effectively represent natural phenomenon. For representing non-natural phenomena effectively, a special type of non periodic time lapse Video, known as differential time lapse video can be used [1]. A differential time lapse video can be generated by the arranging the different frames captured with the help of a capturing device in specific order. Initial frame is stored in the video file. The next frame is compared with the previously stored frame by a pixel to pixel bit mapping algorithm. Only when the pixel value is differed by an amount larger than the Pixel Difference Value (PDV), that particular pixel is treated as a modified pixel [2,3]. Overall the total number of such modified pixels are recorded and If the total number of modified pixels are greater than 15% (Value can change according to the application requirements) of total number of pixels in the frame, than that particular frame is selected and stored in the video file. If the modified pixels are less than the specified value (15% here) than the frame is discarded. All the frames selected by pixel to pixel mapping algorithm are processed by visual watermarking algorithm so as to get date and time stamp on each of the frame. Lossless watermarking technique is used so as to get the finer details.

II. DIFFERENTIAL TIME LAPSE VIDEO

For selecting the frame from the live streaming captured by the video capturing device, edge detection technique, bit wise pixel mapping technique etc can be used. The simplest algorithm should be choosing so as to make it run faster for the real time application [4]. Here we have used a simple bit by bit pixel mapping based algorithm to detect the motion. A simplified algorithm for differential time lapse video is as shown in figure 1. The first frame captured by the capturing device, gets stored as default in the video file for every process. The next frame undergoes a test via pixel

mapping algorithm to check the variations as compared with the previously stored frame. If variations are found upto a specific level decided than the the frame is chosen to be stored in video file and if the variations are less the frame is discarded [5]. This variation calculation is obtained by pixel mapping algorithm. If pixel intensity having the difference value larger than the specified pre-define Pixel Difference Threshold (PDT) level than, this is considered to be as the change in the pixel. Now if the changes in the intensity of the frame is due to the environmental changes than such image may not be useful to be taken in to the final video file. Such images are to be discarded which has changes in the intensity level but does not have any remarkable modifications on the subject under study.

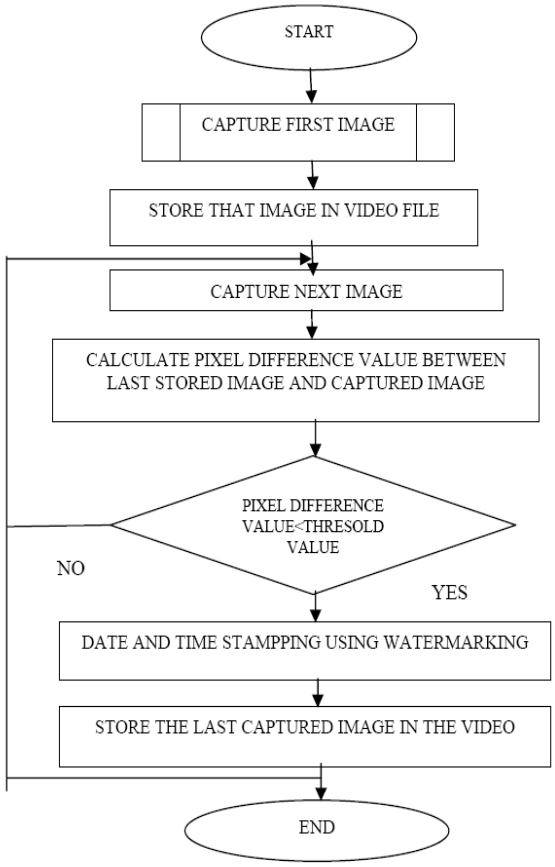

Fig. 1 : Algorithm for Differential Time Lapse Video

III. EFFECT OF ENVIRONMENTAL CHANGES

The figure 2 describes the sequence of images where the pixel values are multiplied by the factor of 1.5 according to which the contrast level changes.

Fig. 2 : Effect of variation in Contrast

The figure 3 describes the sequence of images where the pixel value is added up with a factor of 12, so as to increase the brightness of the frame. The changes in the effects may not be visible for the images in the sequence taken at regular intervals. The changes can be seen if we compare the first and the last image and so on. As per the proposed algorithm the frames should not be selected in the final video file based on differential time lapse video only due to the changes in the brightness or contrast or both which are the environmental factors and does not show much changes in the subject under study. To avoid such situations the pixel difference threshold value is targeted to be set around 20 or higher, so that the effect of the brightness and contrast are eliminated from the differential time lapse video.

Fig. 3 : Effect of variation in Brightness

IV. SELECTION CRITERIA OF FRAME

The effect of the pixel difference cutoff can be studied and understood with the help of an example in which the sequences of photographs are taken at periodic or regular interval of time as described in the figure 4.

Table 1 - THE PIXEL DIFFERENCE VALUE FOR DIFFERENT PDT AND PDC FOR FIGURE 2.4 (READING X/150)

0	374	1318	1993	2477	2905	3472	4064	4365	4572	4695	4947	5023	5352	5405	5411				
374	0	674	1659	2289	2762	3452	4124	4500	4709	4841	5036	5186	5617	5627	5653				
1318	674	0	572	1410	2077	2806	3492	3980	4204	4422	4617	4793	5184	5287	5309				
1993	1659	572	0	425	198	2146	2838	3338	3646	3924	4256	4457	4867	4955	5027				
2477	2289	1410	425	0	467	1521	2395	3035	3408	3707	4105	4328	4812	4861	4984				
2905	2762	2077	198	467	0	635	1788	2619	2981	3414	3887	4157	4742	4842	4943				
3472	3452	2806	2146	1521	635	0	583	1496	2103	2578	3080	3382	3394	4257	4404				
4064	4124	3492	2838	2395	1788	583	0	396	1125	375	2234	2716	3292	3514	3769				
4365	4500	3980	3338	3035	2619	1496	396	0	403	1088	1787	2307	2847	3117	3413				
4572	4709	4204	3646	3408	2981	2103	1125	403	0	391	1139	1820	2492	2766	3034				
4695	4841	4422	3924	3707	3414	2578	375	1088	391	0	360	1160	1983	2377	2739				
4947	5036	4617	4256	4105	3887	3080	2234	1787	1139	360	0	314	1092	1714	2194				
5023	5186	4793	4457	4328	4157	3382	2716	2307	1820	1160	314	0	348	1000	1653				
5352	5617	5184	4867	4812	4742	3394	3292	2847	2492	1983	1092	348	0	290	837				
5405	5627	5287	4955	4861	4842	4257	3514	3117	2766	2377	1714	1000	290	0	193				
5411	5653	5309	5027	4984	4943	4404	3769	3413	3034	2739	2194	1653	837	193	0				

The pixel difference values are calculated for pixel difference threshold equals to 20 and 30, shown in table 1. The reading on right-top above diagonal zero are for pixel difference threshold set to 20, while the reading on left-down below diagonal zero are for pixel difference threshold set to 30. The color cutoff map is shown for different pixel difference cutoff values set to 5000, 9000, 12000, 17000, 21000 and 25000. The reading shown in the table should be multiply by 100 to get actual value of pixel difference cutoff. It is easily seen from the table as the time difference increased the difference in pixel values are increased. However, at one stage this difference cross the reference level and that frames are selected for store. It is easily seen from the table that, the effect of threshold again makes large contribution in selection of the frame. If the threshold is kept low too, fine details are also covered. If threshold is kept high, only large movement will be covered. However, we have to trade off between the fine detail and size of the video.

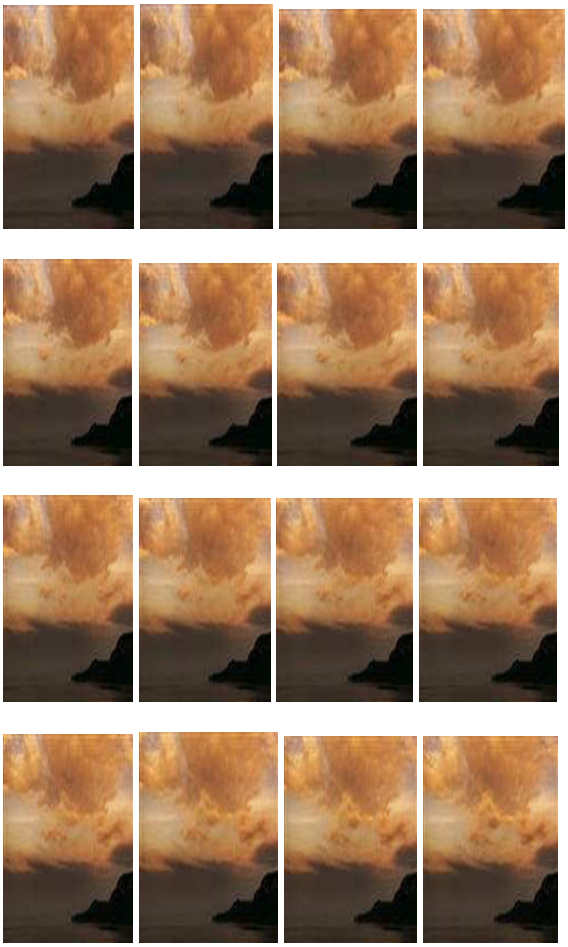

Fig. 4 : Sequential Snapshot

The number of the frame if selected are high some fine details can be covered however size of the video increases does not help the cause too, hence depends on the applications the threshold and the selection criteria should be finalized. The table along with the graph for the sequence of the figure is shown above for the different threshold value like 10, 15 and 20 respectively. In the graph the different color maps are used to shows the different pixel difference value. From the table 1, it is seen that as the time difference increased, the pixel difference value are increases. The pixel difference values are increasing more rapidly in pixel difference threshold set to 20 compared 30. The change in color are made to show that the different cutoff values set to 5000, 9000, 12000, 17000, 21000 and 25000. The selection of PDC value decides which photos are going to be selected for the differential time lapse video.

Case I: PDT = 20; PDC = 3000;

Frames selected are: a, c, e, g, I, j, l, p, s;

Total: 9 Frames

Case II: PDT = 20; PDC = 5000;

Frames selected are: a, d, h, k, q;

Total: 5 Frames

Case III: PDT = 20; PDC = 3000;

Frames selected are: a, c, e, g, I, j, l, p, s;

Total: 9 Frames

Case IV: PDT = 30; PDC = 3000;

Frames selected are: a, d, h, j, m, p, s;

Total: 7 Frames

Case V: PDT = 40; PDC = 3000;

Frames selected are: a, f, I, k, n, q, s;

Total: 7 Frames

V. DATE & TIME STAMPING

The selected frames which have changes as per the algorithm are stored in the final video file. While capturing the frames for the video file, the date and time at which that particular frame has been captured becomes very much important in understanding the finer details of the subject under study such as plant growing or location of the stars in the sky etc. For these date and time stamping a lossless visual watermarking method is used. Here the date and time of the system with which the frame capturing device is connected while implementation is considered to be as the reference time. The stamping method results into the numeric characters that are represented with the help of the binary representation as shown in the figure 5 [6,7,8,9].

Fig. 5 : Time-stamping using Visual lossless Watermarking

With the help of the lossless watermarking algorithm the pattern for each character to be stamped if found. Algorithm also produces resultant pixel image of size 20x18. For each predefined location pixel to pixel mapping is done. In the numeric character if the pixel value is equal to 1, than the respective image pixel is kept as it is. If the pixel value is not equal to 1 than the pixel value is increased by a factor of 30 percent or reduced by same percentage depending on whether the pixel is bright or dark. Figure 6 shows the original, time stamped and recovered image.

Original Image Watermarked Recovered Image

Fig. 6 : Time & Date stamping Analysis

The numbers are stored in the form of binary digits having array of 20x18 characters. The numbers which are denoted by '0' are highlighted and it represents the character to be displayed. With the help of a MATLAB based algorithm time stamping is done for the recorded images. The locations where the time stamp is to be done are fixed within the pixel values ranging from 1:20 x 1:144 for date stamping and 21:40 x 1:144 for time-stamping.

VI. CONCLUSION

One of the vital features of the proposed work is that it plays crucial role in studying the processes which takes large span of time for its completion. The work describes such processes in a very short video file (.avi). The resultant video file size is very less as compared to the total size of the frames taken for that particular subject under study. Generally video file transfer contains information which may not be really needed to describe that event. With the help of the proposed work unwanted information can be removed as it selects only smaller number of frames in which the pixel difference is greater than the specified value. Due to this the bandwidth requirement gets reduced and also the overall transmission cost comes down to an economical value in terms of time and money.

REFERENCES:

[1] http://en.wikipedia.org/wiki/Time-lapse

[2] Handbook of image and video processing by Alan Conrad Bovik, Elsevier Inc., ISBN 0-12-119192-1

[3] Digital Video Processing by A. Murat Tekalp, Prentice Hall Signal Processing Series.

[4] R. Schaphorst, "Videoconferencing and videotelephony," Boston, MA: Artech House Publishers, 1996.

[5] /www.mathworks.com/products/imaq/demos.html?file=/products/demos/shipping/imaq/demoimaq_timelapse1.html.

[6] /www.mathworks.com/matlabcentral/fileexchange/12262-datetime-stamp-in-a-plot

[7] Lossless Visible Watermarking- Shu-Kei Yip

[8] Adnan M. Alattar, "Reversible watermark using the difference expansion of a generalized integer transform", IEEE Trans. On Image Processing, vol. 13, no.8, Aug, 2004.

[9] Avcibas, N. Memon, and B. Sankur " Steganalysis using image quality metrics", IEEE Trans. IP, VOL. 12, PP.221-229, Feb. 2003

◈◈◈

Simulation of the effect of DIE Radius on Deep Drawing Process

Kopanathi Gowtham, K.V.N.S. Srikanth & K.L.N. Murty.
CAD-CAM, Dept. of Mechanical Engineering, Godavari Institute of Engg. & Tech., Rajahmundry, INDIA.

Abstract - This paper "SIMULATION OF THE EFFECT OF DIE RADIUS ON DRAWING PROCESS" is one of the most used Metal Forming Process within the industrial field. Different analytical, numerical, empirical and experimental methods have been developed in order to analyze it. This work reports on the initial stages of finite element analysis (FEA) of a Deep drawing process. The objective of this study is to determine the factors influencing a drawing process and analyzing the process by varying the Die radius and keeping the Friction, Punch radius and Blank Thickness as constant.

In this paper Punches, blank thickness of same geometry and dies of various geometries were drawn by using CATIA software. And an effort is made to study the simulation effect of main process variant namely die radius using finite element analysis. As the FEM code, the commercially available software DEFORM-3D is used here. Aluminium alloy 6061 is used for deep drawing with initial diameter as 56mm.

Keywords- *Die radius; FEA; CATIA V5; Deep drawing process; DEFORM 3D*

I. INTRODUCTION

Mathematical description of the processes of Deep-drawing is very complicated because of varying loading history and complex stress state in each point of material. The parameters introduced in the mathematical models of deep drawing are normally taken from a simplest mechanical test such as uni-axial traction test. Lately some new tests were developed which are closed to forming processes. Deep-drawing of a cylindrical cup occupies a particular place between these tests since it allows to study material hardening, conditions of friction, wrinkling, plastic flow instability, fracture, some others effects.

Drawing is a manufacturing process very used in the industry due to its versatility and good mechanical properties (as good surface finish and dimensional accuracy) of the parts. Successful drawing operations require careful selection of process parameters and consideration of many factors.

The main variables involved in this type of process are :

1. Die radius
2. Friction
3. Punch Radius
4. Blank Thickness.

Deep Drawing

"Deep drawing is a compression metal forming process in which a sheet metal blank is radially drawn into a forming die by the mechanical action of a punch".

A cup-like cylindrical part, having the depth greater than its diameter, is formed as a result of deep drawing.

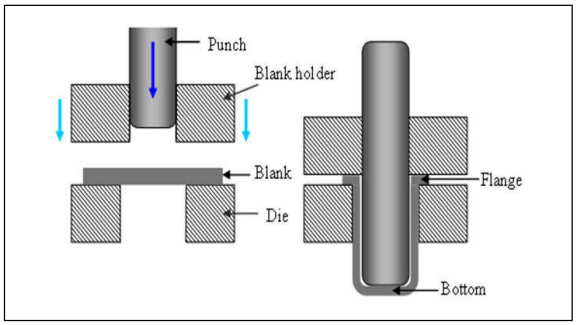

Fig. 1.1 Deep Drawing

Method Of Analysis

In general, the complexity of these processes and the great number of factors involved in them making very difficult to select the parameter values properly. Then, different analytical, numerical and experimental methods are being developed in order to analyze the best combination of them.

Now-a-days analytical methods still continue being studied and developed in spite of numerical methods allow obtaining solutions with high precision and detail levels in the analysis of this type of process.

Finite element method has been used as well in several studies about metal forming processes recently.

The main objective of this paper presented in it is the multi stage deep drawing analysis. According to John Monaghon [1] et al, as the die radius is reduced, this increases the amount of force required to draw the material. The increased force on the punch and the greater difficulty in getting the material around the die radius causes stretching marks on the cup wall and an uneven thickness distribution. To verify the above experimental results and to validate the simulation done, several simulations were performed by varying the die radius. Furthermore, the effect of the above process parameters on the formability and quality issues are studied.

Outline of this Paper

The outline of this paper is to present the CATIA V5 and DEFORM-3D software, also gives the methodology of various process variables used and how deep drawing has been simulated for those combinations with more emphasis on finite element tool used. The results of Deep Drawing process are in the form of graphs and also figures with short discussions. And lastly of this paper, the main conclusions are recapitulated.

II. LITERATURE REVIEW

The stamping of thin metallic sheets is a widely used industrial material forming process. It allows production of thin walled parts with complicated shapes such as automotive panels or structural parts. The process consists of the plastic deformation of an initial at blank subjected to the action of a rigid punch and die while constrained on the periphery by a blank holder.

The main variables involved in this type of process are :

- Die Radius
- Friction
- Punch Radius
- Blank Thickness.

These factors determine the maximum punch load in drawing, the sheet-thickness variation after drawing, and the maximum limit drawing ratio. If the height of the work piece in industrial production is too high, multi-redrawing is necessary in order to obtain a successful product.

The finite element method has recently been sufficiently developed for the analysis of metal forming processes. Hence, much research has been performed using the finite element method. The purpose of this study is to clarify the mechanics of ductile fracture in bulk metal forming processes.

The following four kinds of ductile fracture criteria, that is to say, freudenthal's fracture criterion, Cockcroft and latham's fracture criterion, Brozzo et al.'s fracture criterion and oyane's fracture criterion are used. These four kinds of ductile fracture criteria are used in the analysis of deep drawing. The analytical results of the work using Cockcroft and latham's fracture criterion and using Brozzo et al.'s fracture criterion agree satisfactorily with the experimental result.

Damage Mechanics

Damage specifies the damage factor at each element. Fracture occurs when the damage factor has reached its critical value. Critical value of Damage Factor must be found through physical experimentation. The basic idea of damage mechanics is to translate the underlying microscopical failure phenomena to a macroscopical description that can be used in a phenomelogical model. In all cases, the models are considering one or more parameters and when these parameters reach a critical value failure is expected.

In this case more properties are needed, for instance the strain rate, stress tri-axiality and temperature. Most crash simulations of today do not use damage models due to a lack of information on which damage models that under given conditions give reliable predictions, and how the damage parameters should be determined.

Phenomelogic Failure Models :

The Phenomelogical models describe the failure in the material in terms of mechanical variables such as stress, strain, temperature, strain rate etc. In all models presented in this paper the failure model is a function which depends of these variables and if the functions reach a critical value, failure is expected in the material.

Stress Dependent Failure Criteria

One of the simplest models to predict failure is to consider that failure occurs when the stress reaches a critical value. Below follows a short review of some of the basic stress dependent failure criteria. All the models presented are isotropic, i.e. they have the same property in all directions of the material.

Maximum Principle Stress Criterion

The maximum principle stress criterion is also known as the Coulomb or Rankine failure criterion. It only depends on the principle stress to predict failure. To predict failure one considers two material parameters

describing the maximum allowed stress in compression σ_c and tension σ_t, respectively, and state that failure is not to be expected as long as the principle stresses is in between these values, i.e

$$-\sigma_c \leq \{\sigma_1, \sigma_2, \sigma_3\} \leq \sigma_t .$$

III OVERVIEW

Deep Drawing

"Drawing is a operation in which the cross-sectional area of a bar is reduced by pulling it through a converging die'' i.e. the process consists of reducing or changing the cross-section of work piece such as wires, rods, plates, making pass them through a die by means of a pulling force (a tensile force), applied on the exit side of the die.

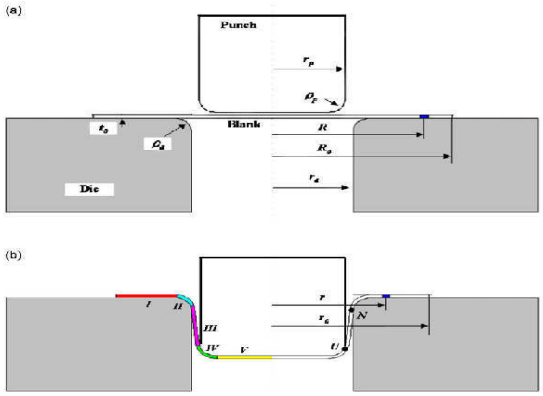

Fig. 3.1 – Deep drawing for a circular cup (a) initial stage and (b) intermediate stage.

Typical Stages of a Deep Drawing process are as follows:

1. **Shearing** a blank (round rectangular or other shape).
2. **Clamping** the blank on the die.
3. **Stretching** the blank by the punch forcing it into the die cavity.
4. **Returning** the punch and removal the part from the die.
5. **Trimming** the excess blank.

IV. METHODOLOGY

The Deep drawing processes have been analyzed for different combinations of process variables. The various assumptions and combinations are used in this study to investigate an effect of process variables on deep drawing process is presented in this chapter.

The material used in this analysis is Al 6061 an Aluminum alloy. The initial diameter is taken as 56 mm. The Deep drawing speed used here is 0.9 mm/sec. The friction between the blank and the punch, die interface has taken constant as 0.3.

Combinations Of Process Variables

The various combinations of the process variables are i.e. Die radius, friction, damage value, effective stresses and strains, Max. Principle stresses and strains.

1. Variation Of Die Radii With Constant Friction And

   Effective Stress

   1) 4------0.3-------148.
   2) 5------0.3-------155.
   3) 6------0.3-------163.
   4) 7------0.3-------188.
   5) 8------0.3-------172.

2. Variation Of Die Radius With Constant Friction And Damage Value

   1) 4------0.3-------6.51.
   2) 5------0.3-------5.35.
   3) 6------0.3-------8.30.
   4) 7------0.3-------3.99.
   5) 8------0.3-------5.50.

3. Variation Of Die Radius With Constant Friction And Effective Strain

   1) 4------0.3-------5.48.
   2) 5------0.3-------4.46.
   3) 6------0.3-------4.45.
   4) 7------0.3-------2.83.
   5) 8------0.3-------4.79.

4. Variation Of Die Radius With Constant Friction And Max. Principal Stress

   1) 4------0.3-------199.
   2) 5------0.3-------169.
   3) 6------0.3-------178.
   4) 7------0.3-------203.
   5) 8------0.3-------175.

5. Variation Of Die Radius With Constant Friction And Max. Principal Strain

1) 4------0.3-------4.40.
2) 5------0.3-------4.02.
3) 6------0.3-------3.85.
4) 7------0.3-------2.45.
5) 8------0.3-------3.69.

6. Variation Of Die Radius With Constant Friction And Max. Load per Stroke.

1) 4------0.3-------12749.17.
2) 5------0.3-------13507.11.
3) 6------0.3-------13913.89.
4) 7------0.3-------13971.84.
5) 8------0.3-------13952.45.

V. RESULTS AND DISCUSSION

Different simulations with different die radii were performed. According to John Monaghon [1] et al. , as the die radius is reduced, it increases the amount of force to draw the material, the increased force on the punch & greater difficulty getting the material around the die radius causes stretching marks on the cup wall and an uneven thickness distribution.

To verify the above experimental results and to validate the simulation done, several simulations were performed by varying the die radius.

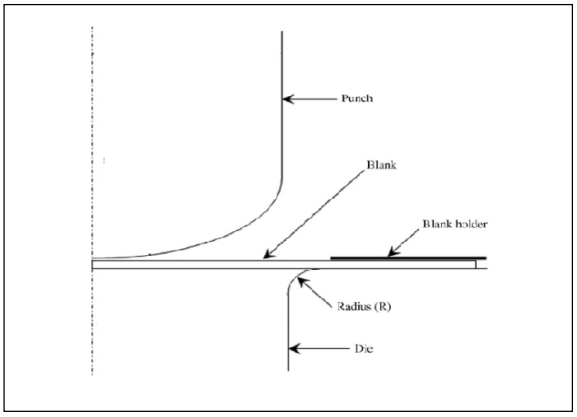

Fig. 6.1 : Geometry of The Die Profile

The following figures from 6.1 to 6.5 are the drawn cups showing effective stress values for different die radii ranging from 4mm to 8mm respectively.

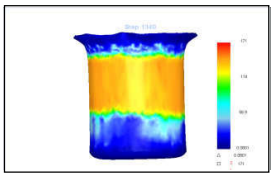

Fig. 6.2 Effective stress Values for 4mm Die radius.

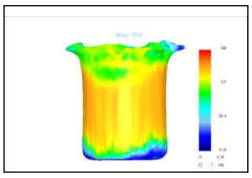

Fig. 6.3 Effective stress values for 5mm Die radius

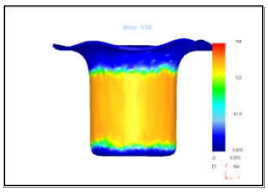

Fig. 6.4 Effective stress values for 6mm Die radius.

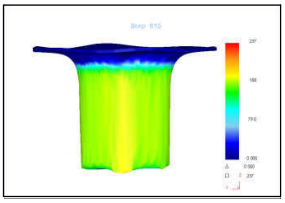

Fig. 6.5 Effective stress values for 7mm Die radius.

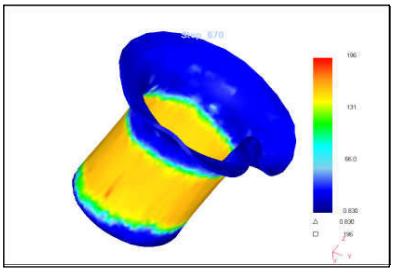

Fig. 6.6 Effective stress values for 8mm Die radius.

Comparing the effective stress values of the drawn cups, it was found that, effective stress value was increasing as the die radius is decreased as shown in Fig. 6.1-6.5. Comparing the Max. principal stress values of the drawn cups, it was found that, max. Principal stress values are increasing as the die radius is decreasing.

Comparing the effective strain values of the drawn cups, it was found that, effective strain value is decreasing as the die radius is decreasing.

Comparing the Max. Principal strain values of the drawn cups, it was found that, max. Principal strain values are decreasing as the die radius is decreasing.

Comparing the damage values of the drawn cups, it was found that, damage value is minimum for a die radius of 7mm and this die radii is recommended as an optimum die radii.

Comparing the load required of the drawn cups, it was found that, load is increasing as the die radius is decreasing.

Further, when the die radius was too small, the material, after considerable thinning process experienced Ear-ring type defect because, as the die radius was too small, the amount of force required to

draw the material was large and the shear component of the load required in the deformation process is increased.

As for the above case, more force is needed to draw the material, it causes Stretching Marks and the end face of the cup twisted itself in its edge, forming earring type of error.

From the simulation performed, it is proved that, As the die radius is reduced,

- ❖ This increases the amount of force to draw the material
- ❖ The increased force on the punch & greater difficulty getting the material around the die radius causes stretching marks on the cup wall.
- ❖ Uneven thickness distribution.

With the above results, it can be seen that the simulation performed is validated.

Effect Of Process Variables On Damage Value

Fig. 6.7 shows the analysis result to investigate the effect of variation in die radii on damage value when the friction between the die and the blank are considered to be constant as 0.3 respectively and the die radii varies as 4, 5, 6, 7, 8mm.

For the die radii equal to 4mm, as the 56mm blank passes through the first die, damage value near the blank is found to be about 2.34 and damage value increases gradually and the region that damage increased its value is generated after it passes through 5th die. Similarly for other die radii equal to5, 6, 7, 8mm the damage value as the blank passes through the dies is tabulated and it is shown in table 6.1.

From fig. 6.7, By comparing the damage values of the drawn cups, it was found that, damage value is minimum for a die radius of 7mm and this die radii is recommended as an optimum die radii.

Table 6.1: Damage Values After Each Die Pass For Different Die Radius

No. of Drawing Die	**Max. Principal Stress**				
	Die radius of 4mm	Die radius of 5mm	Die radius of 6mm	Die radius of 7mm	Die radius of 8mm
1	199	169	178	203	175
2	161	122	155	172	146
3	122	94	96.74	111.2	87.4
4	65.5	50.7	31.1	67.4	28.1
5	11.79	14.5	4.85	4.28	8.21

Table 6.2: Effective strain after each die pass for different Die radius.

No. of Drawing Die	Damage Values				
	Die radius of 4mm	Die radius of 5mm	Die radius of 6mm	Die radius of 7mm	Die radius of 8mm
1	6.51	5.35	8.30	3.99	5.50
2	5.47	4.54	5.87	3.22	4.64
3	4.53	3.56	4.54	2.51	3.77
4	3.60	2.72	3.44	1.47	2.42
5	2.34	1.31	2.79	0.49	1.21

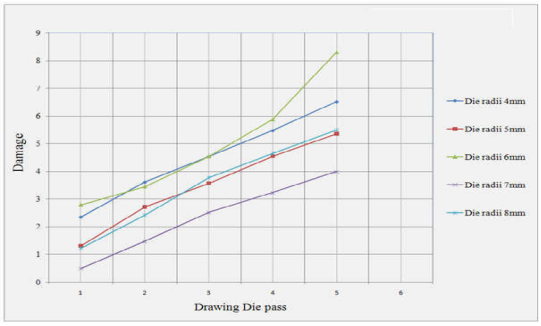

Fig. 6.7 : Damage Values After Each Die Pass For Different Die Radius.

Effect Of Process Variables On Effective Strain

Fig.6.8 shows the analysis result to investigate the effect of variation in die radii on effective strain when the friction between the die and the blank are considered to be constant as 0.3 respectively and the die radii varies as 4, 5, 6, 7, 8mm. Table 6.2 shows effective strain developed in drawing operation during each pass, for different die radii.

Comparing the effective strain values of the different die radii, it was found that, effective strain is decreasing gradually for a given die radii with lower strain after first pass. For a given constant friction, effective strain is decreasing with increase in die radii.

Table.6.8 shows the values of these effective strains. Effective strains is decreasing for larger die radii. For die radii of 4, 5, 6, 8mm the effective strain is almost constant with little variation and for 7mm die radii showing an decrease in effective strain.

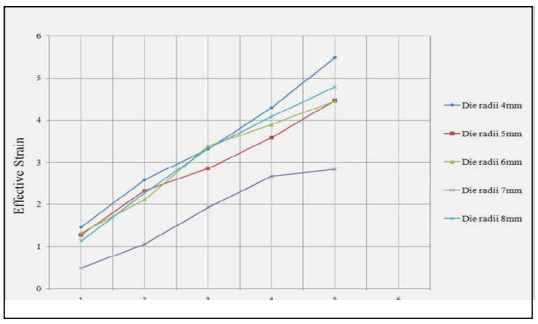

Fig. 6.8 : Effective strain after each die pass for different Die radius

Table 6.3: Effective stress after each die pass for different Die radius.

No. of Drawing Die	Effective Strain				
	Die radius of 4mm	Die radius of 5mm	Die radius of 6mm	Die radius of 7mm	Die radius of 8mm
1	5.48	4.46	4.45	2.83	4.79
2	4.29	3.58	3.89	2.67	4.08
3	3.31	2.85	3.38	1.93	3.33
4	2.58	2.32	2.11	1.06	2.28
5	1.46	1.27	1.32	0.49	1.13

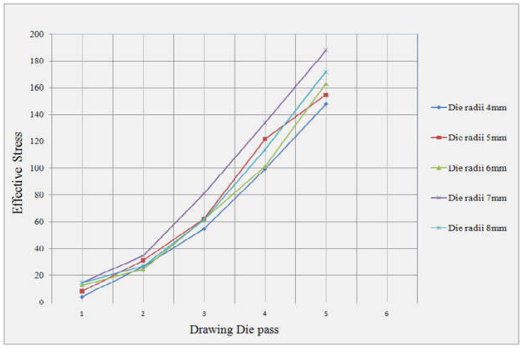

EFFECT OF PROCESS VARIABLE ON LOAD REQUIRED

Effect of die radii

Fig. 6.12 shows the analysis result to investigate the effect of variation in die radii on load required during drawing operation, when the friction between the die and the blank are considered to be constant as 0.3 respectively and the die radii varies as 4, 5, 6, 7, 8mm. Table 6.6 shows the load required in drawing operation during each pass, for different die radii.

The load required for a given die radii increases as the blank passes through the next die with highest load required for the third pass. For a given constant friction, the load required increases with increase in die radii. This is because for larger die radii the length of contact between the blank and die is high, thus it cause significantly high frictional losses, thus load required is high.

The load fluctuates periodically with increase in time. The load in actual drawing operation fluctuates gradually with time, while the load in the analysis fluctuates significantly for each die pass with increase in time. The reason for the fluctuation of the load in the analysis is, since the number of elements which come into contact with the drawing die is limited, the load fluctuates markedly when a node comes into contact with the drawing die or separates from the drawing die.

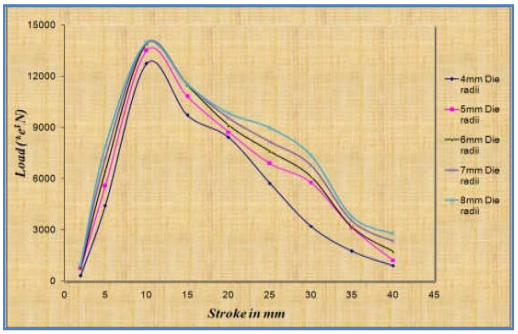

Fig. 6.12 Load per stroke for different Die radius.

VI CONCLUSIONS

It is a finite element analysis based simulation has been done using Deform-3D for the deep drawing process.

1. The effect of die radius on the formability and quality characteristics of deep drawing process has been done.
2. It has been found that as the die radius is reduced, the amount of fore required to draw the material is increased.
3. A decreased die radius created stretching marks and earring type quality problems.
4. Because of the above issues, an optimum die radius was an important parameter to be obtained from the simulation studies.

5. It has been found that a die radius of 7mm gave an optimum deform levels with minimum damage.
6. It was found that the result of the simulation studies were in line with the experiments conducted by prof. john monaghon[1] et al., whose results have been published in journal of material processing technology.
7. The developed model, as it is validated can be used to simulate any problems in deep drawing process for any material.

REFERENCE :

[1] MARK COLGAN, JOHN MONAGHAN, Deep Drawing Process : Analysis And Experiment, Journal Of Materials Processing Technology 132(2003)35– 41.

[2] DIETER G. E., (1986), Mechanical Metallurgy. Mcgraw-Hill.

[3] Metal Forming Process by R.KALPAKKAM JAIN.

[4] B.AVITZUR, Handbook of Metal Forming Processes, Willey, NewYork,1983.

[5] M.G. COCKCROFT, LATHAM D.J., Ductility and the Workability of Metals, Journal Of The Institute Of Metals, 1968; 96:33-9.

[6] Development Of An Analytical Model For Warm Deep Drawing Of Aluminum Alloys, HONGSEOK KIMB, MUAMMER KOC,JUNNIB, Journal Of Materials Processing Technology 197(2008)393–407.

[7] J. BEDDOES, M.J. BIBBY, Principles Of Metal Manufacturing Processes, ARNOLD PARIS, 1999, pp. 152–161.

[8] Influence Of The Die Arc On Formability In Cylindrical Cup-Drawing, YOU-MIN HUANG, JIA-WINE CHEN, Journal Of Materials Processing Technology 55 (1995) 360-369.

[9] M. COLGAN, J. MONAGHAN, An Elastoplastic Finite Element Analysis Of A Deep Drawing Process, J. MATER. Process. Technol. (2000).

[10] Numerical Simulation And Analysis On The Deep Drawing, R. PADMANABHANA,, M.C.OLIVEIRAA, J.L. ALVESB, L.F. MENEZESA, Journal Of Materials Processing Technology 200(2008)416–423.

[11] Numerical Damage Prediction In Deep-Drawing Of Sheet Metals, M. KHELIFAA, M. OUDJENEB, Journal Of Materials Processing Technology 200(2008)71–76.

[12] Analytical Model For Deep-Drawing Of A Cylindrical Cup, R.A. NAZAROV, Z. AYADI, S.A. NIKULIN.

[13] Influence Of Process Parameters On The Deep Drawing, R. PADMANABHANA,∗, M.C. OLIVEIRAA, J.L. ALVESB, L.F. MENEZESA. Finite Elements In Analysis And Design 43(2007)1062–1067.

◈◈◈

Simulation of Vehicular Frontal Crash-Test

Tejasagar Ambati, K.V.N.S. Srikanth & P. Veeraraju

Dept. Mechanical Engineering, Godavari Institute of Engg & Tech., Rajahmundry, INDIA

Abstract **-** This paper **"SIMULATION OF FRONTAL CRASH-TEST"** The simulation of vehicle crashes by using computer softwares has become an indispensible tool for shortening automobile development time and lowering costs. It also has huge impact on the crashworthiness of an automobile.

This work reports on the simulated crash test of an automobile. The objective of this work is to simulate a frontal impact crash of an automobile and validate the results. The aim is also to alter some of the materials of the components with a view to reduce the forces experienced during the crash. Computer models were used to test the crash characteristics of the vehicle in the crash. The model used here was that of a Chevrolet C1500 pick-up truck.

The software used for the simulation is LS-DYNA. It is widely used by the automotive industry to analyze vehicle designs. It accurately predicts a car's behavior in a collision.

The results obtained by the simulation were then validated by comparing it with the test results of the same test performed by the NCAC (National Crash Analysis Center)**..**

Keywords **-** *CRASH TESTS; FEA; LS-DYNA; Proposing alternative materials;*

I. INTRODUCTION

In modern engineering analysis it is rare to find a project that does not require some type of simulation for analyzing the behavior of the model under certain specified conditions. The advantages of simulation are numerous and important. A new design concept may be modeled to determine its real world behavior under various load environments, and may therefore be refined prior to the creation of drawings, when few dollars have been committed and changes are inexpensive. Once a detailed CAD model has been developed, simulations can analyze the design in detail, saving time and money by reducing the number of prototypes required. An existing product which is experiencing a field problem, or is simply being improved, can be analyzed to speed an engineering change and reduce its cost.

The finite element method is comprised of three major phases: (1) *pre-processing*, in which the analyst develops a finite element mesh to divide the subject geometry into sub-domains for mathematical analysis, and applies material properties and boundary conditions, (2)*solution*, during which the program derives the governing matrix equations from the model and solves for the primary quantities, and (3) *post-processing*, in which the analyst checks the validity of the solution, examines the values of primary quantities (such as displacements and stresses), and derives and examines additional quantities (such as specialized stresses and error indicators).

Crash- Test

A crash-test is a form of destructive testing usually performed in order to ensure safe design standards in crashworthiness and crash compatibility for automobiles or related components. To test the cars safety performance under various conditions and during varied types of crashes, vehicle manufacturers crash test their cars from different angles, different sides and with different objects, including other vehicles.

The most common types of crash tests are listed below.

- Front impact test
- Front offset crash test
- Side impact test
- Roll over test

Method Of Analysis **(LS-DYNA)**

Crash-testing requires a number of the test vehicle to be destroyed during the course of the tests and is also

time consuming and uneconomical. One new recent trend that is gaining vast popularity is computer simulated crash-testing. Here instead of a real vehicle, a FE (Finite Element) model of the vehicle is generated and is used to carry out the different tests that were carried out before using actual vehicles.

There are several software packages that are equipped to handle the crash-testing of vehicles, but one of the most popular is from Livermore Software Technology Corporation called LS-DYNA.

With LS-DYNA, automotive companies and their suppliers can test car designs without having to tool or experimentally test a prototype, thus saving time and expense. While the package continues to contain more and more possibilities for the calculation of many complex, real world problems, its origins and core-competency lie in highly nonlinear transient dynamic finite element analysis (FEA) using explicit time integration. The application of LS-DYNA covers a wide range of industries.

Outline of this Paper

The outline of this paper is to present the dynamic analysis of a vehicle using LS-DYNA software, also proposes some alternative materials in order to reduce impact shock and to increase the toughness of the body parts and decrease the weight. The main purpose was the reduction of the weight of the vehicle, the lower values of the results is not unexpected. The Test model 2 will experience lower forces as a result of its lower weight. Than the test model .

II. LITERATURE REVIEW

Simulated crash-testing is being increasingly by various institutes to study the outcome of a vehicular in various situations under different conditions. The advantage of simulation is that the FE models can be reused again and again and also the user has the freedom to change any of the parameters of the test and also the user can vary the material properties as well as the type of material of the parts in the vehicle.

The FE model was then used to simulate crash test. The FE software used here to carry out the simulation was LS-DYNA. One of the tests carried out was the Frontal-offset crash at 40 mph. Before the simulation could be carried out, several other preprocessing conditions have to be specified. The test results were verified using results from actual crash-test reports. Present runtimes on high-end workstations for LS-DYNA vehicle models are still measured in days, while multi-body run-times are typically less than 1h, even for the most complex models.

Thacker et.al [1] conducted crash-testing simulation study of a 1997 Honda Accord. Originally, a real vehicle was obtained and then the vehicle was stripped down to its basic parts, each component was identified, labeled, and the material evaluated. Data that could be efficiently extrapolated from existing sources were collected

A similar study was carried out by Cheng et.al [2], wherein the aim of the study was to reverse engineer a 1997 Honda Accord DX Sedan and to develop a FE model of the vehicle to be that can be successfully used in computational simulations of full frontal, offset frontal, side, and oblique car-to-car impact testing

The crashworthiness was then compared to existing physical data of a 2007 Jeep Wrangler that has been manufactured with all safety standards and technology. These comparisons were made to evaluate the crashworthiness of the pre safety standards.

NHTSA Crashworthiness

Every year the NHTSA (National Highway Traffic Safety Administration) evaluates crash safety for cars and trucks. NHTSA chooses new vehicles, which are predicted to have high sales volume or have improved safety equipment.

Tests are conducted to measure how well occupants are protected in a head-on collision. Based on the result from the test, the vehicle is given a one to five star rating, five stars being the most protective and one being the worst. The crash test ratings are only meaningful when comparing vehicles within the same weight class. Federal law requires all passenger cars to pass a 30 mph frontal crash while the NCAP test involve crashing into a fixed barrier at 35 mph. Instruments are placed in the vehicle to record the response of the structure during the crash. Anthropomorphic dummies are placed in the driver and passenger seats for the test, they measure the force of the impact to the chest, head and leg. These readings are the basis for the five start rating. The test program deals only with crashworthiness and indicates how well a car can protect its occupants in a frontal collision

Alternative Materials

Due to the age of the vehicle, the majority of the components were constructed of mild steel. However, in light of recent developments in manufacturing processes, the use of lighter substitutes to steel in the construction of the vehicle components has been steadily increasing. One of the most widely substitutes for steel is aluminum. In considering the total life-cycle of an automobile covering four stages (pre-manufacturing, manufacturing, use, and post-use), it is apparent that during the operational stage of a vehicle,

aluminum is proven to be a reliable alternative for traditional materials currently used in automotive body structures largely due to its cost effectiveness and superior performance due to light weight

In Test model 1, the materials used are the original materials that were used to manufacture the vehicle. However, in Test model 2, the materials used were updated in relation to the increased use of lighter alloy metals for manufacturing automobiles. The materials that were use in the two test models are

- AA 3005
- AA 5182
- AA 5454
- A 319
- ASTM A 514

Material		**Test Model 2**
Aluminium	AA 3005	Radiator
	AA 5182	Door, Hood, Fonder, Wheel housing
	AA 5454	Tire rim
	A 319	Engine
Steel	ASTM A514	Rail

Tab: Materials Used for Test model 2

III. OVERVIEW

Simulation a frontal impact crash-test of a vehicle model moving at a velocity of 15.65m/s or 35mph (≈56.3kmph) in to a rigid immovable barrier is to be carried out and analyzed. It is assumed that the brakes are not applied during the crash event. The results obtained will then be validated and compared with the results of the same crash analysis performed by the NCAC (National Crash Analysis Center). The reason for comparing with the NCAC is that the institute has already conducted the same test under the same conditions by using a physical test vehicle. Then developed a finite element model of the vehicle by the process of reverse engineering. Then again carried out the same test under the same test conditions on the finite element model and validated their results by comparing with the results obtained from the physical test.

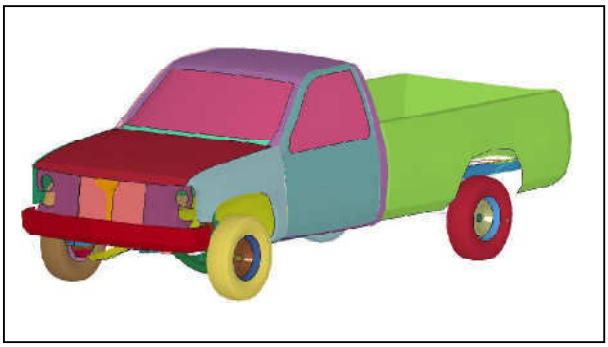

Fig: FE model of a Chevrolet C-1500

	NCAC Model	Test Model1	Test Model2
Weight(kg)	2013	1884	1654
Number of parts	251	65	65
Number of elements	58313	10729	10729

Tab: Comparison NCAC model and Test models

IV. METHODOLOGY

The frontal-impact crash-testing is conducted using a Chevrolet C1500 as the test FE model. The vehicle has an initial velocity of 35 mph (approx. 56 kmph) before it impacts the wall. The simulation is given a termination time of 0.15secs. The reason for termination time is that for rigid barriers, deceleration rates are very high. Numerous instrumental tests carried out in the past show that most energy transfer in a head-on or frontal vehicle impact with a rigid barrier occurs within 0.2 seconds and can be as short as 0.07 to 0.02 seconds

To the generated model simulation is done in 3 steps

1. Pre processing
2. Solver
3. Post processing

The post-processor is used to read the database file from the simulation engine and displaying the results graphically.

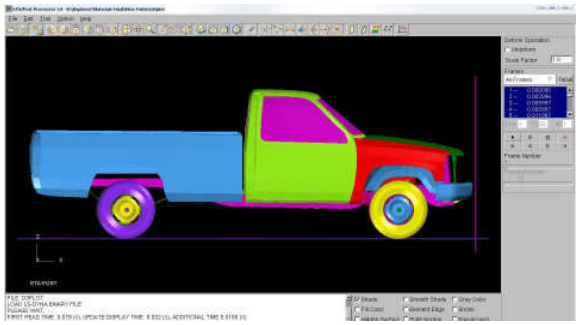

ELEMENT FORMULATION

The completed model contains approximately 65 parts, 61 materials and 10693 elements and 11060 nodes. Structural components and specific element types used in the model include

- Solid elements
- Belytschko - say shell element
- Hughes-Liu beam element

BOUNDARY CONDITIONS

The function of the boundary conditions is to create and define constraints and loads on finite element models. To simulate a full vehicle car crash, all loads and boundary conditions that occur in the actual crash event need to be modeled. Just as a car is subjected to gravitational loads in real life, the simulated model should have a representative gravity force applied. Friction forces between the tires and the road surface play an important role in how the vehicle behaves on impact, so these have to be accounted for in the simulation. The tires in real life are filled with air and will affect the severity of the impact. Modeling of the tires has to be able to simulate the interaction of the tires upon impact. A velocity has to be applied to the vehicle in a manner as to not impart any unrealistic acceleration or cause the simulation to run for an extended amount of time. Fortunately, Ls-Dyna provides methods to simulate all of these requirements

V. RESULTS AND DISCUSSION

Two simulations were carried out for the frontal impact; the Test model 1 had the same materials as the NCAC model while in the Test model 2, newer materials for the parts were employed. The results obtained were then validated with the results obtained of similar simulations performed by the NCAC.

The sequence of images shown below is the image of the vehicle before and after it impacts the rigid wall with the specified velocity of 35mph (≈56kmph). A collection of images showing the impact of the Test model 1 as it impacts the wall from time t=0 to t=0.15secs at time intervals 0, 0.05, 0.10 and 0.15sec.

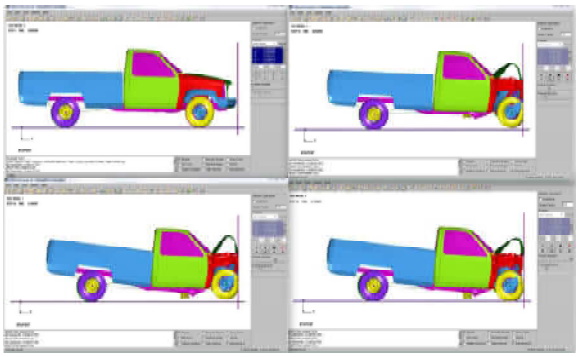

Fig Crash sequence of Test model1

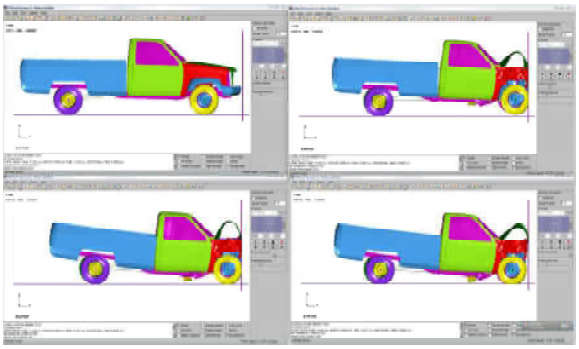

Fig Crash sequence of Test model 2

ENERGY BALANCE GRAPHS

First of all, the energy balance graphs between the Test model 1 and Test mode 2 are compared to comprehend the performance of Test model 2 with respect to Test model 1

Graphs showing the Kinetic energy, Internal energy and the Total energy Vs Time obtained after the simulation are displayed for both the simulations and also for the NCAC test.

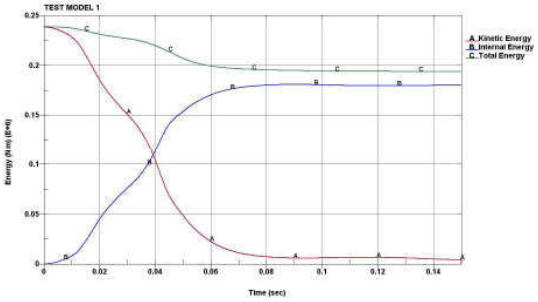

Fig: Energy balance graph of test model1

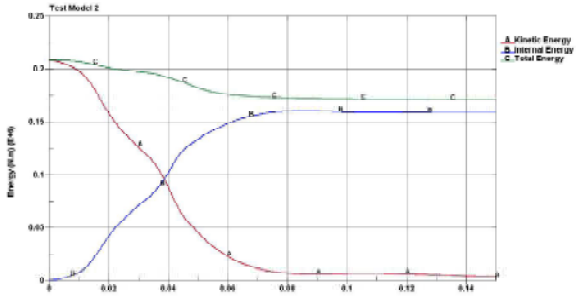

Fig: Energy balance of Test model 2.

As observed, the most of the energy of the impact is absorbed by the bumper, radiator, engine and the rails. These components absorb most of the energy of the crash before the tires impacts the wall. The maximum values of kinetic energy of the Test model 1 and Test model 2 are 239.126kJ and 208.301kJ respectively. For the Test model 2, whose main purpose was the reduction of the weight of the vehicle, the lower values of the results is not unexpected. The Test model 2 will experience lower forces as a result of its lower weight.

DECELERATION Vs TIME

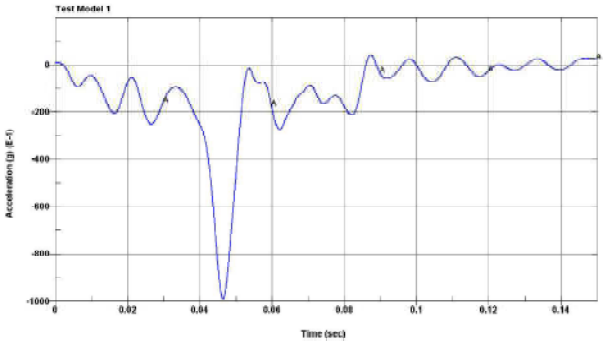

Fig: Acceleration Vs Time graph of Test Model 1

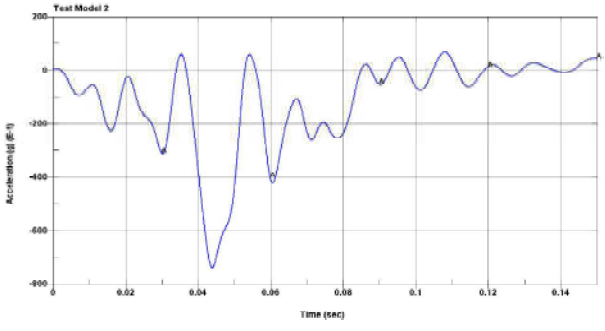

Fig: Acceleration Vs Time graph of Test Model 2

As can be seen from the graph, there is a small difference between the deceleration profile of the Test model 1 and the Test model 2 The maximum deceleration for the Test model 1 and the Test model 2 are found to be 98.94 g and 84.83 g respectively

Since the deceleration is related to the mass of the body and as is known that the Test model 2 has a lower mass than Test model 1 as given in Tab 3.1. Therefore, the lower value of the deceleration of the Test model 2 is not unexpected

VELOCITY Vs TIME

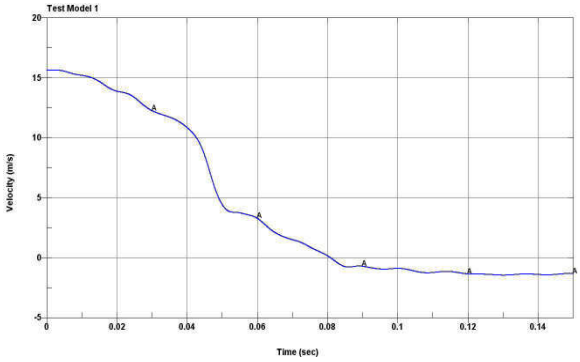

Fig: Velocity Vs Time graph of Test model 1

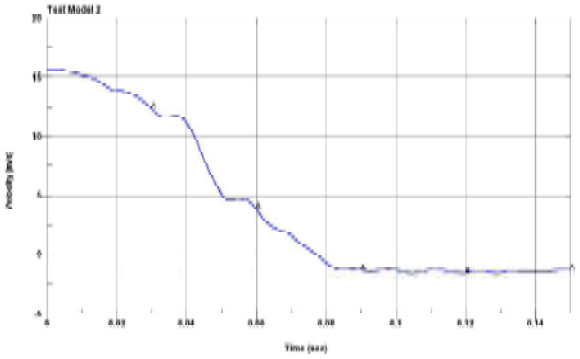

Fig: Velocity Vs Time graph of Test model 2

As can be seen from the graph, the velocity profiles of both the Test models follow very similar profiles. Here also there is the presence of a small negative velocity towards the end of the crash event. This is caused as a result of the forces generated due to the impact of the vehicle against the wall.

SCOPE OF FUTURE WORK .

The FE model can be used for further simulation of in the simulations of the offset frontal impact test, where one side of the front of the vehicle is impacted against a

barrier or another vehicle. Other tests include the side impact test, where a vehicle is impacted from the side by and oncoming vehicle and oblique car-to-car impacts the two or more vehicle take part in a collision. Rollover simulation can also be carried out wherein the vehicle rolls on its sides due to the cause of an impact or other factors

Further crash-testing involving the effects of the crash forces on the occupants of the vehicle can also be carried by using FE models of test dummies. Human-surrogate dummies called Anthropomorphic Test Devices (ATDs) could be placed inside the FE vehicle models and an entire crash test event could be simulated. The FE dummies are used to simulate the behavior of a vehicle occupant in the event of a crash. These FE dummies can then be placed inside the vehicle and the crash-simulation performed, they can provide various insights into the dynamic behavior of the human body in the event of a crash. This, however, requires detailed occupant compartment geometry as well as a detailed dummy model. This could easily double the FE models complexity and greatly increase the needed computer resources

VI. CONCLUSIONS

The overall objective of the work was to simulate a Frontal crash-test and validate the results of the simulations obtained from the crash-test. Simulation was performed using the LS-DYNA software package.

1. The results of the simulations were validated by comparing with the results of the NCAC model simulation.
2. As was observed, the bumper, engine and the rails absorb most of the energy before the wheel impacts the wall. Almost half of the energy of the crash is absorbed by these components after about 0.04sec of the crash initiation.
3. It has been observed that there is minimum deformation of the cabin and also there was minimum intrusion of the components into the cabin. Therefore, it can be assumed that the occupants in the cabin would not be caused any injury by a component intruding into the cabin in the event of the crash.
4. Due to the limited availability of computer resources, a simpler model of the test vehicle was chosen, which ultimately caused the inaccuracies of the results. As the number of elements of the test models is lower than that of the NCAC model, therefore, there are certain inaccuracies in the results.
5. For more accurate results a more accurate model would be required but the computer resources required for the simulations would have been much higher. Therefore a compromise had to be found wherein the simulation could be performed without the result deviating too much.
6. The graphical results obtained all showed that the test models behavior were similar to that of the NCAC model throughout the crash event.
7. The slightly different behavior of the Test model 2 can be attributed to the fact the material of the components were changed which had change the some of the outcome of the simulation.

VII REFERENCES

[1] J.G. Thacker, S.W. Reagan, J.A. Pellettiere, et.al, "Experiences during development of a dynamic crash response automobile model", Journal of Finite Element Analysis and Design 30 (1998) 279-295.

[2] Z.Q. Chenga, J.G. Thackera, W.D. Pilkeya, W.T. Hollowellb, et.al, "Experiences in reverse-engineering of a finite element automobile crash model", Journal of Finite Elements in Analysis and Design 37 (2001) 843–860.

[3] Abdullatif K. Zaouk , Nabih E. Bedewi, Cing-Dao Kan, et.al, "Validation of a non-linear finite element vehicle model using multiple impact data", The George Washington University FHWA/NHTSA National Crash Analysis Center.

[4] M.A. Virginia, "Crashworthiness of a Pre-NCAP Safety Standard Light Truck and Corresponding Suspension Analysis", Wichita State University (2001).

[5] Gary R. Consolazio, Jae H. Chung, Kurtis R. Gurley, "Impact simulation and full scale crash testing of a low profile concrete work zone barrier", Journal of Computers and Structures 81 (2003) 1359–1374.

[6] S. W. Kirkpatrick, "Development and Validation of High Fidelity Vehicle Crash Simulation Models", SAE Publications, Presented at the 2000 International Congress and Exposition (2000) SAE Paper No. 00PC-248.

[7] Geoff Davis, "Materials for Automobile Bodies", Elsevier, U. K. (2003) 10-60.

[8] J.O. Hallquist, "LS-DYNA Keyword User s Manual", Livermore Software Technology Corporation (1997).

[9] Zhipeng Zeng, Yanshu Zhang,Yi Zhouc, et.al, "Superplastic Forming of Aluminum Alloy Car Body Panels", Materials Science Forum 475-479 (2005) 3025-3028.

[10] U.N. Gandhi and S. J. Hu, "Data-Based Approach in Modeling Automobile Crash", Jouranal of Impact Engineering 16 (1995) 95-118.

[11] A. Deba, M.S. Mahendrakumara, C. Chavan, J. Karve, D. Blankenburg, S. Storenb, "Design of an Aluminium-Based Vehicle Platform For Front Impact Safety", Journal of Impact Engineering 30 (2004) 1055–1079.

◈◈◈

Application of Conditional Shortest Path Routing in Delay Tolerant Networks

Vamsi Krishna Pichika

Sri Vasavi Engineering College , Tadepalligudem

Abstract - This article studies Delay tolerant networks (DTNs) where each node knows the probabilistic distribution of contacts with other nodes. Delay tolerant networks are characterized by the sporadic connectivity between their nodes and therefore the lack of stable end-to-end paths from source to destination. Since the future node connections are mostly unknown in these networks, opportunistic forwarding is used to deliver messages. Based on the observations about human mobility traces and the findings of previous work, we introduce a new metric called conditional intermeeting time. We propose Conditional Shortest Path Routing (CSPR) protocol that route the messages over conditional shortest paths in which the cost of links between nodes is defined by conditional intermeeting times rather than the conventional intermeeting times. When a node receives a message from one of its contacts, it stores the message in its buffer and carries the message until it encounters another node which is at least as useful (in terms of the delivery) as itself. Through trace-driven simulations, we demonstrate that CSPR achieves higher delivery rate and lower end-to-end delay compared to the shortest path based routing protocols that use the conventional intermeeting time as the link metric.

I. EXISTING SYSTEM

A connected hypercube with faulty links and/or nodes is called an injured hypercube. A distributed adaptive fault-tolerant routing scheme is proposed for an injured hypercube in which each node is required to know only the condition of its own links. Despite its simplicity, this scheme is shown to be capable of routing messages successfully in an injured n-dimensional hypercube as long as the number of faulty components is less than n. Moreover, it is proved that this scheme routes messages via shortest paths with a rather high probability, and the expected length of a resulting path is very close so that of a shortest path.

Since the assumption that the number of faulty components is less than n in an n-dimensional hypercube might limit the usefulness of the above scheme, a routing scheme based on depth-first search which works in the presence of an arbitrary number of faulty components is introduced. Due to the insufficient information on faulty components, however, the paths chosen by this scheme may not always be the shortest. To guarantee all messages to be routed via shortest paths, the authors propose to equip every node with more information than that on its own links. The effects of this additional information on routing efficiency are analyzed, and the additional information to be kept at each node for the shortest path routing is determined.

II. PROPOSED SYSTEM

In this proposed system, we redefine the intermeeting time concept between nodes and introduce a new link metric called conditional intermeeting time. It is the intermeeting time between two nodes given that one of the nodes has previously met a certain other node. This updated definition of intermeeting time is also more convenient for the context of message routing because the messages are received from a node and given to another node on the way towards the destination. Here, conditional intermeeting time represent the period over which the node holds the message. To show the benefits of the proposed metric, we propose conditional shortest path routing (CSPR) protocol in which average conditional intermeeting times are used as link costs rather than standard intermeeting times and the messages are routed over conditional shortest paths (CSP). We compare CSPR protocol with the existing shortest path (SP) based routing protocol through real trace- driven simulations. The results demonstrate that CSPR achieves higher delivery rate and lower end-to-end delay compared to the shortest path based routing protocols. This show how well the conditional intermeeting time represents internode's link costs (in the context of routing) and helps making effective forwarding decisions while routing a message. Routing algorithms in DTN's utilize a paradigm called store-carry-and-forward.

We generated the multiple messages from a random source node to a random destination node at each t seconds. Clearly, CSPR algorithm delivers more messages than SPR algorithm.

III. ALGORITHM DESCRIPTION

Our algorithm basically finds conditional shortest paths (CSP) for each source-destination pair and routes the messages over these paths. We define the CSP from a node n0 to a node nd as follows:

$$CSP(n_0, n_d) = \{n_0, n_1, \ldots, n_{d-1}, n_d \mid R_{n0}(n_1|t) + d-1 \sum_{i=1} T_{ni}(n_{i+1}|n_{i-1}) \text{ is minimized.}\}$$

Here, t represents the time that has passed since the last meeting of node n_0 with n_1 and $R_{n0}(n_1|t)$ is the expected residual time for node n_0 to meet with node n_1 given that they have not met in the last t time units. $R_{n0}(n_1|t)$ can be computed as in with parameters of distribution representing the intermeeting time between n_0 and n_1. It can also be computed in a discrete manner from the contact history of n_0 and n_1.

Assume that node i observed d intermeeting times with node j in its past.

Let $\tau_i^1(j), \tau_i^2(j), \ldots \tau_i^d(j)$ denote these values. Then,

$$R_i(j|t) = \left(\sum_{k=1}^{d} f^k{}_i(j)\right)/|\{T^k{}_i(j \geq t\}|) \text{ where,}$$

$$f^k{}_i(j) = \begin{cases} T^k{}_i(j)-t & \text{if } T^k{}_i(j) \geq t \\ 0 & \text{otherwise} \end{cases}$$

Here, if none of the d observed intermeeting times is bigger than t (this case occurs less likely as the contact history grows), a good approximation can be to assume $R_i(j|t) = 0$.

IV. MODULES DESCRIPTION

1. Networking Module

Client-server computing or networking is a distributed application architecture that partitions tasks or workloads between service providers (servers) and service requesters, called clients. Often clients and servers operate over a computer network on separate hardware.

2. Shortest Path Module

In multi-hop wireless networks, packets are transferred through routes that could be composed of multiple relay nodes between sources and destinations. In many multi-hop wireless networks, shortest path routing is often used for its simplicity and scalability, and this is closely approximated by straight line routing for large multi-hop wireless networks. Thus, in this paper, we will focus on straight line routing for delivering packets from sources to destinations.

3. Straight Line Routing Module

Both simulations and analysis show that the relay load over the network, imposed by straight line routing, depends on the model of the traffic pattern. Even if the system settings are identical and straight line routing is commonly adopted, the relay load induced by "random" traffic could be distributed differently over the network. This paradoxical result is a consequence of the famous Bertrand's paradox. Thus, in contrast to traditional belief, there are many scenarios in which straight line routing itself can balance the load over the network, and in such cases explicit load-balanced routing may not help mitigate the relaying load.

4. Multi Hop Module

Analyze the load for a homogeneous multi-hop wireless network for the case of straight line routing in shortest path routing is frequently approximated to straight line routing in large multi-hop wireless networks. Since geographical and geometric attributes of nodes and routes affect the nodal load, we employ results from geometric probabilities to solve the problem

Based on our analytical results, we are able to show the precise relationship between the number of nodes and the load at each node, and the geographical distribution of the relaying load over the network for different scenarios. Interestingly, straight line routing itself can balance the relay load over the disk in certain cases.

V. FUTURE ENHANCEMENT:

In future work, we will look at the performance of the proposed algorithm in different data sets to see the effect of conditional intermeeting time in different environments. Moreover, we will consider extending our CSPR algorithm by using more information (more than one known meetings) from the contact history while deciding conditional intermeeting times. For this, we plan to use probabilistic context free grammars (PCFG) and utilize the construction algorithm. Such a model will be able to hold history information concisely, and provide further generalizations for unseen data.

◈◈◈